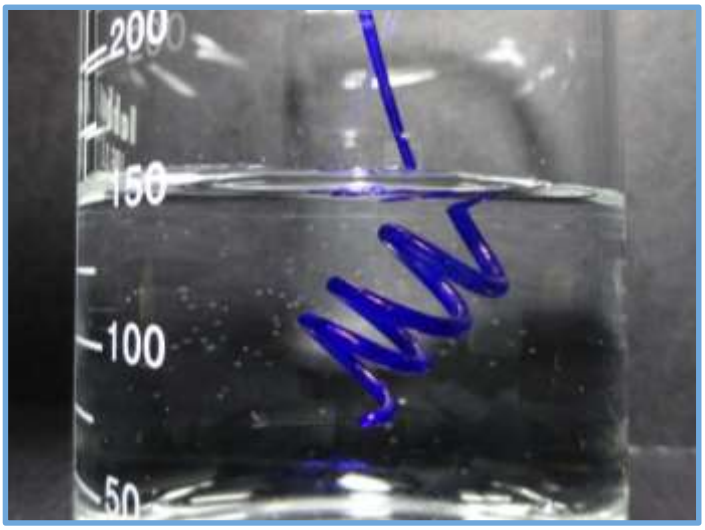

Biodegradable thermoplastic elastomers: Tuning viscoelastic properties and shape memory

Susana Petisco Ferrero 2015

Universidad del País Vasco Euskal Herriko Unibertsitatea

Ingeniaritza Goi Eskola Teknikoa
Escuela Técnica Superior de Ingeniería
Bilbao

This Thesis has been performed at:

ZIBIO Group, Department of Mining-Metallurgy

Engineering and Materials Science

Faculty of Engineering

Bilbao,

Spain

Network of Functional Biomaterials,

National University of Ireland Galway

Galway,

Ireland

Supervisor: Jose-Ramon Sarasua Oiz

A mi familia,

Enjoying the way,

Acknowledgements

Acknowledgements

In the following lines, I would like to express my gratefulness to those colleagues, friends and relatives who have supported me along this episode of my life.

Of course, the first acknowledgement is for my supervisor Prof. Jose Ramon Sarasua for his encouraging support since I was an undergraduate student, for nurturing in me the scientific interest on materials, undertaking me in his Research Group and allowing me to develop and mature with the cherish of a mentor.

Secondly, I would like to thank the technical support of Dr. Raúl Villanueva and Dr. Jagoba Iturri both from CICBiomagune as well as Dra. Mª Belén Sanchez and Alex Díez from SGIker respectively.

I want to specially acknowledge the kindness of Prof. Dr. Antxon Santamaría and Mª Mercedes Fernandez for their accessibility and generous contribution to this thesis.

I also thank my laboratory colleagues, friends and technicians for the scientific discussions, technical support and the so many good times.

I cannot forget Prof. Wenxin Wang and his Research Group for their generosity in undertaking me amongst his team during my stay in NUIG, Ireland and fostering new relationships and showing me the friendly side of excellence. I would also like to express my gratitude to Prof. Peter McHugh and Anna Bobel for the scientific exchange and motivating discussions.

I would also like to address a kind regard to the Department Professors, for their encouraging words and readiness along those years.

Finally, I reserve my deepest recognition to my family for their warmness and impinge me the fundamentals of hardworking.

Table of contents

Summary/Resumen

Summary

Polymers offer a special property spectrum for applications, extending the range of activities of mankind. With only a few decades separating their first commercial development from their present pervasive use, synthetic polymers are so well integrated into the fabric of society that we take little notice of our dependence on them. These range of properties, being completely different from those of the more traditional engineering materials, happen to be a consequence of their molecular structure which is in turn determined by production. From the combination of chemical intra-bond and van der Waals inter-bond forces distinct melting crystallizing and glassy transitions are achieved.

However interesting properties may polymers exhibit from an academic standpoint, it is their practical use which determines their relevance. Such was the case of polymers synthesized from glycolic acid and other α-hydroxy acids, which were not appreciated until an application where their instability was relevant was outlined such as their use as biodegradable medical devices. Thus, the efficient use of materials which implies the complete utilization of material properties, requires a multidisciplinary approach whereby material properties are harmonised with the functionalities demanded by such an application.

In this context, the motivation of the research work of this Thesis has been to gain a deeper understanding of viscoelasticity and shape memory from a Materials Engineer perspective, settling the correlation amongst structure and properties of lactide derived biodegradable systems with regard to specific applications.

In the first chapter, a complete characterization of the physical properties of several commercial (co)polymers has been conducted. It has been shown that, compared to the very regular poly(L-lactic acid) (PLLA), the addition of DLA or other comonomers, such as glycolide (GA) and ε-caprolactone (CL) reduce the crystallization capability as well as the glass transition temperature (T_g) so that at room temperature the poly(L-lactide-co-ε-caprolactone) (PLCL) copolymer exhibited a markedly elastomeric character, with entropy elasticity. Similar observations were also made on poly(rac-DL-lactide-co-glycolide) (PDLGA) at body temperature and on poly(DL-lactide) (PDLLA) at a somewhat higher temperature.

Thus, in search of a material for urological application, such as a temporary catheter in hypospadias repair, their biodegradation was further investigated *in vitro* and *in vivo* using a rat model. According to such investigations it was determined that PDLGA was the fastest copolymer to degrade whereas PLLA was the latest, being this late rate associated to the persistence of crystals formed during the implantation time.

As part of the same chapter, PLCL and PDLGA were blended in different compositions so that a complete spectrum of properties was achieved despite all the studied compositions resulted immiscible as disclosed by the prevalence of the respective T_gs in the calorimetric scan (DSC) and definitely by the two-phase structures observed by scanning electron microscope (SEM).

Secondly, concerned with processing as a necessary step in the chain of value of polymers (and materials in general) towards useful devices, the second chapter was developed where, taking advantage of the thermoplastic nature of polylactides, casting and, more intensely thermoconformation have been explored.

It has been found that solvent diffusion plays the mayor role in solvent casting processing and if poorly controlled, tensile properties are severely affected.

Instead, thermoconformation, is dependent on the rate of cooling from the melt whereby the permanent shape is fixed by solidification below the T_g, as slow rearrangements in sought of thermodynamic equilibrium cause the measurable evolution of properties such as enthalpy and yielding.

Though this phenomenon has been observed since Griffith's studies on ideal elastic solids (glasses) it still remains as an active field of research as the range of temperatures in which it takes place usually include the temperature of practical use and involve higher-order transitions so that the time temperature superposition principle is no longer applicable and extrapolations using parameters obtained from distinct properties cannot in general be made.

Thus, the contribution to this field derived from this Thesis includes the identification of ductile to brittle transition (BDT) in PLLA and the enthalpy relaxation kinetics in PDLGA and in two PLCL copolymers differing on the randomness character.

On the other hand, it has been shown that orientation induced by stretching at $T \sim T_g$ not only increases the elastic modulus (x3) but also promotes ductile fracture as chain molecules, being aligned in the stretching direction, are more conveniently disposed to yield upon application of a tensile stress in the direction of orientation.

Following, compounding with an osteosconductive filler (HA) as a way to impinge increased functionalities on polymeric devices where bones are implied, such as fixation devices, has been investigated. Further, plasma polymerization has been explored and successfully applied on HA particles starting from two different monomers.

It has been shown that the addition of particles does not overshadow the nature of the polymeric matrix as the elastomeric properties of PLCL matrix are preserved (and increased, demonstrating the enhancement of the interface adhesion) and the toughness of the glassy matrix.

As a part of this chapter, the nucleating activity of particles (neat and plasma fucntionalized) has been characterized, disclosing that neat HA is a more active heterogeneous nucleating site than plasma polymerized poly(acrylic acid) particles (HA_{AA}).

The third chapter has been devoted to understanding the thermally triggered shape memory effect of polylactides and identifying the relevant parameters both from the programming conditions and from the intrinsic material properties in order to design an ideal polymer for its application as a biodegradable stent in coronary artery disease (CAD).

The major findings of this chapter can be resumed in that whatever cause of reduction in the amount of entropy elasticity associated with the amorphous phase has a detrimental effect on the recovery of the permanent shape.

Thus, in the case of semicrystalline polymers, the reduction of the amorphous phase is associated with the development of crystallinity whereas in totally amorphous polymers, such reduction is associated to disentanglement and chain slippage between chains and relaxation of these in an unstretched state.

However, these microstructural changes have been observed to develop during the first cycles (programming-recovery), so that once they have fully developed, stable values of recovery are achieved.

Regarding the capacity to fix the temporary shape, it has been shown that narrower and sharper transitions are preferred over broader ones so that vitrification and thus fixation of the shape completes in a more limited temperature range.

Finally, to conclude this summary, it must be emphasised the international character of this Thesis a part of which has been developed under a secondment agreement between the National University of Ireland Galway (NUIG) and the University of the Basque Country (UPV-EHU).

Resumen

Los polímeros ofrecen un amplio espectro de propiedades, permitiendo ampliar las posibilidades del ser humano. Así, transcurridas unas pocas décadas desde su primer desarrollo comercial, los polímeros están tan integrados en la sociedad actual que apenas somos conscientes nuestra dependencia de ellos. Este rango de propiedades, siendo tan diferentes de aquellas propias de los materiales más tradicionales, es consecuencia de su estructura molecular que es a su vez determinada mediante el proceso de producción. Mediante la combinación de enlaces químicos intra e inter moleculares del tipo van der Waals, se consiguen distintas transiciones vítreas y cristalinas. Sin embargo, por muy interesantes que resulten las propiedades de los polímeros desde el punto de vista académico, es la utilidad lo que determina su relevancia. Tal fue el caso de los polímeros sintetizados a partir del ácido glicólico y otros α-hidroxiácidos, que fueron relegados hasta que se intuyó que precisamente su inestabilidad era de especial interés en dispositivos médicos biodegradables. Por este motivo, se desprende que el uso eficiente de los materiales, esto es, el pleno aprovechamiento de sus propiedades, requiere un abordaje multidisciplinar mediante el cual se consiga armonizar las propiedades del material con aquellas funcionalidades demandadas por la aplicación.

En este contexto, la motivación del trabajo de investigación de esta Tesis ha sido profundizar en la comprensión de la viscoelasticidad y de la memoria de forma, desde el punto de vista de un Ingeniero de Materiales, estableciendo las correlaciones pertinentes entre estructura y propiedades de sistemas biodegradables derivados de la lactida, manteniendo la perspectiva de la aplicación.

En el primer capítulo, se ha realizado la caracterización completa de varios (co)polímeros comerciales. Se ha demostrado que, comparado con la altamente regular poli(L-lactida) (PLLA), la inclusión de unidades DL-lactida u otros comonómeros como la glicolida (GA) o la ε-caprolactona (CL) durante la etapa de síntesis, reducen la capacidad de cristalización así como la transición vítrea (T_g), tal que, a temperatura ambiente, el copolímero poli(L-lactida-co- ε-caprolactona) (PLCL) muestra un marcado carácter elastomérico con elasticidad entrópica. Las mismas observaciones se dan en el copolímero poli(racDL-lactida-co-glicolida) (PDLGA) a la temperatura corporal y en el

poli(DL-lactida) a una temperatura ligeramente superior. Por tanto, en la búsqueda de un material para aplicaciones en urología como la cateterización temporal en la cirugía reconstructiva de hipospadias, se investigó su biodegradación *in vitro* e *in vivo* usando ratones como modelo animal. Gracias a esta investigación, se pudo determinar que el PDLGA era el copolímero que más rápidamente se biodegradó, siendo el más lento el PLLA debido a la persistencia de los cristales de PLLA desarrollados durante el tiempo de implantación. Como parte de este capítulo, se estudia el sistema PLCL-PDLGA, que comprende mezclas de ambos en varias composiciones obteniéndose una gama completa de propiedades a pesar de que las composiciones estudiadas resultaron inmiscibles como se demuestra por la prevalencia de las respectivas T_gs mediante calorimetría diferencial de barrido (DSC), y definitivamente a partir de las imágenes obtenidas mediante microscopía electrónica de barrido (SEM) que muestran dos fases bien diferenciadas.

En segundo lugar, debido a la importancia del procesado como operación necesaria para transformar los polímeros en dispositivos útiles y así aportar valor, se desarrolla el capítulo segundo en el que, aprovechando la naturaleza termoplástica de las polilactidas, se exploran dos métodos de conformación: la vía húmeda con evaporación de disolvente y la termoconformación.

Se determina que, en el proceso por vía húmeda, la difusión del disolvente a través del polímero es el parámetro relevante, que, de no ser estrictamente controlado, perjudica gravemente las propiedades tensiles de los filmes así conformados.

Por otra parte, el parámetro relevante en el termoconformado es la velocidad de enfriamiento desde el fundido, que si bien proporciona la forma final del objeto mediante solidificación al enfriar por debajo de la T_g, sus propiedades están en constante evolución debido a la tendencia al equilibrio termodinámico del líquido subenfriado. Esta tendencia, que se denomina envejecimiento físico, es la responsable de la evolución cuantificable de propiedades como la entalpía o la fluencia. Y, aunque este fenómeno es conocido desde el trabajo de Griffith con vidrios cerámicos (1920), sigue constituyendo un campo activo de investigación ya que el rango de temperatura en el que sucede suele coincidir con la temperatura de utilización del polímero e incluye transiciones de órdenes superiores, no pudiéndose, en general, realizar extrapolaciones a partir de parámetros determinados a partir de otras propiedades.

De esta forma, la contribución de esta Tesis en este campo incluye la identificación de la transición dúctil frágil (BDT) en el PLLA y la cinética de relajación entálpica en el PDLGA y en dos copolímeros tipo PLCL con diferente carácter aleatorio.

Por otra parte, se ha mostrado que la orientación conseguida mediante estiramiento de los polímeros a temperaturas cercanas a la T_g no sólo incrementa el módulo elástico (x3) sino que favorece la fractura dúctil, ya que las cadenas tienen una mejor disposición para fluir cuando se les aplica tensión en la dirección de la orientación.

Como parte de este capítulo dedicado a la conformación, se han preparado dos familias de materiales compuestos de matriz polimérica (una de carácter elastomérico y la segunda de carácter vítreo) mediante la adición de hidroxiapatita (HA), que es una carga inorgánica osteoconductora, con el objetivo de impartir esta propiedad a los materiales para su potencial utilidad en aplicaciones en contacto con tejido óseo. Además, con el fin de mejorar la intercara partícula-matriz, las partículas se han funcionalizado mediante una capa orgánica obtenida por polimerización por plasma.

Así, se ha demostrado que la adición de partículas no anula el carácter de la matriz y que la polimerización por plasma mejora la intercara entre partícula y matriz, alcanzándose mayores valores de elongación en el caso de la matriz elastomérica y superior tenacidad en el caso de la matriz vítrea.

Como parte de este capítulo, se ha examinado la actividad de nucleación de las partículas, encontrándose que la HA es más activa como agente de nucleación heterogénea que las partículas funcionalizadas con poli(ácido acrílico) polimerizado por plasma.

El tercer capítulo se ha dedicado a comprender el efecto de memoria de forma estimulado por temperatura en las polilactidas, identificándose los factores relevantes tanto del proceso de programación de la forma temporal como de las propiedades intrínsecas del polímero con el fin de diseñar un polímero ideal para su aplicación como stent biodegradable en el tratamiento de la enfermedad arterial coronaria (EAC).

Así, las principales conclusiones obtenidas se pueden resumir en el siguiente corolario: aquella causa que provoque una reducción de la elasticidad entrópica asociada

con la fase amorfa tiene un efecto pernicioso sobre la recuperación de la forma. De esta manera, en el caso de los polímeros semicristalinos, la reducción de la fase amorfa se debe al desarrollo de cristalinidad mientras que en los polímeros totalmente amorfos, la reducción se debe al desenmarañamiento y deslizamiento de cadenas y relajación de éstas en un estado no tensionado, que no contribuye a la elasticidad entrópica.

Por otra parte, se observa que estos cambios de la microestructura se desarrollan principalmente durante los primeros ciclos (programación-recuperación), tal que una vez desarrollados, se obtienen buenos y consistentes valores de recuperación.

Respecto a la capacidad de fijación de la forma temporal, se ha visto que se prefieren transiciones estrechas y abruptas, de manera que la fijación de la forma, debida a la vitrificación, se complete en un rango estrecho de temperatura.

Finalmente, para concluir este resumen, quepa destacar el carácter internacional de esta Tesis, que se ha completado con una estancia de larga duración (14 semanas) en el marco de una colaboración entre la Universidad Nacional de Irlanda (NUIG) y la Universidad del País Vasco (UPV-EHU).

Introduction

Introduction

The growth in the use of polymers and composites mirrored the incredible changes that occurred in the twentieth century and also contributed to these changes [1]. The newly introduced materials have not only challenged the older materials such as metals, woods, glasses and leathers for their well-established uses but have also made possible new products which have helped to extend the range of activities of mankind [2]. Without these two kinds of materials, rubbers and plastics, it is difficult to conceive how such everyday features of modern life [2] such as sports, packaging, transport or healthcare.

Beginning in 1930s, the advent of war brought plastics more into demand, largely as substitutes for materials such as natural rubber and gutta percha, which were in short supply [2]. With only a few decades separating their first commercial development from their present pervasive use, synthetic polymers are so well integrated into the fabric of society that we take little notice of our dependence on them [3]. When nylon was introduced in the late 1930s by DuPont, it soon became a favourite in the textile and clothing industry [4]. Seriously, if all the polyester and nylon fibres in use today were to be replaced by cotton and wool, their closest natural counterparts, calculations show that there would not be enough arable land left to feed the populace, and we would be overrun by sheep [5]. The fact is, there simply are no practical natural substitutes for many of the synthetic polymers used in modern society [5] so that historians are beginning to speak of a dawning “Age of Polymers” [2, 6].

This class of materials possesses many interesting and useful properties that are completely different from those of the more traditional engineering materials, and that cannot be explained or handled in design situations by the traditional approaches [5] but happen to be a consequence of their molecular structure [5], whose basis was proposed by Dr. Hermann Staudinger [7] for which he was awarded with the Nobel Prize in chemistry [5]. Figure i illustrates how the material properties and processing properties, which determine the field of applications depend on molecular structure, which is in turn determined by production [5].

The occasional misuse of plastics was damaging to the industry and plastics became surrounded with an aura of disrepute for many years which were at first

considered an “ersatz” material, a substitute of the “real thing” [2]. However, as an understanding of the advantages and limitations of the individual plastics was developed, it was appreciated that it was unfair to blame the plastics themselves [2]. Thus, the efficient use of materials requires the complete utilization of material properties, which are determined by meaningful measuring and testing procedures [6].

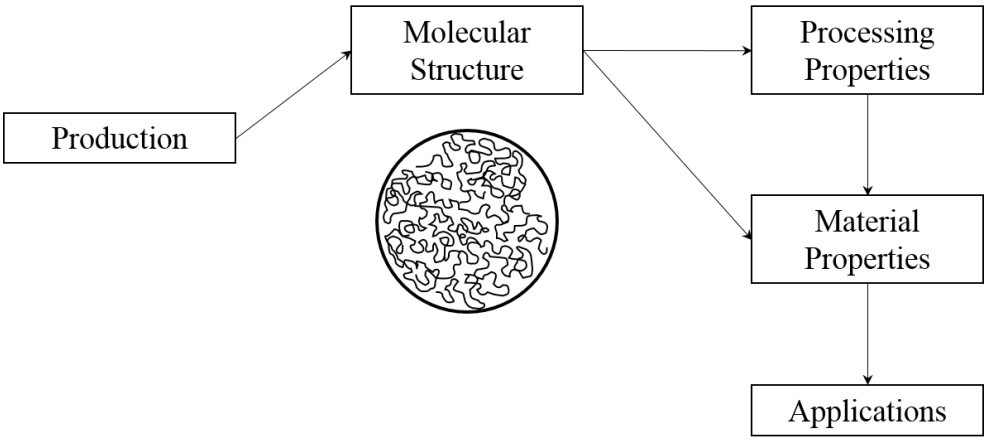

Figure i.- The key role of molecular structure in polymer science and technology [5].

Like all other technical scientific disciplines, polymer testing has a decidedly interdisciplinary character as described in figure ii [6].

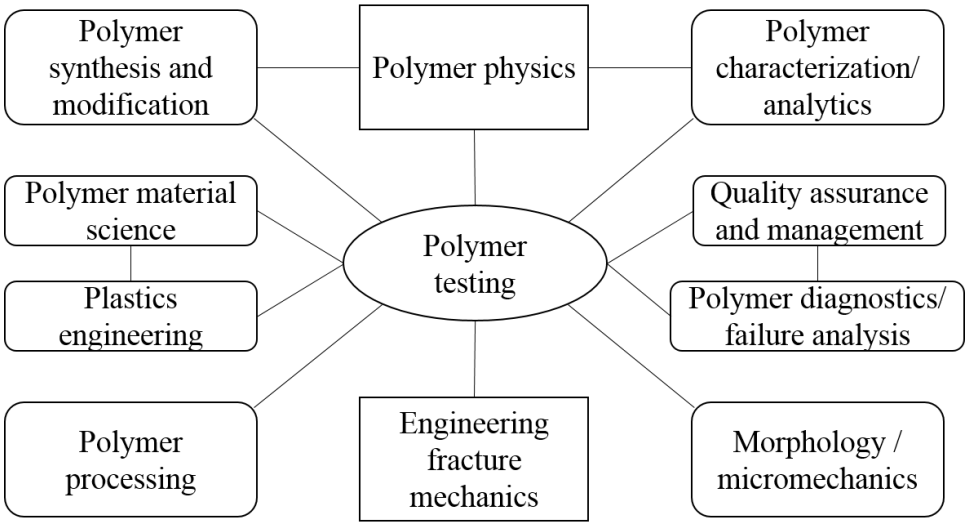

Figure ii.- The interdisciplinary character of polymer testing [6].

The awareness of how to use macromolecules as materials is based on research into methods of synthesizing both to produce new monomers and polymers as well as to introduce new catalyst systems [6]. This in turn necessitated systematic basic research to uncover the fundamental principles affecting polymer synthesis and structure, on the one hand, and microscopic structure and macroscopic properties, on the other [6].

The processing cost and performance per unit weight of polymers became so favourable that capital investments have continually expanded to meet demand [4]. The profits were invested for further research and innovation to bring forth new technologies for a wide variety of applications, resulting in a positive investment cycle [4].

The European plastics industry makes a significant contribution to the welfare in Europe by enabling innovation, creating quality of life to citizens and facilitating resource efficiency and climate protection [8]. More than 1.45 million people are working in about 60,000 companies (mainly small and medium sized companies in the converting sector) to create a turnover in excess of 320bn EUR per year [8].

Among the worldwide trends in the polymer industry is a shift in R&D focus from commodity plastics, produced in massive quantities, to engineering plastics that have superior properties but are produced in lower volumes [3]. In recent years, the emphasis has been on specialty polymers that are expensive yet have specific properties that confer high value [3].

Polymers inherently possess unique structural arrangements that allow them to combine chemical intra-bond and van der Waals inter-bond forces to form distinct melting and crystallizing transitions, which offers a special property spectrum for applications [4]. Still, many polymers would have remained of academic interest had not been found applications for them. Research in the first half of the 20^{th} century with polymers synthesized from glycolic acid and other α-hydroxy acids was abandoned for further development because the resulting polymers were too unstable for long-term industrial uses [9]. However, this very instability leading to biodegradation has proven to be immensely important in medical uses in the last three decades [9].

Beginning with biodegradable sutures first approved in the 1960s [9], fixation devices, catheters and stents have become an invaluable tool in the armamentarium of medical practitioners and surgeons in clinical situations.

Although progress to date in biomaterials can be considered revolutionary, the results of many published clinical trials demonstrate some common complications resulted from the use of resorbable implants [10] indicating that further development is needed.

Moreover, beyond funding, there is a need to nurture relationships between polymer researchers and practitioners of medical field so that once the healing process and biological function to be replaced is understood [11], tailor materials become available upon application of scientific knowledge.

Following this approach, three clinical situations have been explored where biodegradable materials are of application, focusing on the key functionality that makes a biomaterial suitable for such use.

Hypospadias repair

The first addressed clinical situation has been hypospadias repair.

Hypospadias is one of the most frequently encountered congenital malformations of the genitourinary system with an incidence of 1 to 8 per 1000 male births [12]. The current goals of this challenging reconstructive surgery [13] are creating a straight penis, positioning of the meatus on the penile tip, normalization of erections and voiding, creating a urethra of uniform and adequate calibre, and symmetry in appearance of the glans and shaft [12].

The human urethra consists of anisotropic, visco-elastic tissue with a strain dependent Young's modulus (5±2kPa for 15% uniaxial strain, 11±3kPa for 35% and 21±4kPa for 45%) [14], with an inner diameter of about 5 mm and an outer one of about 12 mm [15]. From an engineering point of view, the urethra functions as a valve constituting a mechanical barrier to urine leakage during bladder filling and a conduit for its release during micturition [16, 17]. The smooth muscle provides an intrinsic,

involuntary sphincter mechanism and the striated muscle, which extends distally from the proximal urethra, is known as the external urethral sphincter and is involved in the voluntary control of continence [18]. The smooth and striated muscle components of the urethra function as a sphincter to produce active urethral closure pressure, and the extracellular matrix (ECM), composed of collagen and elastin, plays a passive role, keeping the urethra from overdistending during increases in bladder pressure and voiding and helping it return to a closed state [18].

Experimental studies involving pharmacological neuromuscular blockage demonstrate the fundamental importance of the urethral musculature in maintaining continence, both at rest and during strenuous activities [17]. Changes in the mechanical properties of the urethra may lead to obstruction and/or incontinence [19].

Construction of the neourethra is performed by using a flap of penile skin, bladder mucosa or buccal mucosa [12] or tunica vaginalis [13]. A careful preoperative evaluation, precise surgical technique, and appropriate postoperative care are required to achieve the desired objectives of hypospadias repair [12].

Even in the hands of the most experienced surgeons hypospadias repair is associated with a number of complications including urethrocutaneous fistula, stricture, diverticula, and persistent chordee [12]. Although the exact etiology of fistulas cannot be defined, two avoidable factors usually underscore the problem: infection and tissue ischemia [12].

Temporary tubularization of the neouretra acts as an effective conduit for the urine during voiding and decreases the accumulation of secretions given off by the traumatized urethra, which may be predisposed to infection [12]. Currently, urinary diversion is performed by means of silicone tubing. However, silicone presents two main disadvantages that menace the effectiveness of hypospadias repair.

Firstly, silicone is non-biodegradable, thus, a secondary procedure is required to remove the temporary conduit, adding extra cost and morbidity to the patient [20] and increasing the risk of an infection derived from a premature withdrawal of the conduit [12].

Secondly, silicone is considerably stiffer than the male urethra [21], which may cause mechanical damage, leading in turn, to urethral dysfunction [18].

The biomechanical properties of the urethra, i.e., elasticity/stiffness, are a function of the amount of passive connective tissue and active muscle elements and their distribution within the tissue layers [16, 17, 22]. Those properties are strictly related to the histological and biochemical composition of the urethra and to its physiological function [22]. Increase in collagen content (i.e., fibrosis, scar tissue) after hypospadias repair may lead to changes in biomechanical properties (increase in stiffness) [22]. When persistent with time, i.e., urethral stenosis, these changes lead to long-term poor functional results and to technical surgical failure [22].

Trauma and injuries of orthopaedic tissues

Trauma and regeneration of orthopaedic tissues are commonly associated with injuries to soft tissues such as ligaments and tendons, or to fractures of bones [23].

Among the most common trauma afflicting the young and physically active population are tendon and ligament injuries [23].

Headed by the anterior cruciate ligament (ACL) reconstruction with over 100,000 interventions performed annually in the United States, rotator cuff tendon repair accounts for more than 75,000 interventions, many of which are accompanied by injuries to the surrounding ligaments and other tissues [24, 25]. In Spain, in 2013, there were 341,831 hospital discharges after osseous-articular system and connective tissue diseases from which, 48,912 were attributable to knee internal disruption [26].

Bone is the most commonly replaced organ with over 800,000 grafting procedures performed in annually in the United States alone [23]. In Spain in 2013, the rate of hospital morbidity due to bone fractures alone was 424 for each 100,000 inhabitants [26].

Tendons and ligaments are fibrous tissues that connect muscle to bone and bone to bone respectively [23]. Their physiological functions include the stabilization and guidance of joint motion, transmission of physiological loads, and the maintenance of the anatomical alignment of the skeleton [27, 28].

The primary constituent of tendons and ligaments is collagen [11] whose parallel arrangement to the direction of applied loads [29], results in one of the strongest tissues in the body [23]. For example, Young's modulus of the human patellar tendon and anterior cruciate ligament (ACL) is approximately 650 and 350MPa, respectively [23, 29]. However, it does not have a strong regeneration capacity [25, 27], with an average turnover half-life of 300 to 500 days [11].

ACL is reconstructed using a biological graft [25], however, the superior graft choice, fixation method, and surgical technique continue to be debated [30]. Generally, despite donor site morbidity [25], autograft tissue is preferred over allograft tissue [30], in order to avoid possible disease transmission and delayed incorporation of allograft tissue as compared with autograft [27, 30, 31].

Due to the significant time- and history-dependent viscoelastic properties of ligaments [11, 28, 32], grafts are commonly prepared on a graft board and are preconditioned in tension prior to implantation [32]. During reconstruction, the grafts are typically fixed on the femoral side and cyclically loaded, followed by application of the initial graft tension and tibial fixation [32].

However, this precautions are not sufficient to eliminate a decrease in graft tension due to postoperative stress relaxation [32]. The long-term improved laxity depends on the healing of the graft within the host bone tunnel [25, 27, 33], which is usually secondary to a pulling out of the graft from the bone tunnel before osteointegration occurs [25, 27, 31, 34].

Bone is a composite material consisting of both fluid and solid phases [11] arranged in a hierarchical and complex structure at many length scales as illustrated in figure iii, making the material of bone heterogeneous and anisotropic [35]. The reported Young's moduli for cortical bone tissue have been shown consistently to be about 20-22GPa along the axis of long bone and about 12-14GPa transversely [36], while the reported Young's moduli for trabecular bone tissue range from 1 to over 20GPa [36].

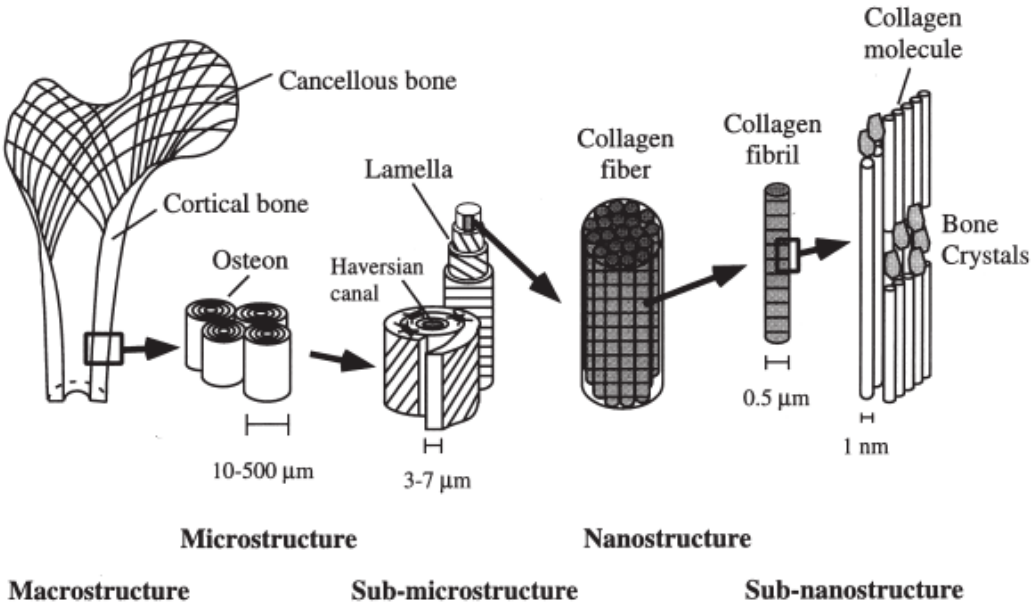

Figure iii.- Hierarchical structural organization of bone: (a) cortical and cancellous bone; (b) osteons with Harvesian systems; (c) lamellae; (d) collagen fibre assemblies of collagen fibrils; (e) bone mineral crystals, collagen molecules, and non-collagenous proteins [35].

Two main solid phases, one organic and another inorganic, give bones their hard structure [11]. An organic extracellular collagenous matrix is impregnated with inorganic materials, especially hydroxyapatite ($Ca_{10}(PO_4)_6(OH)_2$) (consisting of the minerals calcium and phosphate) [11]. Unlike collagen, apatite crystals are very stiff and strong [11]. However, a bone's strength is higher than that of either apatite or collagen because, the organic material gives bone its flexibility, while the inorganic material gives bone its resilience [11].

Bone is populated largely by three cell types: osteoblasts, osteocytes, and osteoclasts [23], which, being sensitive to their mechanical environment, are responsible for synthesis and maintenance of the extracellular matrix components, and degradation of the matrix during tissue remodelling [29].

Mechanical stimulus or stress in the skeleton is probably the major factor in the maintenance of the normal balance between the dynamic process of bone formation and resorption [37]. When physiological stress is diminished, osteoporosis rapidly develops [37].

Protection from stress occurs if two components with different moduli of elasticity form one mechanical system [37]. When a load is imposed on such a system the component with the higher modulus bears more of the load and so protects the other component [37]. This situation is present when a rigid metal plate is fixed to a long bone [37]. Some investigators have demonstrated that in the fixation of fractures long bones by rigid plates this mechanism leads to osteoporosis, leading to fatigue fracture after removal of the plate [37]. Table i resumes some mechanical data of metals in comparison with those of cortical bone [37].

Table i.- Some mechanical data of metals used for implants of cortical bone [37].

	Modulus of elasticity GPa	**Ultimate tensile strength = UTS MPa**	**Fatigue limit as percentage of UTS %**
316 Stainless steel	200	960	45
Titanium (T130)	110	400	50
Cortical bone	6-20	80-150	25-40

Given the complex nanoscale organization of bone, the ideal device must be biomimetic with nanoscale organization, able to support bone growth (osteoconductive), induce bone formation (osteoinductive), and structurally integrate the host bone tissue (osteointegrative) [23].

To achieve the goal of improved osteointegration, conventional hydroxyapatite (HA) is well known for its biocompatibility and is widely available commercially with a Ca/P ratio of 1.67 [27]. In contact with bone, it can promote tendon osteointegration through increasing new bone formation in a tendon-to-bone healing [34]. The mechanism is associated with CaP which is easily resorbed by osteoclasts, and subsequently after the resorption of CaP new bone tissue is formed on the tendon surface by osteoblasts [34]. It has been successfully applied to treat bone defects or articular cartilage defects and to induce bone ingrowth into and/or onto the soft tissue or metal implants in large experimental animals [34].

Thus, in the second chapter, devoted to conformation of polymers with enhanced properties and increased functionalities, two biodegradable polymers have been compounded with hydroxyapatite (HA), a calcium phosphate ($Ca_{10}(PO_4)_6(OH)_2$), similar to the inorganic content of bone [29, 38, 39] for their potential application in orthopaedics.

Following, in the third chapter, factors affecting the shape memory of polymers for its importance in minimally invasive surgery and stenting of blood vessels have been unravelled.

Coronary artery disease

Coronary artery disease (CAD) affects over 15 million people in the United States and it is the leading cause of death for men and women [40].

CAD affects the arteries that supply blood to the heart [40]. It occurs when the passageway through the coronary arteries, or heart arteries, becomes narrowed by a build-up of plaque, including cholesterol, fatty deposits, calcium, and other substances [40].

In severe cases, where a combination of lifestyle changes and medical treatment [40] is not effective, percutaneous transluminal coronary angioplasty (PTCA) is performed [41]. During this procedure the heart doctor threads a small tube (known as a catheter) through the groin or arm which then passes through an artery to the site of the blockage [40]. A small balloon located on the tip of the catheter is then slowly inflated to open the blockage [40].

This procedure can be performed with a balloon catheter alone, or can involve the placement of a coronary stent which expands to fit the size of the artery and helps keep blood flowing freely [40]. Over time, the artery wall heals around the stent [40].

Since Sigwart et al. [42] reported the first implantation of a self-expandable, stainless steel stent in human coronary arteries, various intracoronary stents have been tested in an attempt to prevent occlusion and restenosis after angioplasty [41].

Most of these stents are made of metals with a variety of designs which differ significantly in their geometry, composition and implant methods [41]. However, early

and late complications such as thrombotic closure and restenosis have been reported with metallic stent devices [41]. In addition, as a metal stent remains in the body indefinitely, it may interfere with future clinical procedures [41]. Moreover, the stent becomes a permanent foreign body with potentially important interactions due to the type of metal, electrostatic charges and possible physical irritation from individual filaments leading to long-term effects [41]. The mismatch in mechanical behaviour between the stent and vessel wall can result in excessive intimal proliferation and a high risk of thrombosis [41]. Continuous barotrauma and localized areas of necrosis may be induced by the long-term expandable forces generated by the stent attempting to return it to its unconstrained size [41]. Individual allergy is also a concern to those who are hypersensitive to the metals that make up the device [41]. Permanent implantation could also generate problems due to mechanical stability and corrosion, eventually resulting in the perforation of the vessel wall [41].

The problems with metallic stents have encouraged significant efforts to develop new stents to produce a non-thrombogenic stent site and obviate the problems of restenosis and neointimal hyperplasia [41]. Thus, biodegradable polymer stents are being investigated to prevent thrombosis and restenosis [41].

Biodegradable polymer stents have the potential to remain in situ for a predicted period of time keeping the vessel wall patent and then degrading to non-toxic substances [41]. Therefore, after completion of their functions and resorption of the stents, the vessel wall can preserve its normal function and surgical procedures to remove the stent are avoided [41]. The degradation rate of the stent can be controlled by the degree of polymerization and processing methods [41]. The release profiles of drugs from a biodegradable stent can also be adjusted by the degradation behaviour [41].

Agrawal and co-workers [43] reported a bioabsorbable intravascular stent made of poly(L-lactic acid) (PLLA) [43]. The collapse pressure of the braided PLLA stents surpassed the target pressure of 300 mmHg by a wide margin [43], thus, based on its mechanical properties and in vivo assessment, it was concluded that PLLA is a very strong candidate for use as a material for bioabsorbable polymeric stents [41].

However, reported tissue reactions to PLLA and longer than expected biodegradation rates linked to crystallinity, fostered the research on microstructure changes behind the shape memory functionality and alternative polymers whose shape memory triggering temperatures were closer to body temperature.

Finally, this first introductory chapter would not be concluded without a brief allusion to regulation upon medical devices.

Regulatory commitments

In Europe, medical devices should, as a general rule, bear the CE mark to indicate their conformity with the provisions of the corresponding Directive to enable them to move freely within the Community and to be put into service in accordance with their intended purpose [44, 45].

Thus the CE mark indicates that the device meets the essential requirements which apply to it, taking account of the intended purpose of the device [45].

The procedure to assess the conformity of the medical device with regulation depends on the class of the device. Accordingly, there are four product classes and the classification rules are based on the vulnerability of the human body taking account of the potential risks associated with the technical design and manufacture of the devices [45].

The above mentioned classifications as well as assessment procedures are resumed in figure iv [46]. Class I devices include low level of vulnerability associated with these products, therefore, the conformity assessment procedures for Class I devices can be carried out, as a general rule, under the sole responsibility of the manufacturers [45]. For Class IIa devices, the intervention of a notified body should be compulsory at the production stage; whereas, for devices falling within Classes IIb and III which constitute a high risk potential, inspection by a notified body is required with regard to the design and manufacture of the devices; whereas Class III is set aside for the most critical devices for which explicit prior authorization with regard to conformity is required for them to be placed on the market [45].

According to the classification criteria, most of implantable devices fall into Class III classification as they are inserted in the body in the context of a surgical operation, and have a biological effect or are to be wholly or mainly absorbed in the body [45]. Essential requirements include general requirements, such as safety for patients and users, and specific requirements regarding design and construction, where chemical, physical and biological properties as well as infection and microbial contamination are specifically addressed [45].

More specifically, the technical file of the medical device must contain every detail of the design and manufacturing including product specifications such as testing data and reports, functionality studies, wet lab or bench top testing, materials certificates and/or reports on stability, biological tests, cleanroom-surveillance, certificates, risk management- documentation [47], clinical data [48], product validation, (sterilization, manufacturing, production) [49].

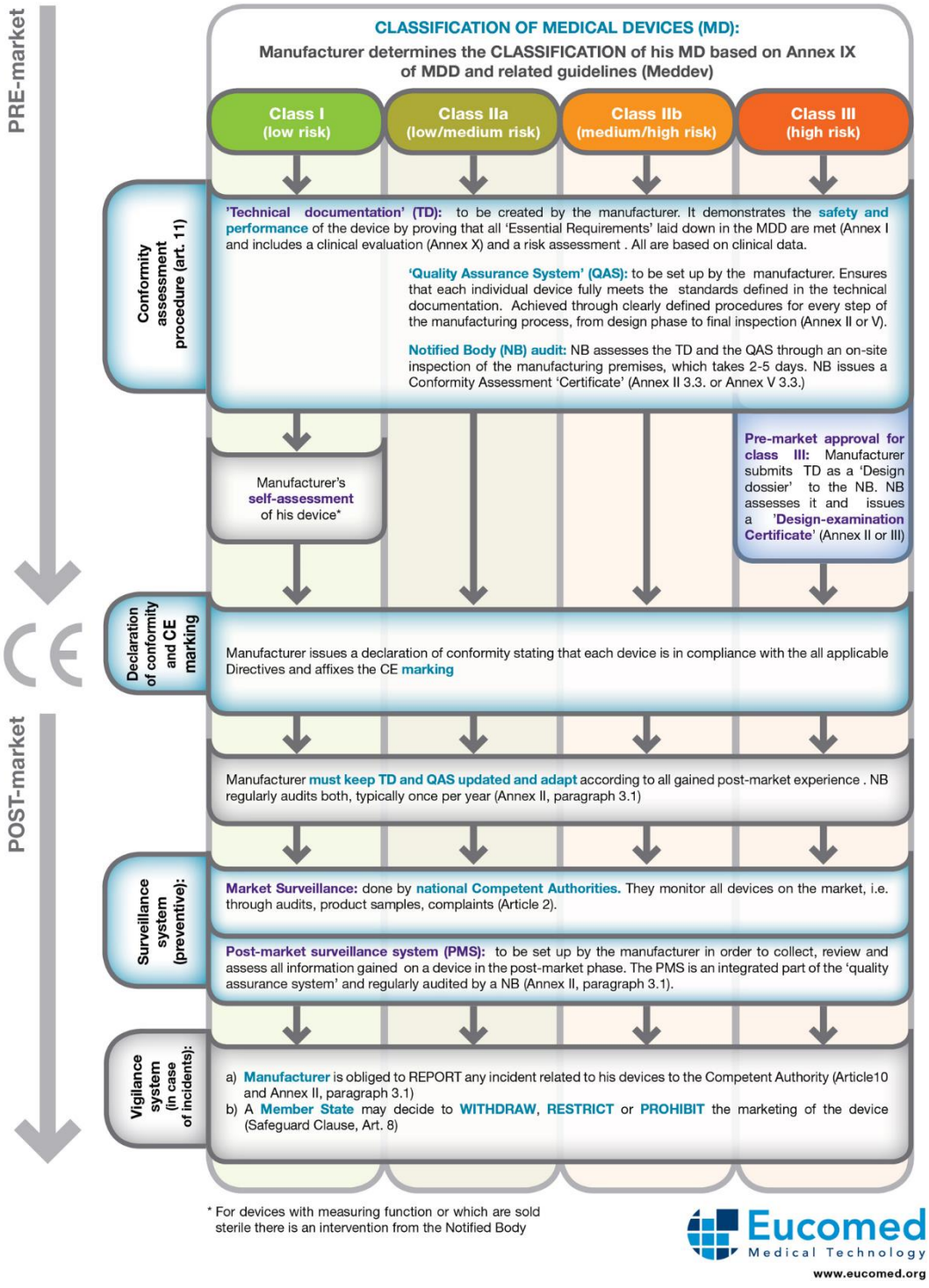

Figure iv.- EU regulatory framework for medical devices [46]

The estimated time to achieve CE marking in Class III products is estimated in at least 3-4 years, for the lowest technology readiness level (TRL) according to the Spanish authorities as long as conformity is fully supported [50]. Thus, considering the difficulty

in transferring a new material into a fully medical device, it can be understood that the current commercially available biodegradable devices are based on a limited number of approved biocompatible polymers [21, 31, 39, 41, 43, 51-64] and combinations thereof [61, 65-71] while understanding of their shortcomings [10, 15, 20, 21, 27, 31, 33, 34, 41, 52, 53, 55, 57, 59, 61, 63, 67, 72-77] encourages the multidisciplinary research [9, 11, 14, 16-19, 22, 28, 36, 75, 78, 79] in sought of the "next generation" of polymers with enhanced and increased functionalities [62, 80, 81].

References

[1] Gerdeen, J. C., Lord, H. W., Rorrer, R. A. L., Engineering design with polymer and composites, CRC Taylor & Francis group, Florida, 2006, pp. 1-2.

[2] Brydson, J., Plastics materials, Butterworth-Heinemann, Oxford, 1999, pp. 1-18

[3] Committee on Polymer Science and Engineering, National Research Council, Polymer Science and engineering: the shifting research frontiers, The national academies press, Washington, 1994, pp. 2-34.

[4] Lee, S. T., History and trends of polymeric foams: from process/product to performance/regulation in Polymeric foams CRC Taylor & Francis group, Florida, 2009, pp. 1-2

[5] Rosen, S. L., Fundamental principles of polymeric materials, John Wiley & sons, New York, 1993, pp. 1-4.

[6] Grellmann, W., Seidler, S., Polymer testing, Carl Hanser Verlag, Munich, 2007, pp. 1-4.

[7] Staudinger, H., Transactions of the Faraday society, 1933, 29, 18-32

[8] http://www.plasticseurope.org/plastics-industry.aspx

[9] Middleton, J. C., Tipton, A. J., Biomaterials, 2000, 21, 2335-2346

[10] Ambrose, C., Clanton, T. O., Annals of Biomedical Engineering, 2004, 32, 171-177

[11] Pal, S., Mechanical properties of biological materials in Design of artificial human joints and organs, Springer science and business media New York, 2014, pp. 20-40

[12] Retik, A. B., Atala, A., Urologic clinics of North America 2002, 29, 329-339

[13] Rosito, T., Pires, J., Garrone, G., Liguori, R., Otoni, S., Ortiz, V., Koff, W., Macedo Jr. A., Journal of Paediatric Urology, 2008, 4 (S1), S59

[14] Müller, B., Ratia Garcia, J., Marti, F., Leippold, T., Journal of Biomechanics, 2008, 41 (S1), S61

[15] Marti, F., Leippold, T., John, H., Blunschi, N., Müller, B., Physics in medicine and biology, 2006, 51, 1361-1375

[16] Jankowski, R. J., Prantil, R. L., Fraser, M. O., Chancellor, M. B., de Groat, W. C., Huard, J., Vorp, D. A., American Journal of Physiology - Renal Physiology, 2004, 286, F225-F232

[17] Jankowski, R. J., Prantil, R. L., Chancellor, M. B., de Groat, W. C, Huard, J., Vorp, D. A., American Journal of Physiology - Renal Physiology, 2006, 290, F1127-F1134

[18] Prantil, R. L., Jankowski, R. J., Kaiho, Y., de Groat, W. C., Chancellor, M. B., Yoshimura, N., Vorp, D. A., American Journal of Physiology - Renal Physiology, 2007, 292, F1229-F1237

[19] Thind, P., Lose, G., Colstrup, H., Urological research, 1991, 19, 241-244

[20] Lange, D., Chew, B. H., Therapeutic Advances in Urology, 2009, 1, 143-148

[21] Idzenga, T., Pel, J. J., M., van Mastrigt, R., Neurourology and Urodynamics 2006, 25, 451-460

[22] Lalla, M., Riis, C., Jørgensen, C. S., Danielsen, C. C., Jørgensen, T. M., Journal of Paediatric Urology 2011, 7, 404-411

[23] Subramony, S. D., Erisken, C., Chuang, P. J., Lu, H. H., Nanofiber-Based integrative repair of orthopaedic soft tissues in Nanotechnology in tissue engineering and regenerative medicine, CRC Taylor & Francis group, Florida, 2011, pp. 2-1-2-12

[24] Bach, Br, Arthroscopy: The Journal of Arthroscopic and Related Surgery, 2000, 16, E10, 1-6

[25] Kuang, G. M., Yau, W. P., Lu, W. W., Chiu, K. Y., Knee Surgery, Sports Traumatology, Arthroscopy, 2010, 18, 1038–1051

[26] http://www.ine.es/jaxi/tabla.do

[27] Shi, P., Teh, T. K. H., Toh, S. L., Goh, J. C. H., Biomaterials, 2013, 34, 5947-5957

[28] Weiss, J. A, Gardiner, J., C., Bonifasi-Lista, C., Journal of Biomechanics, 2002, 35, 943–950

[29] Lee, J. M., Tissue Mechanics. Wiley Encyclopaedia of Biomedical Engineering, 2006, pp. 1-16

[30] Wasserstein, D., Sheth, U., Cabrera, A., Spindler, K. P., Sports health, a multidisciplinary approach, 2015, 7, 207-215

[31] Yang, J., Jiang, J., Li, Y., Li, H., Jing, Y., Wu, P., Yu, D., Chen, S., International Orthopaedics (SICOT), 2013, 37, 515–521

[32] Ciccone, W., Bratton, D. R., Weinstein, D. M., Elias, J. J., The journal of bone and joint surgery, 2006 88-A, 1071-1078

[33] Cho, S., Li, H., Chen, C., Jiang, J., Tao, H., Chen, S., International Orthopaedics, (SICOT), 2013, 37, 507–513

[34] Li, H., Ge, Y., Wu, Y., Jiang, J., Gao, K., Zhang, P., Wu, L., Chen, S., International Orthopaedics, (SICOT), 2011, 35, 1561–1567

[35] Rho, J. Y., Kuhn-Spearing, L., Zioupos, P., Medical engineering and physics 1998, 20, 92-102

[36] Turner, C. H., Rho, J., Takano, Y., Tsui, T. Y., Pharr, G. M., Journal of biomechanics, 1999, 32, 437-444

[37] Tonino, A. J., Davidson, C. L., Klopper, P. J., Linclau, L. A., The journal of bone and joint surgery, 1976, 58-B, 107-113

[38] Thompson, I. D., Hench, L. L., Proceedings of the Institution of Mechanical Engineers, Part H: Journal of Engineering in Medicine, 1998, 212, 127-136

[39] Bleach, N. C., Nazhat, S. N., Tanner, K. E., Kellomäki, M., Törmälä, P., Biomaterials, 2002, 23, 1579-1585

[40] http://www.bostonscientific.com/

[41] Peng, T., Gibula, P., Yao, K., Goosen, M. F. A., Biomaterials, 1996, 17, 685-694

[42] Sigwart, U., Prel. J., Mirkoritch, V., Joffre, F., Kappenberger, L., New England journal of medicine, 1987; 318, 701-706.

[43] Agrawal, C. M., Haas, K. F., Leopold, D. A., Clark, H. G., Biomaterials, 1992, 13, 176-182

[44]http://ec.europa.eu/growth/sectors/medical-devices/regulatory-framework/legislation/index_en.htm

[45] Council Directive 93/42/EEC of 14 June 1993 concerning medical devices.

[46] Eucomed's response to the Commission's proposal for the revision of the EU Medical Devices Directives, 2013

[47] EN ISO 14971 Medical devices. Application of risk management to medical devices.

[48] EN 14155-1/-2 Clinical investigation of medical devices for human subjects.

[49] Recommendation NB-MED/2.5.1/Rec5

[50] Arce, A., Lanuza, A., from Federación de empresas de tecnología sanitaria (FENIN), personal communication (2013).

[51] Melchels, F. P. W., Feijen, J., Grijpma, D. W., Biomaterials, 2009, 30, 3801-3809

[52] Liatsikos, E. N., Karnabatidis, D., Kagadis, G. C., Katsakiori, P. F., Stolzenburg, J. U., Nikiforidis, G. C., Perimenis, P., Siablis, D., European association of urology and European board of urology, 2007, 5, 77-88

[53] Isotalo, T., Halasz, A., Talja, M., Tammela T.L., Paasimaa, S., Törmälä P., Journal of Endourology. 1999, 13, 525-530

[54] Kemppainen, E., Talja M., Riihelä, M., Pohjonen, T., Törmälä, P., Alfthan, O., Urological research, 1993, 21, 235-8

[55] Isotalo, T.M., Nuutine, J. P., Vaajanen, A., Martikainen P. M., Laurila, M., Törmälä, P., Talja, M., Tammela, T.L., British journal of urology international, 2006, 97, 856-859

[56] Isotalo, T., Tammela T.L., Talja, M., Valimaa, T., Törmälä, P., The Journal of Urology, 1998, 160, 2033-2036

[57] Isotalo, T., Talja, M., Välimaa, T., Törmälä, P., Tammela, T.L., Journal of endourology, 2002, 16, 759-762

[58] Stack, R. S., Califf, R. M., Phillips, H.R., Pryor, D. B., Quigley, P.J., Bauman, R.P., Tcheng J. E., Greenfield J.C. Jr. The American journal of cardiology, 1988, 62 (10 Pt 2), 3F-24F

[59] Giessen, W. V., Lincoff, A., Schwartz, R., Beusekom, H.V., Serruys, P., Holmes, D., Ellis, S. G., Topol, E. J., Circulation, 1996, 94, 1690-1697

[60] Tamai, H., Gaki, K., Kyo, E., Kosuga, K., Kawashima, A., Matsui, S., Komori, H., Tsuji, T., Motohara, S., Uehata, H., Circulation, 2000, 102, 399-404

[61] Ormiston, J. A., Webster, M. W. I., Armstrong, G., Catheterization and cardiovascular interventions, 2007, 69, 128-131

[62] Ormiston, J. A., Serruys, P. W. S., Circulation cardiovascular interventions, 2009, 2, 255-260

[63] Bergsma, J. E., de Bruijn, W. C., Rozema, F. R., Bos, R. R. M., Boering, G., Biomaterials, 1995, 16, 25-31

[64] Talja, M., Tammela, T., Pétas, A., Valimaa, T., Taari, K., Viherkoski, E., Törmälä, P., The journal of urology, 1995, 154, 2089-2092

[65] Isotalo, T., Alarakkola, E., Talja, M., Tammela, T. L., Välimaa, T., Törmälä, P., the journal of urology, 1999, 162, 1764-1767

[66] Eury, R. P., EP0604022A1. Multilayered biodegradable stent and method for its manufacture, date of priority: 22-12-1992

[67] Mani, G., Feldman, M. D., Patel, D., Agrawal, C. M., Biomaterials, 2007, 28, 1689-1710

[68] Venkatraman, S., Tan, L., Joso, J., Boey, Y., Wang, X., Biomaterials, 2006, 27 1573-1578

[69] Ormiston, J. A., Serruys, P. W., Regar, E., Dudek, D., Thuesen, L., Webster, M. W. I., Onuma, Y., Garcia-Garcia, H. M., McGreevy, R., Veldhof, S., Lancet, 2008, 371, 899-907

[70] Tams, J., Joziasse, C. A. P., Bos, R. R. M., Rozema, F. R., Grijpma, D. W., Pennings, A. J., Biomaterials, 1995, 16, 1409-1415

[71] den Dunnen, W. F. A., van der Lei, B., Schakenraad, J. M., Blaaw, E., Bartels, H., Pennings, A. J., Robinson, P. H., Microsurgery, 1996, 17, 348-357

[72] Sandfeldt, L., Reducing the Morbidity of transurethral resection of the prostate based on patient selection, fluid absorption, and blood loss. Doctoral Thesis, Karolinska university press, Stockholm, Sweden, 2001.

[73] Azuma H., Chancellor M.B., Reviews in Urology, 2004, 6, 98-99

[74] Lincoff, A., Furst, J., Ellis, S., Tuch. R., Topol, E., Journal of the American college of cardiology, 1997, 29, 808-816

[75] Bobel, A., Petisco, S., Sarasua, J. R., Wang, W., McHugh, P. E., Computational bench testing to evaluate the short-term mechanical performance of a polymeric stent, Cardiovascular engineering and technology, 2015, 10.1007/s13239-015-0235-9

[76] Grogan, J. A., Leen, P.E. McHugh, P. E., Journal of the mechanical behaviour of biomedical materials, 2012, 12, 129-138

[77] Pétas, A., Tajla, M., Tammela, T. L. J., Taari, K., Välimaa, T., Törmälä, P., British journal of urology, 1997, 80, 439-449

[78] Streng, T., Santti, R., Talo, A., Neurology and urodynamics, 2002, 21, 136-141

[79] Laaksovirta, S., Talja, M., Välimaa, T., Isotalo, T., Törmälä, P., Tammela, T. L., The journal of urology, 2001, 166, 919-922

[80] Grube, E., Sonoda, S., Ikeno, F., Honda, Y., Kar, S., Chan, C., Gerckens, U., Lansky, A. J., Fitzgerald, P. J., Circulation, 2004, 109, 2168-2171

[81] Serruys, P. W., Ormiston, J. A., Onuma, Y., Regar, E., Gonzalo, N., Garcia-Garcia, H. M., Nieman, K., Bruining, N., Dorange, C., Miquel-Hébert, K., Veldhof, S., Webster, M., Thuesen, L., Dudek, D., Lancet, 2009, 373, 897-910

Chapter 1. A search of a polylactide system for urological application: mechanical properties and biodegradation behaviour

Introduction

Polylactides

Polymers based on lactic acid (PLA) are a most promising category of polymers made from renewable resources [1]. The lactic acid monomer is produced metabolically in two forms: L-lactic acid (with an S-stereocenter at the α-carbon) and D-lactic acid (R-stereocenter). PLA of high molecular weight is most commonly made by ring-opening polymerization (ROP) of the ring-formed dimer, dilactide (lactide: 3,6-dimethyl-1,4-dioxane-2,5-dione) which is made by depolymerisation of the polycondensed lactic acid (LA; 2-hydroxypropanoic acid) [1].

Unmodified PLA is comprised of macromolecules having a molecular architecture determined by its stereochemical composition (L-and D- lactic acid) [2]. Both *meso*- and DLA induce irregularity in the otherwise very regular poly(L-lactic acid) (PLLA) molecular architecture. Molecular imperfections are responsible for the decrease in both the rate and the extent of PLLA crystallization [2].

However, PLLA has certain shortcomings that limit its applications. Therefore, different approaches have been investigated to tailor the thermo-mechanical properties of the final material, amongst which have to be mentioned copolymerization [3, 4] (random, block and graft), change in molecular architecture (hyperbranched polymers, star shaped, or dendrimers), functionalization or blending with other polymers [5].

Typical comonomers that have been used for lactic acid or lactide copolymerization are glycolic acid or glycolide (GA) and ε-caprolactone (CL) [5]. The monomer distribution (random or block) in the copolymer depends on the monomer pairs, the nature of the catalysts, and the polymerization conditions [5].

Physical properties such as crystallinity, glass transition temperature (T_g), melting temperature (T_m), hydrophobicity and mechanical properties can be significantly affected by such modifications [5].

Thermal properties

In compatible and not too strongly polar systems, the glass transition temperature of the copolymer can be derived from assumption of:

$1/T_g=w_1/T_g(1)+w_2/T_g(2)$ (equation 1)

Where w_1 and w_2 refer to the weight fraction of the two comonomers, whereas $T_g(1)$ and $T_g(2)$ represent the glass temperatures of the two corresponding homopolymers [6]. Conversely, deviations from the linear behaviour would be featured by convex upwards or downwards in a glass transition-composition representation [7].

When cooled from elevated temperatures, liquids that are crystallisable can behave in two qualitatively different ways, depending on whether or not crystallization actually takes place [8] as explained below with the aid of figure 1.1.

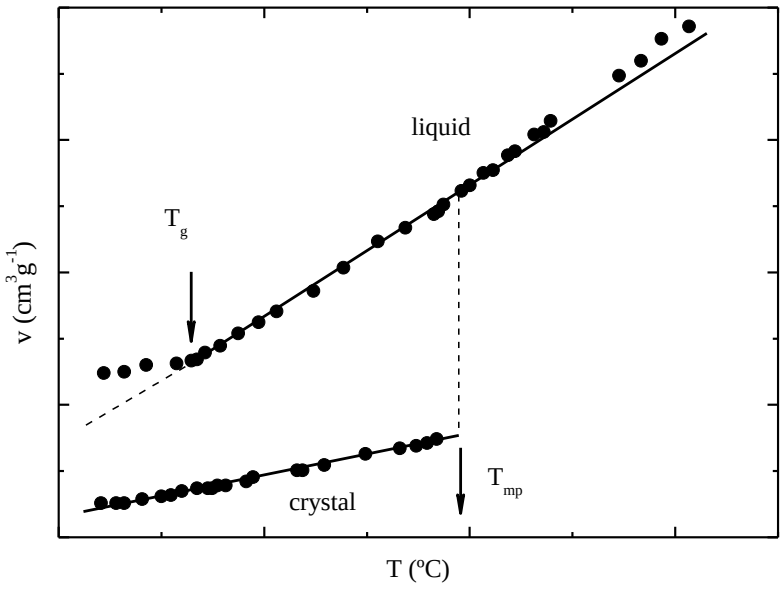

Figure 1.1.- Specific volume vs temperature from [8]

Crystallinity is the regular ordering of atoms and molecules in unit cells and in a three-dimensional lattice [9]. Conversely, glasses are defined structurally as liquids due to the lack of long-range order [8].

Although crystallization is favoured in linear polymer chains, polymers do not achieve 100% crystallinity as the ability of the chains to diffuse from the melt regions to regions around the nuclei decreases due to the rapid increase in viscosity as the melt undergoes cooling [9]. On the other hand, if the melt is cooled and crystallization does not take place, or is prevented, then at a temperature T_{mp} there is a transition from a supercooled melt to a rigid glass [10]. Below the glass transition temperature (T_g) the rate of supercooled liquid contraction slows and the volume runs essentially parallel to but above the crystalline line [8]. The change in liquid contraction rate, or decrease in thermal expansion coefficient, marks the location of the glass temperature T_g [8].

The physical properties of the melt, such as the specific heat capacity and thermal expansion coefficient change in a specific manner in the vicinity of the glass transition and, in principle, any of these can be followed to investigate the glass transition [10].

Differential scanning calorimetry (DSC) is the most popular thermal analysis technique [11]. The basic principle of DSC is that, when the sample undergoes a physical transformation such as crystallization, melting or phase transition, more or less heat will need to flow to the sample than to the reference to maintain both at the same temperature [11]. Thus, an exothermic or endothermic heat, depending on the thermal properties of the sample, is measured as a function of temperature or time [11]. Amorphous thermoplastics are characterized by the presence of only the glass transition temperature but do not exhibit any melting temperature [9].

Mechanical properties

Tensile test is regarded as the fundamental test in mechanical material testing among static and quasi-static testing and measuring methods [12]. The conventional tensile test runs at a constant crosshead speed loading the specimen slowly and steadily until fracture occurs [12]. The total deformation of mechanically loaded polymers has several regions, whereby the absolute amount of such components depends on effective loading time and acting temperature [12].

The elastic region prevails as long as there is a bijective relationship between its stress and deformation states, i. e., entirely reversible in the mechanical as well as

thermodynamic sense [12]. With respect to different thermodynamic causes, we distinguish between energy elasticity and entropy elasticity [12]. The structural cause of energy-elastic behaviour is a change in atomic distance and valence angle in the macromolecule while simultaneously storing elastic potential energy, is typically very small [12]. In such materials, this region corresponds to a reversible strain of <0.1% and given a linear relation between stress and strain, is completely described by Hooke's law [12]. The proportionality constant between stress and strain is called the elastic modulus E [12]. Instead, entropy elasticity refers to the tendency of macromolecules to return to their entropically most advantageous, i. e., coiled, state subsequent to deformation [12]. Entropy-elastic behaviour up to strains of several hundred percent can be observed, whereby the relationship between stress and deformation is non-linear [12]. In such cases, it is common to determine the E modulus as a secant modulus at an agreed deformation, i. e., 0.05-0.25% [12], 100%-500% [13], 20%-500% [14], 100%-300% [15, 16].

After the elastic deformation, polymers exhibit a mechanically reversible but time-dependent deformation behaviour (viscoelasticity). Based on load level, a principle distinction is made between the linear-viscoelastic and the non-linear viscoelastic deformation component [12].

Linear viscoelastic deformation is reversible, but time- and temperature-dependent [12]. In contrast, in the non-linear viscoelastic deformation, molecular entanglements are released and the polymer properties depend not only on time and temperature, but also on the level of mechanical load [12].

In this deformation region, which is characterized by the beginning of microstructural material damage, molecular migrations take place leading to irreversible yield process and thereby to permanent deformation [12]. However, depending on the temperature and test time scale the same substance can behave mechanically in either solid-like or liquid-like fashion [8, 17].

A polymer tested in the glassy state at low temperatures, shows an elastic modulus E in the range of GPas. As the test temperature is increased the modulus falls rapidly through the region of T_g where the polymer is viscoelastic and the modulus is very rate

and temperature dependent. At a sufficiently high temperature, the polymer becomes rubbery.

If the polymer is not crosslinked the modulus decreases rapidly and flows like a viscous liquid. Otherwise, if the polymer is crosslinked the modulus actually increases with increasing temperature, although over a narrow range of temperature the modulus remains approximately constant at 10^6Pa [10].

This form of response which combines both liquid-like and solid-like features is termed viscoelasticity [17]. The prominence of viscoelasticity in polymers is not unexpected when one considers the complicated molecular adjustments which must underlie any macroscopic mechanical deformation [18].

In a polymer, each flexible threadlike molecule pervades an average volume much greater than atomic dimensions and is continually changing the shape of its contour as it wriggles and writhes with its thermal energy [18]. Under stress, a new assortment of configurations is obtained; the response to the local aspects of the new distribution is rapid, the response to a long-range aspect is slow [18].

To understand material response for small disturbances, two time scales must be considered. One characterizes the test (τ_E), and the other, the material (τ_S) [8]. Response to disturbances depends on the persistence of microscopic arrangements. If testing rate greatly exceeds the rate of molecular rearrangements, the response is solid-like. At the other extreme of slow testing relative to structural relaxation rate, the response is liquid-like [8].

Dynamic experiments, allow to explore the effect of time in the response of the material by the application of an oscillating stress which is varied periodically, usually with a sinusoidal alternation at a frequency ν in cycles/sec (Hz) or ω ($=2\pi\nu$) in radians/sec [18]. If the viscoelastic behaviour is linear, the strain will also alternate sinusoidally but will be out of phase with stress [18]. Due to the phase shift δ between stress and strain, its modulus has to be introduced as the complex modulus E* to describe the stress-strain relationship E*=E'+iE" [12].

This complex modulus can be regarded as a vector in the complex plane whose direction is given by the phase angle δ and its amount by the ratio of stress and strain amplitudes. Using simple trigonometric relations, a real part E' and an imaginary part E" can be distinguished [12].

The real part E' is called the storage modulus and it is a measure of the energy stored during deformation [12, 19], while the imaginary part viscous flow is proportional to the energy lost due to friction and internal motions [12, 19].

The relation between the loss modulus (E") and the storage modulus (E') is called loss factor (tan δ) and characterizes the damping behaviour [12]. As the material becomes elastic, damping becomes smaller, whereas in the glass transition region, it describes a maximum, which is usually taken as the T_g value.

After the glass transition, coordinated movements of the amorphous portion of the chain span along the temperature scale, describing the rubbery plateau whose length is related with the chain entanglements [20].

Continued heating the melt state is reached, where large-scale chain slippage occurs and the material flows [20]. Further heating causes the thermal degradation of polymers.

Degradation

It has been reported that the thermal degradation of PLA predominantly consists of random main-chain scission and unzipping depolymerisation reactions [21]. As a consequence of thermal degradation when PLA is melt processed during the manufacturing of industrial products at high temperatures, undesired molecular weight reduction and weight loss occur [21], leading to a detriment in the mechanical properties.

On the other hand, the degradation mechanism that makes PLA and their copolymers so attractive for biomedical applications is the hydrolytic degradation of their ester groups in the presence of water [22]:

$$-COO-+H_2O\rightarrow-COOH+HO-$$

Since this process is acid-catalysed [23], it has been questioned if the low-pH environment produced thereof would cause a strong inflammatory response [24] in the surrounding tissue. Thus, despite the biocompatibility of polylactides has been strongly supported [24-26], it must be reckoned that the local low-pH environment within and surrounding the device [23, 27] constitute an active field of research.

Blends

As it has been mentioned, compounding and blending are useful strategies either to increase functionalities or to overcome certain shortcomings. Compounding PLA with bioactive fillers [27-33] provides osteoconductivity to the biodegradable PLA matrix. Blending with other polymers [34, 35] imparts flexibility and toughness to the PLA matrix [36].

From a thermodynamic point of view, a mixture of polymers constitute a miscible system if the polymer blend is homogeneous down to the molecular level, associated with the negative value of the free energy of mixing ($\Delta G_{mix} \cong \Delta H_{mix} \leq 0$), whereas the system will be immiscible whenever ($\Delta G_{mix} \cong \Delta H_{mix} > 0$) [37].

Between the two situations lie the partially miscible systems, which are systems miscible only under certain restricted conditions. Perhaps the most unambiguous criterion of polymer miscibility is the detection of a single transition whose temperature is intermediate between those corresponding to the two component polymers. At the other extreme, blends of immiscible polymers that segregate into distinct phases exhibit glass transition identical in temperature and width to those of the unblended components [38].

In such systems, the resultant properties depend on the amount and properties of the individual polymeric components as well as the mode of the dispersed material, and the interaction between the phases [39].

In rubber-toughened plastics, two types of behaviour have been observed [40]. In blends that dissipate fracture energy mainly by matrix crazing, the greatest toughness is achieved at an optimum rubber particle size [40]. On the other hand, in blends that dissipate fracture energy mainly by matrix yielding, a sharp brittle-tough transition occurs

at a critical rubber particle size, or when the interparticle distance is at the critical value [40].

The size and shape of the dispersed phase are much controlled by the interfacial tension, rheological properties, and the complex strain field during processing operations [40, 41], whereby a fine nodular dispersed phase is generally sought [39-42]. Mean diameter of the dispersed phase is related to the ratio of the melt viscosities of the dispersed phase (η_{dp}) and the polymer matrix (η_m) [3]. Minimized diameters of the dispersed phase, strongly improving phase dispersion, are achieved as the viscosity ratio (η_{dp}/η_m) tends to 1, i. e. when the viscosity of the dispersed phase is comparable to that of the matrix [3].

The aim of this chapter is to set the basis for the design of a biodegradable polymer for its application as a flexible device for its use in urology. For this, pure PLLA with be compared with three of its copolymers, in terms of thermal, mechanical and biodegradability properties and correlations among the properties and microstructural issues will be established.

Materials and methods

Poly (L-lactide) (PLLA) homopolymer, Purasorb PDLG racDL-lactide/glycolide copolymer (PDLGA) of 53/47 molar ratio; Purasorb PDL poly-DL-lactide (PDLLA) of 51/49 molar ratio and Purasorb PLC 7015 of 70/30 L-lactide/ε-caprolactone (PLCL) molar ratio copolymer were all supplied by Purac Biochem (The Netherlands).

The molecular weight of the samples was determined by GPC using a Waters 1515 GPC apparatus equipped with two Styragel columns (102 - 104 Å). Chloroform was used as an eluent at a flow rate of 1 mL min^{-1} and polystyrene standards (Shodex Standards, SM-105) were used to obtain a primary calibration curve.

Differential Scanning Calorimetry (DSC) was used to determine the thermal transitions and analyse the phase structure of polylactides. It was performed on a Q-200 Calorimeter from TA Instruments, calibrated with pure indium and sapphires. Sample weights ranged from 5 to 10mg.

The tensile tests were conducted in an Instron 5565 testing machine at room temperature under a constant crosshead speed of 5mm/min. Data recording and subsequent analysis was performed using Bluehill software. Tensile test specimens consisted on dumbbell samples punched from 1 mm thickness sheets obtained by rapid cooling (quenching) from the melt in a hot plate press Collin PE200.

Polymer blends were processed in a two screw internal mixer (Brabender) at a constant speed of 20rpm for 10 minutes at 200ºC. After blending, sheets of 1mm thickness were obtained by water quenching from the melt in a hot plate press.

Dynamic mechanic thermal analysis (DMTA) was performed in tensile mode at 1Hz, 0.5N and 25μm and relevant temperature range for each polymer. Testing conditions were selected from preceding isothermal force-strain tests in order to guarantee the elastic regime during the test.

The *in vitro* degradation of the polymers was studied by monitoring the evolution of Molecular weights by gel permeation chromatography (GPC) after immersion in phosphate buffer saline for specific periods of time.

The degradation of bioresorbable polymers was studied in animal urinary bladder model. Wistar rats were divided into 5 equal groups according to the used polymers. A three mm length tube was fixed to the bladder wall by laparotomy. Animals remained in individual housing and kept under daily control of hematuria during the first 15 days and weekly weight and urine control for pH and lactate. Three individuals were sacrificed per group at 4^{th}, 10^{th}, and 16^{th} week after insertion. Remaining polymer was collected for further characterisation and bladder tissue for histologic study.

Results and discussion

Table 1.1 resumes the molecular characterization of the studied polymers. As it can be noted, PDLLA shows the highest molecular weight as well as the highest polydispersity index. Conversely, the lowest molecular weight was measured for the PDLGA copolymer. The lowest polydispersity index was recorded for PLLA.

Table 1.1.- Molecular characterization of the polymers.

	Determined by GPC	
	M_n	**D**
	(g/mol)	**(-)**
PLLA-PL18	120,000	1.25
PDLLA-0303001995	350,000	1.92
PDLGA-0701000351	96,000	1.70
PLCL-0508001260	107,000	1.62
PLCL-1008000233	112,000	1.77

Thermal characterization

The first thermal event observable in figure 1.2 during the heating scan of PLLA is the glass transition temperature at 55ºC. Further heating reveals a broad exothermic peak in the range 91-152ºC centred about 108ºC corresponding to the cold crystallization and a second exothermal just before the endothermic melting peak centred about 183ºC. The later endotherm occurring just before the melting peak has been attributed to a recrystallization process by means of which a more imperfect crystalline form of PLLA recrystallizes in a more perfect crystal polymorph [43]. Integration of these peaks, and substituting in equation 2 with ΔH_m^0=106 J/g [44], reveals an overall crystallinity of ~10%.

$$X_c(\%) = \frac{\Delta H_m - \Delta H_{cc}}{X_{PLLA}\Delta H_m^0} * 100 \text{ (equation 2)}$$

Being PLLA optically pure, and having a stereo-regular chain microstructure, it is a crystallisable polymer. However, as the rate of crystallisation is to some extent slower than the rate of cooling, only a small proportion of the material has crystallized.

In contrast, PDLLA containing 53% L/lactide and 47% D/lactide repeat units randomly distributed along the chain microstructure lacks any crystallisation capacity; therefore only one thermal event corresponding to the glass transition at 48ºC is observable in its thermogram.

A similar conclusion follows from observation of the thermogram of PDLGA. The random distribution of 51 % repeat units of DL-lactide and 49 % of glycolide, yields a glass transition temperature at 45ºC as revealed in its DSC scan.

Finally, PLCL, with a molar composition of 70% L-lactide / 30% ε-caprotactone shows a T_g at 20ºC. The lack of subsequent thermal events indicates a fully amorphous phase were the measured T_g corresponds to a very good approximation to the theoretical value predicted from equation 1 based on the relative quantities of the comonomers and their corresponding T_gs.

However, though no signs of crystallization have been observed under the scanning conditions, due to the stereo-regularity of the 70% L-lactide, it is expected that PLCL crystallized under specific conditions.

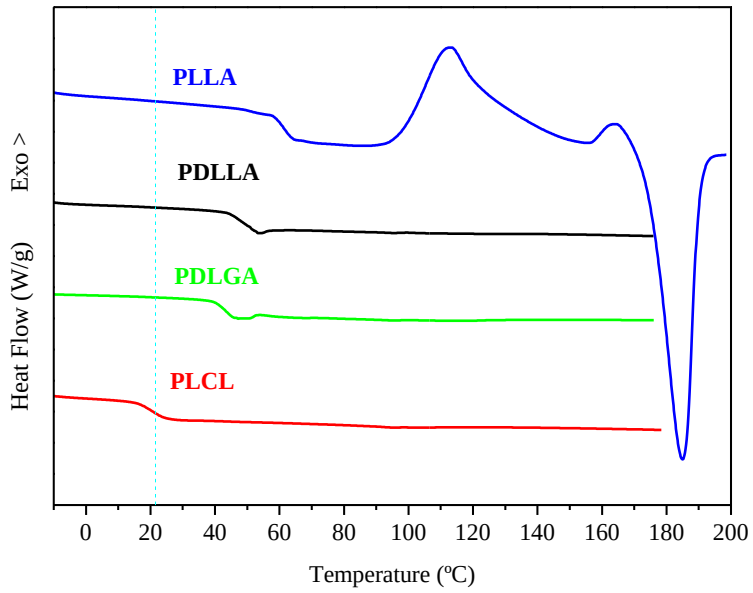

Figure 1.2.- DSC heating scans of the four polylactides.

As it can be noted from table 1.2, the lowest recorded T_g was that of PLCL which is approximately located at room temperature (RT), whereas the other scanned polymers exhibited their corresponding transitions at temperatures well above RT.

In the same table, the 10% crystallinity of PLLA supports the already mentioned superior stereoregularity of PLLA.

Table 1.2.- Thermal properties including glass transition temperature, T_g, cold crystallization temperature, T_{cc}, melting temperature, T_m, and crystallinity degree, X_c, as determined by DSC.

	T_g ºC	T_{cc} ºC	T_m ºC	X_c %
PLLA	55	108	183	10
PDLLA	48	-	-	-
PDLGA	45	-	-	-
PLCL	20	-	-	-

Mechanical characterization

The stress-strain behaviour of these polymers has been studied by the classical tensile test at room temperature and a constant crosshead speed of 5mm/min. From the recorded values represented in figure 1.3 the elastic modulus and other relevant parameters such as yield stress and breaking stress have been extracted and are resumed in table 1.3.

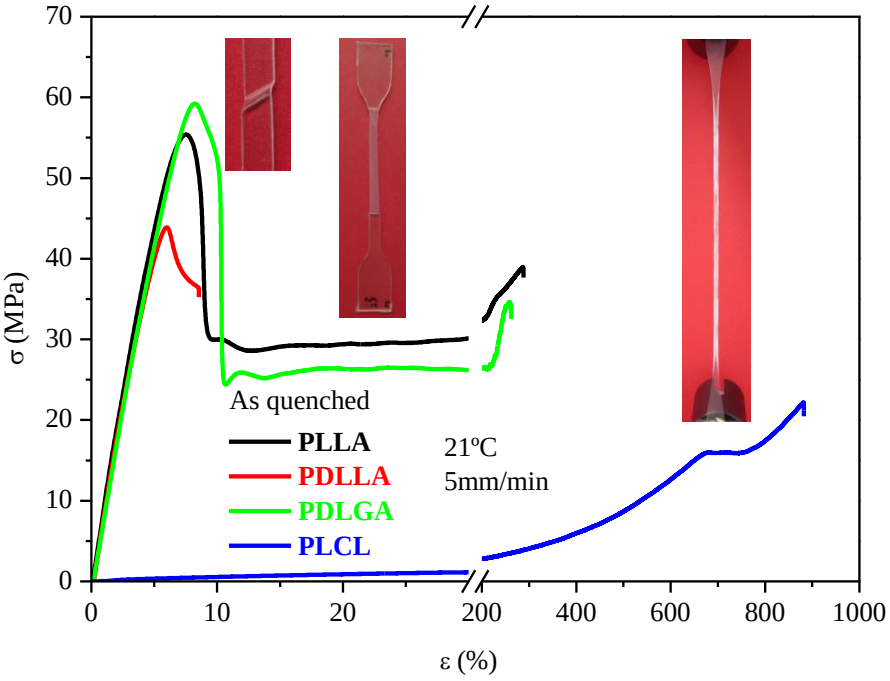

Figure 1.3.- Stress-strain diagram.

The stress-strain graph of PLLA runs essentially linear during the elastic region until it reaches a maximum (yield point) and a subsequent sudden drop.

The yield point notes the beginning of the irreversible plastic deformation caused by strain localization of shear bands and is macroscopically observable by the formation of a neck. The neck stabilizes at the point of the shallow load minimum after which deformation proceeds at a relatively constant force by propagation of the neck shoulders along the test zone of the sample. When the neck advances into the clamping regions of the sample the stress raises until rupture occurs.

The tensile behaviour described here corresponds to that of a glassy polymer tested below its glass transition temperature. As it was seen in the DSC analysis, PDLLA and PDLGA are also well below their T_g at the test temperature, hence, their behaviour is essentially the same as the one described for PLLA, but for the lack of neck propagation in PDLLA.

In contrast, PLCL stretches uniformly without neck formation until strain hardening and whitening are noted. However, after rupture, broken pieces recover their original length and white colour is no longer observed.

These observations correspond to the elastic recovery of rubber and they can be explained by the entropy spring definition given by Treloar [45]. This theory considers the rubbery state as a random coil of polymer chains. Under the application of stress, polymer chains uncoil and as fewer conformations are available the entropy of the system is lowered. Removal of the applied stress allows the chains to recover their randomly coiled conformations, leading to the rubber elasticity.

Consequently, macroscopic observations of transparency to opacity and again, transparency correspond respectively to random, aligned and random microscopic evolution of chains upon application and release of tensile stress.

In table 1.3, mechanical properties from tensile tests are resumed where values of yielding for glassy polymers correspond to respective coordinates where strain location was noted. Conversely, according to previous explanation of observed elasticity in PLCL, values of yielding are omitted for it.

Regarding the elastic modulus, which in the case of glassy polymers corresponds to the Young's modulus whereas in PLCL it corresponds to the secant modulus, a three orders of magnitude difference between glassy and PLCL further highlights the contrasting observed behaviour.

The tremendous standard deviation in strain at rupture for PDLGA and PLLA requires further comments. The explanation behind these values indicates that whereas some samples could accommodate plastic deformation leading to neck propagation, drawing of other samples was interrupted, as in the case of PDLLA immediately after yielding. As this phenomenon will be further developed in subsequent chapters, it is sufficient to say here that this premature failure is a consequence of physical aging.

Table 1.3.- Mechanical properties including modulus of elasticity (E) where for PDLLA, PLGA and PLLA corresponds to the Young's modulus whereas for PLCL E is the secant modulus at 2% strain, yield stress, σ_Y, yield strain, ε_Y, rupture stress, σ_R and rupture strain, ε_R.

	E	**σ_Y**	**ε_Y**	**σ_R**	**ε_R**
	MPa	**MPa**	**%**	**MPa**	**%**
PDLLA	1012±63	45.4±6.9	6.0±0.2	41.0±4.6	7.4±1.1
PLCL	7.3±2.9*	-	-	20.7±3.2	815±102
PDLGA	940±106	57.8±2.2	7.6±0.6	44.9±9.5	147±161
PLLA	972±41	54.6±2.3	7.7±0.7	35.1±5.2	166±146

The viscoelastic behaviour has been studied by means of DMA. The evolution of storage modulus and of tan δ with temperature is plotted in figure 1.4.

At low temperatures, the four polymers are in a glassy state where the chains are essentially frozen and molecular arrangements in order to accommodate the imparted strain takes longer than the time scale of the experiment. The energy loss due to friction and internal motions is negligible, and the storage modulus displays values between 2-3GPa.

As the experiment proceeds, the storage modulus becomes highly temperature dependant undergoing a drop of three orders of magnitude. At a molecular level, this

transition is due to the relaxation of the main chain caused by the heating program. Accordingly, tan δ, which indicates how efficiently the polymer losses energy to molecular rearrangements and internal friction, describes a maximum, which can be taken as a measure of the T_g; although the values are a few degrees higher than those obtained by DSC.

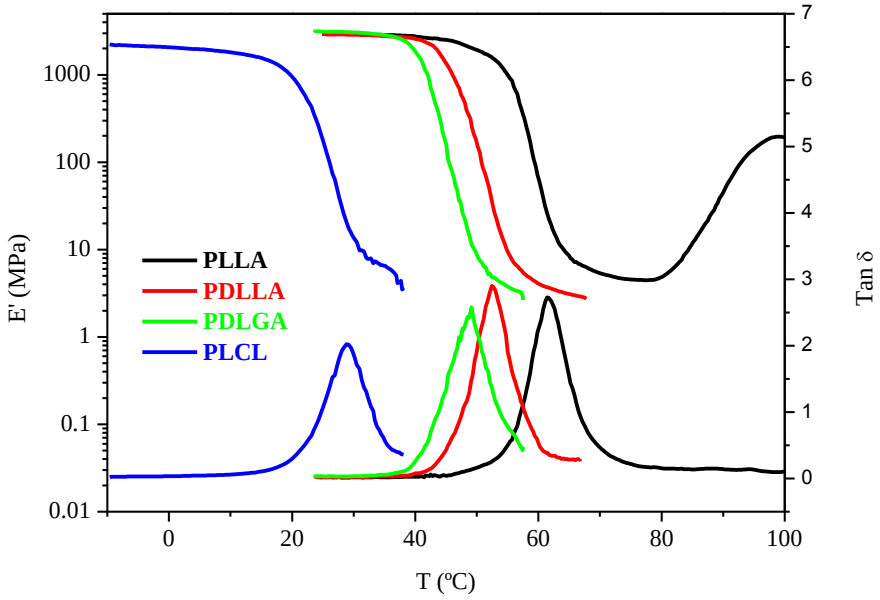

Figure 1.4.- Storage modulus and tan δ vs. temperature of the as quenched polymers.

It is important to note that damping of PLCL takes place while the other polymers are in the glassy state, which is in agreement with the observed tensile behaviour.

Following the α relaxation, the storage modulus describes a short plateau (rubbery modulus) after which amorphous polymers irreversibly flow featuring liquid-like. At this stage, the structure equilibrates rapidly relative to the perturbation rate, so the work expended in imposing a perturbation is effectively dissipated immediately, being the stored free energy negligible and the material flows. In contrast, a sudden increase in rigidity is noted for PLLA indicating crystallization enhanced by the mobility of chains, which is in agreement with the cold crystallization observed by DSC.

Degradation

Figure 1.5 shows the evolution of the number average molecular weight (M_n) with degradation time (days) in phosphate buffer saline. Molecular weights of polylactides were determined by gel permeation chromatography (GPC). It is observed that PDLGA undergoes the fastest reduction in M_n, followed by PLCL and PLLA. The different biodegradation rate can be attributed to the different degradation sensitivity of the repeat units and to the different amorphous/semicrystalline features of the polymers studied. Accordingly, the presence of the hydrophobic methyl group in the repeating unit of PLA, improves the hydrolytic stability, whereas the high hydrophilicity of the glycolide units accelerate the degradation rate [46]. The molecular weight of PLCL is seen to decrease smoothly at an intermediate rate between pure PLLA and PDLGA, due to the intermediate degradation time of ε-caprolactone units [28, 47].

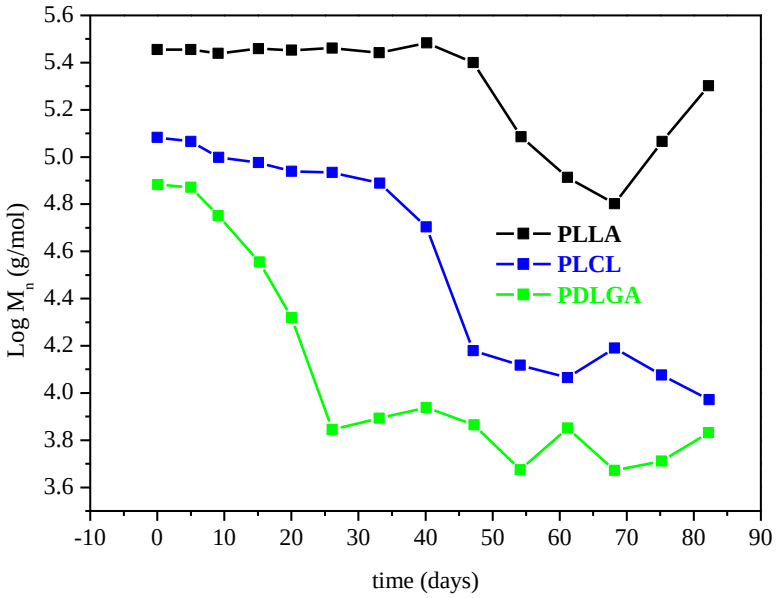

Figure 1.5.- Number average molecular weight (M_n) evolution with biodegradation time (days) *in vitro*.

Figure 1.6 resumes the state of biodegradation of the biomaterials studied in vivo. As it can be observed, silicone tube only shows a slight increase of opacity, indicating that it has remained unchanged during the study. For the same period, PLLA remains quite unaltered in shape, although it shows opacity and it has grown calcification on its

surface. Interestingly, PLCL has developed a significant opacity and the broken pieces of the tube suggest brittle fracture. Finally PDLGA degradation is very advanced in week 4th and from 3 tube parts placed in the bladder (one per specimen), only a small part of one of them remains at week 4th, indicative that in vivo degradation is nearly complete at this time. Only some calcification was appreciated.

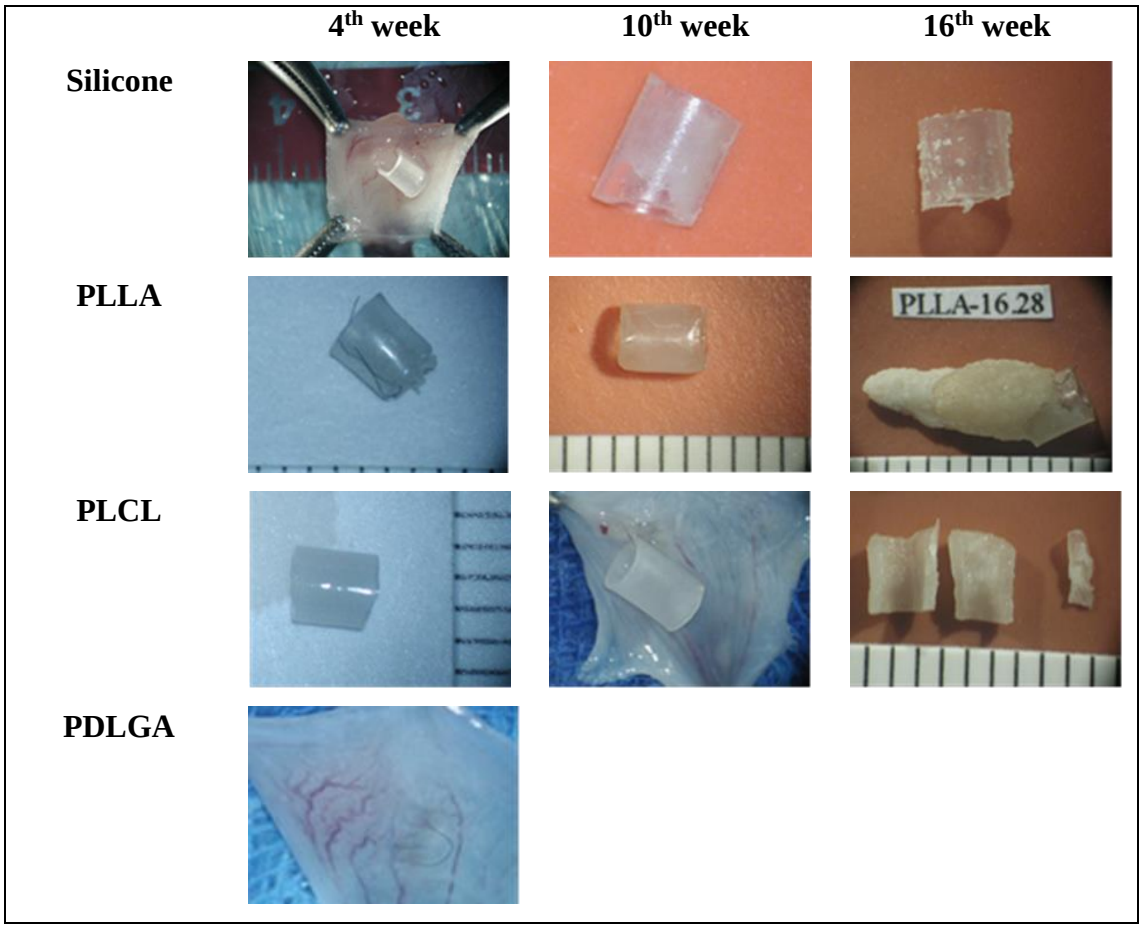

Figure 1.6.- Sequence of biodegradation of the biomaterials studied in vivo.

Observed opacity agrees with reported crystallization in PLLA and PLCL [48] which in the case of PLCL is preceded by a phase separation mechanism [49-51]. The morphology of remaining pieces suggests that as chain scission occurred in PLLA segments, and PCL segments were more easily hydrolysed leading to cracking of small particles from the film [47]. Calcifications were also detected in vessel walls during a long term follow up study of PDLLA copolymeric stent [52]

According to the *in vitro* and the *in vivo* results, PDLGA has proven to be the fastest biopolymer to biodegrade, followed by PLCL and PLLA respectively. As water is preferentially diffused in the amorphous phase where more free volume is available, PDLGA, having an amorphous structure degrades faster. Conversely, PLLA and PLCL are prone to develop crystallinity as observed by the opacity of the extracted parts, thus, their degradation is considerably delayed as the diffusion of water molecules to the chains inside the rigid crystalline regions is prohibited.

Blends

Thermal properties

In order to combine the biodegradability of PDLGA and the flexibility of PLCL the miscibility and mechanical properties of the system PDLGA-PLCL were studied. Figure 1.7 shows the DSC analysis of the PDLGA-PLCL blends obtained by mechanical mixing. The scans of pure copolymers show one thermal event corresponding to their respective glass transition, whereas the blends display two thermal events. Applying the single glass transition miscibility criteria, the detection of two thermal events, denotes poor compatibility between pure copolymers revealing a phase-separated mixture, where each component retains its T_g as highlighted in figure 1.8.

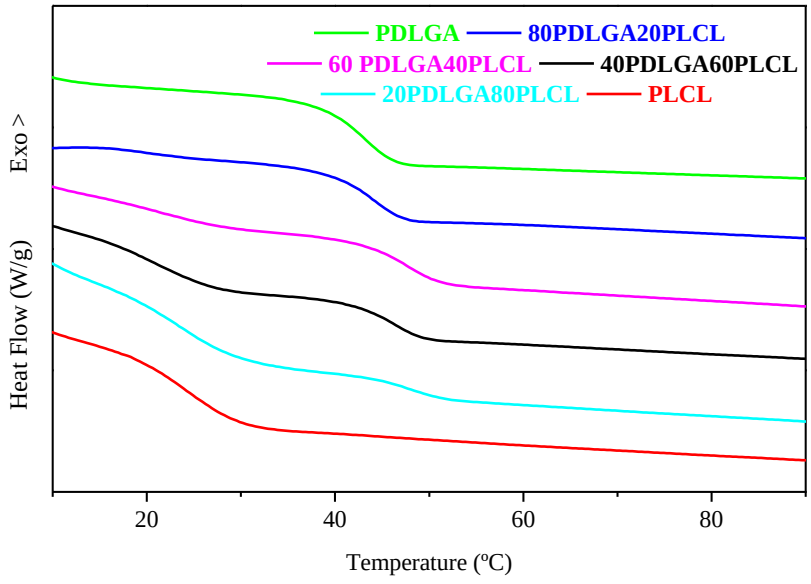

Figure 1.7.- DSC analysis of the PLGA-PLCL blends

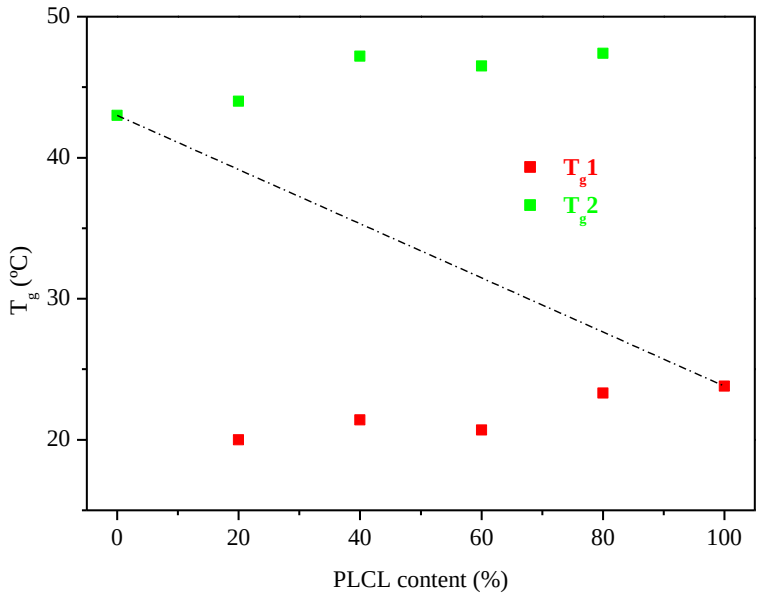

Figure 1.8.- Glass transition temperatures regarding the PLCL content of the mixture.

Representation of the detected T_gs for each of the compositions studied reveals a clear deviation from the one single T_g miscibility criteria represented by a dashed line where a decrease of the measured T_gs in comparison with those of pure copolymers is also noted. It is suggested that the increased interfacial area of the biphasic mixtures, provides free volume to chain segments that show an advanced glass transition due to an enhanced mobility at lower temperatures [53, 54].

Mechanical properties

The nominal stress-strain graph of figure 1.9, displays a whole spectrum of tensile properties ranging from elastomeric for high PLCL content mixtures, to glassy for increasing content of PDLGA. However, a worsening in the tensile properties of PDLGA is noted, which can be associated with thermal degradation occurred as a consequence of the severe processing conditions.

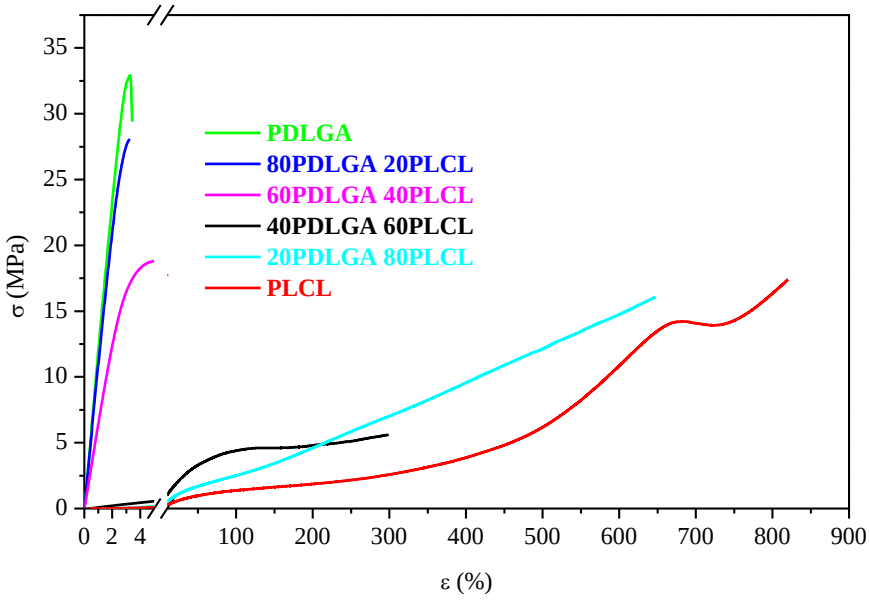

Figure 1.9.- Nominal stress-strain graph of the studied system.

Table 1.4.- Mechanical properties calculated from the tensile tests.

	E MPa	σ_Y MPa	ε_Y %	σ_R MPa	ε_R %
PDLGA	1180±69	36±3	4.5±0.5	34±4	4.8±0.4
80PDLGA20PLCL	1119±70	28±1	4.1±0.3	26±2	5±1
60PDLGA40PLCL	650±50	19±1	7.3±0.2	17±1	13±1
40PDLGA60PLCL	17±4 (*)	6±1	142±3	8±1	382±43
20PDLGA80PLCL	7±2 (*)	17±1	682±27	17±1	682±27
PLCL	3±1 (*)	15±1	679±12	19±1	840±13

The elastic modulus of the high PDLGA content in the above mixtures given in table 1.4 have been calculated as the Young's modulus whereas the elastic modulus of the high PLCL content corresponds to the secant modulus at 2% strain. As it can be noted in figure 1.10, with the exception of 80PLGA20PLCL composition, mixtures showed a negative deviation from ideal values (miscibility) as represented by the dashed line.

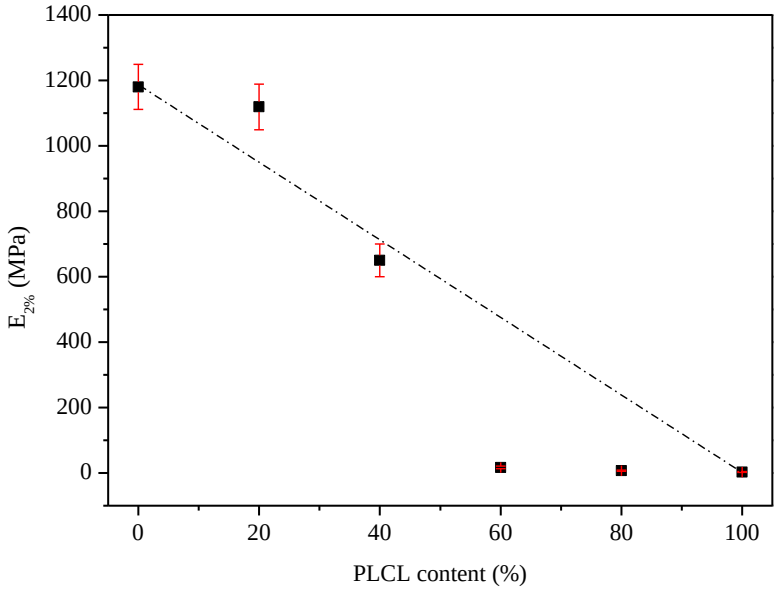

Figure 1.10.- Secant modulus at 2% strain against PLCL content

Careful observation of tensile strength in table 1.4 discloses a minimum with intermediate PLCL content that can be better explained taking into consideration fracture surfaces in figure 1.11.

These show two-phase structures where the majoritarian component constitutes the matrix and the minor the dispersed phase. In all cases, the contour of the phases is clearly defined indicating the lack of compatibility between them. Besides, from their appearance, two opposite failure mechanisms can be easily distinguished depending on the majoritarian phase. On the one hand, images a and c show an irreversibly deformed PDLGA matrix, with ovoid segregates of PLCL and cavities surrounded by uneven surfaces, indicating that the strain energy dissipation mechanism has been plastic deformation of the matrix around stress concentrators (PLCL particles) until rupture. Conversely, neither from the smooth surface of the matrix or from the round PDLGA particles are traces of deformation disclosed, revealing that whereas PLCL matrix has been highly stretched until failure, PDLGA particles had limited to hinder stress transmission along PLCL matrix, without shape alteration. After break, elastically strained PLCL chain molecules snap back to their original position in order to restore their high conformational entropy. Thus, due to the elastomeric behaviour of PLCL

described here, it is inferred that the ovoid shape of PLCL particles noted in figures a and b was impinged during sample conformation and not during tensile testing.

Finally, from the fine particle size and distribution it must be noted that the highest compatibility [3, 39-42] was achieved by 20PDLGA80PLCL composition.

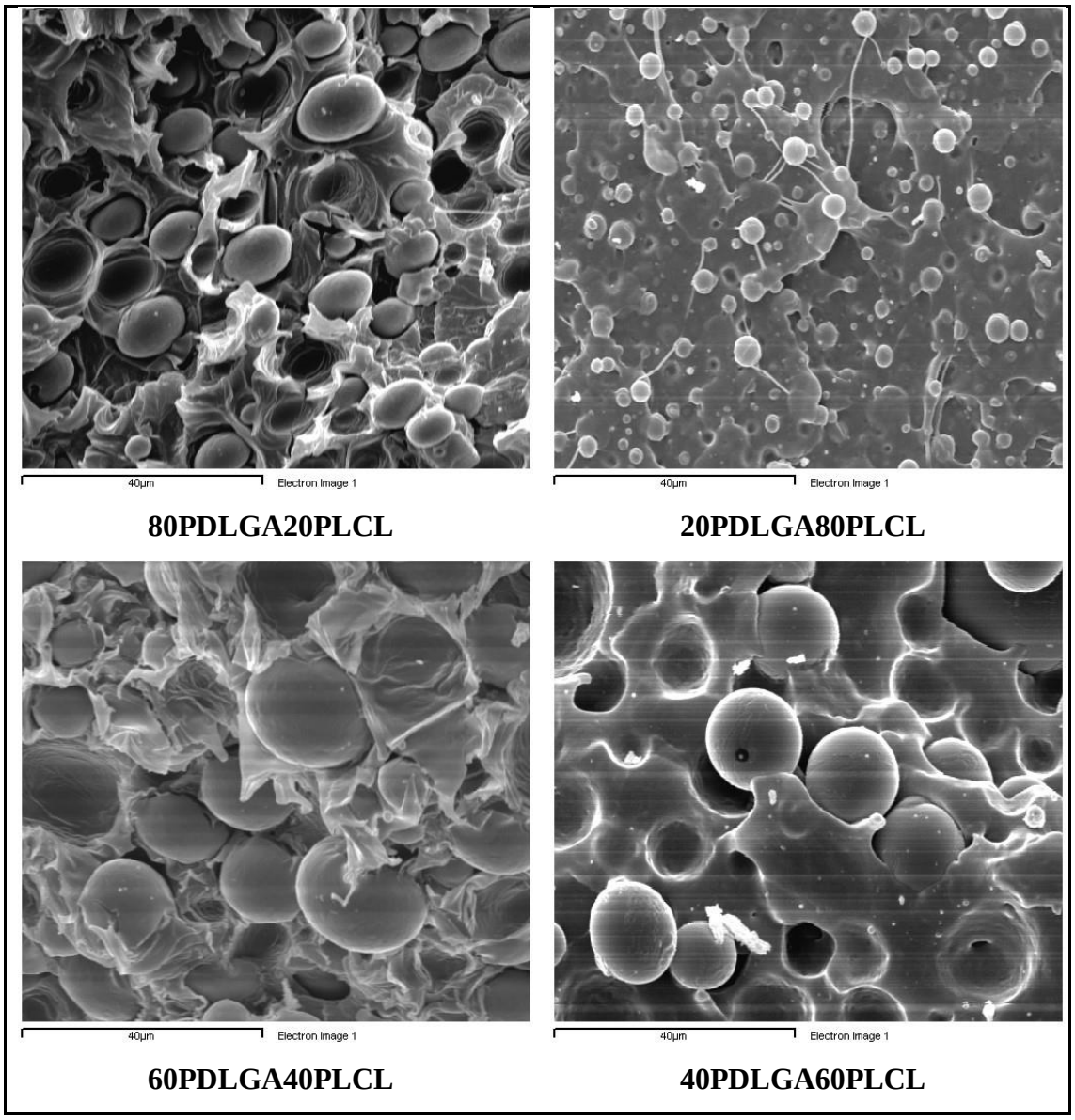

Figure 1.11.- Fracture surfaces after room temperature tensile tests of biphasic mixtures.

Conclusions

As seen from the DSC analysis, the thermal properties of pure PLLA have been substantially modified by the introduction of irregularities in its chain backbone. These alterations restrict the crystallization capacity and bring forward the glass transition at lower values of temperature.

Accordingly, the mere introduction of D units in the chain backbone of pure PLLA has caused a reduction in the T_g of 7-9ºC as measured by DSC and DMA respectively.

Interestingly, the major reduction in the T_g, has been achieved by means of copolymerization of L-lactide with ε-caprolactone in a 70/30 proportion whereby resulting T_g was in the vicinity of room temperature.

Monitorization of the dependence of the storage modulus with temperature by means of DMA discloses the solid-like behaviour of polymers (glassy) at temperatures below their corresponding T_g whereas a three orders of magnitude precipitation as a consequence of a rise in temperature, locates them into the rubbery region. Being this behaviour a common feature amongst polymers, it is the relative position of this transition in regard to the temperature of use that plays the key role.

As it has been shown, the T_g of PLCL coincided with test temperature, causing PLCL to exhibit an elastomeric behaviour with low values of modulus and elastic strains until rupture. Conversely, as test temperature was 25-35ºC below the corresponding T_gs of the other polymers, these behaved as glasses with high modulus and yielding.

On the other hand, crystallinity has been severely affected by the introduction of irregularities in the pure chain backbone of PLLA in different grades. Hence, it has been totally prohibited in the case of PDLLA and PDLGA, whereas after observation of whitening and opacification, it has been hindered in PLCL.

All the biomaterials studied showed biocompatibility with urological tissue and differences in their biodegradation rates where associated with the development of crystallinity, so that PDLGA being totally amorphous was the first to biodegrade. Conversely, pure PLLA was the latest, whereas PLCL displayed an intermediate rate.

Finally, blending PDLGA with PLCL in different proportions has presented an alternative method in order to attain a full spectrum of mechanical properties ranging from toughened PDLGA to reinforced PLCL.

DSC and SEM images revealed a two phase structure, where the highest degree of compatibility was achieved for a 20%PDLGA and 80% PLCL composition.

As the studied system combines the flexibility of PLCL and the high biodegradation rate of PDLGA, it seems a strong candidate for its use in urological applications were empty places after the preferential biodegradation of PDLGA would promote cell colonisation while PLCL maintained its structural role until its biodegradation was completed.

References

[1] Södergård, A. Stolt, M. Industrial application of high molecular weight poly(lactic acid) in Poly(lactic acid) synthesis, structure and properties, processing and applications, Auras, R., Lim, L-T., Selke, S., Tsuji, H., John Wiley & sons, Inc. New Jersey, 2010, pp. 27.

[2] Detyothin, S., Kathuria, A., Jaruwattanayon, W., Selke, S., Auras, R. Poly(lactic acid) blends. Auras, R., Lim, L-T., Selke, S., Tsuji, H., John Wiley & sons, Inc. New Jersey, 2010, pp. 227.

[3] Signori, F., Coltelli, M. B., Bronco, S., Polymer degradation and stability, 94, 74-82 (2009)

[4] Garlotta, D., Journal of Polymers and the Environment, 9, 63-84, (2002)

[5] Albertsson, A. C., Varma, I. K., Lochab, B., Finne-Wistrand, A., Kumar, K. Design and synthesis of different types of poly(lactic acid). Auras, R., Lim, L-T., Selke, S., Tsuji, H., John Wiley & sons, Inc. New Jersey, 2010, pp. 43.

[6] Fox, T. G., The Bulletin of the American Physical Society, 1956, 1, 123-123

[7] Gordon, M., Taylor, J. S., Journal of applied chemistry, 1952, 2, 493-500

[8] Graessley, W. W., Polymer liquids & networks: Dynamics and rheology. Graessley, W. W., Garland Science Taylor & Francis group, New York, 2008, pp. 51.

[9] Ibeh C. C., crystallinity and crystallization in polymers and plastics in Thermoplastic materials, Ibeh, C. C., CRC Press Taylor & Francis, London, 2011, pp. 91.

[10] Haward, R.N. and Young, R.J. Introduction. In The Physics of Glassy Polymers, Haward, R.N. and Young, R.J., Eds.; Chapman and Hall: London, 1997, pp. 3.

[11] Zhang, S., Li, L., Kumar, A., Macro and micro thermal analyses in Materials characterization techniques, CRC Press Taylor & Francis, London, 2009, pp. 267.

[12] Grellmann, W., Seider, S., Mechanical properties of polymers in Polymer testing, Carl Hanser Verlag, Munich, 2007, pp.93, 110.

[13] Kresge, E. N., Polyolefin –Based Thermoplastic elastomers in Thermoplastic elastomers, Carl Hanser Verlag, Munich, 2004, pp.97.

[14] ASTM D412-83 Tensile Properties of Rubber/Elastomers - ASTM D412 Plastic Test Standard

[15] Maláč, J., Polymer Testing, 2005, 24, 790-792

[16] Maláč, J., Polymer testing, 2006, 25, 650-655

[17] Ward, I. M., Hadley, D. W., Principles of linear viscoelasticity In An Introduction to the mechanical properties of solid polymers, Ward, I. M., Hadley, D. W., John Wiley & sons, Inc. West Sussex, 1993, pp. 45.

[18] Ferry, J. D., the nature of viscoelastic behaviour in Viscoelastic properties of polymers. Third edition. John Wiley & sons, Inc. New York, 1980, pp. 2, 11.

[19] Menard, K. P. Dynamic testing in Dynamic mechanical analysis a practical introduction, CRC press, Texas, 1999, pp. 64.

[20] Menard, K. P. Time-temperature scans: transitions in polymers in Dynamic mechanical analysis a practical introduction, CRC press, Texas, 1999, pp. 94.

[21] Nishida, H., thermal degradation in Poly(lactic acid) synthesis, structure and properties, processing and applications, Auras, R., Lim, L-T., Selke, S., Tsuji, H., John Wiley & sons, Inc. New Jersey, 2010, pp. 401.

[22] Tsuji, H., Hydrolytic degradation in Poly(lactic acid) synthesis, structure and properties, processing and applications, Auras, R., Lim, L-T., Selke, S., Tsuji, H., John Wiley & sons, Inc. New Jersey, 2010, pp. 345.

[23] Fu, K., Pack, D. W., Klibanov, A. M., Langer, R., Pharmaceutical research, 2000, 17, 100-106

[24] Lendlein, A., Langer, R., Science, 2002, 296, 1673-1676

[25] Sarasua, J. R., López-Rodríguez, N., Zuza, E., Petisco, S., Castro, B., del Olmo, M., Palomares, T., Alonso-Varona, A., Journal of materials science: Materials in medicine, 2011, 22, 2513-2523

[26] Ramos, J. L., Aldazabal, P., Zuza, E., Sarasua, J. R., Arrieta, A., Villanueva, A., Eizaguirre, I., Cirugía pediátrica, 2013, 26, 91-94

[27] Ekholm, M., Hietanen, J., Tulamo, R. M., Muhonen, J., Lindqvist, C., Kellomäki, M., Suuronen, R., Journal of materials science: materials in medicine, 2006, 17, 139-145

[28] Wang, L., Chen, H., Zhang, L, Chen, D., Pang, X., Xiong, C., Journal of Polymer Research, 2011, 18, 329-336

[29] Senköylü, A., Ural, E., Kesenci, K., Simsek, A., Ruacan, S., Fambri, L., Migliaresi, C., Piskin, E., The international journal of artificial organs, 2002, 25, 1174-1179

[30] Wilberforce, S. I. J., Finlayson, C. E., Best, S. M., Cameron, R. E., Polymer, 2011, 52, 2883-2890

[31] Bleach, N. C., Nazhat, S. N., Tanner, K. E., Kellomäki, M., Törmalä, Biomaterials, 2002, 23, 1579-1585

[32] Gomes, M. E., Azevedo, H. S., Moreira, A. R., Elä, V., Kellomäki, M., Reis, R. L., Journal of tissue engineering and regenerative medicine, 2008, 2, 243-252

[33] Thompson, I. D., Hench, L. L., Proceedings of the institution of mechanical engineers. Part H, 1998, 212, 127-137

[34] Todo, M. Park, S. D., Takayama, T., Arakawa, K. Engineering fracture Mechanics 2007, 74, 1872-1883

[35] Södergård, A. Stolt, M, Progress in polymer science, 2002, 27, 1123-1163

[36] Dethyothin, S., Kathuria, A., Jaruwattanayon, W., Selke, S. E. M., Auras, R. Poly(lactic acid) blends in Poly(lactic acid) synthesis, structure and properties, processing and applications, Auras, R., Lim, L-T., Selke, S., Tsuji, H., John Wiley & sons, Inc. New Jersey, 2010, pp. 227.

[37] Utracki, L. A., Introduction to polymer alloys and blends in Polymer alloys and blends, Utracki, L. A., Hanser publishers, Munich 1989, pp. 2.

[38] MacKnight, W. J., Karasz, F. E., Fried, J. R., Solid state transition behaviour of blends in Polymer blends, Paul, D. R., Newman, S., Academic Press Inc, Orlando, 1978, pp. 11, 188, 229

[39] Choi, G. D., Jo, W. H., Kim, H. G., Journal of applied polymer science, 1996, 59, 443-452

[40] Wu, S., Polymer engineering and science, 1987, 27, 335-343

[41] Serpe, G., Jarrin, J., Dawans, F., Polymer engineering and science, 1990, 30, 553-565

[42] Wu, D., Zhang, Y., Yuan, L., Zhang, M., Zhou, W., Journal of polymer science: Part B: Polymer physics, 2010, 48, 756-765

[43] Ohtani, Y., Okumura, K., Kawaguchi, A., Journal of Macromolecular Science, Part B: Physics, 2003, 42, 875-888

[44] J. R. Sarasua, R. E. Prud'homme, M. Wisniewski, A. L. Borgne, N. Spassky, Macromolecules, 1998, 31, 3895-3905

[45] Treloar, L. R. G., The physics of rubber elasticity, Claredon press, Oxford 1975

[46] Ma, Z., Zhao, N., Xiong, C., Bulletin of materials science, 2012, 35, 575-578

[47] Jeon, O., Lee, S. H., Kim, S. H., Lee, Y. M., Kim, Y. H., Macromolecules, 2003, 36, 5585-5592

[48] Ugartemendia, J. M., Larrañaga, A., Amestoy, H., Sarasua, J. R., Polymer degradation and stability, 2014, 108, 87-96

[49] Fernández, J., Etxeberria, A., Ugartemendia, J. M., Petisco, S., Sarasua, J. R., Journal of the mechanical behaviour of biomedical materials, 2012, 12, 29-38

[50] Sarasua, J. R., Petisco, Fernández, J., Lejardi, A., Ugartemendia, J. M., European Conference on Biomaterials, 24th, Dublin, Ireland, Sept. 4-8, 2011, 2012, 135-142.

[51] Sarasua, J. R., Ugartemendia, J. M., Petisco, S., Fernández, J., SPE Eurotec 2011, Barcelona (Spain), 14-15 November 2011

[52] Hietala, E. M., Salminen, U. S., Ståhls, A., Välimaa, T., Maasilta, P., Törmälä, P., Nieminen, M. S., Harjula, A. L. J., Journal of vascular research, 2001, 38, 361-369

[53] Wilberforce S. I. J., Finlayson, C. E., Best S. M., Cameron, R. E., Polymer 2011, 52, 2883-2890

[54] Ash, B. J., Siegel, R. W., Schadler, L. S., Journal of polymer science: Part B: Polymer physics, 2004, 42, 4371-4383

Chapter 2. Polymer Processing: From grains to devices

Subchapter 2.1. Casting and Thermoconformation. Self-Reinforcing

Introduction

A cornerstone of materials science is processing of materials [1]. It has become increasingly realized that simultaneously combining the steps of synthesis and processing can sometimes lead to better control of microstructure [1]. This combined approach can provide new materials of outstanding performance [1].

Rational control of microstructure in polymers includes simultaneous control of packing at several length scales as, due to their inherent conformational diversity, each molecule has an enormous number of structural states of similar energy to choose from [1]. In accordance, materials scientists have discovered various post-synthesis ways to influence and control the microstructure from the earliest days of forging, rolling and annealing heat treatments [1].

In thermoplastics (TP), the change from a fluid, processible melt to a solid article is fast and reversible [2]. This change takes place on cooling, or in some cases, following the addition and removal of a solvent [2]. Although much less important in tonnage terms than processing in the molten and rubbery states, solution, suspension and polymerisation casting processes have a useful role in polymer technology [3]. Solution processes are used mainly for coating, film casting and fibre spinning, i.e. in processes where the distance the solvent has to diffuse out of the solution once coated, cast or spun is short [3]. The main problem in such processes is to achieve a control of the setting of the shape once formed [3]. Regulation of this diffusion process is important if products of even quality are to be obtained [3].

Thermoconformation

The ability of TPs to become fluid on heating and then solidify on cooling allows manufacturers to produce articles using the fast processing equipment (injection moulders, blow moulders, extruders etc.) that have been developed for plastic industry [2]. The rate of cooling does not only affect the production rates, but must be considered as a key factor influencing the properties of the product [3].

When a liquid is in equilibrium at any given temperature, there is an average statistical relation between its molecules that is unique because any change in temperature, even if infinitesimal, will change it accordingly [4]. Such a change in the average statistical relation, which corresponds to an equilibrium condition, requires many processes or readjustments involving the molecules of the liquid [4]. Although some of these adjustments are completed almost instantaneously, time is undoubtedly an important factor in the development of many others, especially if their process is affected by viscosity [4]. If the time required for the full development of the sluggish readjustments that are demanded by a given change in temperature, exceeds the time required to accomplish the temperature change, the liquid can be brought to a temperature in a state of non-equilibrium [4].

In this regard, thermodynamics constitutes a general framework in order to study manifold manifestations [5]. Therefore, using the thermodynamic variables such as volume or enthalpy, the equilibrium state at different temperatures can be described as shown schematically in figure 2.1.1.

The representation of figure 2.1.1 assumes that when cooling from the melt, a substance can either crystallize or transform to a glass depending upon the experimental conditions [6]. Had the crystalline state been allowed to form, a step change would have been observed at T_c. Conversely, a rapid heating or cooling from any temperature at which a glass is in equilibrium causes departures from these curves [4] as shown schematically by traces q_1 and q_2, leading to corresponding structural states A and B respectively.

Accordingly, these cooling rates, q_1 and q_2, are seen to give rise to two different glass transition temperatures, T_g (q_1) and T_g (q_2), defined by the intersections of the equilibrium liquid line and the asymptotic glassy line. The observed glass transition is essentially a Deborah number (DN) effect, named after the prophetess Deborah who declared that what appeared to mortals to be stationary, such as non-volcanic mountains and the size of the oceans are not necessarily so to an eternal deity [7]. The Deborah number is defined as the ratio of timescales of the observed and the observer, and the glass transition is seen when these two timescales for structural relaxation cross over and DN passes through unity [7].

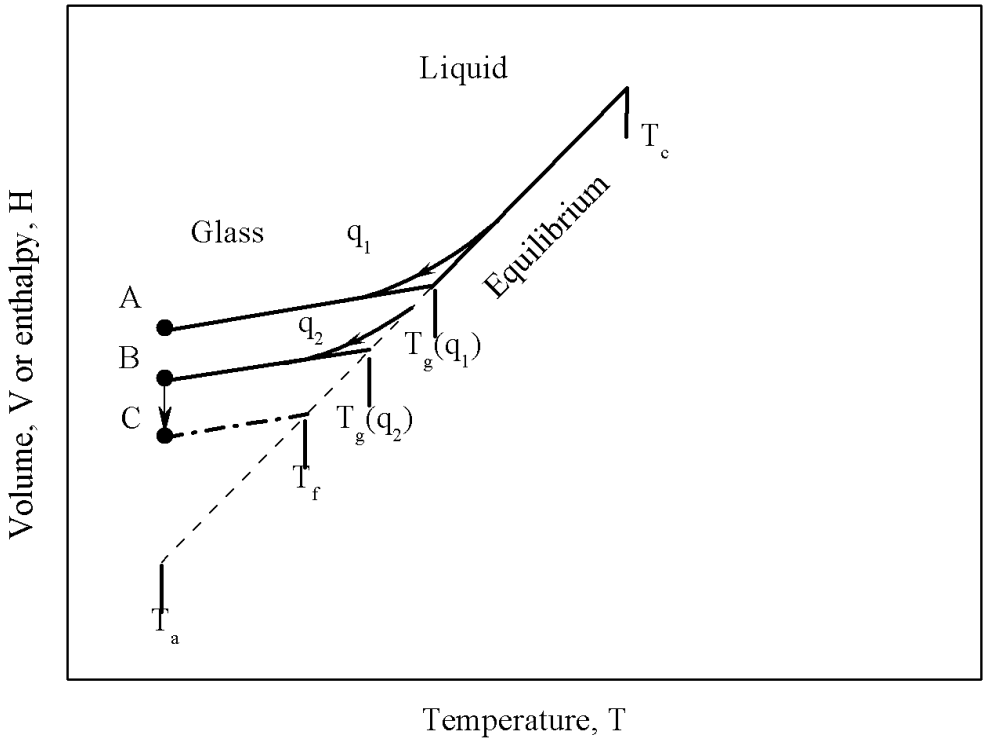

Figure 2.1.1.- Illustration from [6] of the temperature dependence of the volume (or the enthalpy H) of an amorphous material in the glass transition region.

Physical aging

As already mentioned, the configuration of a glass is not completely fixed, therefore if a glass is kept under constant temperature (or pressure), the spontaneous variation of its properties can be observed, which reflects the structure rearrangement [5] in a gradual approach to equilibrium termed “physical aging” [8].

Although there are studies based on thermal density fluctuations which show that physical aging is accompanied by an increase in local order, conformational analysis using Raman spectroscopy reveals little or no change in helical tg’t conformer population during the physical aging process [9] in accordance with FTIR investigations on Polycarbonate [10]. Therefore, losses of configurational entropy measured by enthalpic changes [11] were associated to extremely local rearrangements compatible with a densified structure [10].

Another aspect of physical aging is the nonlinearity or so called memory effect by which relaxation from a particular state depends not only on what that state is, but also on how that state was reached [12]. Accordingly, a glass contracts and evolves heat when equilibrium is approached from an undercooled condition (glass B to state C depicted in figure 1) but it expands and absorbs heat when equilibrium is approached from a superheated condition [4, 5]. Furthermore, the rates at which these heat effects develop depend on the rate at which the difference between actual and equilibrium temperatures is decreased and they are therefore controlled by the inelastic deformability [4].

Physical aging occurs in broad temperature ranges below T_g, and spans until the first secondary transition (T_β) [8]. For many polymers, the aging range includes the temperature range of practical interest [13].

It is also important to recognize that, although physical aging occurs in a wide variety of glasses and affects a large number of properties, the aging kinetics of a particular material are generally different for different properties [12]. Along with small decreases in the volume and enthalpy of glassy polymers on aging or annealing, rather profound changes are observed in some of the mechanical properties [14]. Thus, changes in one property cannot in general be predicted using parameters obtained from another property [12].

Of particular concern in the processing and application of polymers is the loss of general ductile behaviour of many polymers on aging or annealing at temperatures below their respective glass transition temperatures [14]. In fact, aging is a gradual continuation of the vitrification around T_g, therefore it will affect all those properties which in their dependence on temperature undergo drastic changes at T_g [13].

Increases of the yield stress in the range of 10MPa [15] and a severe reduction of notched impact strength [16] have been reported for PC after annealing under different conditions. Further evidences of ductile to brittle transition (BDT) in polymers have been given for PVC and PMMA [17] or PLLA [18, 19].

Modes of failure

Brittle fracture

Ward and Orowan [20], and latter Legrand [21] attributed BDT in polymers to a competition between fracture stress and yielding stress [22] where the preferential process, determines the mode of failure. Their argument was based on the energetic balance proposed by Griffith [23], who explained brittle fracture of elastically stressed solids by the presence of very small cracks that generate small volumes of stress concentration around them where the theoretical strength was overcome.

The concept of theoretical stress is linked to the existence of molecular cohesive forces that preserve the continuity of solids and liquids. The simplest way of obtaining a rough estimate of the molecular cohesion of a solid is from its surface energy [20]. Therefore, two new surfaces (of fracture) can be created in an elastically stressed isotropic solid if the elastic energy provides the surface energy of the surfaces of fracture [20]. Hence, the order of magnitude of the fracture stress σ_m must be

$$\sigma_m = \sqrt{\frac{2\alpha E}{a\pi}}$$ (equation 1) [20, 24]

Where σ_m is the tensile strength, α is the surface energy, E is the elastic modulus and a is the distance to overcome by external forces, that corresponds to the interatomic distance between two consecutive covalently bonded carbon atoms.

Yielding

In ductile fracture, on the other hand, the work done against the cohesive forces is usually negligible compared with the work of plastic deformation that has to be done in order to extend the crack [20].

Ductile mode of failure is featured by the yield or flow stress. Out of the realm of classical plasticity considerations and the aim to establish the yield criterion [25], early attempts to explain the plasticity of glassy polymers were based on modifications of the concepts of viscoelasticity [26].

Thus, the plastic deformability of polymers was first attributed to the heat generated accompanying the deformation which was assumed to raise the temperature above that of the glass transition [26]. However, simultaneous measurements of temperature during yield behaviour on polycarbonate, disclosed to be insufficient to be the cause of the strain softening (0.1ºC; strain rate: $5.2*10^{-3}min^{-1}$) [27].

Alternatively, based on the concept that molecular transport (mobility) in liquids and glasses was determined by the statistical redistribution of the free volume [28], it was suggested that stress-induced free volume [29] would produce the same molecular mobility existing at the glass transition temperature [26].

Years later, measures based on ortho-positronium lifetime studies of free volume in polycarbonate (PC) and polystyrene (PS) provided quantitative evidences of an overall increase of free volume on cold rolled samples that had underwent significant plastic deformation [30, 31], demonstrating that yield and the formation of free volume are governed by the same process [17]. However, Eyring's theory of activated flow [32] provided a narrow framework upon which, the yield behaviour of PC was fitted whereas yielding of PVC involved a secondary transition that required the addition of a second term in a generalized theory [33].

Conversely, the double kink model [26] considered secondary and other higher-order relaxation processes only as accompanying viscoelastic strains affecting the elastic stiffness of the surrounding continuum which momentarily stores the energy of activated molecular kink configurations [26].

In any case, the presence of β relaxation observed at low temperatures [34] has a different temperature dependence than primary or α relaxation [13], giving rise to thermo-rheological complexity [35], where the method of reduced variables and equations derived thereof are no longer applicable.

Self-reinforcing

The practical importance of yielding and cold-drawing found application in the technology of synthetic fibres after the pioneering work of Bailey [36], who disclosed that uniaxial orientation by stretching produced improved tensile strength and elongation to break in the stretch direction. More recently, self-reinforced composite materials [37-46] have taken advantage of the preferential structural arrangement [47].

An amorphous polymer is said to be molecularly oriented when the directions in space of the chain segments are not distributed randomly [48]. According to the statistical theory of rubber elasticity [49], upon application of an external stress, portions of molecular chains between network junctures tend to uncoil elastically, increasing the population of trans conformers and the Kuhn length which are harder to deform [50]. At the same time, enhanced by high temperature, new secondary bonds are formed in relaxed positions [51] which do not contribute to the strain hardening effect.

Therefore, to produce the highest levels of orientation, it is necessary to stretch the polymer rapidly to high stretch ratios at the lowest possible temperature, although limits beyond which fracture rather than stretching takes place must not be overcome [52].

A second effect of molecular orientation is the frozen-in entropy stress [48], which manifests itself when the temperature is varied. The frozen-in orientation, results in a negative contribution to the reversible coefficient of thermal expansion that causes the material expansion on cooling and contraction on heating [48, 53]. This thermal instability is the so called shape memory effect [54] that can be programmed in order to have multifunctional materials. However, limitations to this effect have been found due to the development of strain induced crystallization, demanding special attention to the study of the resulting changes in microstructure as a consequence of the programming conditions, as it will be explained in the third chapter.

The aim of the following section is to explore two alternative processing techniques i. e. solvent casting and compression moulding, of use in the plastic industry.

The evolution of the thermal and mechanical properties will be explained on the basis of the resulting microstructure analysis that will be characterized using different techniques.

Especial interest will be focused on the peculiarities of physical aging, which will be studied from different approaches, such as retardation enthalpy, stress relaxation and yielding.

Finally, hot drawing will be studied as an alternative post-synthesis method to influence the microstructure of amorphous and semicrystalline compression moulded polymers.

Materials and methods

Table 2.1.1 includes the relation of polymers used in this study. Their molecular weights (M_w) as well as their polydispersity index (D) were determined by GPC with reference to polystyrene standards. PLLA PL18, and copolymers were supplied by Purac Biochem (The Netherlands). PLLA Biomer L9000 was supplied by Boehringer Ingelheim (Germany).

Table 2.1.1.- Resume of polymers and their molecular weight, polydispersity index and test.

Name	Ref	M_w (kDa)	D	Test/study
PDLGA 55/45	110600655	100.3	1.65	MDSC, DMA
PDLGA 55/45	0701000351	164.0	1.51	S-R
PLCL 70/30	RDT 0971	177.5	1.69	DSC
PLCL 70/30	1008000233	198.2	1.77	DSC, S-R
PDLLA 51/49	0303001995	540.0	2.28	S-R
PLLA PL18	0710001980	150.0	1.25	S-R
PLLA Biomer	L9000	160.0	1.7	Tensile

The mole fraction of PLLA and PCL, as well as, the degree of randomness (η) of the L-Lactide/ε-caprolactone copolymers were determined by ^{1}H and ^{13}C Nuclear magnetic resonance spectroscopy in a Bruker Avance DPX 300, which corresponds to

300.16 and 75.5 MHz frequencies for ^{1}H and ^{13}C respectively, in 5mm o.d. sample tubes using 0.7ml of CDCl3 at room temperature (≈30ºC).

Conformation and thermo(mechanical) treatments

0.2mm thickness films were obtained by solvent evaporation from a 10% w/v solution (2g/20ml) of PLCL in chloroform. Another set of films was obtained by quenching from 180ºC into iced water bath.

Annealing treatments of pellet samples of PDLGA and PLCL were carried out in the DSC. Those included a previous heating step simulating the thermoconformation process by which samples were initially heated to 100ºC or 180ºC in order to erase the previous thermal history and maintained at this temperature for 20 minutes. Then they were cooled down following different cooling rates depending on the microstructure or energetic target. In the case of PDLGA, the selected cooling rates of 0.5 or 50 °C min^{-1} lead to corresponding energetic states as will be discussed later. For both PLCLs, cooling ramp was set to 50ºC/min in order to achieve a fully amorphous state. Annealing conditions were selected in order to maximize the aging effects. Accordingly annealing temperature of PDLGA samples was 37ºC (8ºC below corresponding T_g) and 8ºC for PLCL (14-16ºC below that of PLCLs).

The oriented states were obtained by stretching dumbbell samples of PDLLA, PLCL, PLGA and PLLA at 55ºC, 39ºC, 45ºC and 60ºC respectively to ε=600% at a constant crosshead speed of 5mm/min. In order to obtain reproducible data, relaxations under such strain at each corresponding temperature were carried out [49] for 5minutes before quenching to room temperature.

Thermal crystallizations on PLLA and PLCL were carried out in an oven. Time and temperature for PLLA were 3h and 100ºC whereas PLCL required ~20 days at 45ºC.

Thermal characterization

The resulting states from the conformation procedure and subsequent annealing treatments were evaluated from the first scan in a Differential Scanning Calorimeter

(DSC) Q-200 from TA Instruments, calibrated with pure indium and sapphires, where 5-10mg samples were heated from -60ºC or room temperature up to 180-200ºC (depending on the polymer) at 10ºC/min. Thermal properties such as glass transition temperature (T_g), its associated heat change (ΔC_p) and enthalpic relaxation (δ_H) using a linear base line, cold crystallization and melting enthalpies (ΔH_{cc} and ΔH_m), where applicable, were therefore obtained by means of TA universal software. From integration of these peaks, the overall crystallinity degree was calculated according to equation 1 considering the enthalpy of fusion of the polylactide crystal $\Delta H_m^0 = 106 J/g$ [55]

$$X_c(\%) = \frac{\Delta H_m - \Delta H_{cc}}{X_{PLLA}\Delta H_m^0} * 100 \text{ (equation 2)}$$

When a more detailed study of the enthalpic relaxation was desired, as in the case of PDLGA, modulated scans were performed on 4-6mg samples where a sinusoidal heating ramp of 0.75°C modulation amplitude and 120s period was run at 0.5ºC/min. To correct the frequency effect, after the heating process above T_g, the samples were cooled under the same MDSC conditions as used for heating. Any peak area in the non-reversing signal on cooling can only be caused by the frequency effect. Thus, this area was subtracted from the peak area obtained on heating to calculate the peak area that corresponds just to the enthalpic recovery.

Thermogravimetric analysis was performed by means of a TGA Q50 from TA instruments in the temperature range from room temperature to 600°C, with a heating rate of 5ºC/min under 60ml/min nitrogen flow on 10-20mg samples. Solvent content of cast films was thus evaluated by determination of the weight loss experimented by the samples in the range of ≈ 100ºC, well below the thermal degradation temperature of the polymers.

X-ray diffraction

The X-ray powder diffraction patterns were collected by using a Philips X'Pert PRO automatic diffractometer operating at 40 kV and 40 mA, in theta-theta configuration and with a secondary monochromator with Cu-Kα radiation (λ = 1.5418 Å). A PIXcel solid state detector in scanning mode with 3.347º of active length was used. The samples were mounted in a generic sample holders and spinning of 4s of revolution time was

applied. Data were collected from 10 to 50° 2θ (step size = 0.0262 and time per step = 150 s) at RT. A fixed divergence and antiscattering slit giving a constant volume of sample illumination were used.

Mechanical and dynamical characterization

Tensile tests and orientation of the samples were carried out in an Instron Universal Testing machine 5565, equipped with a heat chamber, at a constant crosshead speed of 5mm/min. The Young's modulus, the secant modulus, the yield stress and strain and the ultimate stress and strain were calculated from the nominal stress-strain diagram. Tensile tests were conducted under controlled conditions of 21±2ºC temperature and 55±10% relative humidity.

Dynamic Mechanical Analysis was performed in a Mettler Toledo DMA/SDTA 861e, in tensile mode. Force-displacement amplitudes were 3N-30μm for PLCL and 0.5N-25μm for the others. Single frequency tests were conducted at 1Hz whereas isothermal frequency series tests were performed in the range of 50 to 0.05Hz at 5 steps per decade. Starting temperature was 25-30ºC below T_g and end temperature 25-30ºC above T_g as determined by DSC for each polymer.

Results and discussion

Casting. Thermal characterization

Solvent evaporation was monitored by means of sequential thermogravimetric analyses (TGA) conducted at different stages since the polymer solution was poured onto the petri dish. Figure 2.1.2 shows the TGA conducted on a PLCL film 21hours after casting. In there, the evaporation of the solvent can be easily distinguished from the thermal degradation of the polymer, occurring this later at a higher temperature.

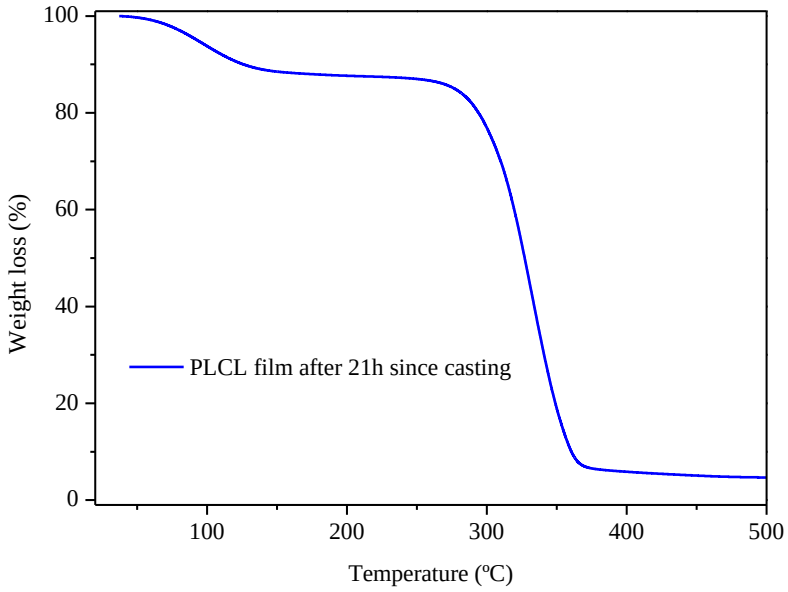

Figure 2.1.2.- Thermogravimetric analysis of the PLCL film 21hours after casting.

As time proceeds, chloroform gradually evaporates from the film as it is reflected in figure 2.1.3 where the weight loss ascribed to solvent evaporation is plotted at the corresponding time of measurement. Taking into consideration that the starting solution was 10%w/v, it follows that solvent evaporated mostly within the early hours, whereas the evaporation rate was severely decreased after 120hours following an asymptotic trend.

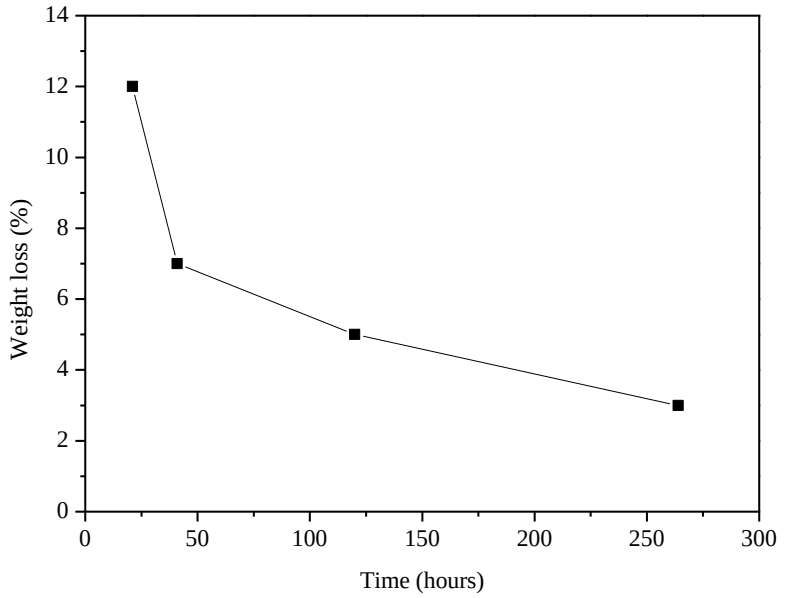

Figure 2.1.3.- Weight loss evolution along drying time.

In an analogous fashion, the evolution of the thermal properties of the cast films was monitored by DSC. For the ease of comparison, a film was obtained by quenching from the melt and further characterized.

The set of thermograms is plotted in figure 2.1.4. In there the gradual evaporation of solvent can be inferred by the evolution of the glass transition temperature towards higher values as well as by the disappearance of the second thermal event.

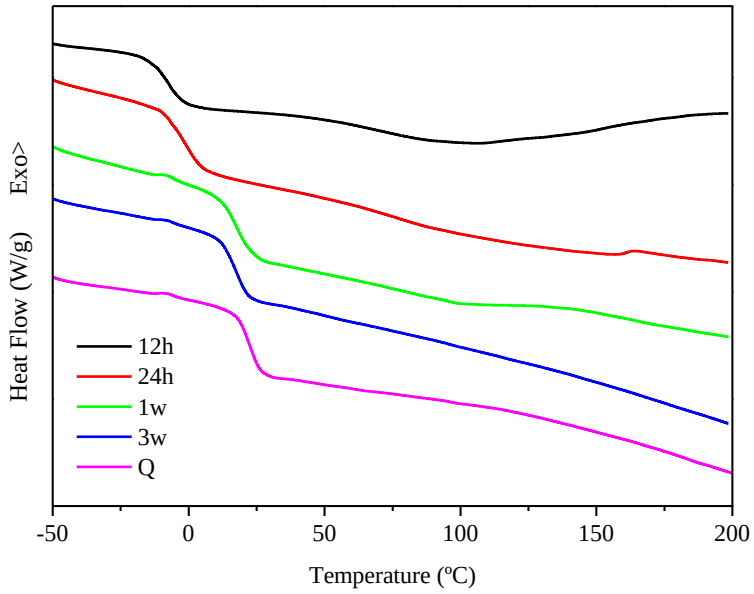

Figure 2.1.4.- DSC thermograms of cast and quenched films of PLCL.

Interestingly, the 3weeks film thermogram is very similar to that of the quenched film, in that the only disclosed event corresponds to the glass transition, although its apparition happens at a somewhat lower value than in the thermogram of the quenched film. This difference is highlighted in figure 2.1.5, where the T_gs from figure 2.1.4 are plotted correspondingly.

According to the early theories of free volume and the liquid lattice model [28] it is suggested that when the solvent is evaporated, it leaves an empty site that can be occupied by the polymer molecules, increasing the number of possible configurations and accordingly configurational entropy. As the solvent evaporation rate is slow, the polymer chains accommodate consequently in a configuration close to that of equilibrium, with a lower value of T_g.

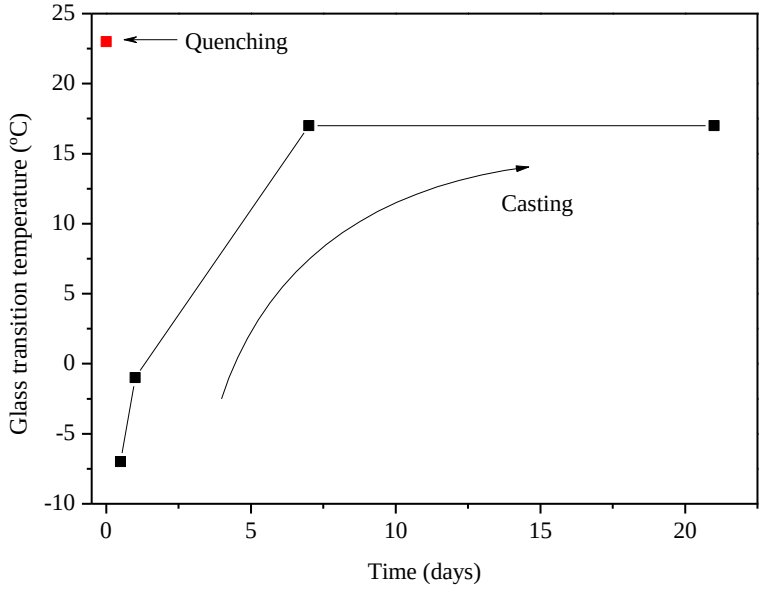

Figure 2.1.5.- Evolution of T_gs with drying time of cast films in comparison with that of the quenched film.

Conversely, when the structural state is reached by rapid cooling from the melt, fluidity decreases many orders of magnitude in a narrow temperature range (glass transition range) [28] and chain molecules cannot rearrange in order to follow the thermodynamic equilibrium, deviating from it. Due to the kinetic nature of the glass transition, the more rapid the cooling is performed, the higher the temperature the deviation is noted, and the higher the T_g.

Casting. Mechanical characterization

Tensile behaviour shown in figure 2.1.6 further discloses the plasticising effect of solvent casting. Being preserved the elastomeric character of PLCL, quenched film exhibited superior stress at break as well as elastic modulus than cast films. In the case of the 24h cast film, the 12% solvent content, as measured by TGA, caused high mobility of chain molecules, reducing intermolecular cohesive forces between chain molecules, thus boosting the deformation imposed by the tensile test at low levels of stress. The 14 days casting film, exhibiting strengthened properties compared to the 24h film, did not achieve the stress levels of the quenched film and broke at lower elongation than the others.

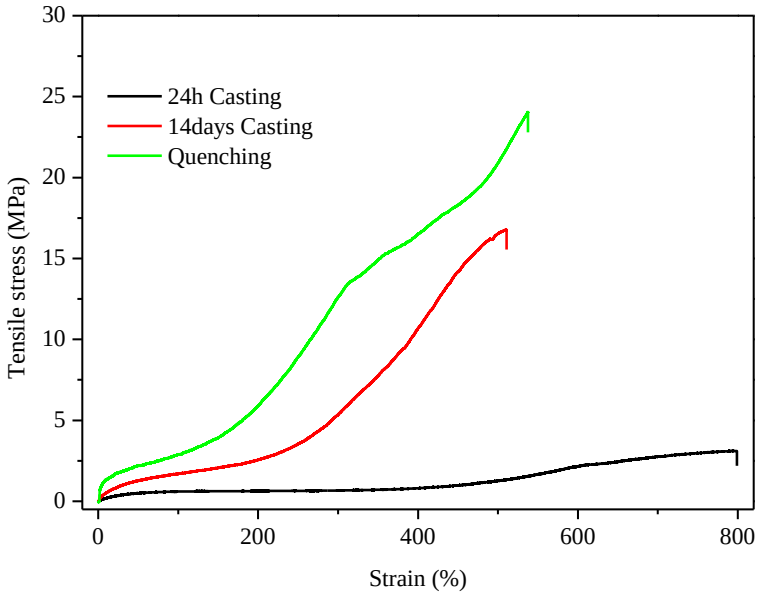

Figure 2.1.6.- Stress-strain graph of quenched and cast films.

Photographs taken from the 14days casting film, as the one shown in figure 2.1.7, revealed the presence of cavities preferentially located at grain boundaries. It is suggested that these cavities may contribute to the mobility of chains in a microscopic scale whereas at a macroscopic scale, not only they reduce the effective section that bears the load during the tensile test, but also promote crack propagation and premature failure.

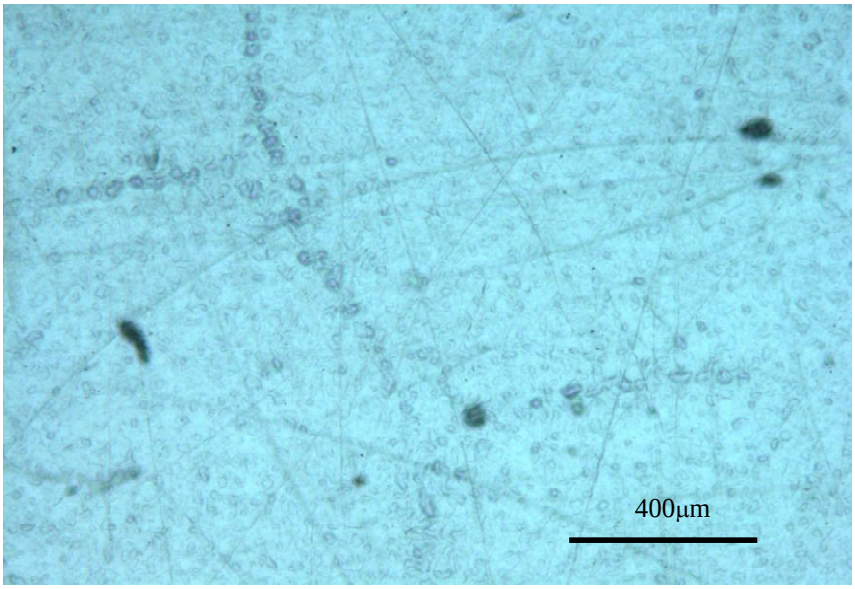

Figure 2.1.7.- Microphotograph of cast film revealing the presence of cavities.

Thermoconformation. Physical aging

Effects of cooling rate

Effects of cooling rate and further annealing on the glass transition temperature and enthalpy relaxation have been studied on glassy PDLGA as a model polymer. Accordingly, two cooling ramps representing a rapid (quenching) and a slow departure from equilibrium have been performed in a modulated differential scanning calorimeter.

The main advantage of modulated scans lies in the separation of overlapping effects allowing to analyse them independently, such as in the case of relaxation enthalpy and glass transition. Upon the application of an oscillating heating ramp, the reversing part of the signal, i.e. the real part of heat capacity C_p, is perfectly in-phase with the modulated heating rate. Conversely, the kinetic processes such as relaxation enthalpy are reflected in the non-reversing part of the signal.

Figures 2.1.8 and 2.1.9 show the reversing and non-reversing C_p respectively of the heating scans after cooling and further annealing at 37ºC at increasing annealing times. In order to minimize errors due to sample preparation or relocation of pans in the same position in the MDSC holder, both sets of annealing treatments were conducted on the same sample in the MDSC. Therefore, for practical reasons the maximum annealing time was restricted to 24hours although further experiments revealed that this time is not enough for enthalpy to reach its equilibrium value at 37ºC. The glass transition temperature (T_g) was defined from the inflection point of the reversing C_p signal. Enthalpy recovery (δ_H) was obtained from integration of the non-reversing C_p signal. In order to delete the frequency effect, a cooling ramp was conducted under the same modulation conditions and subtracted from the values obtained from the heating ramp. The peak temperature (T_p) or maximum of the enthalpic endotherm was also monitored. Complete characterization is resumed in table 2.1.2.

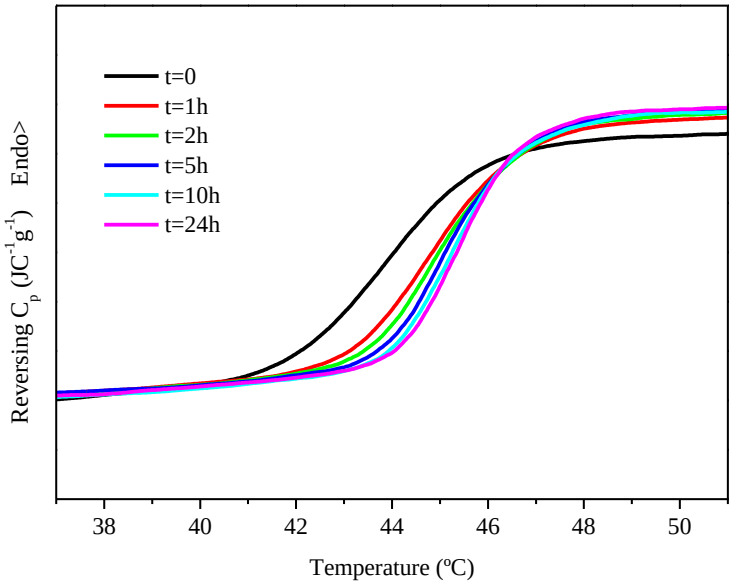

Figure 2.1.8.- Reversing C_p of PDLGA samples aged at 37ºC after being slowly cooled at 0.5ºC/min from 100ºC for the time (in hours) indicated by the legend.

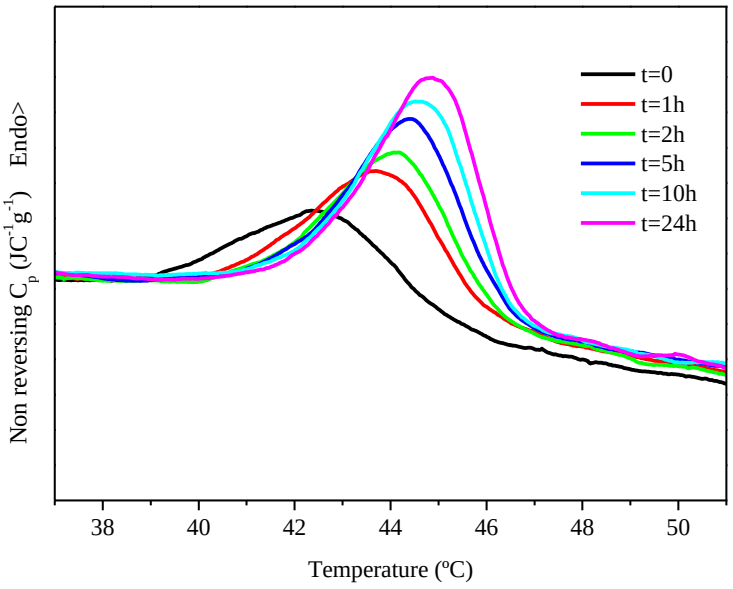

Figure 2.1.9.- Non-reversing C_p of PDLGA samples aged at 37ºC for the time (in hours) indicated by the legend after full annealing at 0.5ºC/min from 100ºC.

As it can be seen in table 2.1.2, rapid cooling yields a higher T_g indicating that departure from equilibrium happened at a higher temperature than by slowly cooling. Accordingly, the lower value of enthalpy relaxation further points to a structural state

closer to the liquid than to the glassy state. Furthermore, the T_p showed a maximum, ("upper peak") indicating a poorly stabilized glass [56] due to the high cooling rate.

Table 2.1.2.- TMDSC results for the PDLGA melts aged at 37ºC after supercoolings from 100ºC following two different cooling rates, that is to say 0.5 and 50ºC/min.

Cooling rate $^oCmin^{-1}$	**Time** h	T_g ºC	δ_H Jg^{-1}	T_p ºC
0.5	0	44.0	1.20	42.5
	1	44.8	1.87	43.7
	2	44.8	1.89	44.2
	5	45.0	2.09	44.5
	10	45.3	2.22	44.7
	24	45.5	2.78	44.9
50	0	44.9	0.39	44.1
	1	44.9	1.38	43.6
	2	44.7	1.83	43.9
	5	44.9	2.13	44.3
	10	45.1	2.20	44.4
	24	45.1	2.70	44.7

Also illustrated in table 2.1.2 is the increase of T_g, δ_H and T_p with isothermal annealing for both set of samples, suggesting a densification of chain molecules as a consequence of excess enthalpy and volume reduction. Accordingly, when the glasses were reheated during the heating scan, more energy was required for the glass transition as reflected by the increase of the area under the endothermic peak. Moreover, because of the reduction of segmental mobility, it was necessary to heat up to higher temperatures to finish the morphological rearrangement which occurred in the glass transition process [18].

Figure 2.1.10 shows the self-retarding kinetics of δ_H where the reduction of free volume as a consequence of physical aging is responsible for the reduction of the rate of properties change [8, 5, 30].

Generally, it is convenient to express the enthalpy changes that occur during isothermal annealing of a glass in terms of alterations in the enthalpy displacement from the equilibrium glassy state, i.e. (Q_E-Q_t). Enthalpy relaxation data expressed in this manner are in terms of properties of the well-defined equilibrium glassy state, rather than those of the generally poorly defined initial state [14].

Thus, a determination of the energy absorption in the T_g region for a corresponding sample in its equilibrium glassy state under the same programming conditions is necessary [14]. For the practical reasons described above, the enthalpy measured after 24hours annealing will be taken as the equilibrium although it is an oversimplification. If more accurate values were sought further annealing should be necessary.

Enthalpy relaxation data obtained from PDLGA during isothermal annealing at 37ºC are given in figure 10 were the excess enthalpy (Q_E-Q_t) is plotted as a function of log time. As it can be noted, the slope of (Q_E-Q_t) /log t is lower for slowly cooling, indicating a slower relaxation rate for full annealed samples.

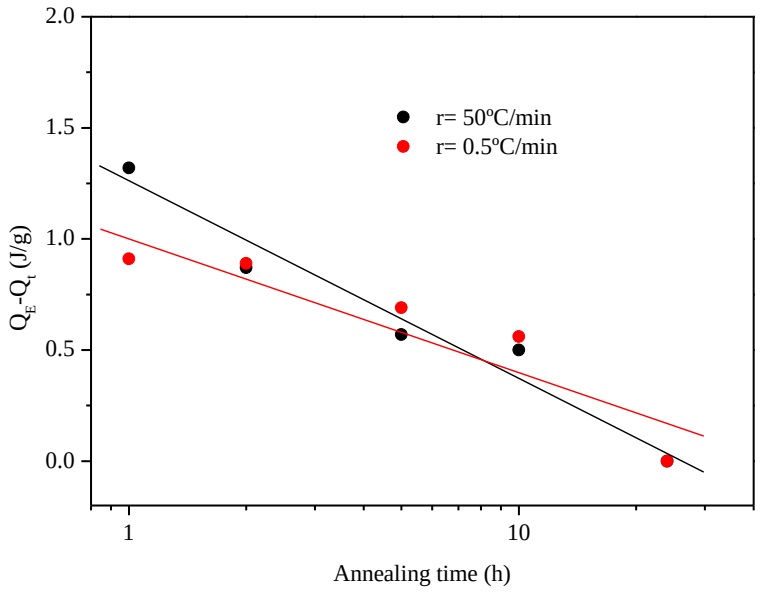

Figure 2.1.10.- Enthalpy relaxation data and linear fitting for both sets of cooling and annealing treatments on PLGA.

Effects of chain topology

In order to gain information of the effect of chain topology on the kinetics of physical aging, two 70/30 poly(l-lactide-co-ε-caprolactone) copolymers with differing sequence lengths have been investigated. Due to the high aspect ratio (C_∞) reported for PLA, it is considered to have a stiff chain backbone [9, 18, 57]. Therefore, the random introduction of caprolactone segments is expected to decrease the overall chain stiffness, whereas a more ordered disruption is not. Molecular characterization by ^{1}H NMR was conducted in order to determine the randomness coefficient (R) according to equation 3

$$R = \frac{(LA-CL)}{2(LA)(CL)} \text{ (equation 3)}$$

where (LA) and (CL) denote the molar fraction of lactide and caprolactone respectively, and (LA-CL) the lactide-caprolactone diad. Thus, the copolymer with R→1 was considered to have higher randomness character, whereas R→0 featured a higher blocky character. The result of molecular characterization is resumed in table 2.1.3.

Table 2.1.3.- Molecular characterization data of PLCL-R and PLCL-B

	Determined by GPC		**Determined by ^{1}H NMR**		
	M_n	**D**	**PLLA**	**PCL**	**R**
Ref.	**g/mol**	**-**	**%**	**%**	**-**
PLCL-R	112,000	1.77	69.2	30.8	0.94
PLCL-B	105,000	1.69	67.1	32.9	0.7

The results of table 2.1.3 indicate that PLCL-B has a larger multiblock character than PLCL-R.

Figure 2.1.11 shows the total heat flow recorded during the heating scans of the annealed samples. As it can be noted, the reversing (glass transition) and kinetic processes (enthalpy relaxation) overlap in the same graph. Isothermal annealing was conducted at 8ºC (T_a=T_g-16ºC) and the associated evolution of thermal parameters is summarized in table 2.1.4. In both samples T_g and enthalpy relaxation increased with aging time although this evolution was more readily seen in PLCL-R than in PLCL-B.

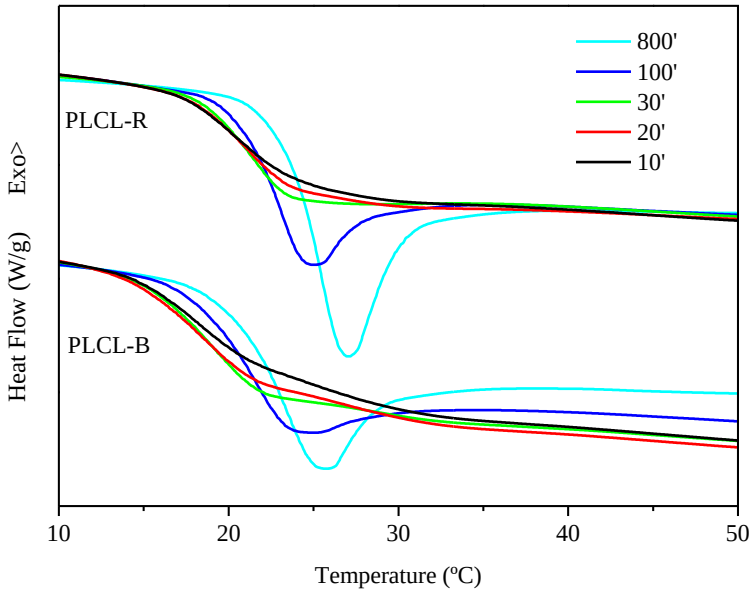

Figure 2.1.11.- DSC curves in the glass transition region of PLCL-R and PLCL-B samples annealed at 8ºC for 10, 20, 30, 150 and 800min.

Table 2.1.4.- Annealing time (t_a) and corresponding measured thermal characteristics: glass transition temperature (T_g), specific heat change (ΔC_p), Enthalpy relaxation (δ_H) and peak temperature (T_p).

Ref.	t_a min	T_g ºC	ΔC_p J/gºC	δ_H J/g	T_p ºC
PLCL-R	10	20.5	0.57	-	-
	20	21.3	0.54	-	-
	30	21.2	0.52	0.27	23.6
	150	22.8	0.50	1.38	25.0
	800	24.6	0.50	2.48	27.0
PLCL-B	10	18.3	0.42	-	
	20	18.7	0.48	-	
	30	18.9	0.47	-	
	150	21.7	0.49	0.74	24.7
	800	23.5	0.51	1.59	25.7

Effects of annealing time

The kinetics of aging was studied from the evolution of the glass transition temperature with annealing time taken as the relaxation time (τ). Considering an Arrhenius dependence of temperature, the more random copolymer gave a higher slope than the blocky copolymer, supporting the idea of a speeded kinetics due to the enhanced flexibility associated to the higher randomness character, thus easing the rearrangements of the chain backbone during structural relaxation. Similar conclusions were disclosed for PDLLA copolymer with increasing D-lactyl content [9].

Further insight into physical aging was sought making use of the Time-Temperature-Superposition (TTS) principle, and master curve construction [51]. This approach, uses temperature to change the scale of time or frequency [35], but its applicability is restricted to thermo-rheologically simple polymers. Hence, the complex modulus obtained from a series of isothermal frequency scans were represented as a function of the corresponding phase angle in figure 2.1.12 according to the Mavridish and Shroff's [58] and van Gurp and Palmen [59] procedure to evaluate the thermorheological complexity, as simplicity cannot be proven [60], of the available data. As it can be noted, data from different temperatures did not superimpose indicating thermo-rheological complexity.

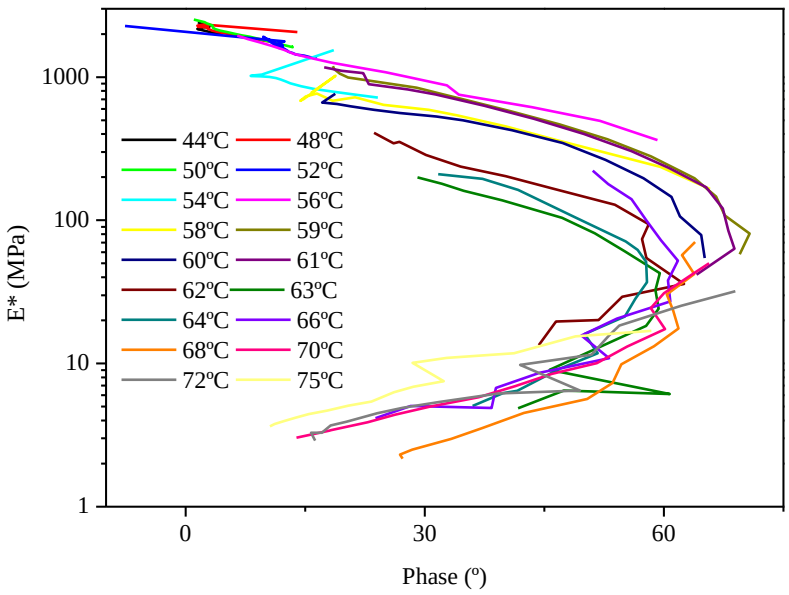

Figure 2.1.12.- Graphical representation of complex modulus E* vs phase lag in degrees.

Therefore, the relaxation process was monitored following a different approach. The dynamic spectra E'(T) and E"(T) were measured at four different frequencies, and from the Arrhenius representation of the corresponding relaxation times against the inverse of E" peak temperature, the activation energy of the glass transition was compared for increasing annealing time.

The shift of the relaxation spectrum towards higher temperatures with increasing annealing times was observed in all cases. As an example, figure 2.1.13 shows the evolution of E'(T) measured at 0.1Hz. In there, the effects of aging can be easily distinguished in the glassy part of the spectrum through the increased value of the storage modulus and its delayed temperature onset whereas the annihilation of the previous history is reckoned by the collapse of the curves in the rubbery region. Besides, in agreement with observations in reversing C_p, the transition from glassy to rubbery state completes in a narrower range of temperature as annealing time was increased.

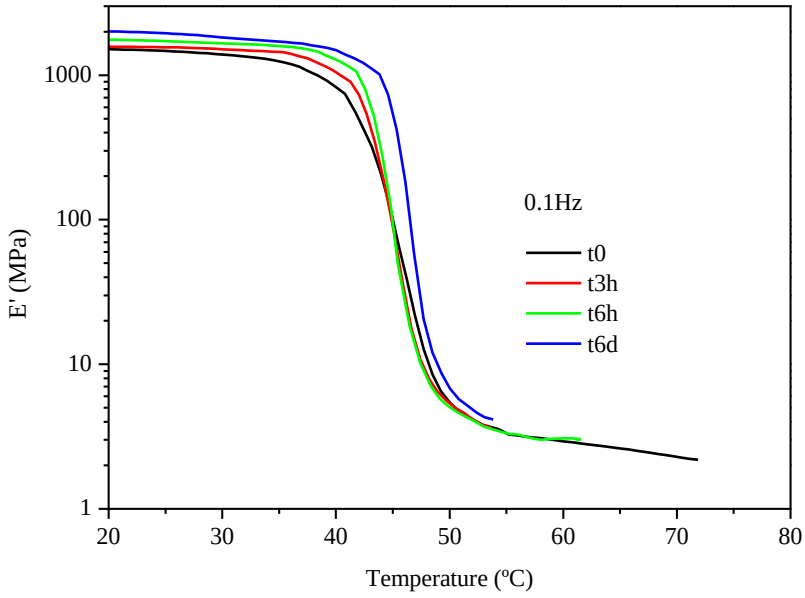

Figure 2.1.13.- Relaxation of storage modulus at increasing annealing times. Tests performed at 0.1Hz in the tensile mode.

Representing the natural logarithm of the inverse of the test frequency (τ) against the inverse of observed temperature peak in E", the activation energy of the transition was estimated from the slope of the linear fitting shown in figure 2.1.14 and resumed in table 2.1.5 supposing an Arrhenius relation

$$\frac{1}{f} = \tau = Aexp^{\frac{\Delta H}{RT}} \text{ (equation 4)}$$

where R= 8.32J/Kmol.

Table 2.1.5.- Resume of temperature peak in E" at indicated frequency and annealing time

Test frequency Hz	**t0 ºC**	**t3h ºC**	**t6h ºC**	**t6d ºC**
0.03	36.6	38.1	38.5	40.9
0.1	40.7	41.5	42.7	44.3
1	42	42.8	43.4	46.6
10	44.7	46.4	45.5	48.1

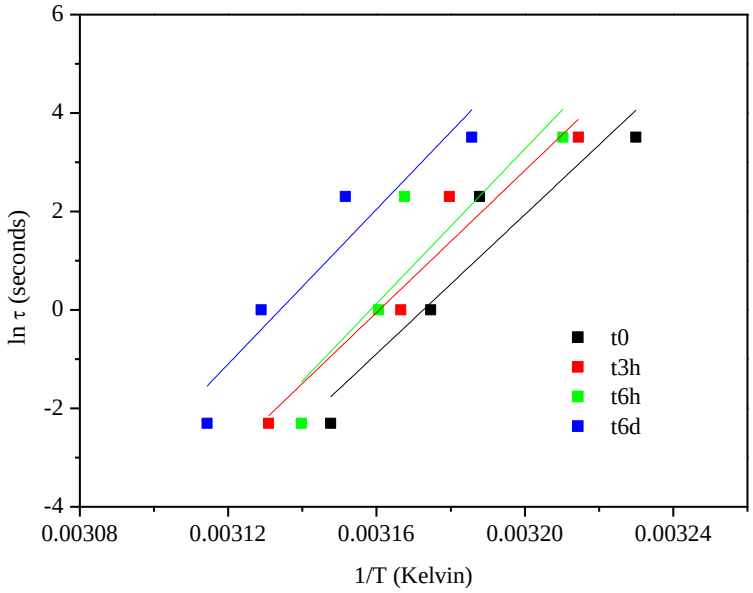

Figure 2.1.14.- Arrhenius plot and linear fit of the observed peak temperatures for increasing annealing time at 37ºC

Table 2.1.6.- Details of linear fit from figure 14.

	ΔH	**Adj. R^2**
	kJ	**-**
t0	588.7	0.8392
t3h	600.4	0.9083
t6h	654.0	0.7311
t6d	653.9	0.8572

From table 2.1.6, it can be seen that the linear fit could be improved, although a clear increasing trend must be reckoned although considering that aging of a glass is a self retarding phenomenon, in which the characteristic relaxation time for the process is a structure (or time) dependent parameter at any $T_a<T_g$ [11], highest differences were expected to happen during the early hours, where deviation (and consequent driving force) between the starting structural state and the equilibrium glassy state is maximum. Conversely, it seems that aging kinetics was more active between 3 and 6 hours' aging, stabilizing at 654kJ.

Ductile to brittle transition

Samples of PLLA were tested at increasing time intervals elapsed since their thermoconformation. Until the test, samples were kept at a constant temperature of 20ºC. Neck formation was observed in all samples tested immediately after conformation, as shown in figure 2.1.15. As aging time increased, the percentage of samples that exhibited neck formation was seen to decrease at the same time that the number of samples that brittle fractured raised. Interestingly, after 120minutes both modes of failure equalled, but after 210minutes the 100% of the samples fractured in a brittle manner.

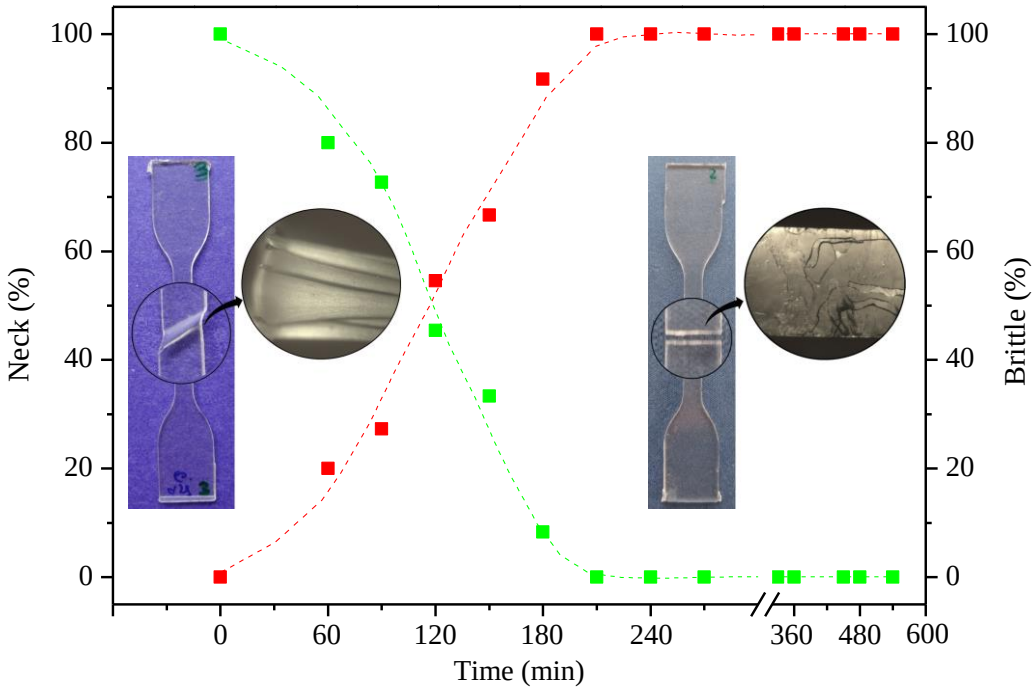

Figure 2.1.15.- Observed modes of failure on PLLA within 24hours.

Microphotographs taken from the surface of failure further disclose the disruption mechanisms. In the microphotograph on the left, sharp edge-on surfaces are due to continued thinning until both parts of the neck finally separate. Conversely, the micrograph on the right side of the graph reveals the surface of fracture caused by normal stresses acting to separate one atomic plane from another [23].

In order to gain full insight into the intrinsic behaviour of PLLA, the true stress-true strain was plotted in figure 2.1.16 where, for the ease of simplicity only the most representative graphs are shown. As indicated in the legend, they correspond to samples immediately tested (t0), and 120 (t120min), 240 (t240min), and 1440 (t1440min) minutes respectively after thermoconformation.

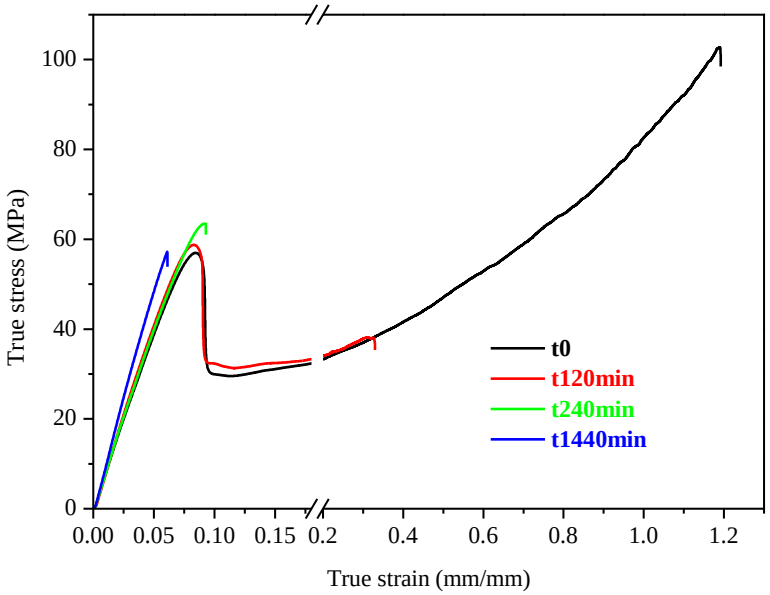

Figure 2.1.16.- True stress-true strain representation of tensile behaviour

The tensile behaviour of samples tested immediately after conformation exhibited a marked yield drop, indicator of strain softening and the consequent macroscopic necking. After yielding, the previous history is erased [29], and the drawing stress (σ_d) showed by the stress drop was independent of previous aging. Further stretching caused cold drawing and subsequent strain hardening as described by the increase in slope until failure by a rupture mechanism. As aging time proceeded, the eventual disappearance of the ductile part was noted until it was relieved by brittle fracture.

As the mode of failure is determined from a competition between yielding and fracture [20, 22], where the preferential process is the more energetically favourable, an estimation of the volumetric energy of fracture (ρ) was obtained from integration of the stress-strain curves. Values calculated thereof yielded $67.5*10^6$ Jm^{-3} for $PLLA_{t0}$ whereas

the corresponding for $PLLA_{t1440}$ was reduced to $1.80*10^6$ Jm^{-3}, quantifying thus the loss of toughness.

The process can be explained considering yielding as a stress activated phenomenon, in which the more aged is the sample, the more mechanical work is required to draw the material out of the rigid glassy state [29]. Accordingly, where ductile behaviour was noted, σ_Y was observed to rise up to 1.6MPa further supporting this idea, whereas as expected, ε_Y and the drawing stress (σ_d) remained essentially unaltered. Based on the theory of cracks developed by Griffith [23] in order to explain brittle fracture of elastically stressed glasses, and the surface energy of PLLA reported by Neuendorf [61] and corrected to room temperature, according to equation 1

$$\sigma_m = \sqrt{\frac{2\alpha E}{a\pi}}$$ (equation 1) [20, 24]

where σ_m is the tensile strength, α is the surface energy, E is the elastic modulus an estimation of the size of the crack a was calculated to be in the order of 6.7nm.

However, it must be reckoned that a more accurate study of the fracture energy should be measured in terms of the strain energy release rate and not by the area under the stress strain graph, because so many other phenomena may be at play [62].

From the conventional representation of the tensile tests, that is regarding the initial cross sectional area, the mechanical properties including the elastic modulus (E) calculated from the slope of the linear part of the graph, the yield strength (σ_Y) taken as the maximum after the elastic segment, the corresponding strain (ε_Y), and the stress (σ_B) and strain (ε_B) at break were obtained and listed in table 2.1.7.

As it can be noted, within experimental errors, the elastic modulus shows an increasing trend for increasing time of aging. It is also noted that whereas the strain at yield was observed at a constant value for increasing time, the necessary stress to produce yielding eventually raised until it was no longer affordable, from an energetic standpoint, being replaced by fracture at essentially the same value of strain.

In the same table, the two opposite modes of failure have been emphasised by separately indicating ductile and fragile values of stress and strain.

Focusing on the values of stress at rupture, three ranges of stress level (~27MPa; ~45MPa and ~54MPa) can be distinguished, that can be better understood with the aid of figure 2.1.17.

Fresh samples failed by collapse after significant drawing, at any point; 1, 2 or 3 in figure 2.1.17, depending on internal defects, giving rise to the severe deviations of strain, but at a constant value of stress ~27MPa. As aging proceeded, the strain at failure advanced backwards, into the post yield region (points 4 and 5), so that high dispersion was observed in σ_B where ductile rupture had developed whereas ε_B leaned to stabilise.

After 3.5hours of aging, yielding was no longer observed, as all samples failed by brittle fracture in the pre yield region (points 6 and 7) around a constant value of stress ~54MPa, which is lower than the previously observed stress at yield of fresh samples, and around a constant value of strain ~10%.

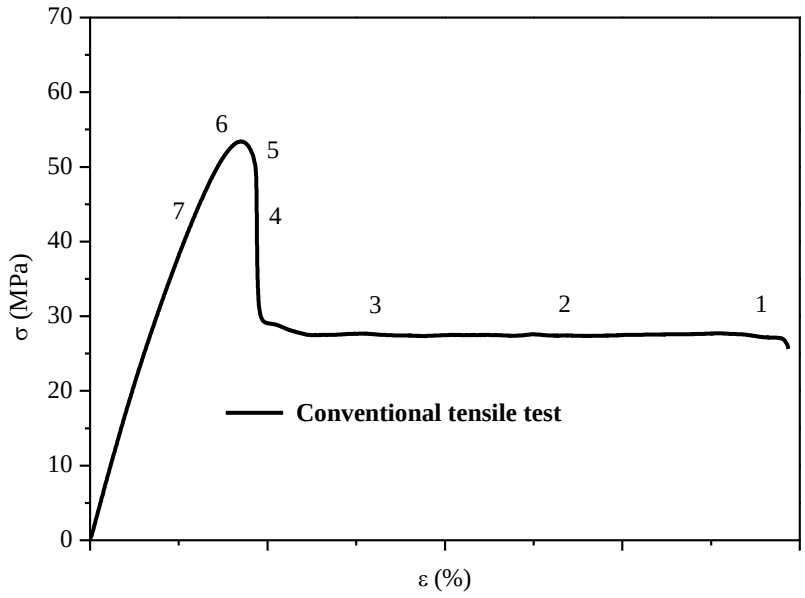

Figure 2.1.17.- Conventional tensile tests with neck formation and cold drawing

Table 2.1.7.- Mechanical properties calculated from tensile tests

				Ductile		Fragile	
	E	**σ_Y**	**ε_Y**	**σ_B**	**ε_B**	**σ_B**	**ε_B**
	MPa	**MPa**	**%**	**MPa**	**%**	**MPa**	**%**
t0	811±15	52±1	9.9±0.3	28±1	38±28		
t60	832±46	54±1	10.1±0.2	27±1	37±39	40±18	9.9±0.5
t90	810±18	55±1	10.2±0.4	29±0.5	37±43	51±4	10.3±0.5
t120	813±38	55±1	10.1±0.2	25±3	32±13	56±6	10.0±0.6
t150	825±52	57±1	10.6±0.8	40±12	20±9	54±3	10.2±0.7
t180	835±36	58±1	9.8±0.7	45±14	15±4	54±2	9.8±0.4
t210	814±34	58±1	10.1±0.5	46±15	14±3	53±2	10±1
t240	789±38					53±6	10±2
t270	841±42					54±5	10±1
t330	833±37					54±2	9.4±0.5
t360	838±49					56±2	10±1
t450	866±35					54±2	9.2±0.6
t480	800±41					57±1	10.7±0.7
t1440	886±47					54±3	9±1

As the reason for necking in tensile specimens is non-uniformity and localization [63], the eventual annihilation of strain softening in favour of uniform deformation can be obtained by increasing the test temperature (figure 2.1.18) or alternatively decreasing the strain rate (figure 2.1.19).

As it can be noted from figure 2.1.18, σ_Y decreased with increasing the test temperature, suggesting the idea of yielding as a type of reaction that proceeded more readily at high temperature [31]. Moreover, although a certain extent of aging can be inferred, a glassy to rubbery transition was observed when test temperature approached the glass transition temperature of PLLA.

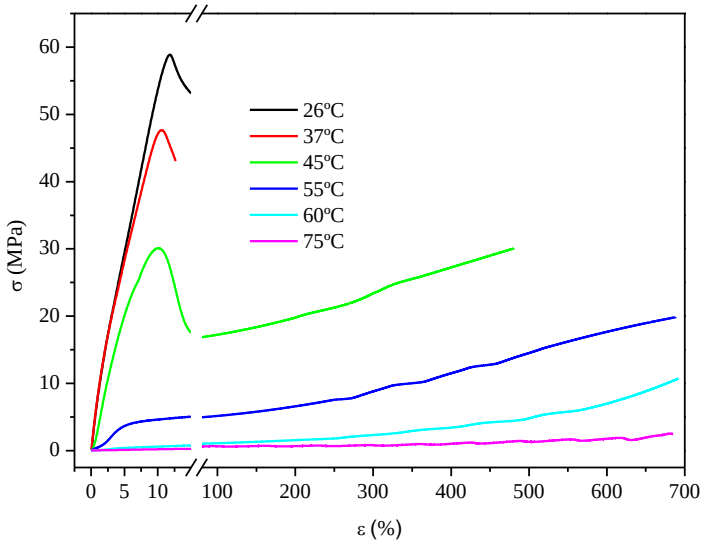

Figure 2.1.18.- Tensile tests of PLLA conducted at indicated temperatures

Further testing at 60ºC, revealed the dependence of yield with strain rate ($\dot{\varepsilon}$) as shown in figure 2.1.19. At this temperature, the reduction and eventual disappearance of stress drop and subsequent delay in strain hardening was noted for decreasing $\dot{\varepsilon}$.

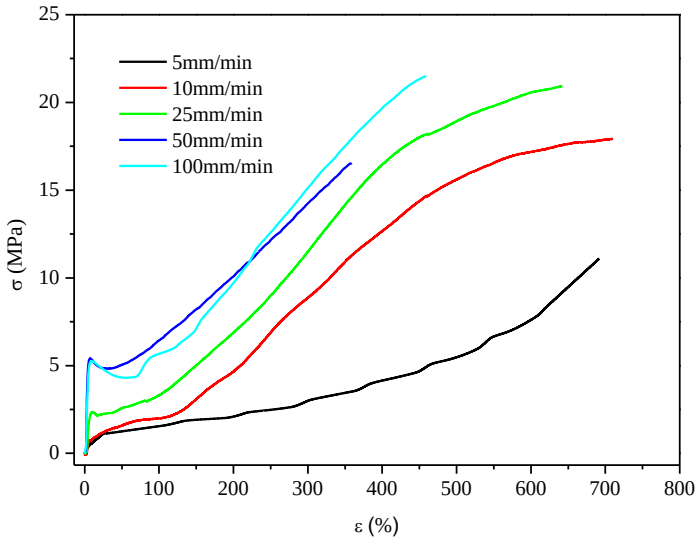

Figure 2.1.19.- Tensile tests conducted on PLLA at indicated strain rates at 60ºC.

Although both observations answer to relaxation, the lack of proportionality suggest the existence of a secondary relaxation, with its own activation energy [33, 64] that would fit into the thermo-rheological complexity as already reported for PLLA [65].

Self-reinforcing

Based on tests performed on PLLA, it was concluded that suitable temperature for orientation lied in the vicinity of T_g. At too high temperatures, deformations can easily be applied but will not result in molecular orientation because of rapid relaxation, whereas when the temperature is too low, the polymer is in the glassy state, such deformations will mostly lead to rupture or if possible at all, require excessively high stresses [66].

Therefore, samples of semicrystalline and amorphous polymers were stretched at $T \approx T_g$ at a constant crosshead speed of 5mm/min up to 600% strain (see figure 2.1.20). In order to obtain reproducible results, samples were allowed to relax for five minutes under constant strain prior to quenching at room temperature for further testing. With the exception of PLCL, all samples kept the impinged strain at room temperature as a result of the vitrification of chain molecules in the oriented state. Conversely, due to the concurrence of the T_g at room temperature, PLCL tended to shrink in order to recover its original length. Therefore, PLCL oriented samples were kept in the freezer until further testing.

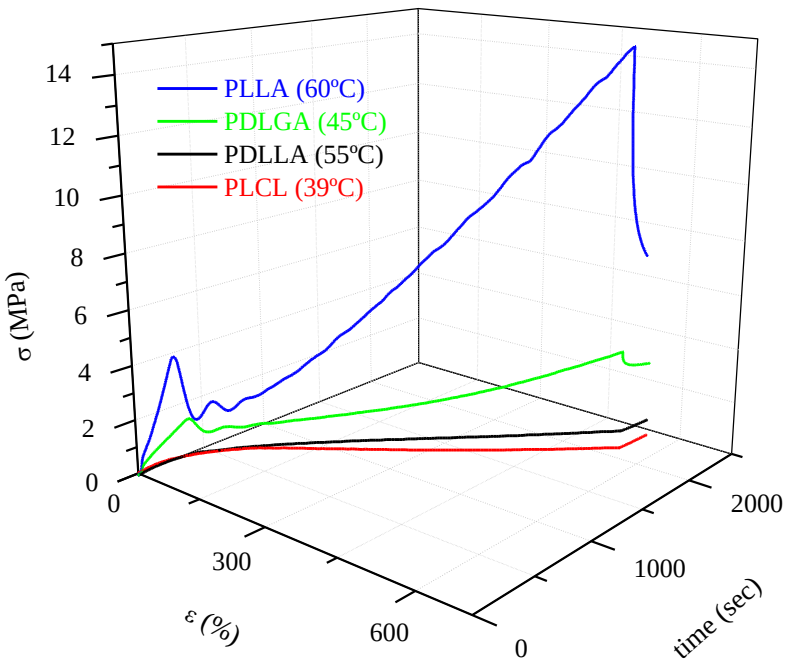

Figure 2.1.20.- 3D representation of the preorientation treatment conducted on PLLA, PDLGA, PDLLA and PLCL at indicated temperatures

Tensile properties

For the ease of discussion, in the following figures, the undeformed as-quenched and, were applicable, thermally crystallized samples, are presented together with those of the oriented ones. Figures 2.1.21 to 2.1.24 show a substantial increase in ductility in the tensile test with higher values of E, and σ_Y, as resumed in table 2.1.8 as well as other relevant values. It is noticed that the orientation produces a threefold increase in elastic modulus, as well as in the ultimate stress. It is also remarkable the increase in ductility of PDLLA when in oriented state, reaching values of 55% strain at rupture.

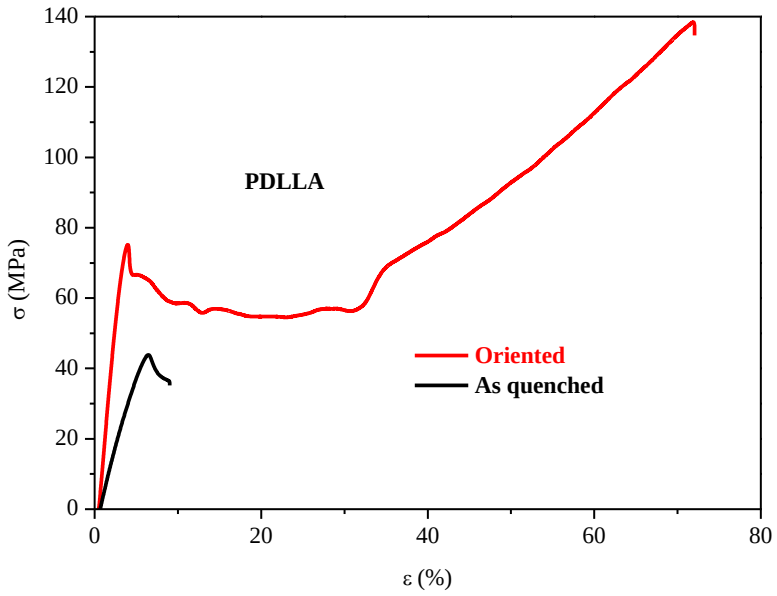

Figure 2.1.21.- Tensile tests of PDLLA

When polymer chains are stretched, they become aligned in the direction of the applied stress, promoting interactions between lateral chains such as hydrogen bridges, electric dipole and polar forces. Although these are always some orders of magnitude smaller than the forces of covalent bonding in the chain [67], they are not present in the isotropic glassy state, resulting in an increased E.

In the extended form, molecules are more prone to flow, therefore, the strain softening effect due to relaxation of amorphous chains is reduced [68], promoting uniform deformation over localization which causes necking or premature brittle failure.

Subsequent cold drawing extends until limited chain extensibility due to junctions (entanglements and/or crystallites) causes the strain hardening effect.

PDLLA, having the highest molecular weight and polydispersity index, showed multiple drops (σ_d) and the longest cold drawing plateau suggesting that despite the initial 600% preorientation, many molecules remained in the coiled conformation and whenever a portion of these relaxed, caused a new drop. Conversely, the lack of σ_d and limited plateau in PLLA suggests the development of strain induced crystallinity, where the strain hardening effect is ascribed to the limited extensibility of the amorphous segments between lamellae [69].

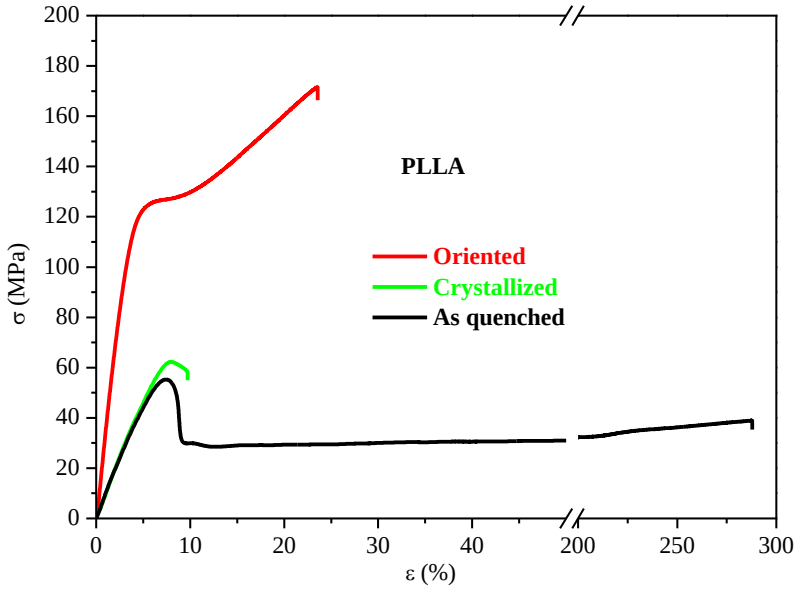

Figure 2.1.22.- Tensile tests of PLLA

Again, the enhanced E is also observable in figure 2.1.23. Following, the observed shorter and more even cold drawing region of oriented PDLGA is consistent with the lower molecular weight and polydispersity index of PDLGA in comparison with PDLLA.

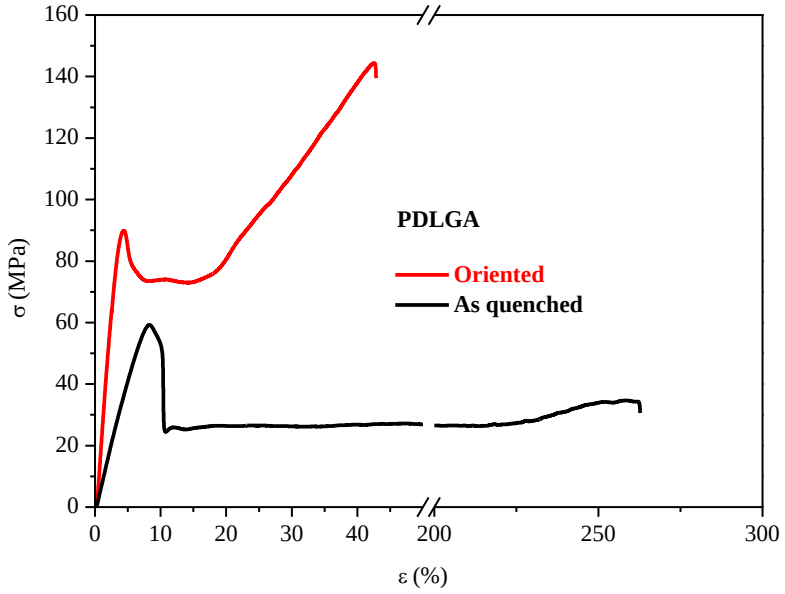

Figure 2.1.23.-Tensile tests of PDLGA

It should be noted here that handling of PLCL was difficult and despite our efforts, some retraction happened, so the evaluated behaviour does not entirely correspond to the initially achieved stretched state. Yet, differences with the isotropic amorphous state could be observed.

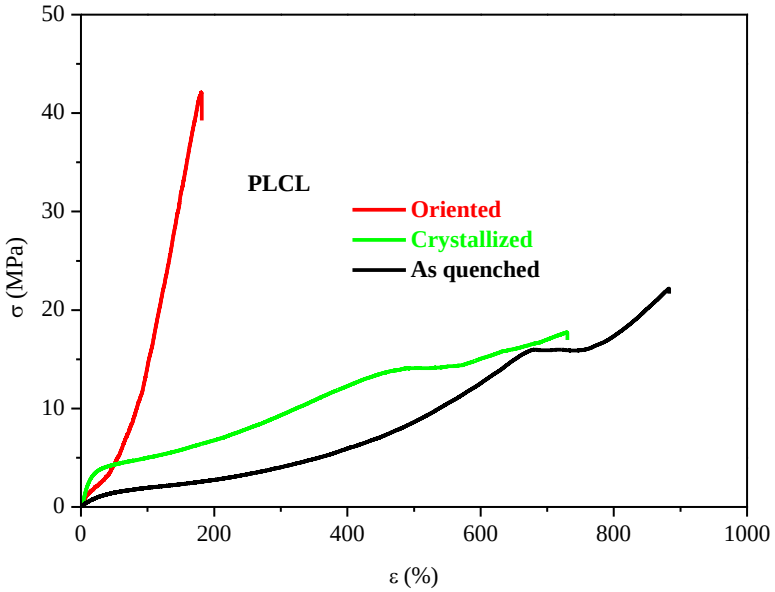

Figure 2.1.24.- Tensile tests of PLCL.

Values from table 2.1.8 mirrored the significant increase of elastic modulus and stress at yield observed in glassy polymers due to orientation. Conversely, in PLCL thermal crystallization caused the highest increase of modulus, preserving the elastomeric character of PLCL as it can be inferred by the high values of ε_R, whereas orientation caused a comparatively premature failure at ~190% strain.

Table 2.1.8.- Tensile properties of the polymers in the as quenched, crystallized and oriented states

	E	**σ_Y**	**ε_Y**	**σ_R**	**ε_R**
	MPa	**MPa**	**%**	**MPa**	**%**
PDLLA_a	1012±63	45.4±6.9	6.0±0.2	41.0±4.6	7.4±1.1
PDLLA_o	2800±126	74.3±2.1	3.5±0.1	113±42	55.1±30.3
PDLGA_a	940±106	57.8±2.2	7.6±0.6	45.9±9.5	147±161
PDLGA_o	3160±215	91.1±2.3	4.0±0.2	137±16	36.4±4.8
PLCL_a	7.3±2.9	16.2±0.6	669±31	20.7±3.2	815±102
PLCL_c	36.0±1.9	14.3±0.4	496±14	16.5±1.7	664±93
PLCL_o	29.6±7.9	23.2±4.1		41.0±2.0	184±17
PLLA_a	972±41	54.6±2.3	7.7±0.7	35.1±5.2	165±146
PLLA_c	1116±78	63.7±1.0	7.7±0.24	57.3±2.3	9.9±2.0
PLLA_o	3727±149	127.1±0.5	6.1±0.1	172±24	23.2±7.2

Dynamic mechanical analysis

Figures 2.1.25 to 2.1.28 show the DMA spectra for all polymers. In all cases, the observed effect of orientation in the storage modulus is an increase of its value, and a delay in its relaxation. As the storage modulus represents the elastic response, these effects are in accordance with observations from the tensile tests, and explained by the same underlying molecular alignment, that being less coiled is harder to deform. Besides, the extended conformation promotes second order interactions between neighbouring chains that must be overcome to allow relaxation. The observed reduction in the height of the damping peak, also ascribed to the increased rigidity of frozen segments, indicates lesser mechanical losses [70]. At this stage, extended chains try to recoil to their high entropic undisturbed dimensions [66, 71], exerting recovery stress [72-74] that plays its role opposing to modulus relaxation. Accordingly, the length of the rubbery plateau where junctures (entanglements) break and reform in new unstressed positions where they no longer contribute to stress [51] is reduced due to the shrinkage phenomenon in comparison to the extended plateau observed in isotropic as quenched samples.

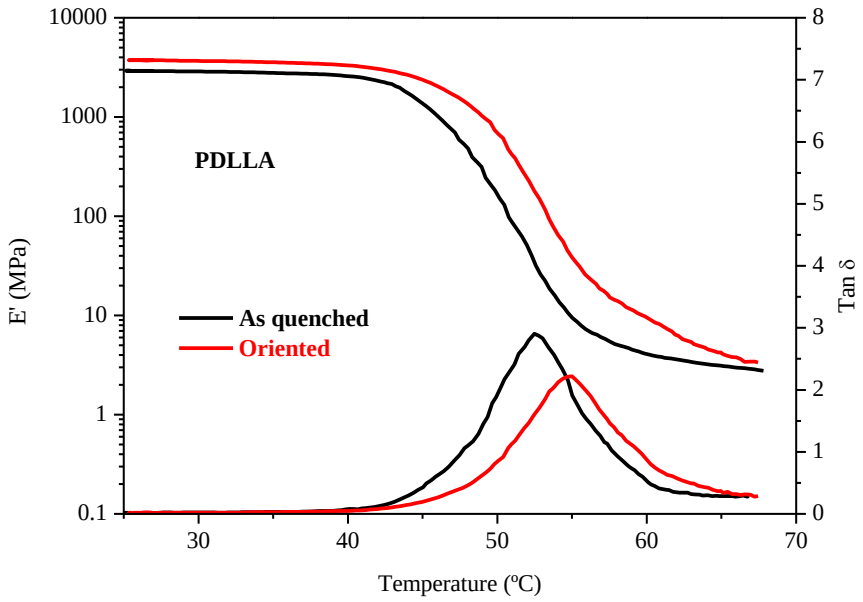

Figure 2.1.25.- Relaxation spectrum and tan δ of PDLLA

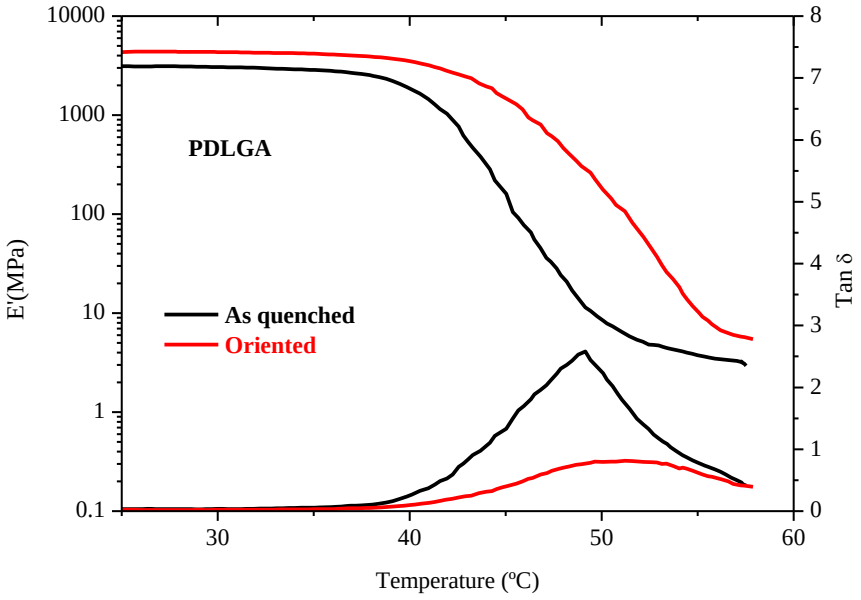

Figure 2.1.26.- Relaxation spectrum and tan δ of PDLGA

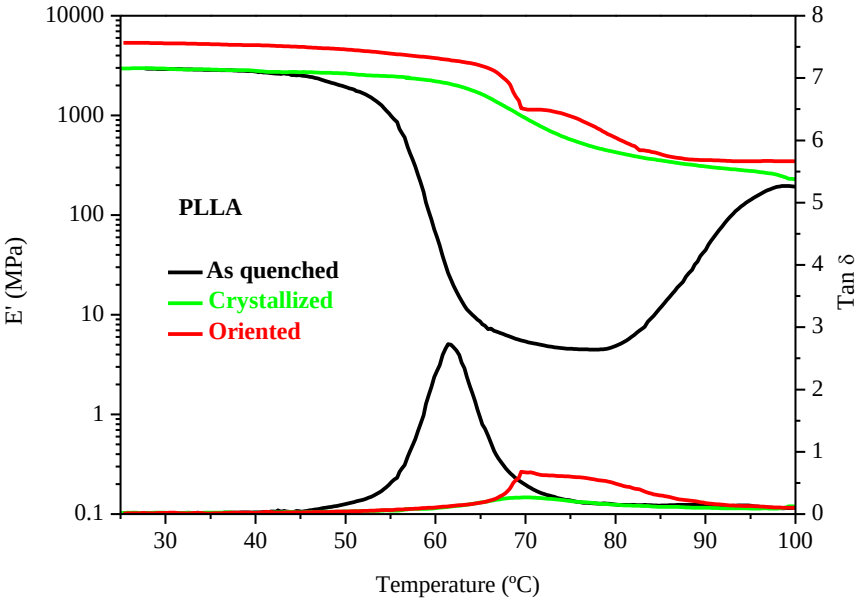

Figure 2.1.27.- Relaxation spectrum and tan δ of PLLA

Conversely, the relaxation of the storage modulus of semicrystalline polymers (PLLA and PLCL) is seen to progress in two steps as temperature triggered opposing effects are taking place simultaneously. On the one hand, as in the case of amorphous polymers, recoiling of amorphous chains oppose to modulus relaxation. On the other, the

development of strain induced crystallization opposes to amorphous shrinkage [49] and tends to stabilize E' at the featuring value of crystalline PLLA at that temperature [75]. It is noteworthy the phase separation phenomenon observable in the relaxation spectra of crystallized PLCL, where the contribution of each comonomer to the total E' is easily perceived.

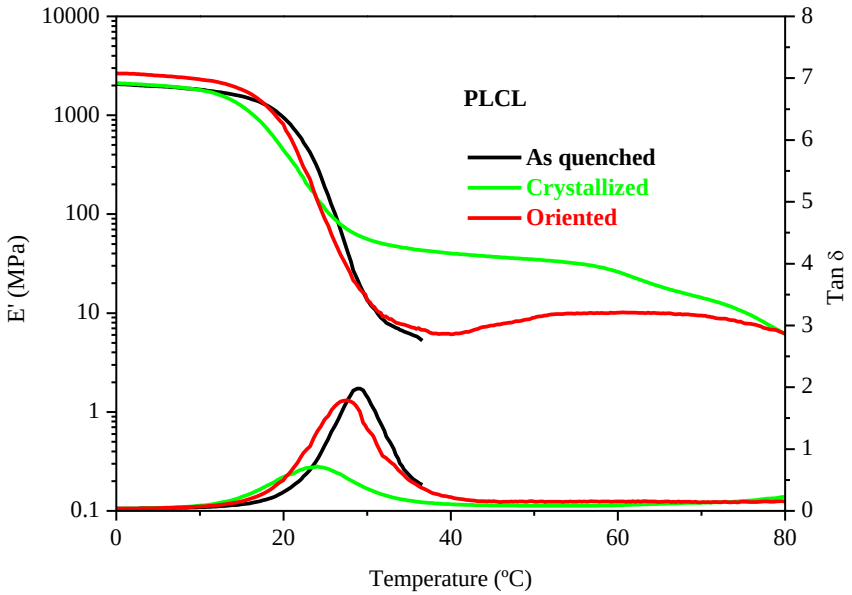

Figure 2.1.28.- Relaxation spectrum and tan δ of PLCL

Thermal properties

Figures 2.1.29 to 2.1.30 show the heating DSC scans from where thermal properties resumed in table 2.1.9 were extracted. In agreement with DMA observations, a further increase in the glass transition T_g was measured. Besides, in prestrained samples, a sharp endotherm ascribed to relaxation of orientation [47, 76], overlapped the glass transition step. Following, an exotherm was also noted. In the case of PLLA and PLCL its appearance is clear and easily correlated to a promoted cold crystallization [71, 77, 78], while in the case of PDLLA and PDLGA it is more subtle and such correspondence cannot be stablished. The sharp enthalpy endotherm, has been ascribed to the relaxation of the metastable structure resulting after orientation [79] and is presumed to contain a significant conformational contribution [80] that in a macro-scale is accompanied by samples shrinkage, a phenomenon that is activated above the glass transition temperature

[77]. Shrinkage although exothermic by nature, does not generate the exotherm in question after the T_g [77]. The correlation between mechanical shrinkage and exothermic heat flow can therefore be only indirectly casual [77].

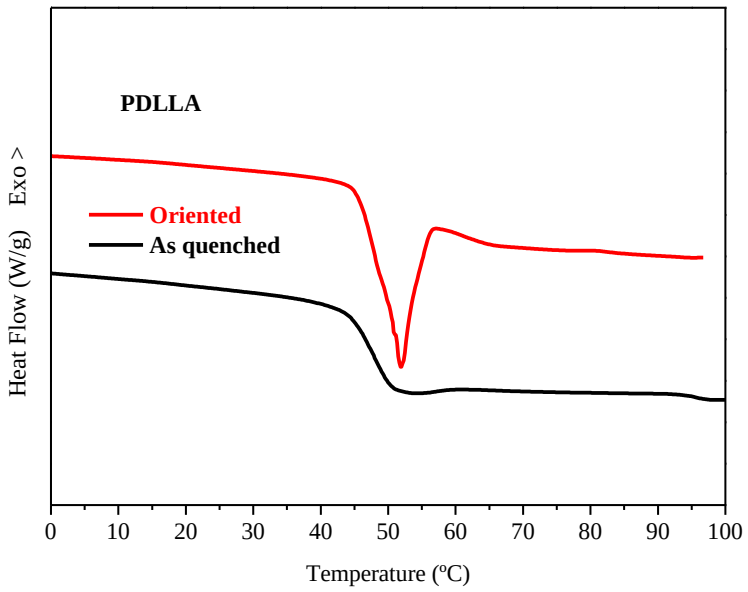

Figure 2.1.29.- Heating scans of PDLLA

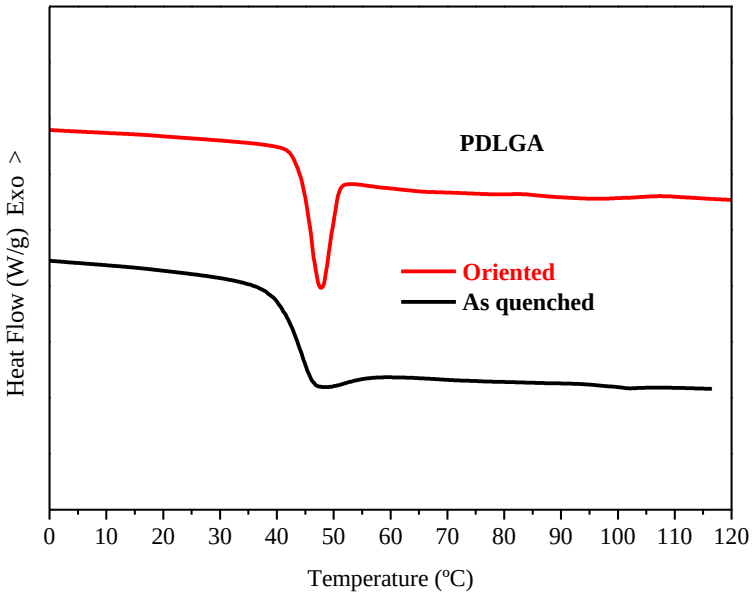

Figure 2.1.30.- Heating scans of PDLGA

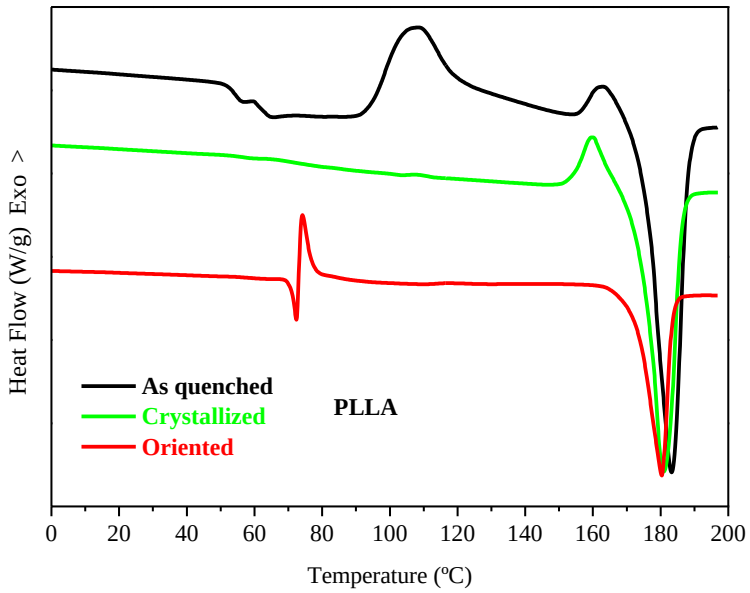

Figure 2.1.31.- Heating scans of PLLA

Careful observation of the glass transition in the as quenched PLLA, discloses a double transition, which has been ascribed to the presence of a rigid amorphous phase [81].

In the same graph, observation of the glass transition in the sample that has been thermally crystallized is very subtle, suggesting that the amorphous phase is arrested in the interlamellar space, whereas the second crystallization is easily seen. This second exothermal peak has been attributed to the recrystallization into the polylactide crystal polymorph of higher perfection [81].

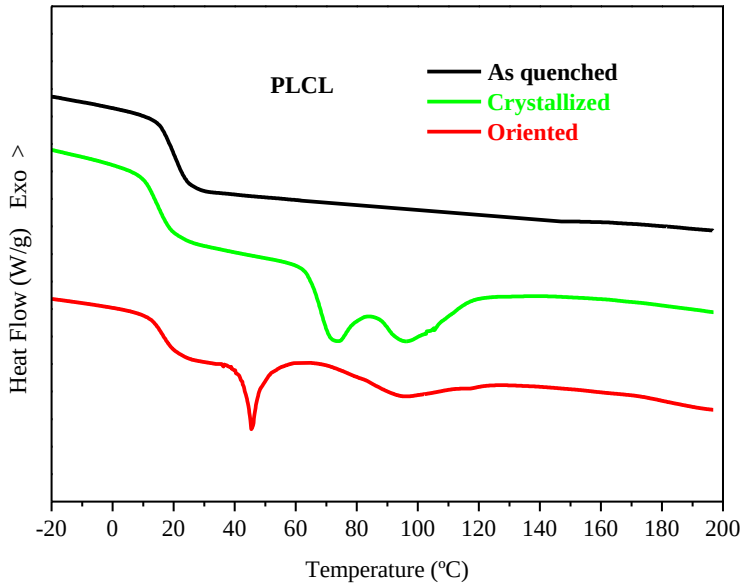

Figure 2.1.32.- Heating scans of PLCL

The thermogram of as quenched PLCL showed the glass transition event indicating a fully amorphous phase. The thermal crystallization was fulfilled by an annealing treatment at 45ºC for 20 days. This treatment, as previously reported in our group [82, 83], entails the appearance of a second T_g at 68ºC with an associated enthalpy relaxation of 1.5J/g and an endothermic peak at ~97ºC associated with the fusion of imperfect α polylactide crystals. The thermogram of the oriented sample disclosed two clearly separated glass transitions, the second one exhibiting the enthalpic recovery ascribed to the metastable oriented structure [79]. Careful observation reveals the presence of cold crystallization, presumably as in the case of PLLA enhanced by strain orientation, followed by a melting peak.

Table 2.1.9 summarizes the thermal parameters determined from Figs. 2.1.29 to 2.1.32, where T_g, ΔH_r, T_m and X_c refer respectively to glass transition, enthalpy relaxation, melting temperature and crystallinity degree. Hereinafter, letter “a” refers to the “as quenched” state; letter “o” to the “oriented” and letter “c” to the thermally crystallized ones respectively.

Table 2.1.9.- Thermal analysis of the as quenched, crystallized and oriented states of the studied polylactides

	T_{g1}	ΔH_{r1}	T_{g2}	ΔH_{r2}	T_m	ΔH_m	X_c
	ºC	J/g	ºC	J/g	ºC	J/g	%
PDLLA_a	48	0.46	-	-		-	-
PDLLA_o	49	4.95	-	-		-	-
PDLGA_a	45	0.70	-	-		-	-
PDLGA_o	46	5.58	-	-		-	-
PLCL_a	20	-	-	-		-	-
PLCL_o	17	-	43	1.98	96	3.71	1
PLCL_c	15	-	68	1.58	97	3.43	3.2
PLLA_a	55	-	-	-	183	55.2	10.2
PLLA_o	72	0.55	-	-	180	64	47.4
PLLA_c	70	-	-	-	181	57.5	44.3

As it can be noted from table 2.1.9, both crystallisable polymers have developed a certain degree of crystallinity as a consequence of the combined stretching and heating, which in the case of PLLA is higher than that obtained by heating only.

X-ray diffraction

In order to further investigate the type of crystals formed thereof, their corresponding X-ray diffraction patterns were collected. The X-ray diffraction pattern is itself sufficient evidence for the existence of a crystalline structure though in some cases, the crystallization is only partial and the crystallites are very small [49]. As expected, the diffractograms of PDLLA and PDLGA showed a halo featuring an amorphous structure. Conversely, PLLA and PLCL samples revealed the existence of crystalline-like structures by the presence of certain scattering peaks. Those peaks were narrower and more intense in the thermally crystallized samples, and their location corresponded to that reported in literature [47, 85-87], as highlighted in figure 2.1.35 and comments, than the observed peaks in the oriented samples. From the less intense signal and higher breadth it was inferred that instead of crystals, long range symmetry structures were achieved.

Some authors have reported the presence of β crystals, termed shish-kebab, after drawing semicrystalline PLLA α crystals at high temperatures, with a featuring reflection at 2θ = 29.9º [84]. However, it was not seen in our diffractogram.

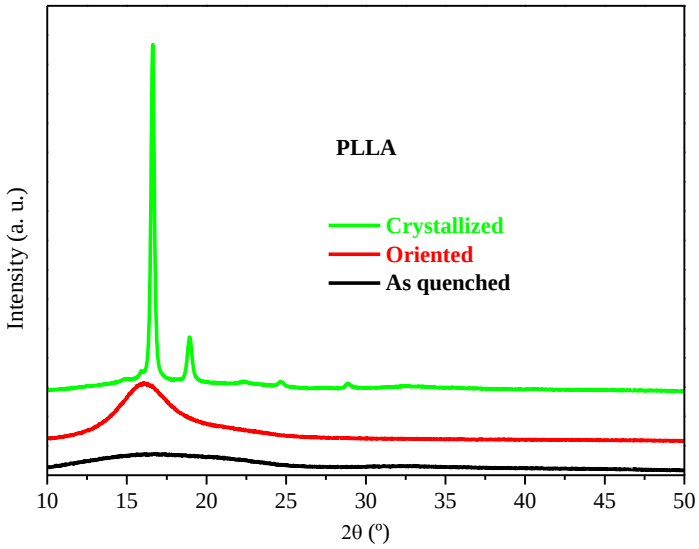

Figure 2.1.33.- Diffractograms of PLLA

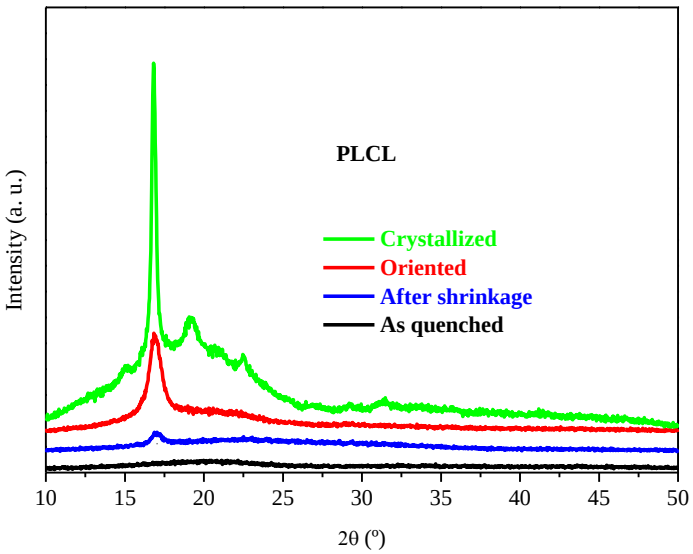

Figure 2.1.34.- Diffractograms of PLCL

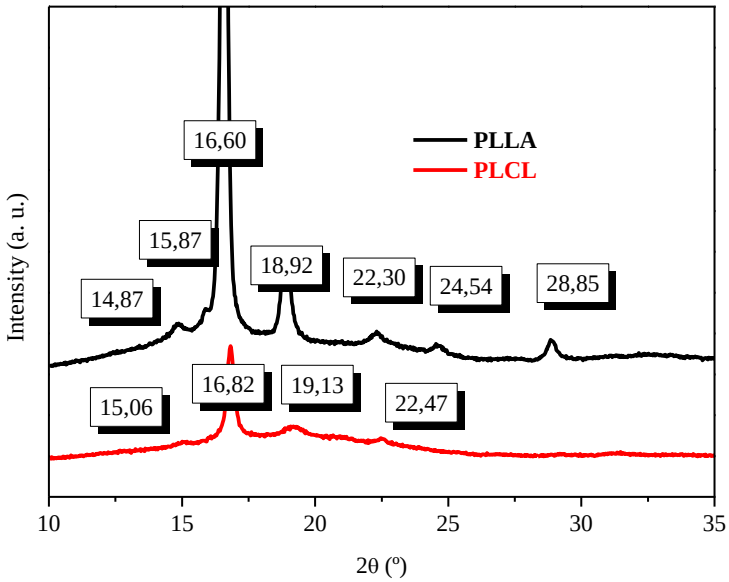

Figure 2.1.35.- Diffractograms of PLLA (black) and PLCL (red) and detail of their diffraction peaks in crystallized state

The main scattering peak at 2θ = 16.6-16.8º, and less intense peaks at ~19 and ~22º of figure 2.1.35 have been attributed to the set of planes (200) or (110), (203), and (015) of the α crystalline form of poly(lactide) respectively [47, 85].

Within experimental errors and deviations amongst reported values of the scattering peaks it can be said that the presence of ε-caprolactone units in the backbone of PLLA has a moderate effect on the shape of PLLA crystals in the copolymer [86]. Furthermore, the typical diffraction peaks of crystalline PCL at 2θ=21.4º cannot be observed in the pattern of the copolymer, which indicates that PCL is fully amorphous phase in the copolymer [87].

Oriented samples were heated above T_g and allowed to shrink, and their diffraction spectra were collected and plotted in figure 2.1.34. The existence of an even less intense band suggested the endurance of the long range symmetry.

The application of the Scherrer equation (eq. 5) to the diffraction peak, allows estimating a crystalline average size or coherent diffraction domain. The estimation of the dimensions of the crystallites depends on the broadening of the spots in the diffraction pattern as the crystal dimensions are diminished [49]. The method is applicable only when

the dimensions are less than 10000Å and becomes increasingly accurate as the dimensions are reduced [49]. In addition may be a broadening due to other factors such as imperfections of the crystal lattice [49]. For these reasons, estimates of the size of the crystallites must be regarded as subject of considerable uncertainty [49].

$$\tau = \frac{K\lambda}{\beta_\tau cos\theta} \text{ (equation 5)}$$

Where τ is the coherent diffraction domain, K is the shape factor, λ is the X-ray wavelength (copper Kα), βτ (=B-b) is the line broadening at half the maximum intensity (FWHM) in radians, being B the observed width, b the instrumental width and θ the Bragg angle. Calculated values for PLLA and PLCL, crystallized (c), oriented (o), and after shrinkage (oHT) are listed in table 2.1.10.

Table 2.1.10.- Parameters used in the Scherrer equation, and calculated domain sizes

	β_τ	**K**	**λ**	**b**	**τ**
	º		**Å**		**nm**
PLLA_c	0.25	0.85	1.5418	0.1	50
PLLA_o	3.13				2-3
PLLA_oHT	3.08				2-3
PLCL_c	0.31				40
PLCL_o	0.84				10
PLCL_oHT	0.67				10

As it can be noted in table 2.1.10, domain sizes were very small, yet coherence of the results must be claimed as obtained value for thermally crystallized PLLA was in close agreement with previously reported size [88] and from comparison between the corresponding values of thermally crystallized and oriented it follows that higher values were obtained by thermal crystallization than those obtained by the combined effect of orientation and heat. It must also be noted that the size of the domains after shrinkage produced by subsequent heating of oriented samples was not altered, indicating irreversible changes in the microstructure.

Conclusions

In the present work, several induced features have been explored from different approaches.

It has been demonstrated that solvent casting, being a handy way to obtain thin films, revealed severely comprised final properties due to the presence of cavities generated during solvent evaporation. Therefore, more rigorous control over the solvent evaporation must be undertaken if films of better quality are sought.

Conversely, thermoconformation is a comparatively fast production process whose main drawbacks are developed after conformation in a thermo-reversible process termed physical aging that preferentially affects amorphous phases. The aging range, delimited by the glass transition temperature and the secondary β transition may include the temperature of practical use. Amongst the observed changes that take place during this structural relaxation are enthalpy relaxation, whose kinetics is favoured by the highest deviation from thermodynamic equilibrium caused by rapid quenching, and by a more random sequence of comonomer segments distribution, that increase flexibility of the chain backbone, making it easier for it to accommodate the structural changes in the approach towards thermodynamic equilibrium.

As a consequence of these structural changes, increasing relaxation times and, of special technological importance, the measured loss of ductility have also been disclosed.

In tensile tests, the loss of ductility has been associated the the increase of the necessary stress in order to cause yielding that, in the presence of small cracks (in the range of 7nm), preferentially caused brittle fracture.

In agreement with this, dynamic mechanical measurements revealed that higher activation energy was demanded for the glassy to rubbery transition in aged glasses.

Alternatively, a general enhancement in ductility as well as an elastic modulus improvement was obtained by pre-stretching glassy polymers at temperatures in the vicinity of their corresponding T_g.

It was speculated that the preferential arrangement of chains favoured physical bonds between chains, which contribute to the raise in E, and, upon application of sufficient stress, yielding.

Further, it was demonstrated that the pre-stretching protocol induced crystallization in semycristalline polymers, and an estimation of their size was calculated upon application of the Scherrer equation.

References

[1] Fetters, L., Model polymers for Materials Science in Materials Science and technology volume 12 Structure and properties of Polymers Edited by Cahn, R. W., Haasen, P., Kramer, E. J., VCH Verlagsgesellschaft mbH, Weinheim, 1993, pp. 19, 194, 197.

[2] Holden, Kricheldorf, Quirk. Thermoplastic elastomers. Hanser Gardner publications, pp. 493

[3] Brydson, J., Principles of the processing of plastics in Plastics Materials, Butterworth Heinemann, seventh edition, Oxford, 1999, pp. 47, 158, 174, 181.

[4] Tool, A. Q., Journal of the American ceramic society, 1946, 29, 240-253

[5] Kovacs, A. J., Fortschritte der hochpolymeren-forschung, 1963, 3, 394-507

[6] Haward, R.N. and Young, R.J. Introduction in The physics of glassy polymers; Haward, R.N. and Young, R.J., Eds.; Chapman and Hall: London, 1997, pp. 3, 87.

[7] Hodge, I. M., Journal of non-crystalline solids, 1994, 169, 211-266

[8] Struik, L. C. E., Physical aging in amorphous polymers and other materials, Elsevier scientific publishing Company, Amsterdam, 1973.

[9] Aou, K., Hsu, S. L., Kleiner, L. W., Tang, F. W., The journal of physical chemistry B, 2007, 111, 12322-12327

[10] Heymans, N., Polymer, 38, 1997, 3435-3440

[11] Brunacci, A., Cowie, J. M. G., Ferguson, R., McEwen, I. J., Polymer, 1997, 38, 865-870

[12] Hodge, I. M., Science, 1995, 267, 1945-1947

[13] Struik L. C. E., Polymer engineering and science, 1977, 17, 165-173

[14] Marshall, A. S., Petrie, S. E. B., Journal of applied physics, 1975, 46, 4223-4230

[15] Bauwens-Crowet, C., Bauwens, J-C., Polymer, 1982, 23, 1599-1604

[16] Bigg, D. M., Polymer engineering and Science, 1996, 36, 737-743

[17] Bauwens, J-C., Polymer, 1980, 21, 699-705

[18] Pan, P., Zhu, B., Inoue, Y., Macromolecules, 2007, 40, 9664-9671

[19] Lizundia, E., Sarasua, J. R., Macromolecular Symposia, 2012, 321-322, 118–123

[20] Orowan, E. Reports on Progress in Physics, 1949, 12, 185-232

[21] Legrand, D. G., Journal of applied polymer science, 1969, 13, 2129-2147

[22] Lyu, S-P., Zhu, X-G., Qi, Z-N., Journal of polymer research, 1995, 2, 217-224

[23] Griffith, A. A., The phenomena of rupture and flow in solids, Philosophical transactions of the royal society of London. Series A, 1920, 221, 169-198

[24] Gonzalez, J. J., Arana, J. L., Mecánica de la fractura, publicaciones de la Universidad del País Vasco, 2002.

[25] Ward, I. M., Journal of materials science, 1971, 6, 1397-1417

[26] Argon, A. S., Philosophical Magazine, 1973, 28, 839-865

[27] Tant, M. R., Wilkes, G. L. Polymer engineering and science, 1981, 21, 874-895

[28] Cohen, M. H., Turnbull, D., The journal of chemical physics, 1959, 31, 1164-1169

[29] Struik, L. C. E., Physical Aging: Influence on the Deformation Behaviour of amorphous polymers from Brostow, W., Corneliussen, R. D., Failure of plastics, Hanser Publishers, Germany, 1979.

[30] Cangialosi, D., Wübbenhorst, M., Schut, H., Picken, S. J., Acta physica polonica A, 2005, 107, 690-696

[31] Crist, B., Yield processes in glassy polymers from Haward, R. N., Young, R. J., The Physics of glassy polymers, Chapman & Hall, London, 1997

[32] Eyring, H., Journal of chemical physics, 1936, 4, 283-291

[33] Bauwens-Crowet, C., Bauwens, J. C., Homes, G., Journal of polymer science: part A-2, 1969, 7, 735-742

[34] Williams, G., Transactions of the Faraday Society, 1966, 62, 2091-2102

[35] Ngai, K. L., Plazek, D. J., Rubber Chemistry and Technology, 1995, 68, 367-434

[36] Bailey, J., US patent 2545868, 1951

[37] Törmällä, P., Clinical materials 1992, 10, 29-34

[38] Majola, A., Vainionpää, S., Rokkanen, P., Mikkola, H. M., Törmällä, Journal of materials science: materials in medicine, 1992, 3, 43-47

[39] Shikinami, Y., Okuno, M., Biomaterials, 1999, 20, 859-877

[40] Nazhat, S. N., Kellomäki, M., Törmälä, P., Tanner, K. E., Bonfield, W., Journal of Biomedical Materials Research Part B: Applied Biomaterials, 2001, 58, 335-343

[41] Bleach, N. C., Tanner, K. E., Kellomäki, M., Törmälä, P., Journal of materials science: Materials in medicine, 2001, 12, 911-915

[42] Niemelä, T., Niiranen, H., Kellomäki, M., Törmälä, P., Acta biomaterialia, 2005, 1, 235-242

[43] Charles, L. F., Kramer, E. R., Shaw, M. T., Olson, J. R., Wei, M., Journal of the mechanical behavior of biomedical materials, 2013, 17, 269-277

[44] Talja, M., Törmälä, P., Rokkanen, P., Vainionpää, S., Pohjonen, T., US patent 5792400, 1998

[45] Törmälä, P., Pentti, R., Laiho, J., Tamminmäki, M., Vainionpää, S., US patent, 4743257, 1988

[46] Törmälä, P., Rokkanen, P., Vainionpää, Laiho, J., Heponen, V. P., Pohjonen, T., US patent 4968317, 1990

[47] Pluta, M., Galeski, A. Biomacromolecules, 2007, 8, 1836-1843

[48] Struik L. C. E., Polymer engineering and science, 1978, 18, 799-811

[49] Treloar, L. R. G., The physics of rubber elasticity, Oxford at Claredon press, second edition, 1974. pp 151, 20, 236, 271, 276

[50] McKechnie, J. I.; Haward, R. N.; Brown, D.; Clarke, J. H. R., Macromolecules, 1993, 26, 198-202

[51] Tobolsky, A. V., Andrews, R. D., The journal of chemical physics, 1945, 13, 3-27

[52] Choi, K. J., Spruiell, J. E., White, J. L., Polymer engineering and science, 1989, 29, 1516-1523

[53] Lendlein, A., Kelch, S., Angewandte chemie international edition, 2002, 41, 2034-2057

[54] Lendlein, A., Langer, R., Science, 2006, 296, 1673-1676

[55] Sarasua, J. R., Prud'homme, R. E., Wisniewski, M., Le Borgne, A., Spassky, N., Macromolecules, 1998, 31, 3895-3905

[56] Hutchinson, J. M., Journal of polymer science: Part B: Polymer physics, 1990, 28, 2127-2163

[57] Meaurio, E., Zuza, E., López-Rodriguez, N., Sarasua, J. R., J. Phys. Chem. B, 2006, 110, 5790-5800

[58] Mavridis, H.; Shroff, R.N., Polymer engineering and science, 1992, 32, 1778-1791

[59] Gurp, M.V.; Palmen, J., Rheological bulletin, 1998, 67, 5-8

[60] Plazek, D. J., Journal of Rheology, 1996, 40, 987-1014

[61] Neuendorf, R. E., Saiz, E., Tomsia, A. P., Ritchie, R. O., Acta biomaterialia 2008, 4, 1288-1296

[62] Ritchie, R. O, Personal communication, 2014

[63] Vincent, P. I., Polymer, 1960, 1, 7-19

[64] Huu, C. H., Vu-Khanh, T., Theoretical and applied fracture mechanics, 2003, 40, 75-83

[65] Muñoz Ugartemendia, J., Muñoz, M. E., Sarasua, J. R., Santamaria, A., Rheologica Acta, 2014, 53,857–868

[66] Schuur, G., Van der Vegt, A. K., Orientation of films and fibrillation in Structure and properties of oriented polymers, Springer, 1997, pp. 416-418

[67] Peterlin, A., Molecular aspects of oriented polymers in Structure and properties of oriented polymers, Springer, 1997. pp 36-38

[68] Andrews, E. H., Pure and Applied Chemistry, 1972, 31, 91-112

[69] Schultz, J. M., Polymer engineering and science, 1984, 24, 770-785

[70] Komalan, C., George, K. E., Kumar, P. A. S., Varughese, K. T., Thomas, S., eXPRESS polymer letters, 2007, 1, 641-653

[71] Mezghani, K., Spruiell, J. E., Journal of polymer science: Part B: Polymer physics, 1998, 36, 1005-1012

[72] Khan, F., Koo, J. H., Monk, D., Eisbrenner, E., Polymer testing, 2008, 27, 498-503

[73] Wong, Y. S., Venkatraman, S. S., Acta materialia, 2010, 58, 49-58

[74] Rousseau, I. A., Polymer engineering and science, 2008, 48, 2075-2089

[75] Hadley, D. W., Ward, I. M., chapter 8: the macroscopic model approach to low strain properties from Structure and properties of oriented polymers edited by Ward page 280

[76] Lee, J. K., Lee, K. H., Jin, B. S., European Polymer journal, 2001, 37, 907-914

[77] Aou, K. Kang, S., Hsu, S. L., Macromolecules, 2005, 38, 7730-7735

[78] Wong, Y. S., Venkatraman, S. S., Acta materialia, 2010, 58, 49-58

[79] Niklason, L. E., Langer, R. S. Transplant immunology, 1997, 5, 303-306

[80] Haward, R. N., Hay, J. N., Parson, I. W., Adam, G., Owadh, A. A. K., Boxnyak, C. P., Aref-Azaf, A., Cross, A., Colloid and polymer science, 1980, 258, 643-661

[81] Sarasua, J. R., Zuza, E., Imaz, N., Meaurio, E., Macromolecular symposium, 2008, 272, 81–86

[82] Ugartemendia, J. M., Sarasua, J. R., SPE-ANTEC Tech. Papers, 2011, 2544

[83] Sarasua, J. R., Petisco, S., Ugartemendia, J. M., Fernández, J. SPE-EUROTEC Tech. Papers, 2011

[84] Takahashi, K., Sawai, D., Yokohama, T., Kanamoto, T., Hyon, S. H., Polymer, 2004, 45, 4969-4976

[85] Sarasua, J. R., López-Rodríguez, N., Zuza, E., Petisco, S., Castro, B., del Olmo, M., Palomares, T., Alonso-Varona, A., Journal of materials science: Materials in medicine, 2011, 22, 2513-2523

[86] Jeon, O., Lee, S. H., Kim, S. H., Lee, Y. M., Kim, Y. H., Macromolecules, 2003, 36, 5585-5592

[87] Li, L. X., Cai, W., Gao, Z., Jun, T. W., Polymer bulletin, 2007, 58, 381-391

[88] Wong, Y. S., Stachurski, Z. H., Venkatraman, S. S. Acta Materialia, 2008, 56, 5083-5090

Subchapter 2.2. Thermoconformation. Compounding

Introduction

Understanding the healing process of the tissue to be replaced and fitting the material design requirements of the implant to the short-term needs of the system avoids the need to meet long term arduous and unrealistic material design demands [1]. Amongst the synthetic polymers, PLA and its copolymers have received considerable attention for their biocompatibility and resorbability [2] making ideal candidates out of them for such applications in surgery where a temporary replacement is needed.

Experimental studies have found sutures, rods, screws and plates made of non-reinforced PLA suitable for fixation of cancellous bone fractures and osteotomies of non-weight loading bones [3]. However, the mechanical properties of these non-reinforced materials are not sufficient for fixation of weight loading bones [3]. The search for strong artificial implants able to perform in load-bearing situations, has led to the development of strong organic/inorganic composites that would combine the flexibility, toughness and bioresorbability of a polymer with the stiffness, strength and osteoconductivity of a ceramic [4]. Their advantage is that biodegradable polymers would allow for bone growth into degraded sections and further permit load transfer from the implant to the bone, thereby lessening the effect of stress shielding [4].

However, many tissues in the body have elastomeric properties [5]. Tendons transmit tensile loads from muscle to bone and are designed to undergo considerable extension and support large tensile forces [1]. Therefore, successful replacement of these tissues requires the development of compliant elastomeric scaffolds that readily recover from relatively large deformations without mechanical irritation to the host [5].

One of the most important parameters to match polymer and application is the relative position of its glass transition temperature (or in the case of crystalline polymers, crystal melting point) regarding the temperature of use (i. e. body temperature), as due to the thermoplastic nature of these polymers, they undergo transitions in their physical properties [6]. Figure 2.2.1 resumes the transitions of the modulus when the temperature is raised. Therefore, if the application requires a stiff material, the polymer of choice must have its T_g at a higher temperature than the temperature of use. Conversely, if a rubbery

material is desired, the selection will be made amongst those polymers having their T_g below the body temperature.

Particularly, in the case of block copolymers which are made of different monomeric units (or segments), or in immiscible systems where each constituent retains its own T_g, two service temperatures can be identified. The lower service temperature depends on the T_g of the soft phase or segment while the upper service temperature depends on the T_g or T_m of the hard phase or segment [6]

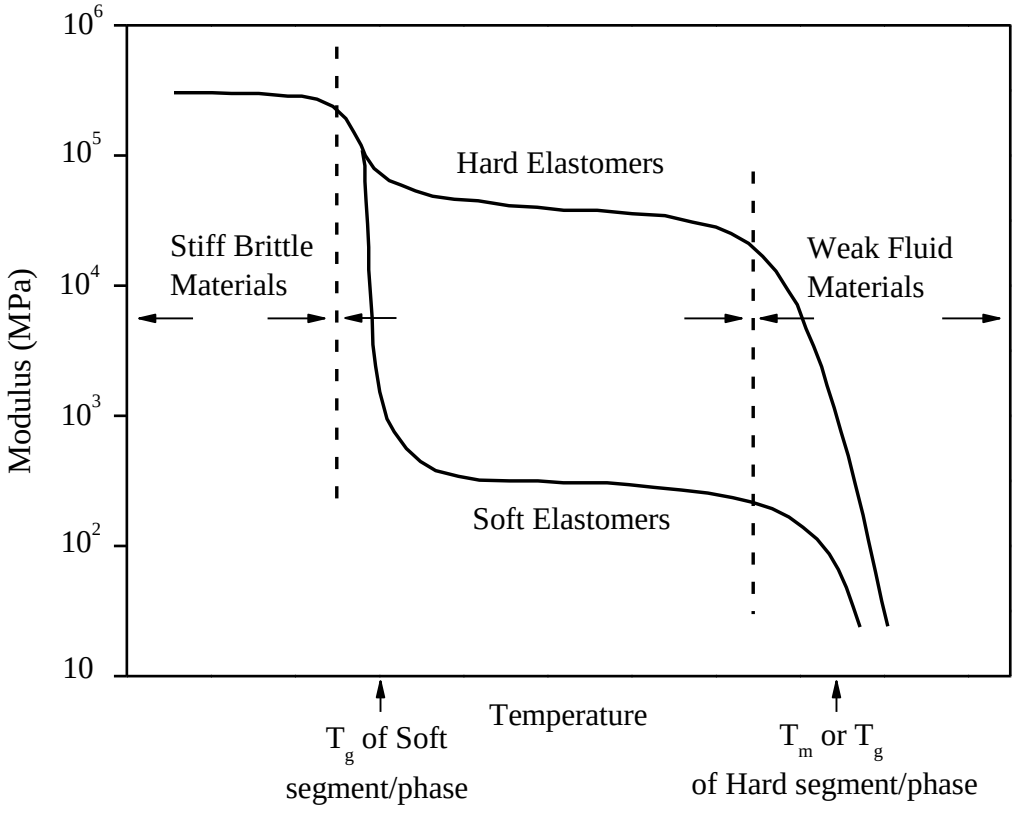

Figure 2.2.1.- Idealized stiffness of several materials at various temperatures, adapted from [6]

Still, the major difficulty lies in the graft integration. Some authors have found that initially excellent biocompatibility of PLA with intramedullary bone turned into deleterious response upon implant degradation and speculated that these adverse effects were due to degradation by-products [7]. Further experiments with bioluminescent bacteria acute toxicity assay on PLA and PGA reported that these polymers produced toxic solutions, probably due to the acidic nature of their degradation by-products [8, 9].

Upon degradation by hydrolysis, PLA produces lactic acid which is incorporated in the tricarboxylic acid cycle and is excreted as carbon dioxide and water [10]. It is possible that when poly(α-hydroxy acids) are implanted in large sizes or in anatomical regions without access to sufficient quantities of body fluids, the resulting release of large amounts of acidic degradation by-products might overwhelm the body's capacity to provide adequate local buffering [10]. Such scenario would lead to a lowering of the local pH and could be detrimental to the surrounding cells and tissue [10].

A three to five year follow-up multicentre study upon ACL reconstruction using the LARS ligament (Ligament Advanced Reinforcement System; Surgical Implants and Devices, Arc-sur-Tille, France) revealed that instead of the fibrocartilage transitional zone found in the native ACL insertion site, an interposed layer of fibrous scar tissue appeared at the interface between the graft and the bone tunnel [11]. It was presumed that the inflammation at the graft-bone interface might induce the scar tissue formation and hamper the graft osteointegration within the bone tunnel [12]. The poor bone-tendon interface has been reported to be the cause of devastating effects in anterior cruciate ligament reconstruction [11-16].

A proposed way to improve the artificial ligament graft healing in the bone is through alleviating the inflammation and promoting graft biocompatibility [12]. The addition of nano-HA into the degradable matrix not only helps maintain the pH at non-toxic levels during degradation by neutralizing the acid degradation products of poly(α-hydroxy acids) but also enhances the bone induction capacity of the scaffold [17]. Hydroxyapatite (HA) has been used for bone repair and tissue engineering due to its biocompatibility, osteoconductivity, and osteoinductivity [17].

Synthetic HA ($Ca_{10}(PO_4)_6(OH)_2$) is closely related to the carbonated apatite that constitutes the mineral component in the bone [4] although some differences may be expected in their chemical composition as bone does not have pure or stoichiometric HA [18]. However, synthetic HA is osteoconductive when porous and believed to aid bone formation in vivo [4]. In contact with bone, HA often develops a mechanically tight bond with bone which may be of a chemical nature [19].

Fiber matrix interfacial adhesion

It is known from the literature on particle reinforced polymer composites that ideally, the reinforcing particles should be well dispersed in the host polymer matrix at a high level of loading, and be well bonded to the matrix phase to achieve maximum reinforcement [20]. Nano-sized HA particles, like other nano-sized particles, have a large surface area that results in a high interfacial energy [20]. In general, these particles will tend to agglomerate both during the preparation of the particles and during the mixing with the polymer phase in an attempt to minimize the free energy of the system [20]. If this occurs in the composite, it can cause a reduction in the reinforcing effect of the particles which will ultimately affect the mechanical properties of the composite [20]. To maintain the stability of the particles, a dispersing agent is necessary [20]. Amongst the reported dispersing agents for HA, poly(acrylic acid) has been identified as a useful alternative because of its biocompatibility in other systems [20].

Often, the mechanical strength of the composite is compromised by the bonding characteristics at the interface between the constituents [21]. A common problem with HA-polymer composites is the weak binding strength between the nano-filler and the polymer matrix since they cannot form strong bonds during the mixing process [17]. Coating particles with a polymer film would lead to the formation of strong bonds with the polymer matrix [17]. A strong interface results in a fibre-reinforced composite with high strength and stiffness [21].

Fibre-matrix interphase adhesion [22] can be analysed by DMA, assuming that composite dissipation is attributable not only to the matrix amount present in the composite, but also to the fibre-matrix interactions at interfaces that will tend to form layers of immobilized interphase [22]. Since inorganic fillers do not contribute to damping, composite dissipation may be given by the eq. 1:

$$\frac{(\tan\delta)_c}{(\tan\delta)_m} = 1 - bV_f \text{ (equation 1)}$$

Where m and c indexes refer to matrix and composite dissipation respectively, V_f is the fibre volume content and b is a parameter introduced to correct the volume fraction

of reinforcement because of the formation of a layer of immobilized interphase resulting from fibre-matrix interactions [22].

Plasma polymerization technology is a useful way to activate nano-HA powder surfaces by creating a degradable film with functional groups at nanoscale thickness [17]. An ideal coating would be biocompatible, ultrathin and degradable, so that the bioactivity of the filler is not shielded [17]. Plasmas modify surface physical-chemical properties keeping however bulk properties unaltered [23]. Plasma generated with gaseous organic monomers can polymerize and crosslink on the exposed surface, forming a dense polymeric coating with specific characteristics [23]. The interest in plasma polymerized films lies in their unique coating properties which include good adherence and conformal coating of substrates [24]. Furthermore, the study of the chemistry of such coatings demonstrates the high retention of monomer functionalities such as carboxylic acid, hydroxyl, ester, sulfone and amine, depending on the starting monomer [24].

The aim of this work is to explore the possibilities of plasma coating particles for two different polymer matrix composites of potential use as load bearing devices in case of stiff PLA matrix and as artificial tendon with improved osteointegration with an elastomeric PLCL matrix. PLCL is a copolymer made of randomly polymerised lactide and ε-caprolactone polymers [25]. PLCL has a good track record in such medical applications as vascular grafts and for periodontal regeneration [25]. The most attractive property of PLCL compared to other synthetic polymers is its elasticity, which is inherent to most natural bone [25]. However, PLCL has a relatively low affinity for osteoblasts [25]. Studies conducted on Coll/HA/PLCL showed that osteoblast-like cells adhered and spread more significantly in the Coll/HA/PLCL scaffold than in the PLCL scaffold [25], suggesting that the Coll/HA/PLCL scaffold provides an appropriate environment for the human osteoblast [25].

Accordingly, two monomers have been used for the plasma polymerized coating following different purposes. With the aim of potentiating the good dispersion of the particles into both matrices, acrylic acid has been used as the starting monomer for plasma polymerization. In order to maximize the bonding interface between HA particles and polymer matrix, chemical affinity has been promoted by the use of ε-caprolactone as the starting monomer for plasma coating in the PLCL matrix composite.

Surface analytical techniques such as XPS and FTIR have been used for the characterization of the polymer coating thin film, whereas mechanical properties of the composites have been measured by DMA and tensile tests.

With a reported elastic moduli of 114GPa [4, 21], the addition of HA particles is expected to increase the strength of both matrices [26] and to have an influence on crystallization kinetics due to their nucleating activity [27]. Although processing temperatures of the composites are low enough to prevent phase and compositional changes of the HA [28], some authors have found that the addition of bioglass particles boosts thermal degradation [29, 30, 31] of the polymeric matrix. Therefore, thermal degradation of the composites will be studied in order to assess the suitability of injection moulding as a processing technique for medical devices with enhanced biocompatibility.

Materials and methods

Hydroxyapatite (Plasma Biotal Ltd, UK), poly(L-lactide-co-ε-caprolactone) (Purasorb PLC 7015 L-lactide/caprolactone copolymer ratio M/M% 70/30, ref 100800233, M_n: 112900g/mol and D: 1.71), and Polylactide PLLA (PL18 M_n: 120000g/mol and D: 1.25), both from Purac Biomaterials, The Netherlands, were used as received without any further purification.

The monomers used for plasma treatments were ε-caprolactone (99%, Alfa Aesar, Germany) and acrylic acid (anhydrous, 99%) from Sigma-Aldrich Chemie GmbH, Germany.

Composite preparation

A series of poly(L-lactide-co-ε-caprolactone)/hydroxyapatite and PLLA/hydroxyapatite composites with HA content of 0%, 10%, 20% and 30% (w/w) were prepared by melt blending into a 15 cm^3 co-rotating twin screw microcompounder from DSM Xplore at processing temperatures between 190 and 200ºC. Dumbbell samples were injection moulded between 200 and 240ºC.

Plasma treatment procedure

The surface modification of hydroxyapatite by plasma deposition was performed in a Pico LF40 (Diener electronic GmbH&Co., Germany). In both cases, the plasma treatments consisted on three steps. First, hydroxyapatite powder was introduced in the plasma chamber and activated for 5min under 0.4mbar of oxygen gas pressure at 700W generator power. After evacuating the plasma chamber, the corresponding monomer was fed into the chamber until 0.3mbar chamber inner pressure was achieved. Then plasma polymerization of ε-caprolactone was performed for 60min under 0.3mbar of monomer gas pressure at 120W generator power whereas conditions for acrylic acid plasma treatment lasted 45min under 70W generator power. Finally, the plasma treated hydroxyapatite powder was deactivated for 5 min under 0.3 mbar of monomer gas pressure with the generator off.

SEM

The HA particles and the tensile fracture surfaces of the composite samples were examined in a scanning electron microscope at various magnifications. SEM micrographs of gold-coated samples were obtained at 15 and 5kV respectively.

Thermal analyses

The thermal stability of composites was verified by TGA using a TA Instruments Q50 thermogravimetric analyser in the temperature range from room temperature to 600°C, with a heating rate of 5ºC/min under 60ml/min nitrogen flow on 10-20mg samples.

A TA Instruments DSC Q200 thermal analysis system was employed for thermal characterisation. In order to investigate the influence of injection processing upon the resulting state 5mg samples cut from the dumbbell samples were heated from -30 to 200°C, at 10°C/min, under nitrogen flow for PLCL system, whereas the PLLA system was evaluated from 0 to 250ºC at 10ºC/min.

With the aim of study the activity of the filler and the effect of the organic layer in the crystallisation behaviour of the composites, each sample was heated to 200ºC and cooled at the following cooling rates: 0.5, 1, 2, 3, 4, 6, 8, 10, 20, 30, 40ºC/min. From DSC measurements, the degree of crystallinity of the composites and the nucleating activity of the fillers were calculated. The degree of crystallinity of the samples was calculated from the ratio of their enthalpy of fusion to the enthalpy of fusion of the polylactide crystal ΔH_m^0 [32]. For this purpose, 106J/g was used for ΔH_m^0 [32]. In all cases, the PLLA content of the composites was corrected according to the TGA measurements conducted on the same samples after the DSC scans.

Nucleating activity (ϕ) was graphically calculated from the ratio of the slopes, log r versus $1/\Delta T_p^2$ with and without the nucleating agent following the method proposed by Dobreva [27]. ϕ is a factor by which the work of three-dimensional nucleation decreases with the addition of a foreign substrate [33]. If the foreign substrate is extremely active, ϕ approaches 0, while for inert particles ϕ approaches 1 [33]. According to ref. [27], in the vicinity of the melting temperature, T_m, the cooling rate, r, and the undercooling, ΔT_p, corresponding to the peak of the DSC crystallization curve are connected as

$$\log r = const_I - \left(B_2/2.3\Delta T_p^2\right) \text{ (equation 2)}$$

for the homogeneous case and for the heterogeneous case [27]:

$$\log r = const_I - \left(B_2\phi/2.3\Delta T_p^2\right) \text{ (equation 3)}$$

Here

$$B_2 = B_1/nT_m, \text{ (equation 4)}$$

where n is the Kolmogorov-Avrami exponent and B_1 is defined by

$$B_1 = \omega(\sigma^3 V_m^2/k_B \Delta S_m^2) \text{ (equation 5)}$$

where ω is the steric shape factor, σ is the specific surface energy, V_m is the molar volume, k_B is the Boltzmann's constant and ΔS_m is the molar entropy of melting [27]. In deriving eqs. (2) and (3), it is assumed that the degree of overall crystallization corresponding to the peak of the DSC curve always has a constant value [27] and that the

kinetics of crystallization are determined by the rate of nucleation [27]. This effect is evident from the simple fact that in the vicinity of T_m the potential barrier for crystal growth is much smaller than the kinetic barrier for nucleation [27]. It is seen from eqs. that the ratio of the slopes of the linear functions, obtained in coordinates, log r versus $1/\Delta T_p^2$ in cooling experiments T→T_m for the homogeneous and for the heterogeneous case, respectively, would give directly the value of ϕ [27].

Dynamic mechanical analysis (DMA) was performed in a Metler Toledo 861e dynamic mechanical analyser. Specimens were placed in the DMA instrument and oscillated to 3N-30μm or 0.5N-25μm amplitude at 1Hz frequency in the tensile mode. The specimens were heated from 5°C to 90°C at a heating rate of 1°C/min in nitrogen atmosphere. The storage modulus (E'), and loss tangent (tan δ) were used to evaluate the glass transition temperature. The intensity of the transition (S) and the fibre-matrix interface adhesion parameter (b) were calculated in order to study the effect of the filler and the coupling agent. S refers to the mobility and content of the amorphous phase and defined as:

$$S = \frac{E'_b - E'_a}{E'_a} \text{ (equation 6)}$$

where E_a' denotes the storage modulus after and E_b' before the transition. A higher value of S means a superior mobility or a higher content of the amorphous phase.

On the other hand, the fibre-matrix interface adhesion parameter (b) can be graphically calculated from the representation in a coordinated axis of $(\tan \delta)_c / (\tan \delta)_m$ against the volume fraction of the reinforcement [22]. When b=1, there is no formation of immobilized layer, and thus the composite damping is given by that of the matrix amount present in the composite [22]. When b>1, the strength of fibre-matrix interactions leads to an immobilized layer to be formed [22]. The stronger the interfacial interactions, the thicker the immobilized layer, and the higher the value of parameter b. The transition point from weak (b<1) to strong (b>1) interphase adhesion corresponds to an ideal composite (b=1) [22].

Tensile tests

Mechanical tests were carried out using an Instron tensile machine 5565 type at a speed of 10 mm/min in the case of PLCL system and at 5mm/min in the case of PLLA system, both at room temperature. Dumbbell tensile specimens of 1mm thickness and 4 mm width were tested.

Young's modulus of the samples was determined from the slope of the stress-strain function at its linear part and the fracture strain was the elongation at break from the tensile curve. The reported mechanical properties were calculated by averaging measurements of five specimens.

XPS

X-ray photoelectron spectroscopy (XPS) was performed in a SPECS (Berlin, Germany) equipped with a Phoibos 150 1D-DLD analyser and a monochromatic Al Kα (1486.6 eV) X-ray source. Wide scans (step energy 1 eV, dwell time 0.1 s, pass energy 40 eV) were used to identify the existing elements. High resolution spectra (C1s, O1s, Ca2p and P2p) were acquired at an electron take-off angle of 90º (step energy 0.1 eV, dwell time 0.1 s, pass energy 20 eV).

Spectrum were analysed by means of CasaXPS 2.3.16, that models the Gauss-Lorentzian contributions after background subtraction (Shirley). The hydrocarbon peak component in the C1s spectra was set at 285.0eV to correct sample charging (other peaks were corrected accordingly).

The concentrations presented from XPS data are in atomic percent excluding hydrogen which the technique does not detect. RSF correction factors were applied to correct differences in element sensitivity of the apparatus.

Results and discussion

Surface functionalization

Surface modification of HA powder by plasma deposition of poly(ε-caprolactone) and poly(acrylic acid) was evaluated by means of TGA, time of deposition from dispersion, XPS, FTIR and SEM.

Figure 2.2.2 shows the weight loss as a consequence of thermal degradation. The weight loss experimented by neat HA at 100ºC can be attributed to the loss of humidity, whereas the degradation of the organic layer measured in ε-caprolactone and acrylic acid treated particles showed a weight loss of 1.3 and 4.4% respectively. The higher weight loss observed in acrylic acid treated particles suggests that a higher deposition of organic layer has been achieved compared with the ε-caprolactone plasma treated particles.

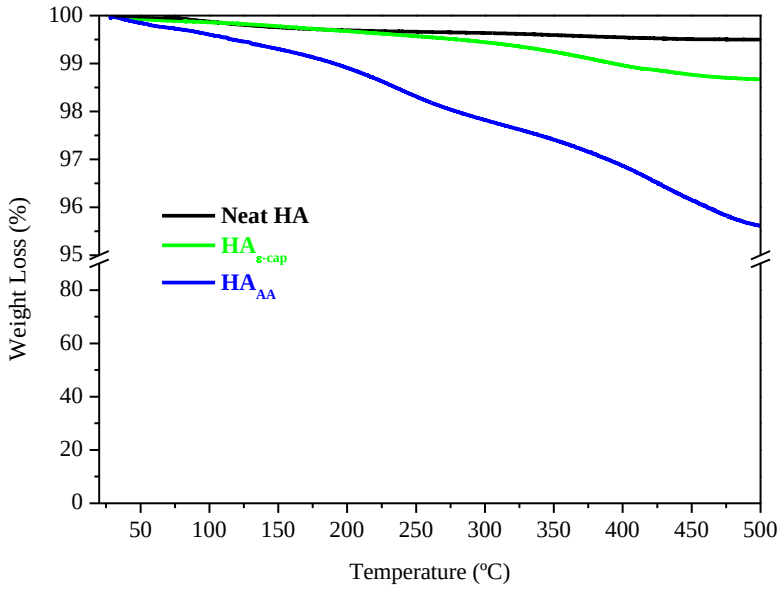

Figure 2.2.2.- Thermal degradation behaviour of neat and plasma treated HA.

Table 2.2.1.- Weight loss calculated from the thermo gravimetric analysis of figure 2.2.1.

	Weight loss **%**
HA	0.521
$HA_{\varepsilon cap}$	1.303
HA_{AA}	4.438

The stability of the HA suspensions with and without poly(ε-caprolactone) plasma treatment was investigated qualitatively by visual observation of their sedimentation rates as shown in figure 2.2.3. HA and $HA_{\varepsilon\text{-cap}}$ particles were dispersed in $CHCl_3$ and were left to sediment for varying times (0, 1', 5' and 90') while photographs were taken. It can be observed, that plasma treated particles kept longer in dispersion than not treated particles, which started sedimentation 1 minute after dispersion. As time elapsed the difference became more noticeable. After 90minutes, approximately all HA particles were observed to sediment, whereas plasma treated particles still showed signs of dispersion.

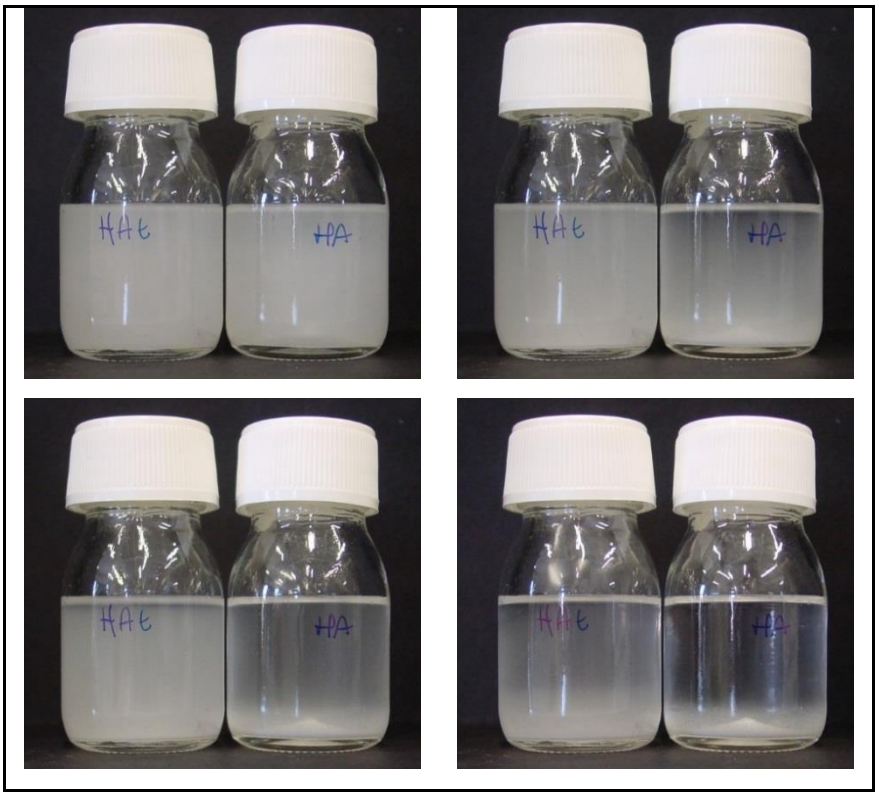

Figure 2.2.3.- Photographs taken after 0, 1', 5' and 90' dispersion of neat and ε-caprolactone plasma treated HA particles in $CHCl_3$.

The XPS wide surveys of the plasma treated Hydroxyapatite particles are showed in figure 2.2.4. In both surveys, the signals of oxygen, carbon, calcium and phosphorus can be distinguished. The presence of Ca and P from the HA, suggests either that the thickness of the deposited layer is less than the XPS analysis depth or that the surface is not uniformly covered, thus revealing the substrate of HA.

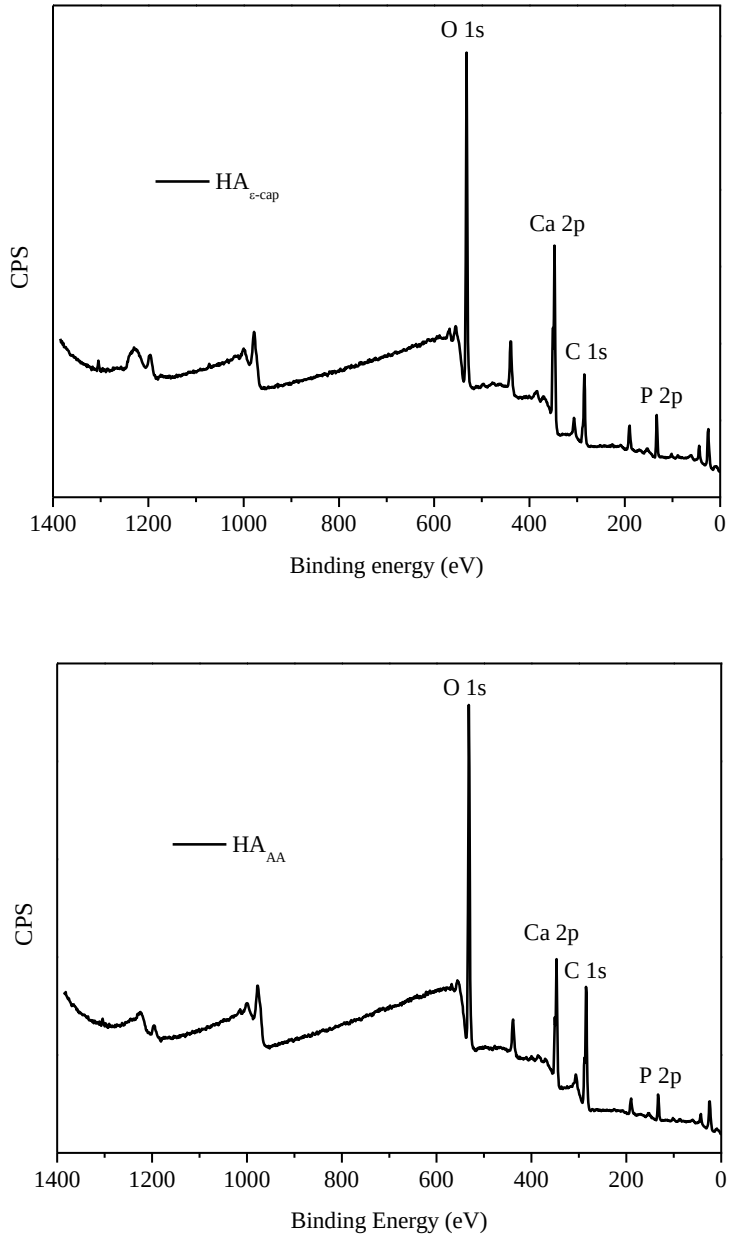

Figure 2.2.4.- XPS wide survey from plasma deposited coatings, a) poly(ε-caprolactone) and b) poly(acrylic acid).

For each plasma treatment, the narrow spectrum of O, C, Ca and P were analysed and their atomic concentration was determined.

The narrow analysis of C1s peak of poly(ε-caprolactone) is shown in figure 5. It can be seen that two peaks [34] corresponding to C-C/C-H and O-C=O respectively, are enough to match the obtained spectra, indicating that only two species are present. The lack of C-O and C=O peaks suggests that no degradation has taken place under the plasma polymerisation conditions and that the O-C=O functionality is fully retained from the monomer structure.

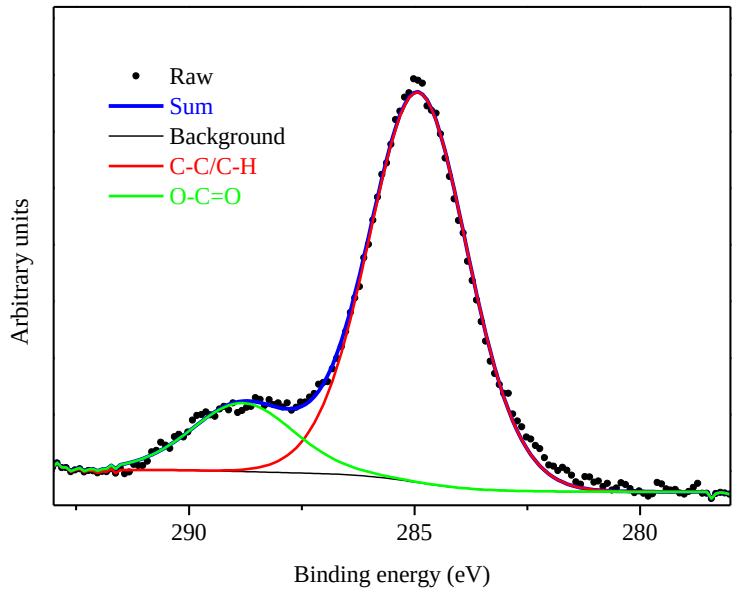

Figure 2.2.5 XPS C1s peaks HA poly(ε-caprolactone).

Results of the poly(ε-caprolactone) plasma treatment are listed in table 2.2.2. Considering the stoichiometry of the existing species, by application of the law of conservation of mass, the source of the elements can be deduced. Therefore, in the case of synthetic HA, its constituents must keep the relation: $Ca_{10}(PO_4)_6(OH)_2$ [18].

Table 2.2.2. Integration parameters of the existing elements: element bonding, position (in eV), full width at half maximum (FWHM), relative sensitivity factors (RSF), integrated area, percentage of atomic concentration, total percentage of the element.

Name	Group	Pos.	FWHM	R.S.F.	Area	% Conc.	%Total
O1s		531.84	2.656	2.93	120314.7	47.96	47.96
C1s	C-C	284.92	2.591	1	18707.5	21.85	25.81
	O-C=O	288.81	2.673	1	3386.5	3.96	
Ca2p	Ca 2p 3/2	347.51	2.377	5.07	51398.3	11.84	16.71
	Ca 2p 1/2	351.14	2.022	5.07	21154	4.87	
P2p		132.7	2.501	1.19	9702	9.52	9.52

Analysing the concentrations of table 2.2.2, it can be seen that the relation found between Ca and P is 1.76, which is near the ratio 10/6 found in the stoichiometric formula. Applying the same reasoning to oxygen, we find that the concentration of this element in HA is 2.4 times that of Ca; therefore, 40.10% from the total oxygen is bound to HA leaving 7.86% which is approximately twice the concentration of C found due to the contribution of the O-C=O group of poly(ε-caprolactone).

The chemical composition of the plasma polymerised poly(ε-caprolactone) was also analysed by FTIR. In order to maximize the signal of the coating, KBr was used as a substrate for plasma deposition. The corresponding spectra is shown in figure 2.2.6 together with the monomer and the conventional polymer for the sake of comparison.

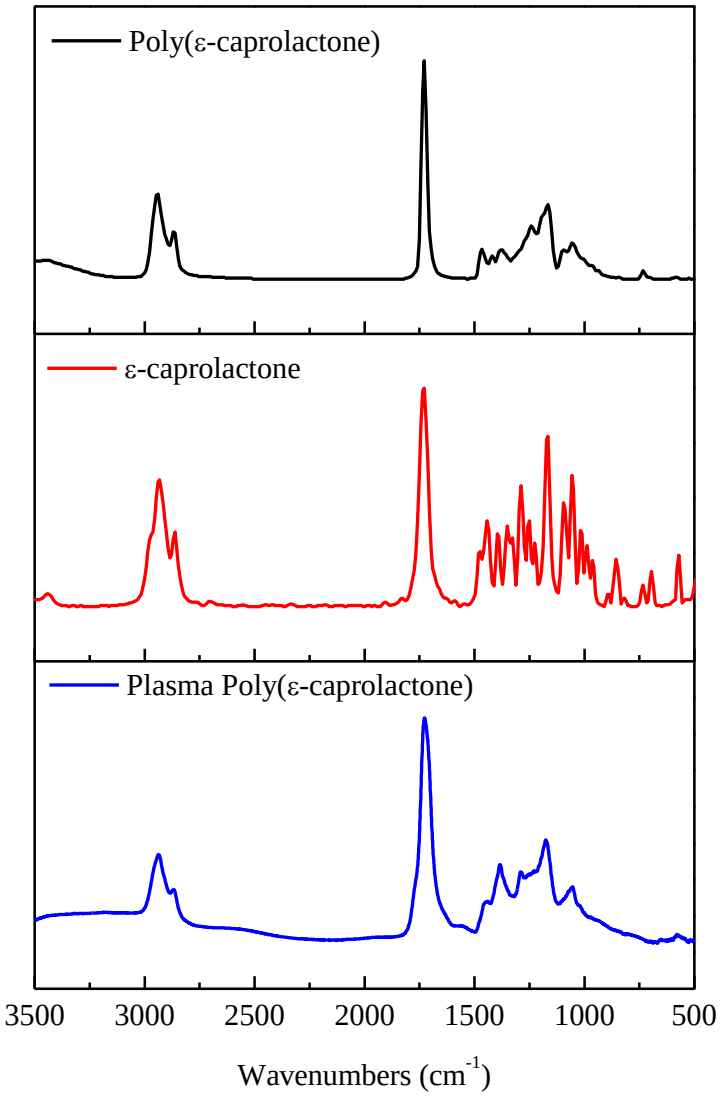

Figure 2.2.6.- FTIR spectra of the conventional polymer poly(ε-caprolactone), monomer (ε-caprolactone) and plasma polymerized poly(ε-caprolactone).

The spectra of the ε-caprolactone shows the C=C absorption band at 1637cm^{-1} and a group of thin absorption bands proper of the cyclic structure of the monomer. The disappearance on the thin absorption bands and the lack of degradation bands indicate that a high conversion of plasma polymerization has been fulfilled without degradation by-products.

The narrow spectra of the poly(acrylic acid) (figure 2.2.7) shows that it can be sufficiently adjusted with two components, indicating that as in the case of poly(ε-

caprolactone) only two species are present. Again, the lack of C-O and C=O peaks suggests that no degradation has taken place under the plasma polymerisation conditions and that the O-C=O functionality is fully retained from the monomer structure.

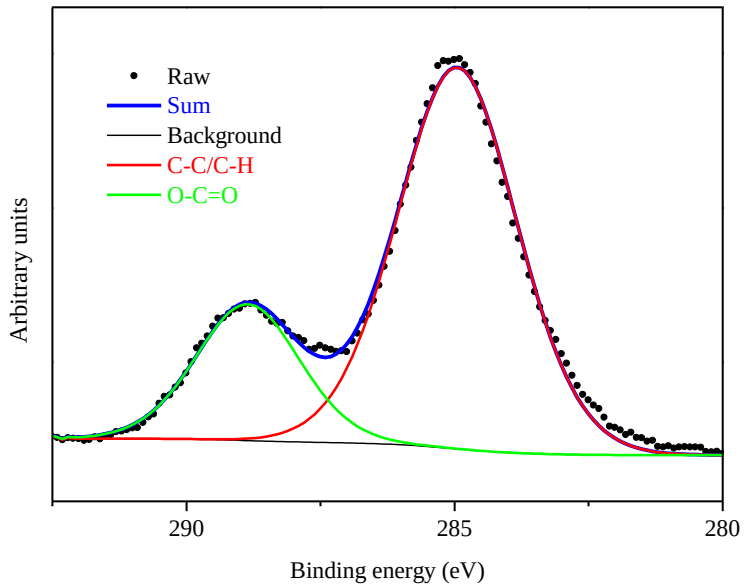

Figure 2.2.7.- XPS C1s peaks HA poly(acrylic acid).

Table 2.2.3 Analysis of the poly(acrylic acid) plasma treated HA XPS spectra.

Name	Group	Pos.	FWHM	R.S.F.	Area	% Conc.	%Total
O1s		532.28	3.074	2.93	106869	43.39	43.39
C1s	C-C	284.95	2.622	1	27158.7	32.31	42.34
	O-C=O	288.86	2.275	1	8431.9	10.03	
Ca2p	Ca 2p 3/2	374.72	2.551	5.07	28807.1	6.76	9.46
	Ca 2p 1/2	351.36	2.033	5.07	11514.5	2.70	
P2p		133.56	2.307	1.19	4807.6	4.81	4.81

From table 2.2.3, the ratio between Ca and P (1.97) is slightly higher than expected (1.67). According to the stoichiometry, the oxygen content due to the HA is 2.4 times the Ca content, leaving 20.69% oxygen which is nearly twice the carbon content due to the acidic group.

FTIR was used to identify functional groups of the plasma polymer film deposited over HA particles. The obtained spectra for the plasma polymerized poly(acrylic acid) is represented in figure 2.2.8 together with the corresponding spectra of the monomer and the conventional polymer.

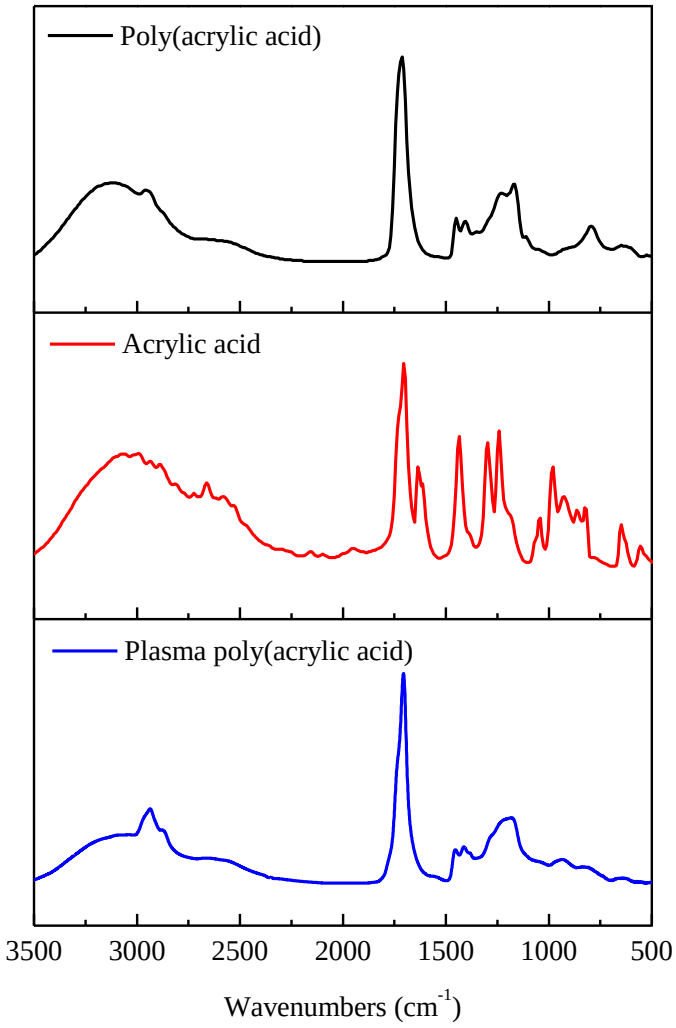

Figure 2.2.8.- FTIR spectra of the conventional poly(acrylic acid), starting monomer acrylic acid and plasma polymerized poly(acrylic acid).

From the plasma polymerized poly(acrylic acid) spectra, C-H (2950cm^{-1}), carbonyl -C=O (1710cm^{-1}) and H-C-H (1459cm^{-1}) can be observed [23]. In there, the lack of the C=C and =CH_2 absorption bands (1637 and 984cm^{-1}) indicated the reaction of the carbon-carbon double bond.

Neat and plasma treated particles were observed by SEM. Photographs taken at several magnifications in figure 2.2.9 show the presence of circular aggregates of about 30μm and fine irregular single particles ranging from 0.1 to 1μm. Aggregates are larger structures of fine particles that tend to combine together and form strongly bonded agglomerates [18, 20]. To form high quality and high performance ceramic polymer composites, the particle aggregates must be broken down during composite processing [18]. Therefore, specially designed processing equipment is often required [35]. In general, irregular shaped particles are preferred to spherical ones because the molten polymer can penetrate to the particle surface during high temperature composite processing and can form a mechanical interlock with the particle, while the smooth surface of spherical particles does not provide such a locking mechanism [18].

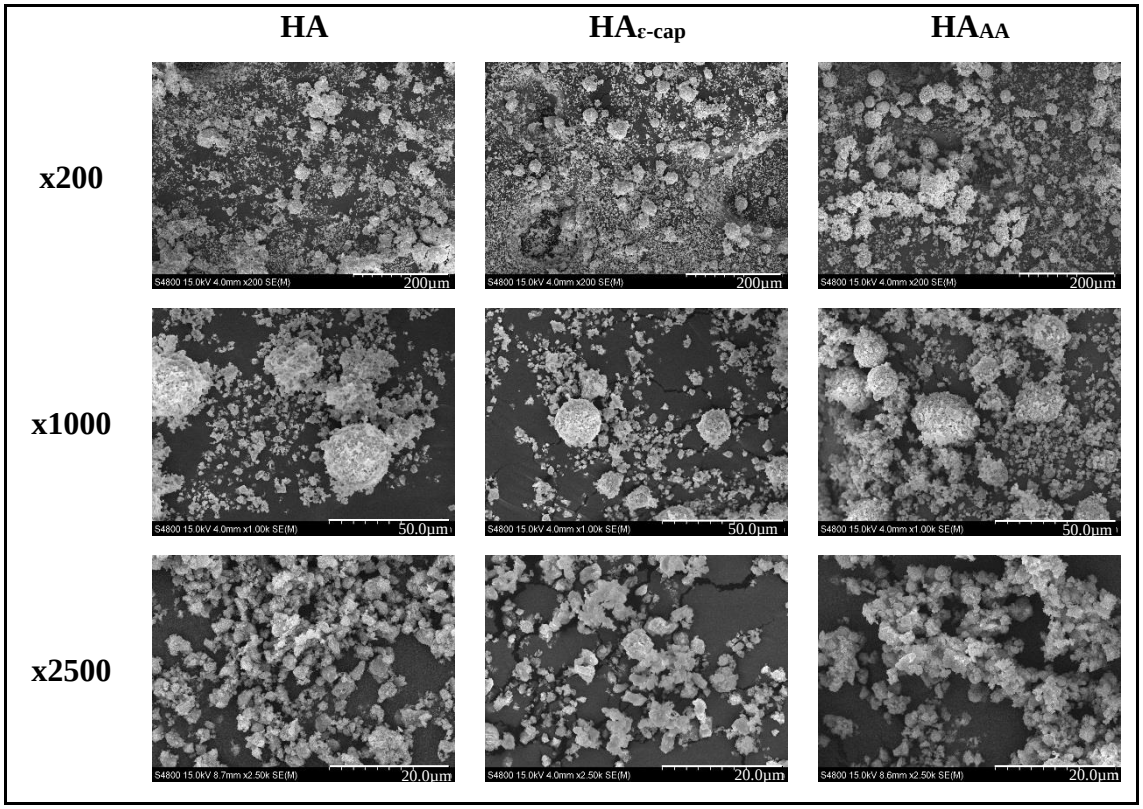

Figure 2.2.9.- SEM photographs of the neat, ε-caprolactone and acrylic acid plasma treated HA particles.

Elastomer matrix composites

PLCL matrix composites were prepared by mixing the appropriate quantities in a twin screw micro-compounder during 15minutes at 200ºC. In this process, HA is intercalated and dispersed in the polymer melt by application of shear forces during compounding [36]. After 15 minutes mixing, composites are injected at 200-225ºC depending on the HA content. Although at these temperatures, phase and compositional changes of the HA are not expected [28], some authors have reported boosted thermal degradation of polymer matrix in bioglass composites processed by thermoplastic techniques [29]. Therefore, thermogravimetric analysis (TGA) was conducted on 10-20mg weight samples cut from the injected samples by heating them under an inert atmosphere from room temperature to 600ºC at 5ºC/min heating rate. TGA provides a good indication of the polymer's bulk degradation rate e. g. for a certain value of residence time at a specified temperature, yet it offers little insight into changes in processing-related properties, which are not always coupled to material loss [37]. However a detailed description of the degradation mechanisms including inherent viscosity measurements, gel permeation chromatography (GPC) [37] or mass spectrometry (MS) and Fourier transform infrared spectrometry (FTIR) [38] are beyond the scope of this study. Accordingly, thermal stability is discussed in terms of the relative position of thermal degradation onset temperature (T_{onset}) regarding that of the neat polymer.

Thermal analysis

The increase in thermal stabilities observed in natural ceramic or clay-polymer composites has been attributed to the higher thermal properties of clay and to the interaction between the clay particles and the polymer matrix [36]. The nanoclays are believed to increase the barrier properties by creating a maze or a "tortuous path" that retard the progress of gas molecules through the matrix resin [39, 40]. Several works with layered silicates and aliphatic polyesters [36, 39-41] or polyurethanes [42] reinforced composites have reported the enhancement of the thermal stability of the polymeric matrix as a consequence of the incorporation of natural (clays) or synthetic ceramics. However, Ray [40] reported a slight degradation of PLA during processing with an

associated reduction in M_w from 177K of PLA to 165K for the 4%montmorillonite. Ignjatovic et al. [43] studied the effect of hot-processing time on degradation of HA/Poly-L-lactide composite biomaterial [43] and found evidences that increasing the hot processing time decreased the thermal stability of PLA matrix [43]. Still, they explained the thermal degradation of PLLA by the final OH groups that "attack" the basic chain at temperatures higher than 500K (223ºC) [43] and did not refer to the presence of impurities, moisture or metals that may catalyse the degradation [44-46]. Moreover, they observed greater thermal stability of composites before hot processing and ascribed it to the presence of HA particles which in the composite acted as barriers preventing heat transfer [43]. Ural et al. studied the degradation of PLCL/HA composites and found that they degraded much slower than pure copolymer and suggested the possibility that HA particles could absorb the degradation products, monomers and oligomers which further reduced the autocatalytic degradation of the polymer phase [47]. Although Ural et al. referred to hydrolytic degradation, it is possible that the same mechanism applies during thermal degradation. Weight loss percentage of neat PLCL and 30% HA content composites are represented in figure 2.2.10. Thermal onset temperature (T_{onset}) and 5 (T_5), 10 (T_{10}), and 60% (T_{60}), weight loss temperatures are listed in table 2.2.4.

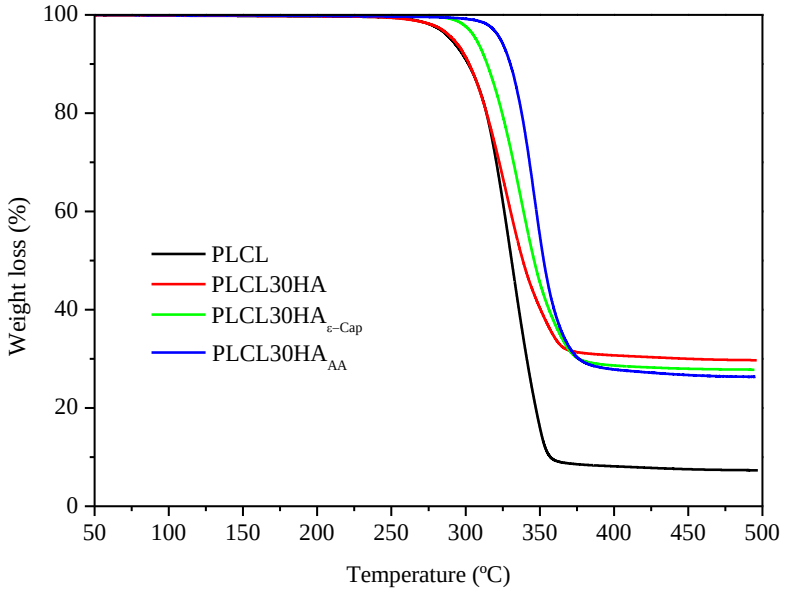

Figure 2.2.10.- Thermogravimetric analysis of the PLCL-30HA system

Table 2.2.4.- T_{onset}, T_5, T_{10}, T_{60} of unfilled and HA and $HA_{\varepsilon\text{-cap}}$ samples

		Neat			
		0HA	**10HA**	**20HA**	**30HA**
T_{onset}	**ºC**	307	294	301	300
T_5	**ºC**	290	287	292	293
T_{10}	**ºC**	303	299	303	302
T_{60}	**ºC**	326	327	332	330
		$HA_{\varepsilon\text{-cap}}$			
		10HA	**20HA**		**30HA**
T_{onset}	**ºC**	310	309		312
T_5	**ºC**	303	303		308
T_{10}	**ºC**	310	310		315
T_{60}	**ºC**	335	334		339
		HA_{AA}			
		10HA	**20HA**		**30HA**
T_{onset}	**ºC**	327	330		330
T_5	**ºC**	320	321		324
T_{10}	**ºC**	327	329		331
T_{60}	**ºC**	346	349		348

As seen from figure 2.2.10 and table 2.2.4, the T_{onset} of HA loaded composites is advanced 6-13 degrees compared to the neat polymer, indicating a moderate effect in the thermal stability due to the addition of neat HA particles. Being the thermal degradation a complex mechanism, it is presumed that impurities may catalyse any of the reactions that take place during the thermal degradation of the polymeric matrix. In contrast a delay in T_{onset} is noted for the plasma coated particles composites, indicating that their thermal stability has been considerably enhanced by the plasma polymerization of the nanoHA, being the most effective the poly(acrylic acid) plasma treatment. Similar results have been reported on coated particles composites [30, 48] although different arguments were outlaid to explain the observed enhancement.

The reason underlying the reported improvement of thermal stability of l-lactide grafted HA particles (g-HA) was a barrier effect of the g-HA particles which slowed down product volatilization and thermal transport which assisted composites with high thermal stability [48].

On the other hand, the proposed mechanism that laid behind the improvement of the thermal stability due to the plasma polymerization of bioglass particles was to avoid the degradation reaction between the $Si\text{-}O^-$ groups present in the surface of bioglass particles and the C=O groups present in the polymer backbone [30, 31].

From TGA, the actual composition of the composites was obtained attributing the weight loss to the organic phase content. Accordingly, considering density values of 1.2 g/cm^3 for PLCL [49] and 3.2 g/cm^3 [4] for HA, the volume fraction of HA was calculated. A summary is listed in table 2.2.5.

Table 2.2.5.- Thermogravimetric analysis of the PLCL system.

	Neat			**$HA_{\varepsilon\text{-cap}}$**			**HA_{AA}**		
	w/w %	**HA %**	**V_{HA} %**	**w/w %**	**HA %**	**V_{HA} %**	**w/w %**	**HA %**	**V_{HA} %**
PLCL0HA	92.7								
PLCL10HA	87.8	12.2	0.05	86.9	13.1	0.05	90.9	9.1	0.04
PLCL20HA	84.4	15.6	0.06	81.3	18.7	0.08	84.8	15.2	0.06
PLCL30HA	70.1	29.9	0.14	72.5	27.5	0.12	73.7	26.3	0.12

From table 2.2.5, no significant deviations in composition from the theoretical values can be inferred.

DSC showed small variations of T_g, ascribed to measurement deviations. Decreasing values of ΔC_p for increasing HA compositions are attributed to the decrease of polymeric content that changes from glassy to rubbery state during the heating scan.

Table 2.2.6.- Glass transition temperature (T_g) and corresponding step in specific heat capacity (ΔC_p) of plain polymer matrix and its composites.

	Neat HA		**$HA_{\varepsilon\text{-cap}}$**		**HA_{AA}**	
	T_g	**ΔC_p**	**T_g**	**ΔC_p**	**T_g**	**ΔC_p**
	ºC	**J/(gºC)**	**ºC**	**J/(gºC)**	**ºC**	**J/(gºC)**
PLCL0HA	20.5	0.492				
PLCL10HA	20.1	0.408	20.8	0.425	20.3	0.410
PLCL20HA	19.7	0.368	20.1	0.412	20.4	0.365
PLCL30HA	21.4	0.329	19.8	0.320	19.5	0.367

Tensile tests

Tensile tests conducted on dumbbell samples are shown in figure 2.2.11. From the obtained graphs, the secant modulus at a 2% strain and stress and strain at rupture were calculated and are resumed in table 2.2.7.

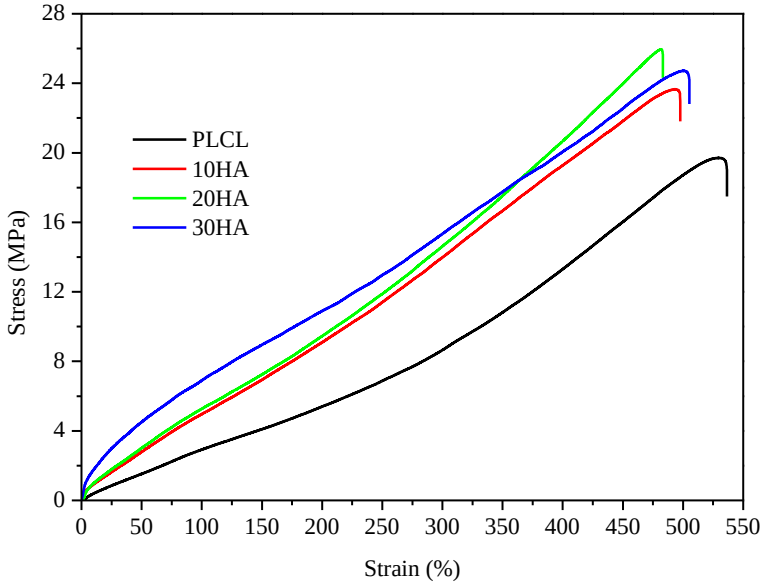

Figure 2.2.11.- Stress-strain graph of neat HA composites

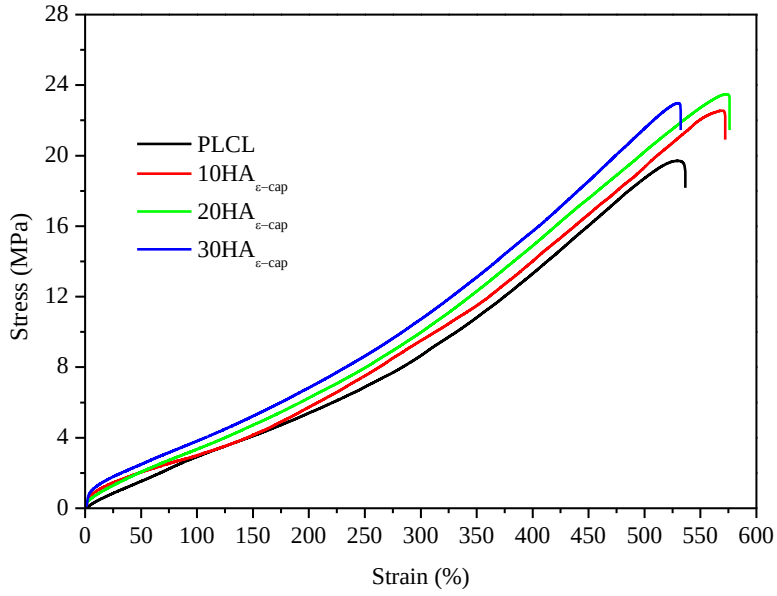

Figure 2.2.12.- Stress-strain graph of $HA_{\varepsilon\text{-cap}}$ composites.

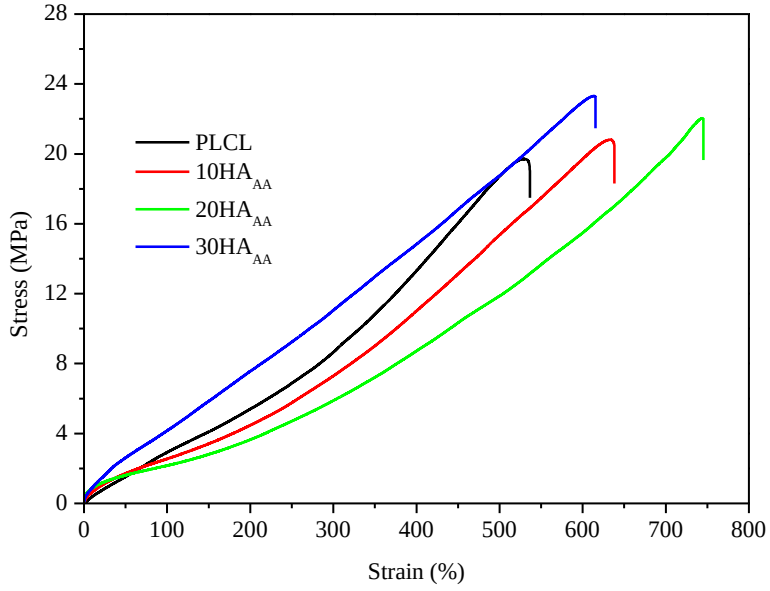

Figure 2.2.13.- Stress-strain graph of HA_{AA} (right) composites.

The tensile graph of PLCL describes the typical elastomeric behaviour with stress-transmission through chain molecules [50] producing arrangement of chains along the stretch direction with strain hardening [51] until slip of chain ends or whole segments and chain scission mechanisms ensue fracture [50]. This fracture theory, correlates sample

strength to limited segmental stress transfer based on observations that the static strength of polymer samples depends on their molecular weight [50]. According to this theory, the introduction of defects or heterogeneities such as a second phase, will affect stress transmission through chain molecules in different ways. If there is a strong interface (e. g., covalent bonds) between reinforcement filler and polymer matrix, load will be transferred to the filler, which will bear the load, increasing the tensile strength of the composite [18]. In contrast, poor bonding strength between polymer and filler serves as a crack path whose growth is subjected to fracture energy and energy dissipation mechanisms at the crack tip [4].

In the studied systems, as depicted in figures 2.2.11 to 2.2.13 and resumed in table 2.2.7, the addition of HA shows an increase in $E_{2\%}$ and in σ_R compared to the neat polymer. However, the obtained data have not been revealed to be very reproducible making it difficult to stablish a correlation with increasing HA, $HA_{\varepsilon\text{-cap}}$ and HA_{AA} content.

The presence of agglomerates (as shown in figures 2.2.15 to 2.2.17), that have endured conformation and impurities on HA surface are thought to have reduced the effectiveness of the plasma coating and contributed to the observed variability on the measured properties. Great variances in surface properties such as contact angle measurements have been ascribed to impurities present in HA [4].

For the ease of discussion, obtained data have been compared to theoretical values predicted according to a model proposed by Nicolais and Narkis [52] which assumes spherical particles with no adhesion between them and matrix, being the load carried by the continuous polymer phase [53]. The tensile strength of the composite, σ_c, is given by

$$\sigma_c = \sigma_m(1 - 1.21V_f^{2/3}) \text{ (equation 7)}$$

where the σ_m is the tensile strength of the matrix and V_f is the volume fraction of the filler. As it can be seen in table 2.2.7, experimental results are higher than predicted values, suggesting some adhesion between matrix and particles and consequent load transfer. The work of adhesion between PLA and HA and between PCL and HA has been reported to be 57±1 and 48±3mJ/m^2 respectively [4]. These values are usually attributed to the formation of a physical bond (e. g. van der Waals and dispersion forces) at the

organic/inorganic interface and the absence of interfacial chemical bonding [4]. Interestingly, the highest values of σ_R and the lowest values of ε_R have been obtained for neat HA composites; whereas plasma coated particles composites achieved higher values of ε_R for lower values of σ_R. This trend suggests that due to the chemical modification of the HA surface, crack propagation has been hampered in favour of higher extended chains.

Corresponding values of ε_R have been plotted in figure 2.2.14. It can be easily noted that the highest extension is obtained for HA_{AA} composites.

Table 2.2.7.- Mechanical properties of PLCL composites.

		$E_{2\%}$ **MPa**	σ_R **MPa**	σ_C **MPa**	ε_R **%**
	PLCL	3.7±0.1	19.7±0.7		532±26
Neat HA	**PLCL10HA**	7.6±0.6	22.7±0.8	16.5	502±27
	PLCL20HA	16.8±5.3	25.1±1.5	15.9	506±40
	PLCL30HA	31.9±0.8	24.9±1.4	13.4	485±36
$HA_{\varepsilon\text{-Cap}}$	**PLCL10HA**	13.8±2.3	23.2±0.6	16.3	563±10
	PLCL20HA	14.6±2.4	23.2±0.6	15.3	580±30
	PLCL30HA	19.7±1.7	21.8±1.0	13.8	558±43
HA_{AA}	**PLCL10HA**	10.3±1.8	21.9±1.4	17.1	606±27
	PLCL20HA	6.2±0.3	23.1±2.1	16.0	706±78
	PLCL30HA	13.4±4.9	22.4±1.0	14.0	671±62

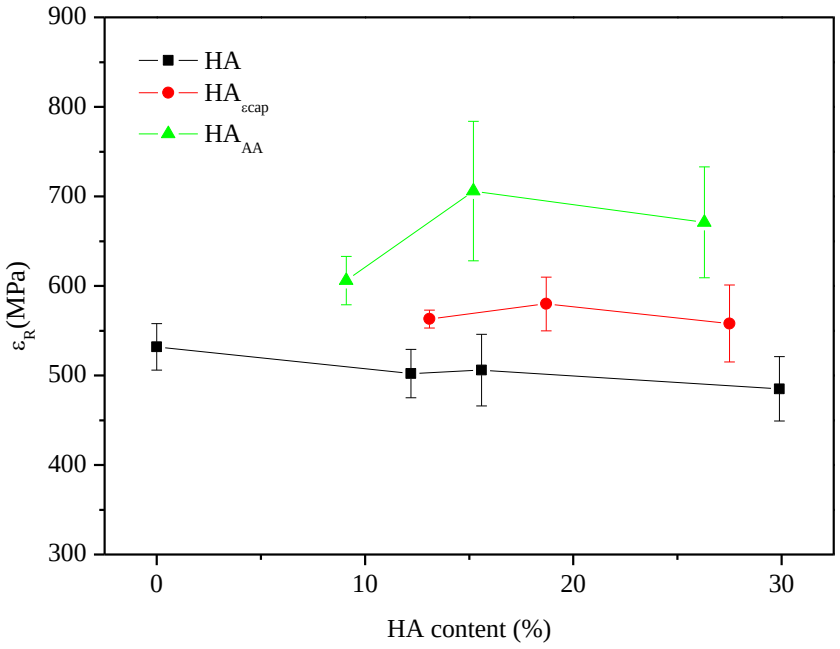

Figure 2.2.14.- Elongation at break vs HA content as determined by TGA.

SEM

Fracture surfaces of the studied composites were observed by SEM at different magnifications (figures 2.2.15 to 2.2.17). SEM microphotographs taken from the neat HA composites (figure 2.2.15), show a two phase separated composite where different sized HA particles are spread onto the polymer matrix, although some aggregates can still be observed. Figures also reveal a close contact between the polymer and the HA particles. At x50 augmentations, the fracture surface is smooth, suggesting elastic crack propagation through organic/inorganic interface. However, a careful observation at higher augmentations, reveals the presence of fibrils indicating that some plastic dissipation mechanisms have been developed at the crack tip.

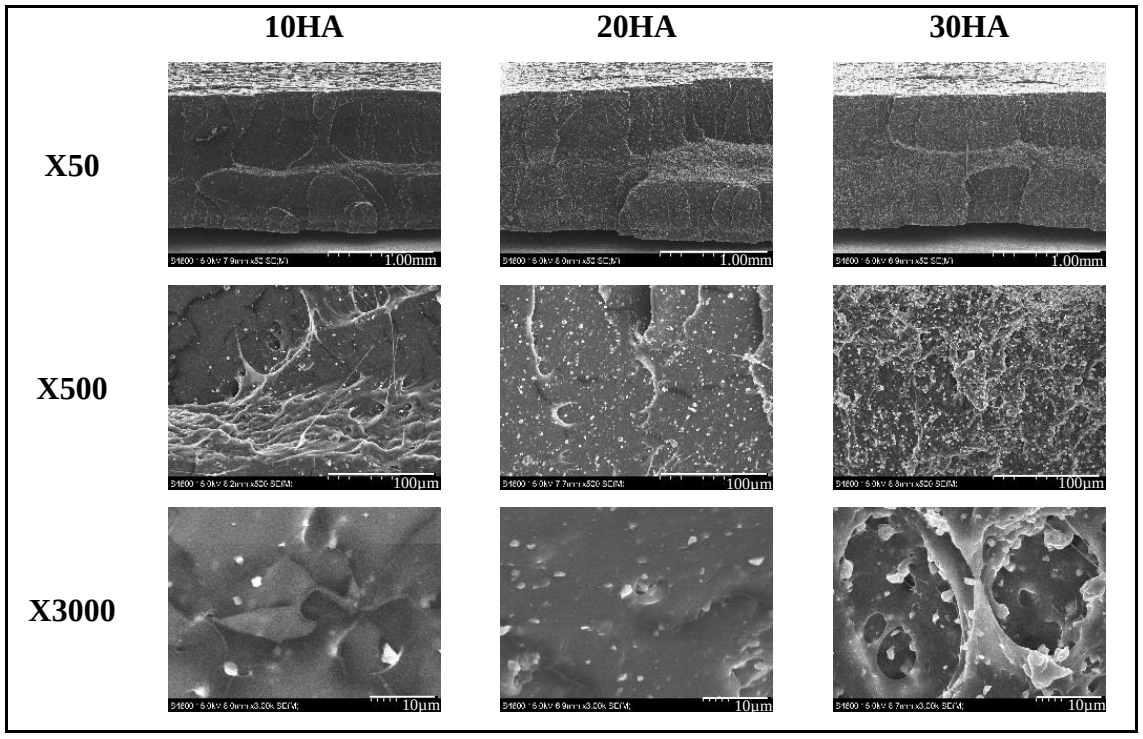

Figure 2.2.15.- SEM photographs of the rupture surfaces of neat HA composites

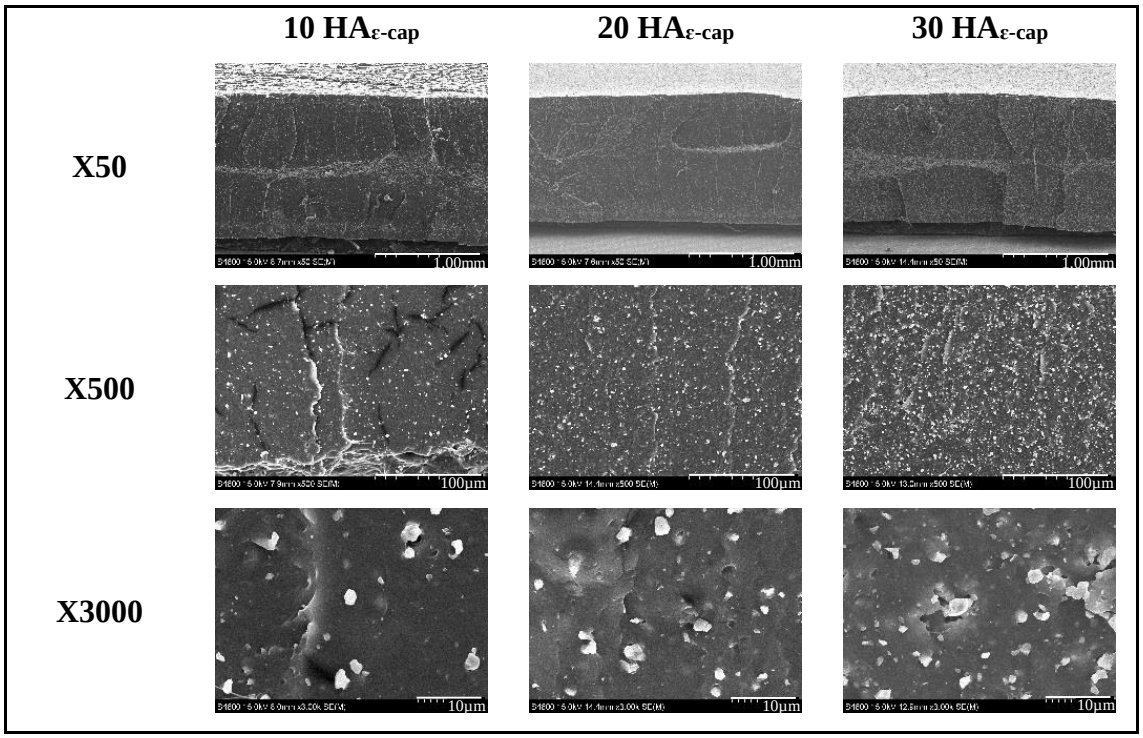

Figure 2.2.16.- SEM photographs of the rupture surfaces of $HA_{\varepsilon\text{-cap}}$ composites

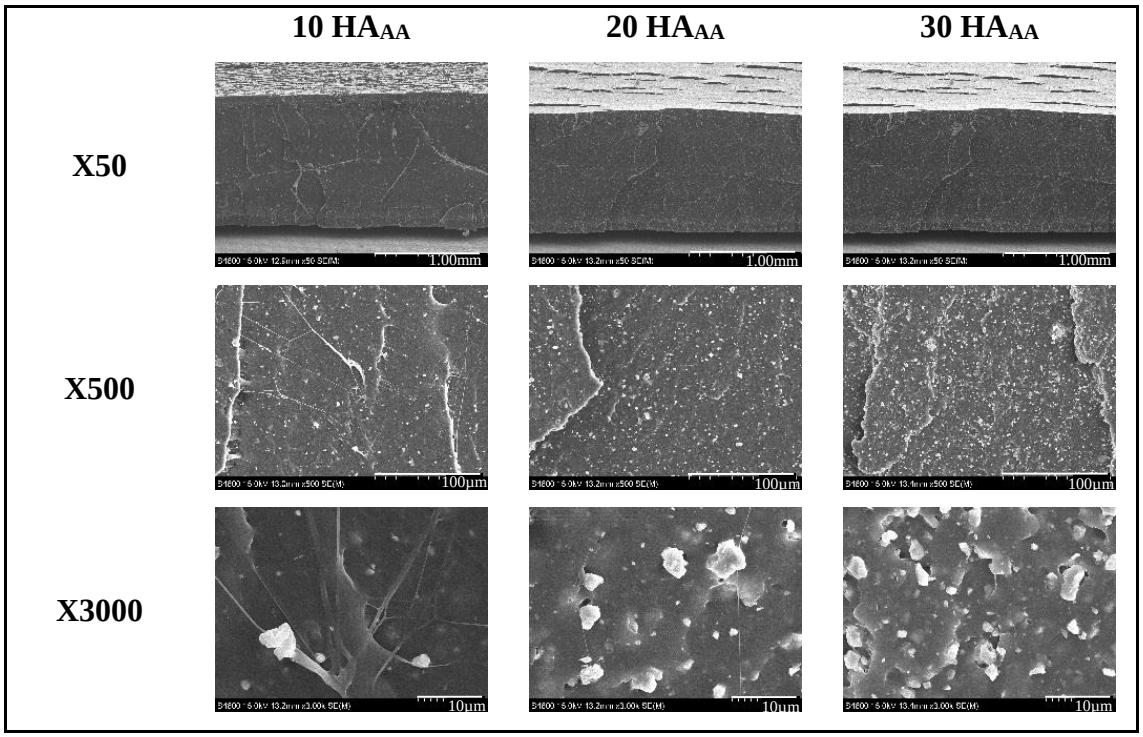

Figure 2.2.17.- SEM photographs of rupture surfaces of HA_{AA} composites

Dynamic mechanical analysis

DMA provides a sensitive test method for chemical and structural changes of polymeric materials and composites as a function of temperature [54]. Pure PLCL and its composites were subjected to low force and displacement amplitude in order to guarantee the elastic regime of the tensile deformation at 1Hz. The storage modulus (E') and the loss factor (tan δ=E"/E') are represented in figures 2.2.18 to 2.2.20. E' represents the elastic component of the properties of a material and is equivalent to the energy stored through the deformation. Being the HA a stiffer material than PLCL, the addition of HA promotes the solid like behaviour as seen by the increase of E' in the rubbery region. Above T_g, when the material becomes soft, the reinforcement effect of particles becomes prominent, due to restricted movement of the polymer chains, and hence strong enhancement of modulus appears [55]. Accordingly, a decrease in tan δ is also observed, although in all cases tan δ >1 indicating the prevalence of the viscous character over the elastic.

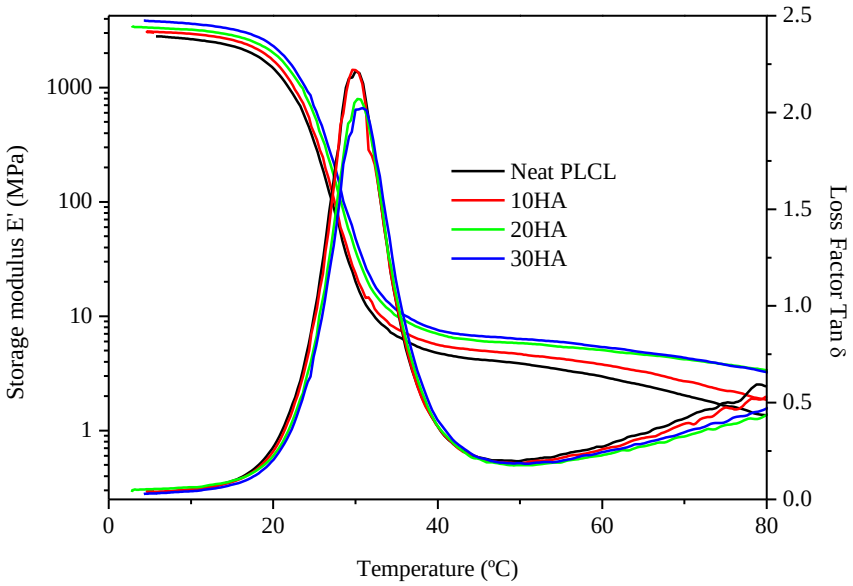

Figure 2.2.18.-Evolution of storage modulus and loss factor of with temperature.

The DMA results of the plasma coated particles show a similar trend than uncoated particles. Increasing the $HA_{\varepsilon\text{-cap}}$ content increases the storage modulus and the highest increase is observed for the 30% composite. The height of the tan δ does not reveal any significant decrease, indicating the damping character of the composites in the transition.

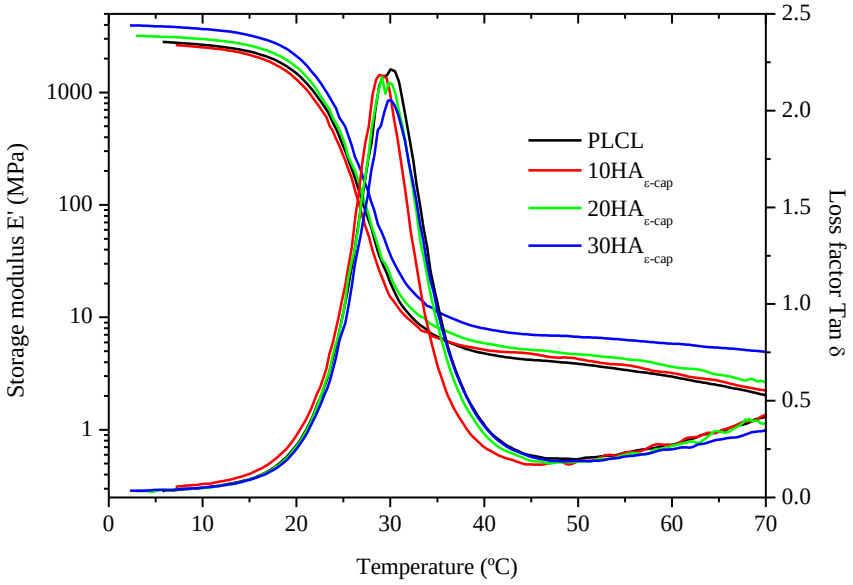

Figure 2.2.19.- Evolution of storage modulus and loss factor with temperature of $HA_{\varepsilon\text{-cap}}$ composites

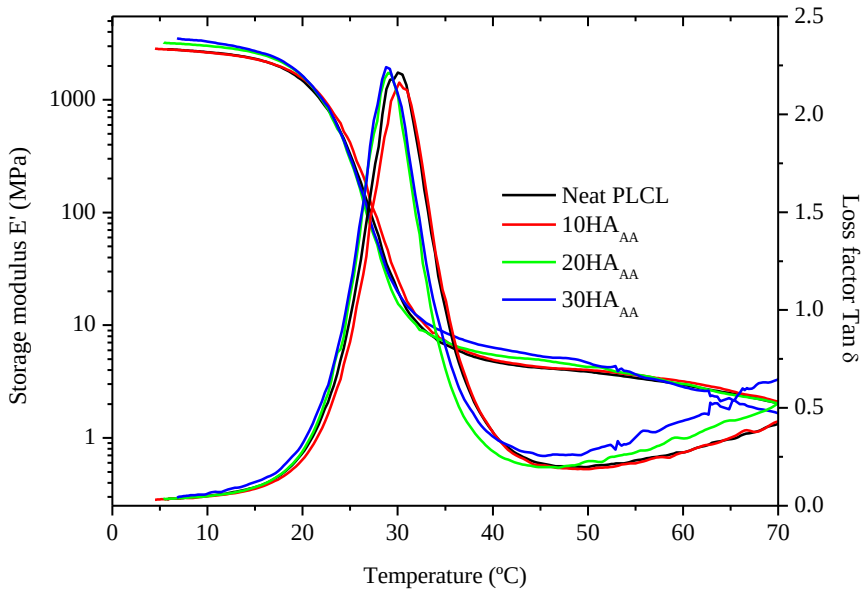

Figure 2.2.20.- Evolution of storage modulus and loss factor with temperature of the poly(acrylic acid) functionalized system.

The intensity of the transition (S) from glassy to rubbery state refers to the mobility and content of amorphous phase. Accordingly, higher S value means a superior mobility or a higher content of the amorphous phase [56]. Thus, corresponding values of E' at 20 and at 40ºC from figures 2.2.18 to 2.2.20 have been substituted in eq. (6) and correspondingly in figure 2.2.21.

Compared to the neat polymer, a reduction of S is observed for HA loaded systems, which is in accordance with the expected behaviour, as the addition of HA particles reduces the content of polymeric phase and therefore its sensibility. However, two opposite trends are observed in figure 2.2.21 depending on the plasma functionalization. Whereas the addition of poly(acrylic acid) treated HA shows a decreasing trend, S seems to increase with the addition of HA and poly(ε-caprolactone) plasma treated particles. The observed increasing trend of S, suggests that although less amorphous phase is present, it has greater mobility. Some authors have ascribed the higher mobility observed in loaded systems with the presence of more polymer free surfaces or free volume [57]. However, in those systems, the facilitated polymer chain mobility has caused a decrease in the glass transition temperature of the composites that has not been observed here. Considering that the HA contribution to the damping is

extremely low compared to that of PLCL matrix, it is possible that new damping mechanisms may be introduced that are not present in the unfilled polymer, which include particle-particle friction where particles are in contact with each other in agglomerates that occur at the higher volume fractions [53].

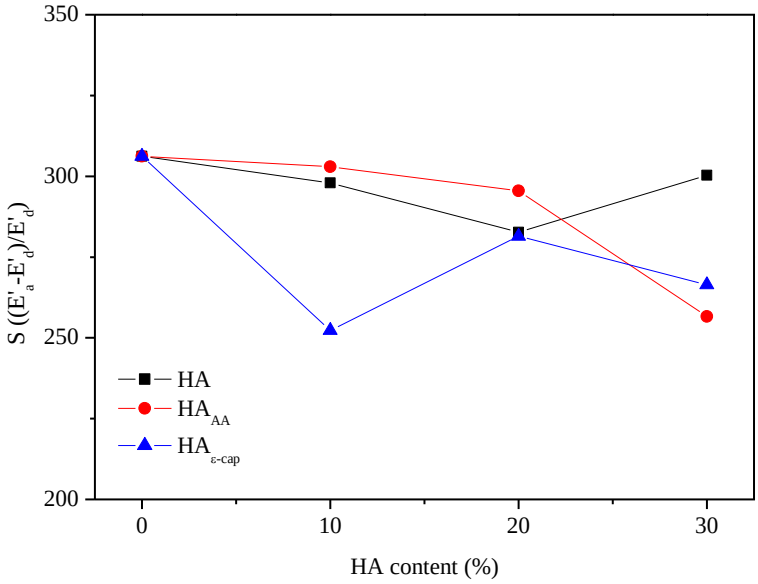

Figure 2.2.21.- Intensity of transition corresponding to HA neat (black), HA_{AA} (red) and $HA_{\varepsilon\text{-cap}}$ (blue) content.

In order to further study the interface, and the formation of an immobilized layer resulting from fibre-matrix interactions [22], the featuring parameter (b) has been graphically (figure 2.2.22) determined by linear fitting of $(\tan \delta)_c/(\tan \delta)_m$ against the corresponding volume fraction of reinforcement fillers deducted from TGA measurements.

Linear fitting of data from figure 2.2.22 gave a negative slope for HA and HA_{ecap} (-0.7021 and -0.2468 respectively) and a positive slope (0.118) for HA_{AA}, being $b<1$ in all cases. Interpretation of $b<1$ suggests that a weak interface has been developed.

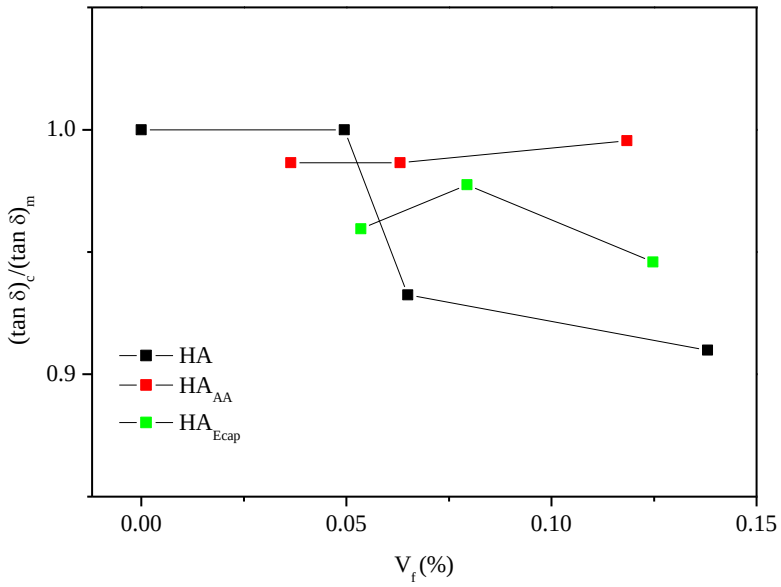

Figure 2.2.22.- Tan δ (composite)/tan δ (matrix) versus fibre volume content (V_f) as determined by TGA

Glassy matrix composites

Thermal analysis

Thermal degradation process of PLA and its composites has been reported to follow a complex mechanism [48] that has been the subject of many publications [58-61]. Although multiwall carbon nanotubes (MWCNTs) have been found to have little influence on the thermal stability at the initial stage of degradation but improved slightly the thermal stability at a higher decomposition level [60], devastating effects on the thermal stability have been reported due to the addition of bioactive glass particles [29].

Graphical representation of the weight loss of neat PLLA and the 30% composites is plotted in figure 2.2.23. From it, an increase of T_{onset} of the poly(acrylic) acid functionalized particles composites indicates an improvement in the thermal stability of the composites as a consequence of plasma coating of the particles, which is in accordance with observations from other authors [30, 31, 48]. Supposing that the reduced thermal stability observed in neat HA composites is associated with the presence of impurities in

HA, plasma coating would create a barrier between impurities and PLA, thus increasing the thermal stability.

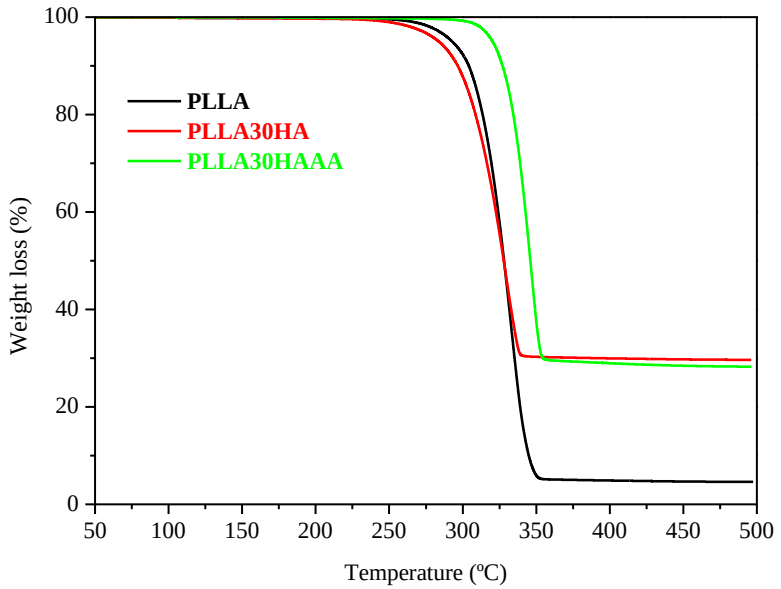

Figure 2.2.23.-Thermogravimetric analysis of neat PLLA and 30% HA composites.

Results of TGA conducted on 10-20mg samples (table 2.2.8) indicate a moderate hastening effect on the onset of thermal degradation for increasing HA content.

Table 2.2.8.- T_{onset}, T_5, T_{10}, T_{60} of unfilled and HA and HA_{AA} samples.

		PLLA	10HA	20HA	30HA
T_{onset}	ºC	319	321	311	303
T_5	ºC	295	306	298	288
T_{10}	ºC	310	315	309	301
T_{60}	ºC	333	337	332	328
			$10HA_{AA}$	$20HA_{AA}$	$30HA_{AA}$
T_{onset}	ºC		328	329	328
T_5	ºC		322	321	321
T_{10}	ºC		327	327	327
T_{60}	ºC		340	343	343

Tensile tests

Mechanical strength and elasticity modulus play a significant role in implantation and exploitation of the biomaterial [43]. The addition of HA, which has a reported Young's modulus of 35-120GPa and a tensile strength of 100-900MPa [4] is expected to have a reinforcing effect on PLLA matrix, although as explained previously, the fracture reinforcement effect is subjected to the interface adhesion between matrix and filler and to plastic dissipation mechanisms at the crack tip [4]. The mechanical properties were calculated from tensile tests conducted on PLLA and its composites. Graphical representation and corresponding fracture surfaces are shown in figures 2.2.24 to 2.2.29.

From figure 2.2.24 the reduction of elongation at break by addition of 10% HA into the polymer matrix can be noted, which suggests an inadequate adhesion of the filler particles to the polymer matrix [26]. Although some authors have reported PLA to be linked chemically with calcium orthophosphates such as TCP or HA [62] by means of a weak ionic bond between Ca in orthophosphates and oxygen in a C=O ester group double bond [26] the bonding strength at PLLA/HA interface has been reported to be in the range of physical bond (20±4MPa) and not in the chemical bonding range [4]. On the other hand, the shape of the fillers is also a key factor in crack propagation being the fibre-shaped fillers more effective than particulate ones [26].

Plasma modified particles seem to produce a considerable reinforcing effect as seen in figure 2.2.24. The observed increased in elastic modulus suggests a better interface between the functionalized particles and the matrix, able to share the applied load efficiently due to the formation of a bond between functionalized particles and PLA matrix. Some authors have reported 6-11GPa of modulus of elasticity in bending mode for a 30-70%wt calcium metaphosphate glass fibre which is in the range of natural cortical bone [62]. However, greater increases have been obtained for fibres. The modulus of elasticity of PLLA composites was increased to 4.3GPa when 5μm particle size HA was used [26].

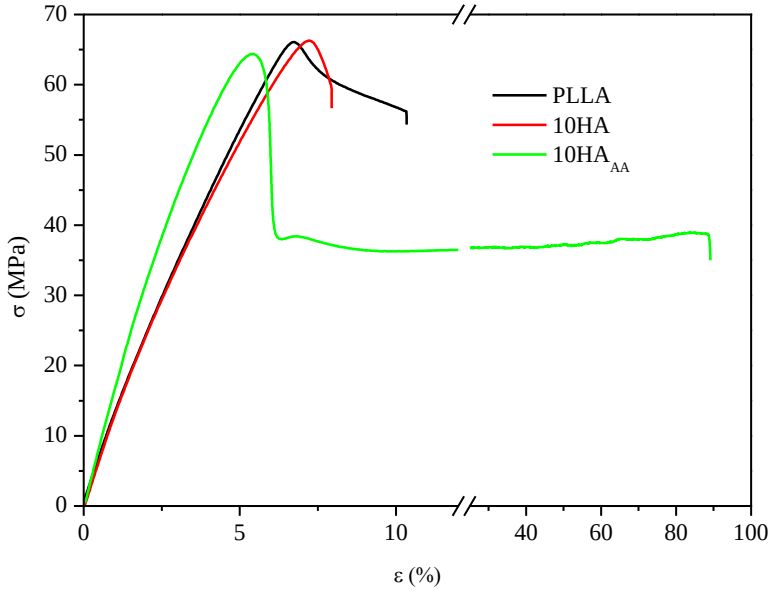

Figure 2.2.24.- Tensile tests conducted on PLLA, 10HA and 10HA$_{AA}$ composites.

Interestingly, the addition of 10%HA$_{AA}$ particles increased the ductile behaviour with neck formation and growth suggesting the development of dissipation mechanisms at the crack tip by plastic deformation.

Figure 2.2.25 shows the tensile tests of 20%HA composition. Again, a higher reinforcement effect is noted as a consequence of plasma coating.

It is worth to note that plasticization mechanisms were observed in some samples whereas others showed brittle surface as revealed in the fracture SEM micrographs of figure 2.2.28.

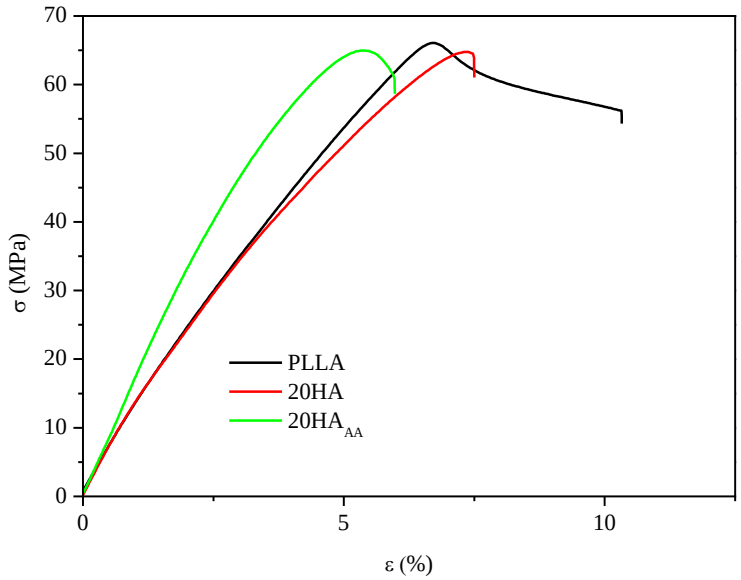

Figure 2.2.25.- Stress-strain graph of PLLA (black) and its composites 20%HA (red) and 20%HA$_{AA}$ (green).

Further increasing the HA content caused discontinuities in the matrix reducing the plasticization capacity and promoting brittle behaviour as evidenced by tensile tests and surface micrographs of figures 2.2.26 and 2.2.29 respectively.

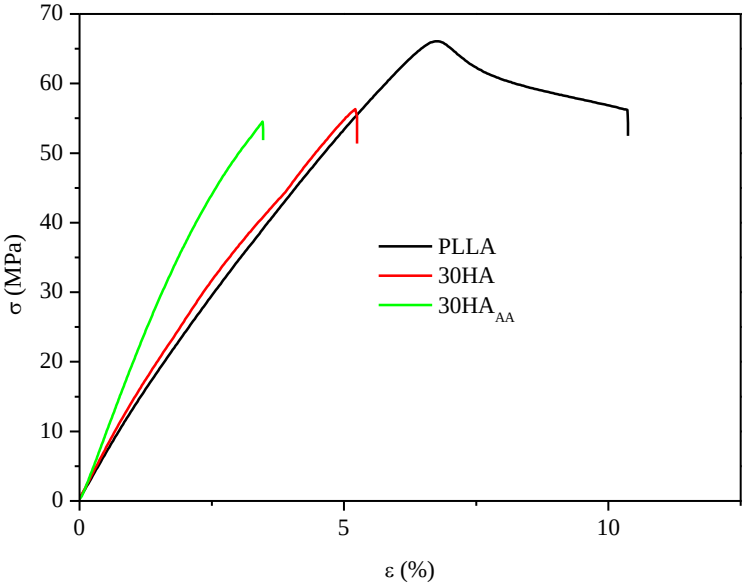

Figure 2.2.26.- Stress-strain graph of PLLA (black) and its composites 30%HA (red) and 30%HA$_{AA}$ (green).

Table 2.2.9.- Mechanical properties of PLLA composites

	E	**σ_Y**	**ε_Y**	**σ_R**	**ε_R**
	MPa	**MPa**	**%**	**MPa**	**%**
PLLA	1360.5±80.2	65.7±0.8	7.3±0.3	57.2±0.7	10.2±0.5
10HA	1404.7±54.0	63.8±5.3	7.2±0.3	58.2±4.8	7.8±0.4
20HA	1571.0±92.8	63.6±1.6	7.5±0.4	62.9±1.5	7.6±0.5
30HA	1564.1±111.4	58.7±3.4	5.9±0.5	58.4±3.2	6.0±0.5
10HA$_{AA}$	1657.2±128.2	63.9±1.0	5.8±0.4	41.0±12.7	57.6±62.2
20HA$_{AA}$	1743.0±79.0	63.3±2.2	5.4±0.3	61.2±1.7	7.0±2.5
30HA$_{AA}$	1873.3±179.8	52.3±9.2	3.7±0.4	52.8±7.0	3.7±0.3

Table 2.2.9 resumes the mechanical properties of the composites and the neat polymer. It can be seen that the addition of neat HA causes a moderate increase in the elastic modulus, whereas the functionalization of these particles with poly(acrylic acid) has a stronger reinforcing effect on the composites.

SEM

The fracture surfaces were analysed by SEM, and corresponding photographs are shown in figures 2.2.27 to 2.2.29.

Fracture surfaces of figure 2.2.27 show the uniform distribution of HA particles onto the surface whereas the presence of aggregates was not observed, indicating that a good dispersion had been achieved during mixing operation.

Photographs at 500 and 3000 augmentations of neat PLLA and neat HA composite displayed even surfaces, in accordance with the scarce plastic strain measured by tensile tests, whereas plasma coated particles were surrounded by a markedly deformed polymer matrix.

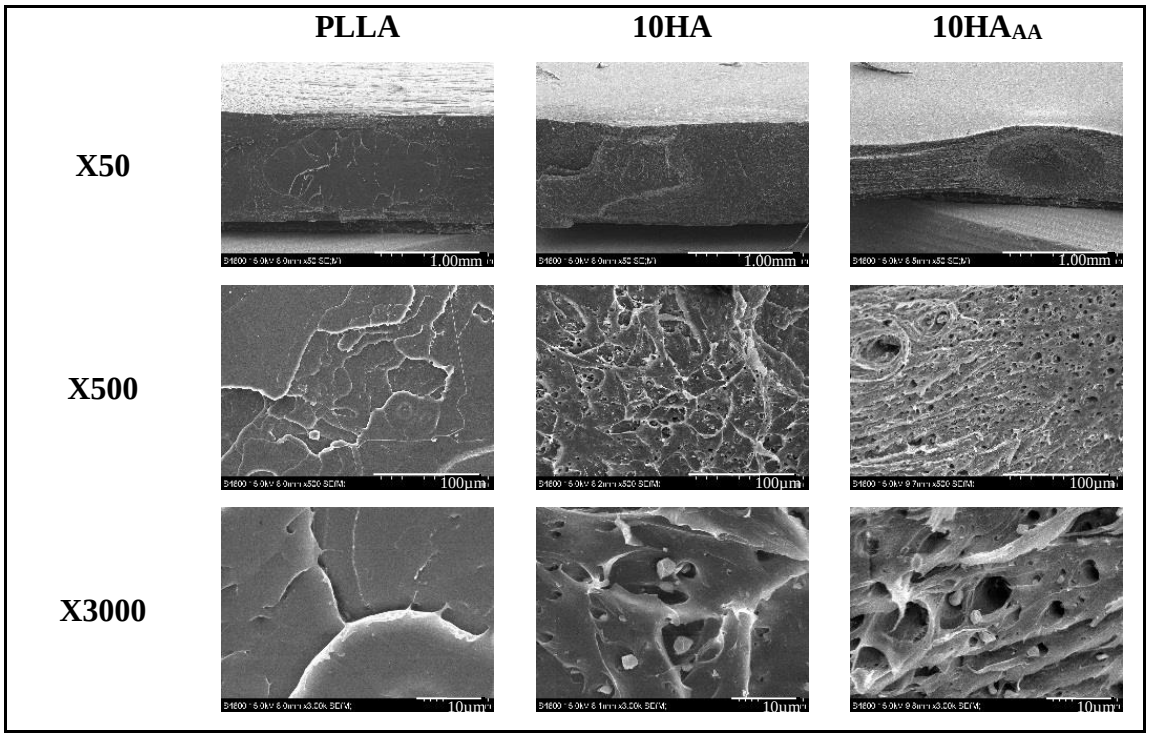

Figure 2.2.27.- SEM photographs of the fracture surface after tensile tests

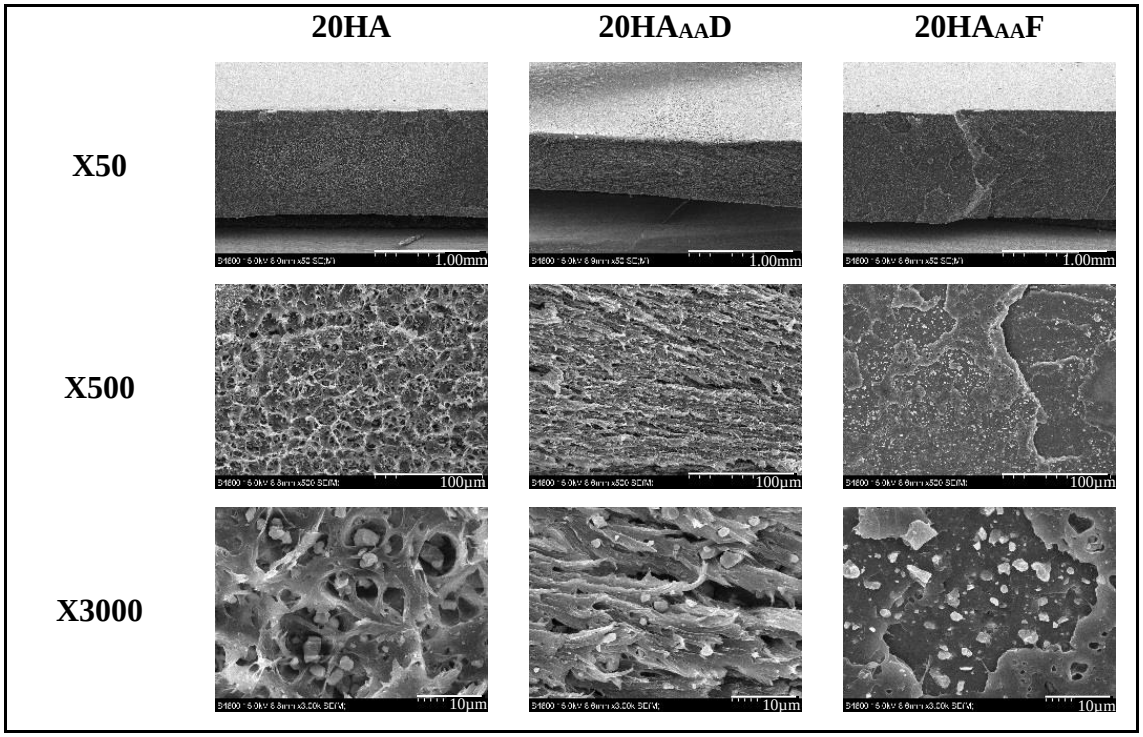

Figure 2.2.28.- SEM photographs of the fracture surface after tensile tests.

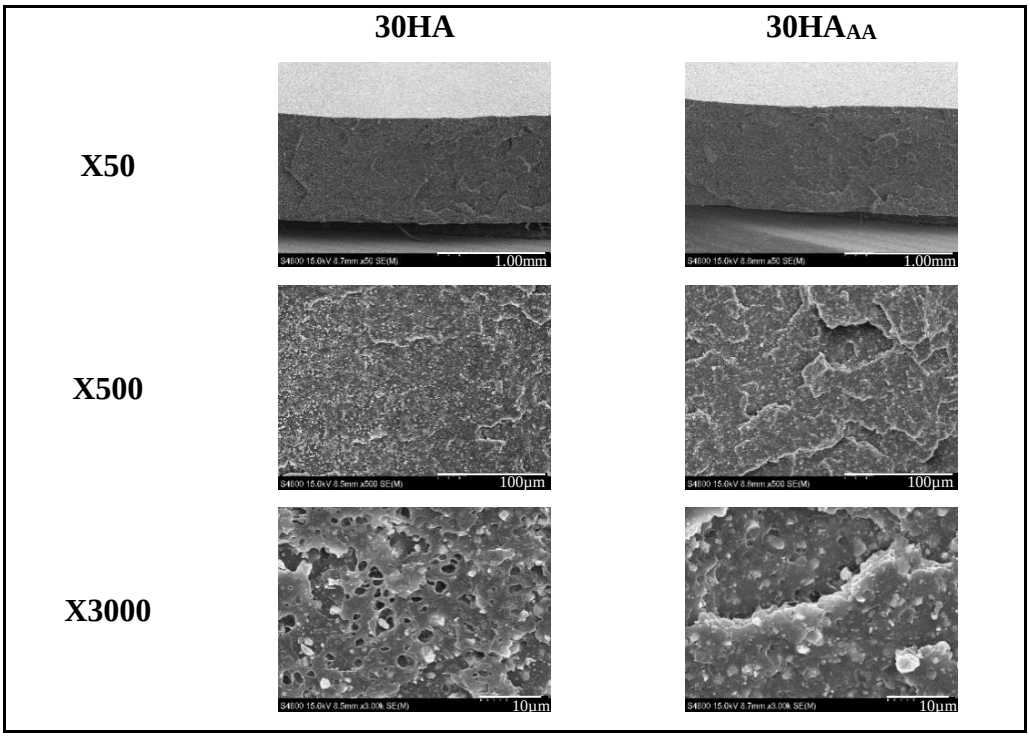

Figure 2.2.29.- SEM photographs of the fracture surfaces.

Observation of the surfaces at x3000 lead to note the presence of smooth irregular voids carelessly distributed onto the surface. From their appearance and the lack of plastic deformation it can be inferred to have been formed during the solidification of the melt as a consequence of the presence of air bubbles. Their existence is thought to have disguised the reinforcement of the HA particles promoting brittle fracture due to stress concentration and reduction of the effective cross section that bore the load during the tensile tests.

Dynamic mechanical analysis

Figure 2.2.30 compares the temperature dependence of E' of neat PLA and 10%HA composites, showing an increase of E' as a consequence of HA addition and further increase for functionalized particles. Moreover, due to the presence of particles, E' after the glass transition maintains at higher values than plain matrix polymer. Similar results have been reported when HA was added to polylactides [54]. Further increasing the temperature shows a recovery in the storage modulus. This recovery is usually ascribed to the cold crystallization promoted during the heating scan. It is observable that

the filled composites exhibit a higher recovery of the storage modulus, suggesting higher presence of crystals. The faster crystallization in filled composites could derive from an amorphous phase with greater mobility resulting in a higher value of tan δ peak [56]. The effect of particles as nucleating agents will be discussed later.

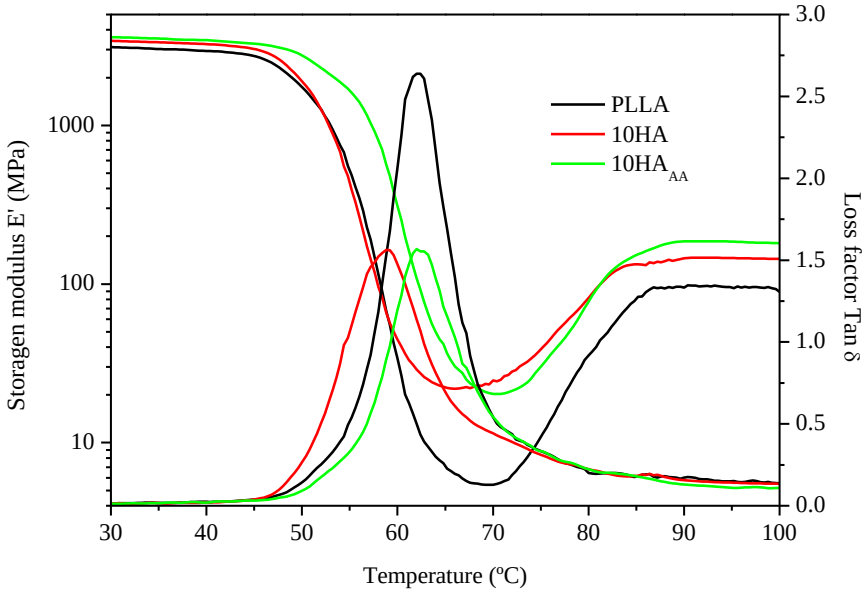

Figure 2.2.30.- Dynamic mechanical analysis of PLLA (black), 10HA (red) and 10HA$_{AA}$ (green).

Differences in tan δ are easily seen in figure 2.2.30. When incorporating HA particles, the loss tangent decreased mainly due to the volume effect [5] although the predominating viscous character of the matrix is preserved as in all cases tan δ>1. Besides, the peak temperature of 10% HA is advanced regarding that of the bare polymer. Some authors have reported the decrease of T_g with increasing nano-particle loading and attributed it to the creation of large interfacial zone leading to dispersed regions of high chain mobility [57, 63]. Conversely, the addition of HA$_{AA}$ particles retarded the apparition of T_g. It is possible that this retardation is due to the partial immobilization of the polymer and a physical blocking of a number of molecular configurations as a result of adsorption onto the filler surface [54]. If an adsorbed layer is more rigid than the polymer matrix, then the glass transition of this layer would be expected to be greater than that of the polymer matrix [54]. Thus, the adsorbed layer of polymer on the filler surface can increase both the modulus and the transition [54].

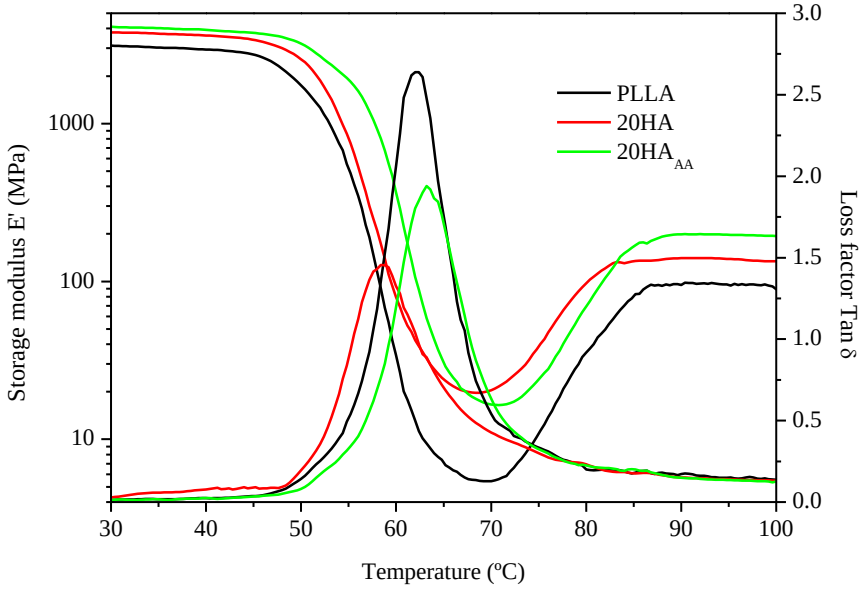

Figure 2.2.31.- Dynamic mechanical analysis of PLLA (black) and PLLA/HA (red) and PLLA/HA$_{AA}$ (green) composites with 20% weight HA.

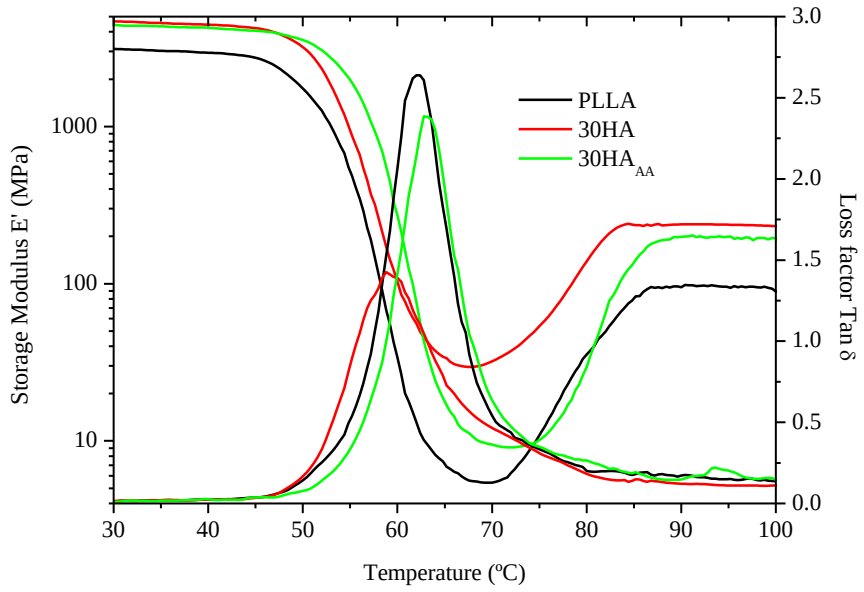

Figure 2.2.32.- Dynamic mechanical analysis of PLLA (black) and PLLA/HA (red) and PLLA/HA$_{AA}$ (green) composites with 30% weight HA.

Figures 2.2.31 and 2.2.32 show the evolution of E' and loss tangent with temperature for 20% and 30% HA composites. Interestingly, increasing the HA$_{AA}$ content promotes the damping character of the composites as evidenced by the growing value

trend observed in tan δ. Apart from this, the observed increase of E' below glass transition and after cold crystallization followed the expected trend.

In order to evaluate the amorphous phase, the intensity of transition (S) was calculated from the DMA data. Obtained values are plotted for each composition in figure 2.2.33.

The intensity of transition is subjected to the amount and mobility of the amorphous phase that changes from glassy to rubbery state because HA in this temperature range displays negligible changes in its mechanical properties [54]. Interestingly, increasing the filler content increases S, indicating an enhanced mobility of the amorphous phase by the addition of particles, noting the highest increase of S in poly(acrylic acid) functionalized particles.

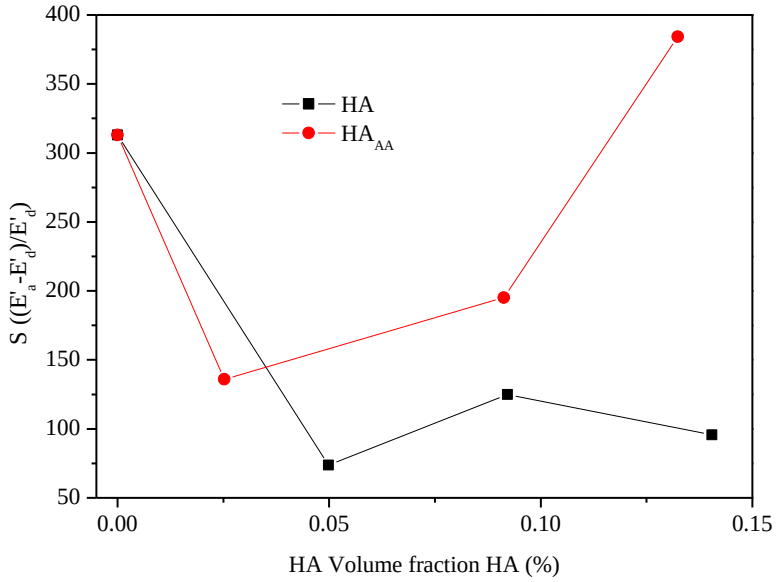

Figure 2.2.33.- Intensity of transition corresponding to HA neat (black) and HA_{AA} (red) volume fraction.

In order to further characterize the fibre-matrix interface adhesion, parameter (b) was graphically calculated from figure 34. Linear fit of the data gave b=-0.5364 for HA composites and b=2.7881 for HA_{AA} composites. Interpretation of b<1 suggest the formation of a weak interface, whereas b>1 suggest a thick immobilized layer [22].

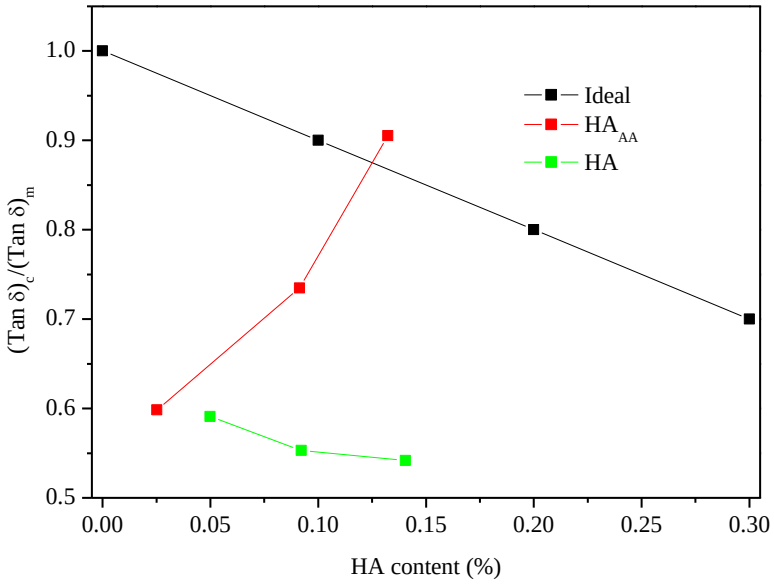

Figure 2.2.34.- Tan δ (composite)/tan δ (matrix) versus fibre volume content (V_f) as determined by TGA.

Following the observed cold crystallization in DMA, a further study on crystallization kinetics of PLLA composites was conducted in order to elucidate the role of HA particles as nucleating agents. Studies on polylactide/layered silicate nanocomposites have shown that the surface of the dispersed silicate act as a nucleating agent for PLA crystallization, leading to the formation of smaller spherulites starting from increased number of nuclei [64]. Therefore, it can be inferred that the strength enhancement observed in filled composites is not only due to the reinforcement effect of particles but to increased crystallinity degree as a consequence of their nucleating activity.

Non-isothermal crystallization kinetics

Since in its amorphous form, the range of applications of PLA is severely limited by its low T_g, many attempts have been made to increase the crystallization rate of PLA [65]. In the present study, the non-isothermal crystallization kinetics of PLLA, 30HA and $30HA_{AA}$ was evaluated. Accordingly, 5mg samples of the above mentioned compositions were submitted to different cooling rates and subsequent heating ramps. Details are showed in figure 2.2.35. Subsequent heating scans revealed that decreasing cooling rates gave place to the apparition of two endothermic peaks that eventually converged into one

single peak as cooling rate was increased. Together with this, the apparition of an exothermic peak just before the melting was observed.

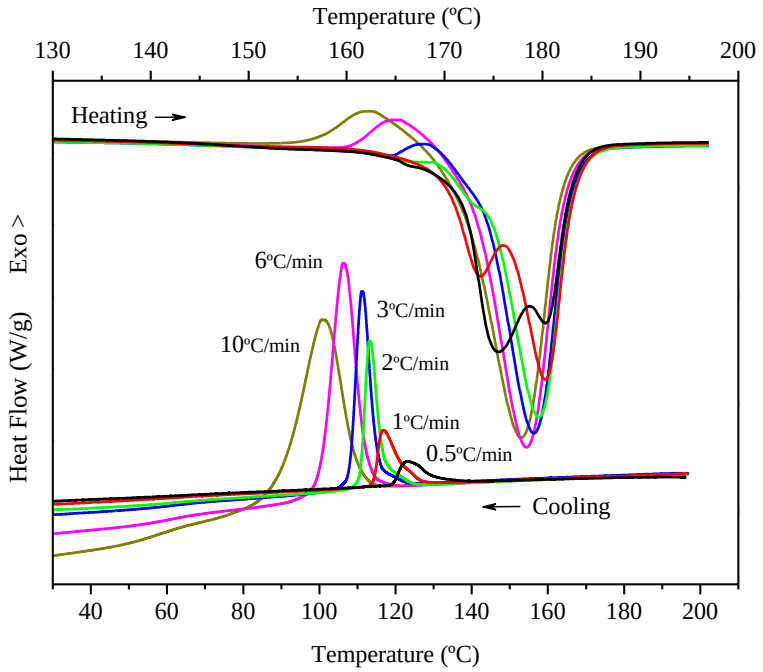

Figure 2.2.35.- DSC thermograms obtained from nonisothermal crystallization and subsequent heating scans of PLLA.

The nonisothermal crystallization thermograms for neat PLLA and 30% HA composites obtained at 8 cooling rates are represented in figures 2.2.36 to 2.2.38. From these curves, the peak temperature (T_p) at which the sample exhibits the fastest crystallization were extracted and used for further calculations. It can be seen that the crystallization exotherm becomes broader and shifts to a lower temperature with increasing cooling rates, as would be expected for crystallization in a nucleation controlled region [65]. It is also noted the eventual displacement of the maximum towards lower values of temperature. This maximum has been attributed to crystallization in the α' polymorph that causes a drastic increase of crystallization rate below 120ºC [66]. According to figures 2.2.36 to 2.2.38, PLLA and $30HA_{AA}$ reached the maximum at 6ºC/min, whereas 30HA at 8ºC/min.

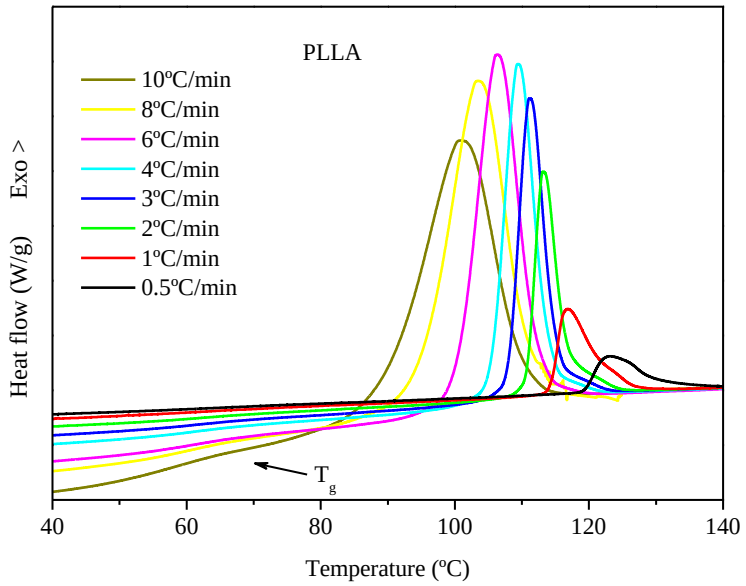

Figure 2.2.36.- DSC thermograms obtained for nonisothermal crystallization of neat PLLA at the indicated cooling rates.

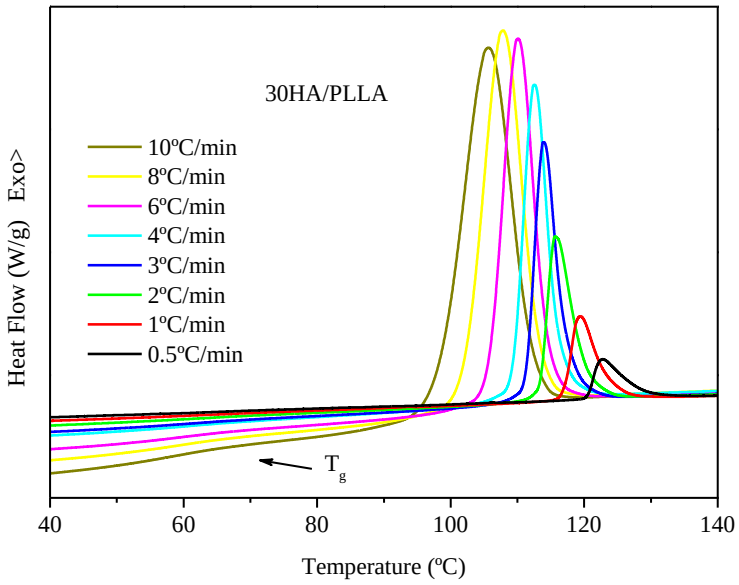

Figure 2.2.37.- DSC thermograms obtained for nonisothermal crystallization of 30HA composite at the indicated cooling rates.

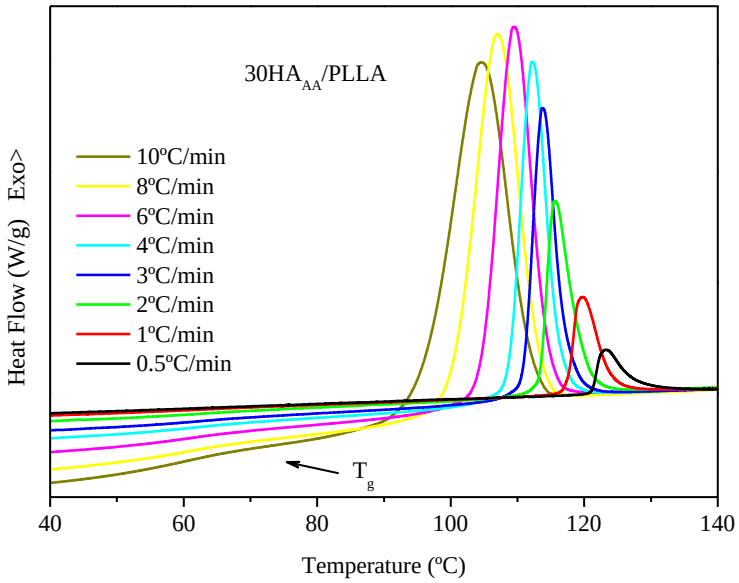

Figure 2.2.38.- DSC thermograms obtained for nonisothermal crystallization of 30HA$_{AA}$ composite at the indicated cooling rates.

It must be pointed out that visual examination of curves 2.2.35 to 2.2.38 may lead to the erroneous conclusion that increasing the cooling rate increases the crystallinity degree, as derived from the enclosed area under the peak. This misleading observation is because time is not represented in this graph. But crystallization enthalpy ($\int_{T1}^{T2} \frac{dH}{dt} dt$) depends on time, so that, as it was expected and mirrored in figure 2.2.39, the slower the crystallization rate, the higher the crystallinity is developed. Thus, the crystallinity degree developed during the cooling scan was calculated and plotted accordingly figure 2.2.39. In the case of pure PLLA no further correction was needed, but in the composites, X_c was calculated according to the polymer fraction content. The polymer fraction in 30HA and 30HA$_{AA}$ composites was corrected according to the measured weight loss obtained from the TGA conducted on the very samples after the DSC cycles.

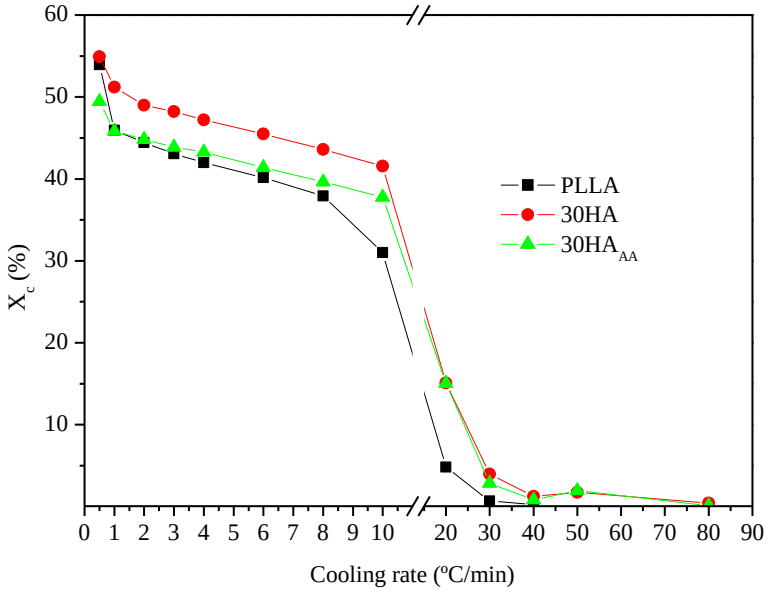

Figure 2.2.39.- Calculated X_c for the corresponding cooling rate.

Representation of X_c against the corresponding cooling rate suggests three regions of crystallization kinetics where the highest X_c values were achieved for the slowest cooling rate. Conversely, cooling faster than 30ºC/min for PLLA or 40ºC/min for 30HA and $30HA_{AA}$ composites led to amorphous structures. Similar results have been reported by other authors [66, 32]. At 0.5ºC/min cooling rate, 30HA followed by pure PLLA exhibited the highest X_c. In the range between 1 and 8-10ºC/min, X_c seem to follow a linear relation with cooling rate. In this region, 30HA showed the highest X_c, whereas pure PLLA exhibited the lowest values. Interestingly, the trend of $30HA_{AA}$ was more similar to pure PLLA than to 30HA. For 10ºC/min cooling rate, X_c of composites was higher than 37% whereas that of PLLA was 31%. From the above discussion it is inferred that HA and HA_{AA} had a different influence upon crystallization. Therefore, their nucleating activity (ϕ) was calculated according to ref. [27] from the ratio of the slopes of log r (being r the cooling rate) versus $1/\Delta T_p^2$ as shown in figure 2.2.40.

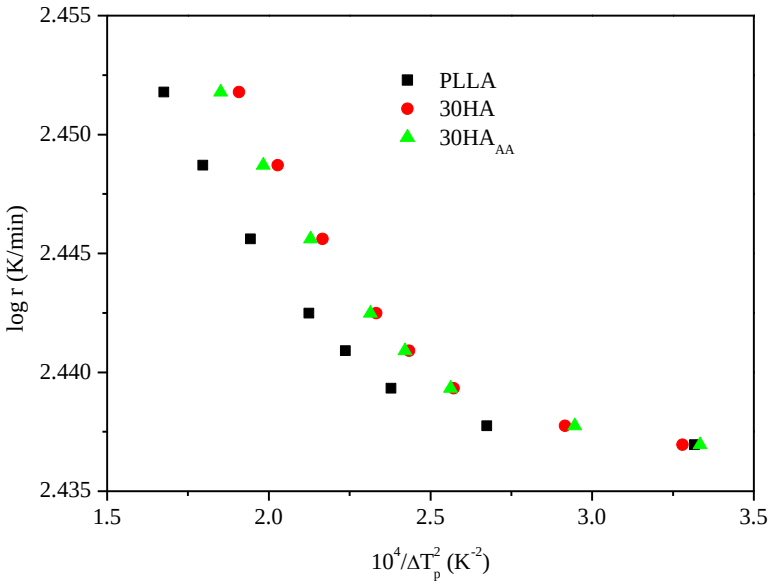

Figure 2.2.40.- Plots of log r versus $1/\Delta T_p^2$ for PLLA and HA and HA_{AA} composites.

Linear fitting of data gave the slopes: -0.0088 for PLLA, -0.0079 for HA and -0.0085 for HA_{AA}, leading to ϕHA=0.89772 and ϕHA_{AA}=0.96591. Interpretation of ϕ, renders that HA is a more active heterogeneous nucleating site than HA_{AA} although both particles are quite inert as their activity factor is near unity.

Considering the influence of the cooling rates on the nonisothermal crystallization process, the activation energy could be determined by calculating the variation of the crystallization peak with cooling rate after Kissinger [67]:

$$\frac{d[ln(\phi/T_p^2)]}{d(1/T_p)} = -\frac{\Delta E_c}{R} \text{ (equation 8)}$$

Where ΔE_c is the crystallization activation energy, and R is the gas constant (8.31J/Kmol). The activation energy can be obtained from the slope of the plot of $ln(\phi/T_p^2)$ versus $1/T_p$, which is represented in figure 2.2.41 for neat PLLA and 30%HA composites. The calculated ΔE_c for neat PLLA, 30HA and $30HA_{AA}$ were -180.27kJ/mol, -228.56kJ/mol and -209.59kJ/mol respectively. ΔE_c values are negative, indicating that the rate of crystallization increased with decreasing temperature, and the crystallization process of polymer is a barrierless and spontaneous process (the lower the value of ΔE_c

the faster the crystallization rate) [66]. The obtained value for PLLA is quite similar to reported values in literature -149.67kJ/mol [66] and -146.86kJ/mol [68]

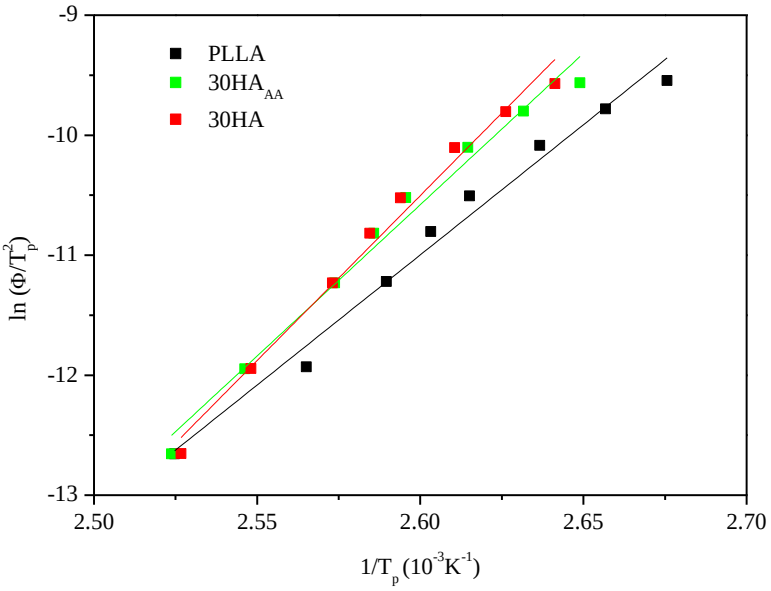

Figure 2.2.41.- Plot of $ln(\phi/T_p^2)$ as a function of $1/T_p$, for neat PLLA (black) and 30HA$_{AA}$ (green) and 30HA (red) composites.

Subsequent heating scans performed after each cooling ramp, revealed the presence of double melting peaks as shown in figure 2.2.42. It was noted that in all cases, the lower melting peak gradually disappeared for increasing cooling rates, being more persistent in the composites than in the neat PLLA. The disappearance of the lower melting peak was accompanied by a shift towards lower temperature of the prevalent melting peak and the apparition of an endotherm just before melting. Interestingly, featuring peaks of 30HA$_{AA}$ were centred at the same temperatures than so of PLLA. According to ref. [32], a double melting is a common phenomenon for polymers that has been described as lamellar rearrangement [69] or annealing whereby crystals of low perfection melt have time to recrystallize a few degrees above and melt in a second endotherm at a higher temperature [32].

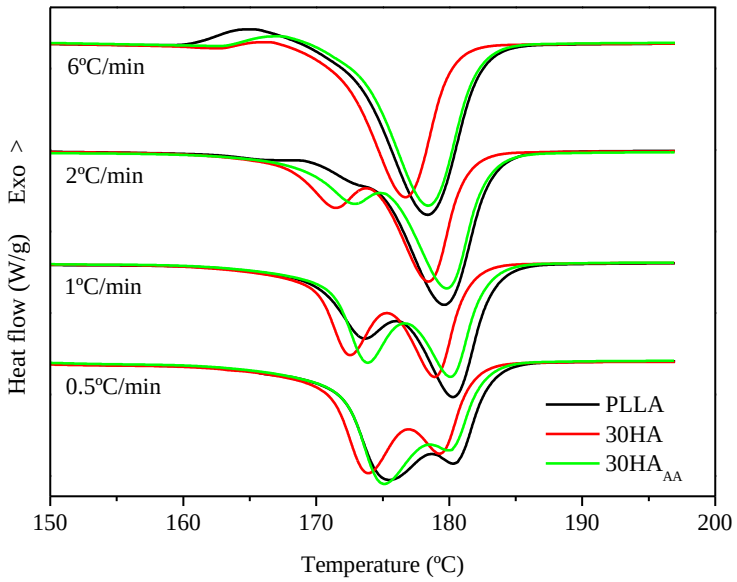

Figure 2.2.42.- Melting curves of PLLA, 30HA and 30HA$_{AA}$ after cooling at the indicated cooling rates.

Conclusions

In this subchapter, plasma polymerization has been successfully performed on an osteoconductive filler (HA) as quantitatively demonstrated by thermogravimetric analysis (TGA), infrared spectroscopy (FTIR), X-ray photoelectron spectroscopy (XPS) and more qualitatively by visual observation of sedimentation of suspended particles in chloroform.

Following, these particles were compounded with two biodegradable and biocompatible polymeric matrices (PLCL and PLLA) for their potential use as fixation devices with enhanced osteoconductivity.

Thermogravimetric analysis revealed a significant enhancement in thermal stability of elastomeric matrix composites, whereas it was more subtle in the glassy matrix composites.

Tensile tests revealed an increased elastic modulus of PLCL composites by the addition of neat HA, whereas composites of plasma coated particles showed enhanced elongation at break.

In PLLA composites, compounding with plasma coated particles caused the highest increase of E. Except for 10% HA_{AA} composites, the addition of particles reduced the strain at break. The presence of smooth irregular voids distributed onto the surface makes us speculate about the presence of air bubbles that may have jeopardized the effect of particles.

Dynamic mechanical analysis of PLCL composites did not reveal spectacular changes, probably due to the low strain regime of the measurements. Conversely, storage modulus and damping of PLLA revealed very sensitive to the addition of particles. In general, the addition of HA particles increased E' in the solid (glassy and recrystallized) states, whereas increasing the HA_{AA} content promoted damping alikeness with neat PLLA.

This alikeness was further observed during the non-isothermal crystallization kinetics evaluation whereby it was concluded that neat HA is a more heterogeneous nucleating site than HA_{AA}.

References

[1] Davis, P. A., Huang, S. J., Ambrosio, L., Ronca, D., Nicolais, L., Journal of materials science: materials in medicine, 1991, 3, 359-364.

[2] Qiu Q. Q., Ducheyne, P., Ayyaswamy P. S., Annals of the New York academic of science, 2002; 974: 556-564.

[3] Majola, A., Vainionpää, S., Rokkanen, P., Mikkola, H. M., Törmälä, P., Journal of materials science: materials in medicine, 1992, 3, 43-47.

[4] Neuendorf, R. E., Saiz, E., Tomsia, A. P., Ritchie, R. O., Acta biomaterialia, 2008, 4 1288-1296

[5] Lei, L., Li, L., Zhang, L., Chen, D., Tian, W., Polymer degradation and stability, 2009, 94, 1494-1502.

[6] Holden, Kricheldorf, Quirk. Thermoplastic elastomers. Hanser Gardner publications pp 493

[7] Suganuma, J.; Alexander, H. J Journal of Applied Biomaterials, 1993, 4, 13-27.

[8] Daniels, A. U., Taylor, M. S.; Andriano, K. P.; Heller, J., Transactions of the orthopaedic research society, 38th annual meeting, 1992, 17, 88

[9] Taylor, M. S.; Daniels, A. U., Andriano, K. P.; Heller, J., Journal of Applied Biomaterials, 1994, 5, 151-157.

[10] Agrawal, C. M., Athanasiou, K. A., Journal of Biomedical Materials Research, 1997, 38, 105-114.

[11] Li, H., Ge, Y., Wu, Y., Jiang, J., Gao, K., Zhang, P., Wu, L., Chen, S., International orthopaedics (SICOT), 2011, 35,1561-1567

[12] Cho, S., Li, H., Chen, C., Jiang, J., Tao, H., Chen, S., International orthopaedics (SICOT), 2013, 37, 507-513

[13] Li, H., Chen, S., Wu, Y., Jiang, J., Ge, Y., Gao, K., Zhang, P., Wu, L., International orthopaedics (SICOT), 2012, 36, 191-197

[14] Shi, P., The, T. K. H., Toh, S. L., Goh, J. C. H., Biomaterials, 2013, 34, 5947-5957

[15] Yang, J., Jiang, J., Li, Y., Li, H., Jing, Y., Wu, P., Yu, D., Chen, S., International orthopaedics (SICOT), 2013, 37, 515-521

[16] Kuang, G. M., Yau, W. P., Lu, W. W., Chiu, K. Y., Knee surgery, sports traumatology, arthroscopy, 2010, 18, 1038-1051

[17] Nichols H. L., Zhang, N., Zhang, J., Shi, D., Bhaduri, S., Wen, X., Journal of biomedical materials research part A, 2007, 82, 373-82.

[18] Šupová, M., Journal of materials science: materials in medicine, 2009, 20:1201-1213

[19] Verheyen, C. C. P. M., Wijn, J. R., Blitterswijk, C. A., Groot, K., Journal of biomedical materials research, 1992, 26, 1277-1296

[20] Noohom, W., Jack, K. S., Martin, D., Trau, M., Biomedical materials, 2009, 4, 015003 (13pp)

[21] Walsh, W.R., Ohno, M., Guzelsu, N., Journal of materials science: materials in medicine, 1994, 5, 72-79.

[22] Sarasua, J. R., Pouyet, J. Journal of thermoplastic composite materials, 1998, 11, 2-21

[23] Villagra Di Carlo, B., Gottifredi, J. C., Habert, A. C., Journal of materials science, 2011, 46, 1850-1856

[24] Alexander, M. R., Duc, T. M., Journal of materials chemistry, 1998, 8, 937-943.

[25] Akkouch, A., Zhang, Z., Rouabhia, M., Journal of biomaterials applications 2014, 28, 922-936

[26] Damadzadeh, B., Jabari, H., Skrifvars, M., Airola, K., Moritz, N., Vallittu, P. K., Journal of materials science: materials in medicine, 2010, 21, 2523-2531

[27] Dobreva, A., Gutzow, I., Journal of non-crystalline solids, 1993, 162, 13-25.

[28] Sim, C. P., Cheang, P., Liang, M. H., Khor, K. A., Journal of materials processing technology, 1997, 69, 75-78

[29] Larrañaga, A. Sarasua, J. R., Polymer degradation and stability, 2013, 98, 751-758

[30] Larrañaga, A., Petisco, S., Sarasua, J. R., Polymer degradation and stability, 2013, 98, 1717-1723

[31] Larrañaga, A., Petisco, S., Sarasua, J. R., WO 2014/049190 Biodegradable Bioglass-Polymer composite having improved thermal stability.

[32] Sarasua, J. R., Prud'homme, R. E., Wisniewski, M., Le Borgne, A., Spassky, N., Macromolecules 1998, 31, 3895-3905

[33] Kim, S. H., Ahn, S. H., Hirai, T., Polymer, 2003, 44, 5625-5634

[34] C. Vilani, D. E. Weibel, R. Zamora, A. C. Habert, C. A. Achete. Applied Surface science, 2007, 254, 131-134

[35] Petisco, S., Larrañaga, A., Sarasua J. R., Solicitud de patente en España nº P201430447 por "SISTEMA Y METODO PARA EL TRATAMIENTO DE PARTÍCULAS SÓLIDAS EN UN AMBIENTE DE ESPECIES ACTIVADAS POR PLASMA"

[36] Feijoo, J. L., Cabedo, L., Giménez, E., Lagaron, J. M., Saura, J. J., Journal of materials science, 2005, 40, 1785-1788.

[37] Ragaert, K., Dekeyser, A., Cardon, L., Degrieck, J., Journal of applied polymer science, 2011, 120, 2872-2880

[38] Persenaire, O., Alexandre, M., Degée, P., Dubois, P., Biomacromolecules 2001, 2, 288-294

[39] Fukushima, K., Tabuani, D., Camino, G., Materials science and engineering C, 2012, 32, 1790-1795

[40] Ray, S. S., Yamada, K., Okamoto, M., Ueda, K., Nano Letters, 2002, vol 2, 1093-1096

[41] Paul, M. A., Delcourt, C., Alexandre, M., Degée, P., Monteverde, F., Rulmont, A., Dubois, P., Macromolecular chemistry and physics, 2005, 206, 484-498

[42] Chen, H., Zheng, M., Sun, H., Jia, Q., Materials science and engineering A, 207, 445-446, 725-730.

[43] Ignjatovic, N., Suljovrujic, E., Budinski-Simendic, J., Krakovsky, I., Uskokovic, D. Journal of biomedical materials research part B: applied biomaterials, 2004, 71B, 284–294

[44] Signori, F., Coltelli, M. B., Bronco, S., Polymer Degradation and Stability, 2009, 94, 74–82

[45] Carrasco, F., Pagèsb, P., Gámez-Pérez, J., Santana, O. O., Maspoch, M. L., Polymer Degradation and Stability, 2010, 95, 116-125

[46] Fernández, J., Etxeberria, A., Sarasua, J. R., Polymer Degradation and Stability, 2013, 98, 1293-1299

[47] Ural, E., Kesenci, K., Fambri, L., Miliaresi, C., Piskin, E., Biomaterials 2000, 217-2154

[48] Li, J., Zheng, W., Li, L., Zheng, Y., Lou, X., Thermochimica acta 493 (2009) 90-95

[49] Muñoz, J., In search of tough polylactides for tissue regeneration: Poly(L-lactide-co-ε-caprolactone) and its blends with Poly (L-Lactide). Doctoral Thesis, UPV-EHU, Basque Country, Spain, 2014

[50] Kausch, H. H., Colloid and polymer science 1985, 263, 306-312

[51] Haward, R. N., Macromolecules 1993, 26, 5860-5869

[52] Nicolais, L., Narkis, M., Polymer engineering and science, 1971, 11, 194-199

[53] Bleach, N. C., Nazhat, S. N., Tanner, K. E., Kellomäki, M., Törmälä, P., Biomaterials, 2002, 23, 1579-1585

[54] Nazhat, S. N., Kellomäki, M., Törmällä, P., Tanner, K. E., Bonfield, W., Journal of biomedical materials research part B: applied biomaterials, 2001, 58, 335-343

[55] Ray, S. S., Maiti, P., Okamoto, M., Yamada, K., Ueda, K., Macromolecules 2002, 35, 3104-3110

[56] Fambri, L., Kesenci, K., Migliaresi, C. Polymer composites, 2003, 24, 100-108.

[57] Wilberforce, S. I. J., Finlayson, C. E., Best, S. M., Cameron, R. E., Polymer, 2011, 52, 2883-2890

[58] Kopinke, F. D., Remmler, M., Mackenzie, K., Möder, M., Wachsen, O., Polymer degradation and stability, 1996, 53, 329-342

[59] Aoyagi, Y., Yamashita, K., Doi, Y., Polymer degradation and stability, 2002, 76, 53-59

[60] Wu, D. F., Wu, L., Zhang, M., Zhao, Y. L., Polymer degradation and stability, 2008, 93, 1577-1584

[61] Wu, D. F., Wu, L. F, Zhang, M., Polymer degradation and stability, 2006, 91, 3149-3155

[62] Kasuga, T., Ota, Y., Nogami, M., Abe, Y., Biomaterials, 2001, 22, 19-23

[63] Wilberforce, S. I. J., Best, S. M., Cameron, R. E., Journal of materials science: materials in medicine, 2010, 21, 3085-3093

[64] Ray, S. S., Yamada, K., Ogami, A., Okamoto, M., Ueda, K., Macromolecular rapid communications, 2002, 23, 943-974

[65] Xiao, H., Yang, L., Ren, X., Jiang,T., Yeh, J. T., Polymer composites, 2010, 31, 2057–2068

[66] Zhou, W. Y., Duan, B., Wang, M., Cheung, W. L., Journal of applied polymer science, 2009, 113, 4100-4115

[67] Blainea, R. L., Kissinger, H. E., Thermochimica Acta 2012, 540, 1– 6

[68] Hao, Q., Li, F., Li, Q., Li, Y., Jia, L., Yang, J., Fang, Q., Cao, A., Biomacromolecules, 2005, 6, 2236-2247

[69] Nijenhuis, A. J., Colstee, E., Grijpma, D.W., Pennings, A.J., Polymer, 1996, 37, 5849-5857

Chapter 3. Shape memory

Introduction

Shape memory materials are stimuli-responsive materials which have the capability of changing their shape upon application of an external stimulus [1] such as heat or light [2, 3, 4] or exposition to a particular environment [5] such as ionic concentration, magnetic field [6], electric field [7], moisture [7, 8] or immersion in water [9, 10].

The shape memory effect (SME) has been reported in alloys, ceramics, hydrogels, polymers [11] and even in human red blood cells [12]. However, comparisons amongst "smart" [1, 2, 5, 7, 13-16] materials are only useful with respect to specific applications because the underlying physical principles are quite different [16, 17]. For instance, the SME of shape memory alloys (SMAs) is based on a martensitic phase transition taking place without diffusion [1], whereas shape-memory polymers have their own special shape-memory mechanism [18].

As the shape memory does not require a specific chemical structure, the intrinsic material properties can be adjusted to the need of specific applications (functionalization) by variation of molecular parameters [15], such as the type of monomer or the comonomer ratio [7, 9]. The on-demand movement [10] as a function of polymers results from a combination of polymer's architecture (morphology) [4, 7] and a shape memory creation procedure, often called programming [4, 9, 19].

Thermoresponsive shape memory polymers (SMPs) [14] are elastic polymer networks equipped with suitable stimuli-sensitive switches [7, 9]. The network of crosslinks, which persist through the temperature and deformation range of operation determine the permanent shape [20], whereas the switches are responsible for the transient [21] or temporary shape [22]. The crosslinks can be chemical bonds (thermosets), physical entanglements (thermoplastics), or small crystalline domains (phase-segregated block copolymers) [20]. Molecular switches [23] make use of reversible thermal transitions such as the glass transition (T_g) or melting temperature (T_m) [24].

To display shape memory functionality relevant to the particular application [1, 7, 9, 25], SMPs must be first processed to receive their permanent shape [23] by

conventional processing methods [9] above a certain temperature (T_{perm}) determined by the nature of the polymer. For instance, in linear block copolymers the hard segments provide the highest thermal transition [1, 4, 7, 9] whereas in semicrystalline homopolymers, the processing temperature is linked to the melting temperature of the crystalline domain [26, 27]. Afterwards, the polymer sample is deformed and the intended temporary shape is fixed [1, 9].

Although the programming process can be performed at a low temperature ($T_{def}<T_{trans}$) [1, 4, 28], generally, higher temperatures ($T_{def}>Tt_{rans}$) are preferred over cold stretching protocols, as the temporary shape is more easily conferred [23] and the shape memory effect is significantly enhanced [4].

Whether the transformation temperature is a glass or a melting transition, the microstructure will require appropriate design to allow for sharp transitions [15]. Melting transitions are usually narrower than glass transitions [15]. However, as melting and crystallization exhibit a large hysteresis on heating and cooling which increases further with increasing cooling or heating rates, the overall thermomechanical cycle associated may still be longer than that based on glass transition [15]. Moreover, very fast cooling rates could jeopardize the extent of crystallization, hampering the shape memory effect [15].

The molecular mechanism underpinning the SME of amorphous SMPs is the dramatic change in the temperature dependence of the chain mobility induced by the glass transition [20] and associated entropy elasticity of the rubbery state [4, 8, 9]. Basic principles of shape memory effects and their application procedure can be best described with their modulus (E)-temperature (T) [28] or frequency (ω) behaviour [29] such as the master curve of a typical linear amorphous polymer shown in figure 3.1. Here, two relaxation processes are obvious: the glass to rubber transition and the terminal zone relaxation [29].

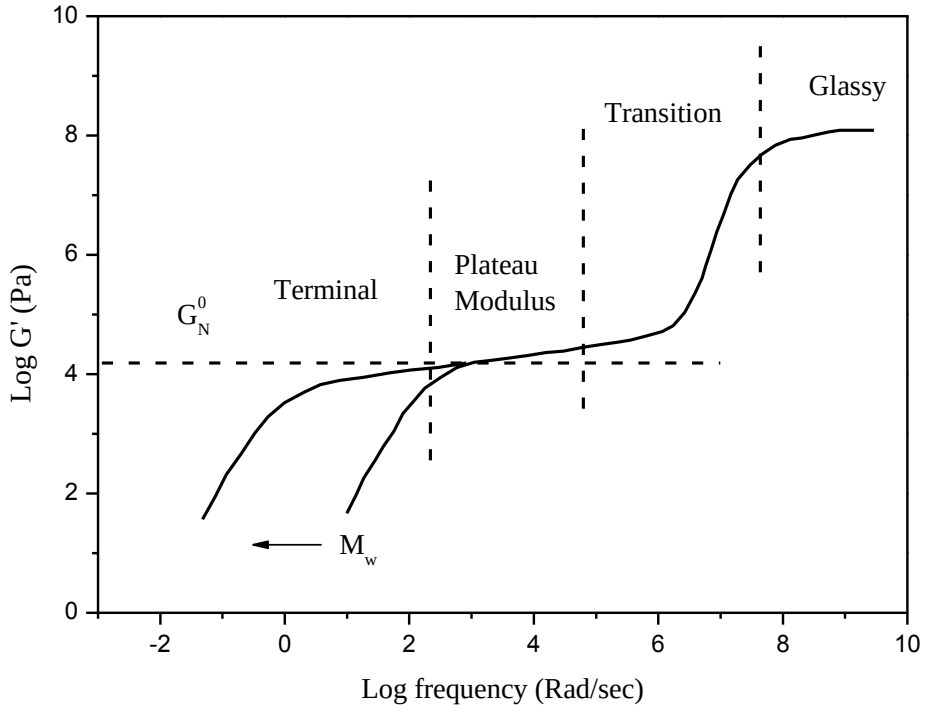

Figure 3.1.- G' mastercurve for a typical linear amorphous polymer

Entropy elasticity

The glass transition is a consequence of submolecular units moving in the same time frame as the measurement frequency (ω) [29]. At high frequencies the apparatus views the material as a glass since the submolecular units cannot move as rapidly as ω and at lower frequencies the material appears less rigid as submolecular unit movement is in the same time frame as ω [29]. At lower frequencies still, a plateau region is observed due to the presence of the transient entanglement network [29]. According to the classic rubber elasticity theory, the plateau modulus G_N^0 is proportional to both cross-link density and temperature, or

$$G_N^0 = \nu k_B T = \rho RT/M_c \quad \text{(equation 1)}$$

where ν is the number density of network chains, ρ is the mass density, R is the universal gas constant, and M_c is the molecular weight between cross-links [4, 8]. In the rubbery region, polymer networks exhibit ‘‘superelasticity’’ wherein the polymer chain segments between cross-link points can deform quite freely and are prone to being twisted

randomly, via rotations about backbone bonds, maintaining a maximum entropy ($S = k_B \ln\Omega$ (equation 2), k_B being Boltzmann's constant and Ω being the number of configurations) and minimum internal energy as macroscopic deformation occurs [1, 8]. Therefore, the associated modulus of elasticity is dictated by the configurational entropy reduction [6, 17] that occurs with deformation of the constituent chains and is therefore often termed ''entropy elasticity'' [8, 4]. When the stress is released, this reduced entropy makes the long polymer chains "snap back" into their original positions [3, 4, 7-9, 26, 28, 30, 31]. Further chain orientation leads to chain slippage and decoupling of crosslinks [32] featuring the terminal zone relaxation [29]. The length of the plateau and the breadth and shape of the terminal zone relaxation, are strong functions of the molecular weight distribution (MWD) [29]. Conversely, chain mobility can be reduced by cooling below the glass transition temperature, freezing the structure in a nonequilibrium configuration and allowing the material to store a deformed shape [20, 28]. The sharper the transition, the more sensitive to temperature is the material [23, 28], and in consequence, the more effectively the deformation is fixed over chain relaxation. Furthermore, a high elasticity ratio ($E_{glassy}/E_{rubbery}$), preferably of two orders of magnitude [15, 28, 33], allows easy shaping at $T>T_g$ and opposes great resistance to deformation at $T<T_g$ [34]. Reheating to above T_g restores the mobility and allows the structure to relax again to an equilibrium random coil configuration of maximum entropy, and the material to recover its memorized permanent shape [20, 23].

For samples with higher storage modulus at high temperature, more deforming energy is needed at T_{def} and more energy are stored with the loss of elastic entropy when cooling down to T_{fix} [34]. As a result, the samples with higher storage modulus and low loss modulus, have higher tendency to return to their original shapes [8, 26, 27, 34-36].

Shape memory effect quantification

Shape memory properties are quantified in cyclic, thermomechanical tensile tests or bending tests [4, 7, 9]. The data obtained from these tests allow the determination of the strain fixity ratio R_f, the strain recovery ratio R_r, the switching temperature T_{switch} [9, 11, 31] and the recovery temperature interval (ΔT_{rec}) [4]. R_f quantifies the ability to fix a mechanical deformation (ε_m) applied in the programming process [9]. R_r quantifies the

ability of the material to memorize its permanent shape after programming using a certain ε_m [9]. The characteristic switching temperature T_{switch}, represents the temperature of the maximum recovery rate (vr) [31] for description of recovery kinetics [31] and is determined as the inflection point of the strain–temperature recovery curve [31]. Finally, the recovery temperature interval is defined as the difference between the temperature at which the recovery starts and the temperature where the recovery is completed [4].

However, these properties depend on such parameters of the test protocols as temperature of deformation, temperature of fixation of the temporary shape, cooling/heating rate, maximum strain, mode of control (strain or stress) [4, 33], therefore, if fully understanding of the SME is sought, appropriate and tailored characterization methods on different levels of hierarchy [4] are needed. In this sense, suitable techniques for the exploration of structure-function relations [12] and gain a detailed knowledge of the molecular mechanism of the SME [1] are nuclear magnetic resonance (NMR), wide and small X-ray scattering, modulated and/or standard differential scanning calorimetry ((M)DSC) and dynamic mechanical thermal analysis (DMTA).

Finally, as a part of a comprehensive characterization, constitutive equations [15] and modelling approaches [4] provide a useful framework for the description and most importantly, the design of SMPs of tailored functionalities for particular applications.

Applications of the shape memory effect

These applications span over various areas of everyday life and include fabrics, intelligent packaging, self-repairing autobodies, switches and sensors [9]. Other application areas can be seen in reusable composite tooling, aerospace industry or nano-actuators [9, 16, 22]. Yet, new shape-memory polymers can be more expensive than established engineering plastics notably at the beginning of the commercialization phase [9]. Therefore, first applications for SMPs can preferentially be found in areas, where only their functionality is really the key technology enabling a specific application [9]. Aerospace and medicine industries seem to be two of these niches [9].

Although a variety of thermoresponsive SMPs have been developed, biodegradability is often required for those intended for use as biomedical materials in

the body [14]. One example of their application is in implant devices for minimally invasive surgery [14]. Degradable implants can be inserted into the body in a compressed (temporary) shape through a small incision [14]. When the device is placed in the correct position, it achieves its application (permanent) shape when its temperature reaches T_{trans} [14]. The device degrades after a defined time period, thus eliminating the need for a second surgery for removal [14].

To date, the most widely used stent polymers are biodegradable poly(L-lactic acid) (PLLA) [37], poly(DL-lactic acid) [38], poly(lactide-co-glycolide) (PLGA) and polycaprolactone (PCL) [24]. For instance, Tamai *et al*. [39] have successfully developed a self-expandable stent using PLLA [24]. However, the self-expansion can only happen at 70◦C which will cause some trauma to the cells. Therefore, although temperatures in the range of 60ºC can be tolerated for short periods of time [40] in areas of the body which are less sensitive to damage by elevated temperatures, several strategies have been explored including as indirect triggering [24, 41], plasticising effect of water molecules [7, 8, 9, 10, 42] or copolymerization [5, 11, 14, 18, 27, 35, 36, 43-47].

The aim of this chapter is to gain further insight into the shape memory effect, exploring the stress-strain-temperature dependence of the shape memory response based on characterization methods on the macroscopic as well as on the molecular and morphological level. Relevant data compiled thereof will serve to two main purposes namely, to fit the network model for a comparative study of the short term mechanical performance of three physical stent geometries [48] and to design a SMP with enhanced performance.

Materials and methods

Commercial (co)polymers

Optically pure poly(L-lactide) Biomer L9000 of M_w= 160kDa and polydispersity index (D)= 1.7, was supplied by Boehringer Ingelheim (Germany). Commercial poly(L-lactide-co-ε-capolactone) copolymer (PLCL 70/30 ref 1008000233; M_w=198.2kDa and D=1.77) and poly(DL-lactide-co-glycolide) (PDLGA 53/47 ref 0701000351; M_w=164.0kDa and D=1.51) were purchased from Purac Biochem (The Netherlands).

Tailored (co)polymers

Statistical poly(L-lactide-co- ε-caprolactone) (PLCL) copolymers of different L-lactide content were synthesized starting from L-lactide monomer (assay > 99.5%), obtained from Purac Biochem (The Netherlands), and ε-caprolactone monomer (assay >98%), provided by Merck. Stannous octoate (assay 95%) was the catalyst employed for the synthesis of the copolymers showing higher blocky character (R ~ 0.40). Bismuth (III) subsalicylate (99.9% metals basis) was added to carry out the polymerization of the random (R → 1) PLCLs. Both catalysts were supplied by Sigma Aldrich. Ring-opening polymerizations (ROP) were conducted in bulk at 130ºC by a one pot-one-step procedure. The synthesis reactions of the $Sn(Oct)_2$-initiated PLCLs (2000:1 comonomers:catalyst molar ratio) were carried out for 24 hours while the copolymerizations induced by BiSS (1500:1 comonomers: catalyst molar ratio) were maintained at the temperature of reaction for 72 hours. The products were dissolved in chloroform and precipitated pouring the polymer solution into excess of methanol in order to remove the catalyst impurities and the monomers that did not react.

Several poly(DL-lactide)s (PDLLA) were synthesized using D,L-lactide monomer (50:50 mix of L-lactide and D-lactide, assay > 99.5%) and different contents of lauryl alcohol, which was added to control the molecular mass of the polymer. Ring-opening polymerizations (ROP) were conducted in bulk by a one pot-one-step procedure. The synthesis reactions using triphenyl bismuth as catalyst (1000:1 comonomers:catalyst molar ratio) were conducted for 24 hours at 130ºC. Afterwards, the products were

dissolved in chloroform and precipitated pouring the polymer solution into excess of methanol in order to remove the catalyst impurities and those monomers that did not react.

Molecular characterization

The molecular weight of the samples was determined by GPC using a Waters 1515 GPC apparatus equipped with two Styragel columns (102 - 104 Å). Chloroform was used as an eluent at a flow rate of 1 mL min^{-1} and polystyrene standards (Shodex Standards, SM-105) were used to obtain a primary calibration curve.

Proton nuclear magnetic resonance (^{1}H NMR) spectra were recorded in a Bruker Avance DPX 300 at 300.16 MHz of resonance frequency, respectively, using 5 mm O.D. sample tubes and following the experimental conditions described in previous works [49]. The signals of the lactide methine, centred at 5.15 ppm, and the signals of the α and ε methylenes of the ε-caprolactone, around 2.35 and 4.1 ppm, from the ^{1}H NMR spectrum can be assigned to the different dyads [50]. The copolymer composition and the microstructural magnitudes of the copolymers were obtained from the average dyad relative molar fractions. Equations 3-7 [51] were employed to obtain the number-average sequence lengths (l_i) of L-LA and CL building blocks, the Bernoullian random number-average sequence lengths $(l_i)_{random}$ and the randomness character (R):

$l_{LA} = \frac{2(LA)}{(LA-CL)}$ (equation 3);

$l_{CL} = \frac{2(CL)}{(LA-CL)}$ (equation 4);

$(l_{LA})_{random} = \frac{1}{(CL)}$ (equation 5);

$(l_{CL})_{random} = \frac{1}{(LA)}$ (equation 6);

$R = \frac{(l_{LA})_{random}}{l_{LA}} = \frac{(l_{CL})_{random}}{l_{CL}} = \frac{(LA-CL)}{2(LA)(CL)}$ (equation 7)

Where (LA) and (CL) are the two comonomer molar fractions, obtained from the integration of the lactide methane signals and the ε-caprolactone methylene signals, and (LA-CL) is the LA-CL average dyad relative molar fraction.

X-ray diffraction

The X-ray powder diffraction patterns were collected by using a PHILIPS X'PERT PRO automatic diffractometer operating at 40 kV and 40 mA, in theta-theta configuration and with a secondary monochromator with Cu-Kα radiation (λ = 1.5418 Å). A PIXcel solid state detector in scanning mode with 3.347º of active length was used. The samples were mounted in a generic sample holders and spinning of 4s of revolution time was applied. Data were collected from 10 to 50° 2θ (step size = 0.0262 and time per step = 150 s) at RT. A fixed divergence and antiscattering slit giving a constant volume of sample illumination were used.

Stress relaxation

An Instron 5565 universal testing machine equipped with an Instron-SFL 3119 temperature controlled chamber was used for the stress relaxation, cyclic and shape memory tests. Stress relaxation tests were performed at three test temperatures 60, 65 and 70ºC and five strain levels (ε=100, 200, 300, 400 and 500%). ISO 527-2 type 5A dumbbell specimens were stretched at a constant strain rate of 50mm/min until the required deformation and then held at constant strain for 900s while monitoring stress decay.

Isothermal cyclic tests

Cyclic tests were programmed by means of the test profiler module included in the Bluehill software. Dumbbell samples were stretched isothermally until the maximum strain (ε_m=200, 400%) at 50mm/min and unloaded until the initial zero strain position allowing for shape recovery. After the recovery time (6' or 60') had elapsed, the second cycle was started at 50mm/min. some tests were deliberately interrupted for further characterization of stretched/recovered samples (refer to figure 2). From complete tests, the strain fixity ratio R_f and strain recovery ratio R_r were calculated according to equations $R_f = \frac{\varepsilon_u}{\varepsilon_m} * 100$ (equation 8); $R_r = \frac{\varepsilon_m - \varepsilon_u(N)}{\varepsilon_m} * 100$ (equation 9)

In cases were more than 2 cycles were performed, the dependence on number of cycles of shape fixity and shape recoverability, was calculated by following equations $R_f(N) = \frac{\varepsilon_u(N)}{\varepsilon_m} * 100$ (equation 10); $R_r(N) = \frac{\varepsilon_m - \varepsilon_u(N)}{\varepsilon_m - \varepsilon_p(N-1)} * 100$ (equation 11)

Where $\varepsilon_p(N)$ represents the residual strain after heating at T_{HIGH} in the N^{th} cycle [33]. R_f is the ratio of ε_u to maximum strain ε_m, and R_r is the ratio of recoverable strain to deformed strain in each cycle N. For the sake of comparison, and despite otherwise indicated, values of ε_p and ε_u at σ=0.33MPa were used for calculations.

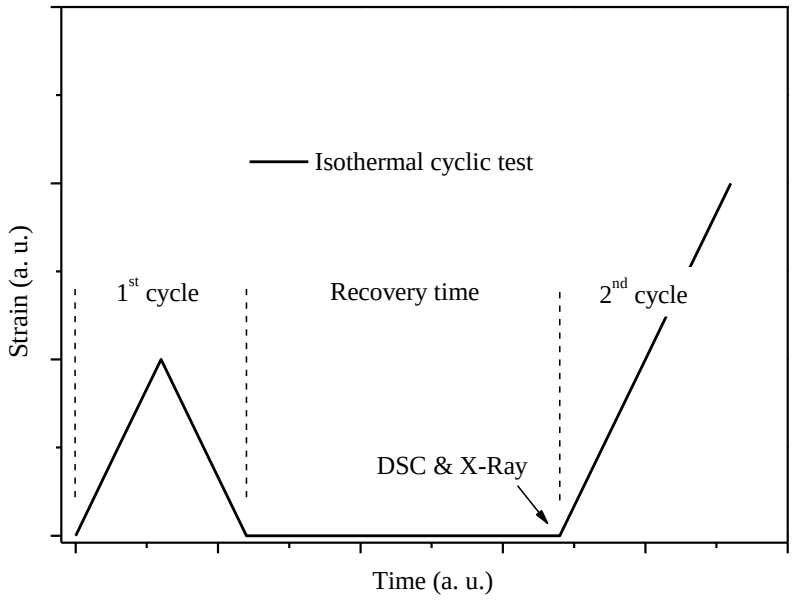

Figure 3.2.- Isothermal stretch and recovery cyclic tests until X00% strain and further elongation

Shape memory tests

Shape memory tests consisted on a heating-stretching-cooling protocol [4] where a single cycle includes programming the test piece and recovering its permanent shape [1]. Unless otherwise indicated, the test piece was first heated up to a temperature T_{high} above the switching temperature T_{trans} and stretched to the maximum strain ε_m [1]. Then, the sample was cooled down below the transition temperature T_{trans} under a constant strain ε_m to a temperature T_{LOW}, thus fixing the temporary shape [1]. Retracting the clamps of the tensile tester to the original distance of 0% strain caused the sample to bend [1]. After

heating the sample up to $T_{HIGH}>T_{trans}$, it contracted and the permanent shape was recovered [1]. Then the subsequent cycle was started. The thermomechanic test (schematically depicted in figure 3.3) was accomplished by separately programming the mechanic test by means of the test profiler module contained in the Bluehill software and the thermal cycles with the iTools software of the temperature controller (eurotherm 2408).

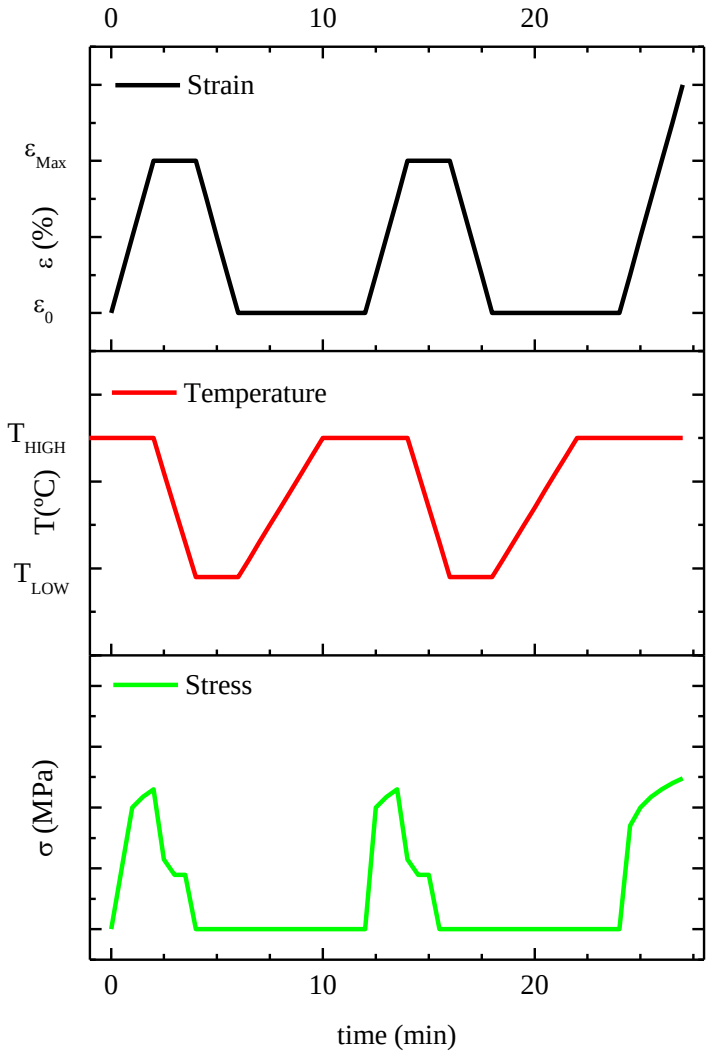

Figure 3.3.- Schematic representation of shape memory test protocol including strain and temperature segments as well as observed stress evolution.

As the effect of temperature and strain were variables to be studied separately, different values were set. Nevertheless, the common features are resumed as follows. Loading and unloading of the sample was performed at 50mm/min strain rate. ε_m was

maintained constant for 2 minutes while temperature was lowered to T_{LOW}. Then stress is completely removed by unloading at 50mm/min. Next temperature is raised in 4 minutes until T_{HIGH} is achieved, thus triggering the shape memory effect.

Dynamic mechanical analysis

Dynamic Mechanical Analysis was performed in a Mettler Toledo DMA/SDTA 861e, in tensile mode. Force-displacement amplitudes were 0.3N-20μm for PLCL samples and 0.5N-25μm for PDLGA and PDLLA samples. Single frequency tests were conducted at 1Hz whereas isothermal frequency series tests were performed in the range of 50 to 0.05Hz at 5 steps per decade. Starting temperature was 25-30ºC below T_g and end temperature 25-30ºC above T_g as determined by DSC for each polymer.

Dynamic viscoelastic analysis

The dynamic viscoelastic behaviour in the terminal zone of synthesised PDLLA samples was investigated using an ARG2 TA Instruments rheometer with a parallel plate fixture of 25 mm diameter. Isothermal dynamic frequency tests were conducted in the linear viscoelastic regime in the molten state.

Thermal analysis

Differential scanning calorimetry was run on 5-10mg samples at a heating rate of 10ºC/min by means of a Q-200 MDSC from TA Instruments, calibrated with pure indium and sapphires in standard mode for determination of thermal properties. First order transitions such as crystallization and melting corresponded to endo- and exothermic peaks respectively, from whose integration, the overall crystallinity degree was calculated according to equation 12 [52]

$$X_c(\%) = \frac{\Delta H_m - \Delta H_{cc}}{X_{PLLA}\Delta H_m^0} * 100 \text{ (equation 12)}$$

considering the enthalpy of fusion of the polylactide crystal $\Delta H_m^0 = 106 J/g$ [52].

The glass transition (T_g) was defined by the inflection point of the endothermic step in heat capacity.

When a more detailed study of the enthalpic relaxation was desired, modulated scans were performed on 4-6mg samples where a sinusoidal heating ramp of 0.75°C modulation amplitude and 120s period was run at 0.5ºC/min. To correct the frequency effect, after the heating process above T_g, the samples were cooled under the same MDSC conditions as used for heating. Any peak area in the non-reversing signal on cooling can only be caused by the frequency effect. Thus, this area was subtracted from the peak area obtained on heating to calculate the peak area that corresponds just to the enthalpic recovery.

Results and discussion

Effect of programming conditions

Stress relaxation tests

Stress relaxation tests were performed at three temperatures located above the glass transition temperature but below the cold crystallization temperature of PLLA. As it can be seen in figures 3.4 and 3.5, at these temperatures dumbbell samples stretched uniformly, showing an elastomeric trend. As expected, the lower the test temperature the higher drawing stress was demanded for a fixed level of strain.

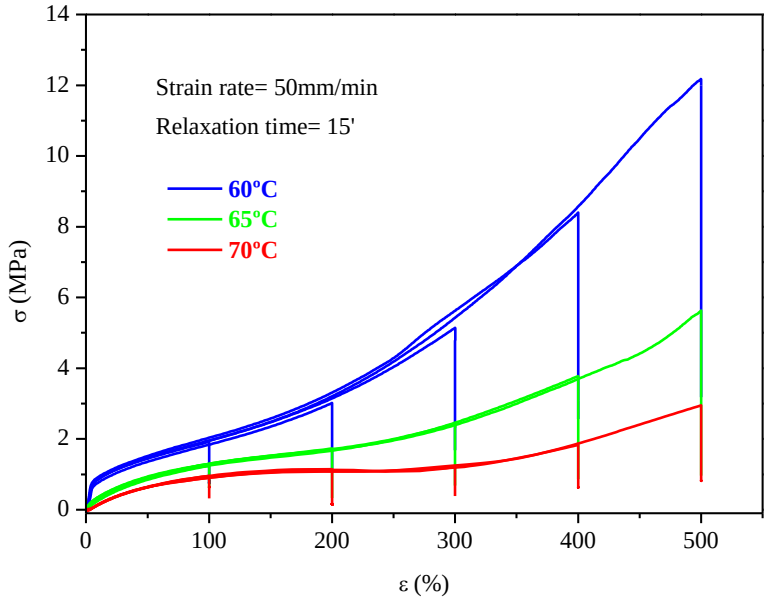

Figure 3.4.- Stress strain resumed representation of the stress relaxation tests

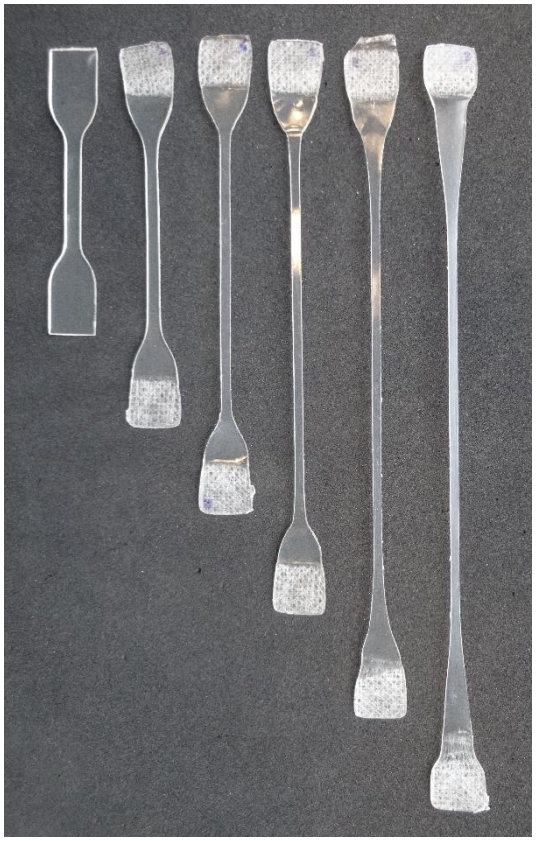

Figure 3.5.- Photographs of unstretched and relaxed samples showing uniform elongation.

Stress evolution during the loading and relaxation steps is illustrated in figure 3.6.

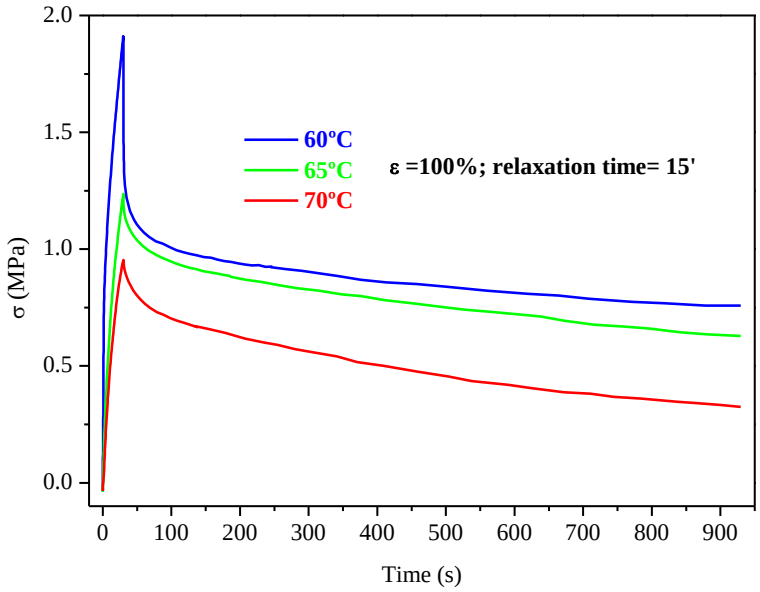

Figure 3.6.- Loading to ε=100% and stress relaxation at 60, 65 and 70ºC.

From the stress relaxation tests, the relaxation strength (Δ) was calculated according to equation 13 [53], and obtained values are resumed in table 3.1 and figure 3.7.

$$\Delta = \left(\frac{\sigma_0 - \sigma_f}{\sigma_f}\right) \text{ (equation 13)}$$

For 60 and 65ºC relaxation tests, relaxation strength increased with strain although the relaxation at ε=200% and 65ºC, showed an exceptional value. Samples tested at 70ºC showed the same anomaly at ε=200% and a direct relation between relaxation strength and strain seemed not straightforward.

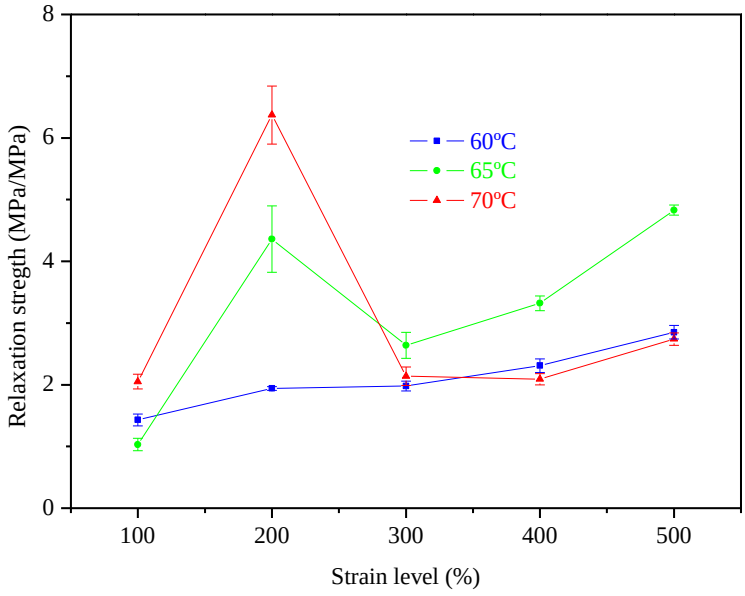

Figure 3.7.- Relaxation strength

Table 3.1.- Relaxation strength

	$\Delta_{60ºC}$ MPa/MPa	$\Delta_{65ºC}$ MPa/MPa	$\Delta_{70ºC}$ MPa/MPa
ε=100%	1.4±0.1	1.0±0.1	2.1±0.1
ε=200%	1.9±0.0	4.4±0.5	6.4±0.5
ε=300%	2.0±0.8	2.6±0.2	2.1±0.2
ε=400%	2.3±0.1	3.3±0.1	2.1±0.1
ε=500%	2.9±0.1	4.8±0.1	2.7±0.1

Thermal analysis

After the stress relaxation tests, samples of 5mg were cut from the central part of the stretched specimens and their thermal properties were determined by DSC. For the ease of discussion only the most representative traces are shown in figure 8, including the corresponding of the original as quenched PLLA. The glass transition is revealed by the step in the base line. The onset of cold crystallization is located at ~93ºC describing the featuring exotherm that spans until the endothermic fusion of the crystals centred at 173ºC. Integration of these peaks allow to calculate the energy involved in the respective

processes, from whose difference according to equation 12 [52], the crystallinity degree of the as quenched PLLA was estimated to be ~8%.

From the upper part of figure 8, it can be said that a 100% strain did not significantly affect the position and shape of the glass transition event but prompted the cold crystallization and the apparition of a second endotherm just immediately before the melting peak for the three temperatures considered. In the lower part of the same figure, the thermograms revealed meaningful changes in the microstructure when strain was increased to ε=500%. Firstly, the glass transition event is clearly delayed and under the highest test temperature it is severely hindered. Moreover, the cold crystallization peak is observed to advance to lower temperatures and eventually disappeared under the most extreme conditions.

Based on the corresponding thermograms of lower test temperatures (60 and 65ºC), it is suggested that two overlapping effects are taking place simultaneously annihilating the DSC signal. On the one hand, relaxation of oriented chains manifests itself by the enthalpic relaxation after the glass transition as seen in traces labelled 60 and 65ºC. The second overlapping effect is the crystallization enhanced by chain orientation, as already seen for lower strain levels. However, the prevalence of the cold crystallization in samples stretched at 60ºC make us infer the presence of different types of crystals i. e.: strained crystals and unstrained crystals or recrystallization of formerly ones. The observed second crystallization exothermic as well as the shoulder on the 70ºC melting peak further support this suggestion.

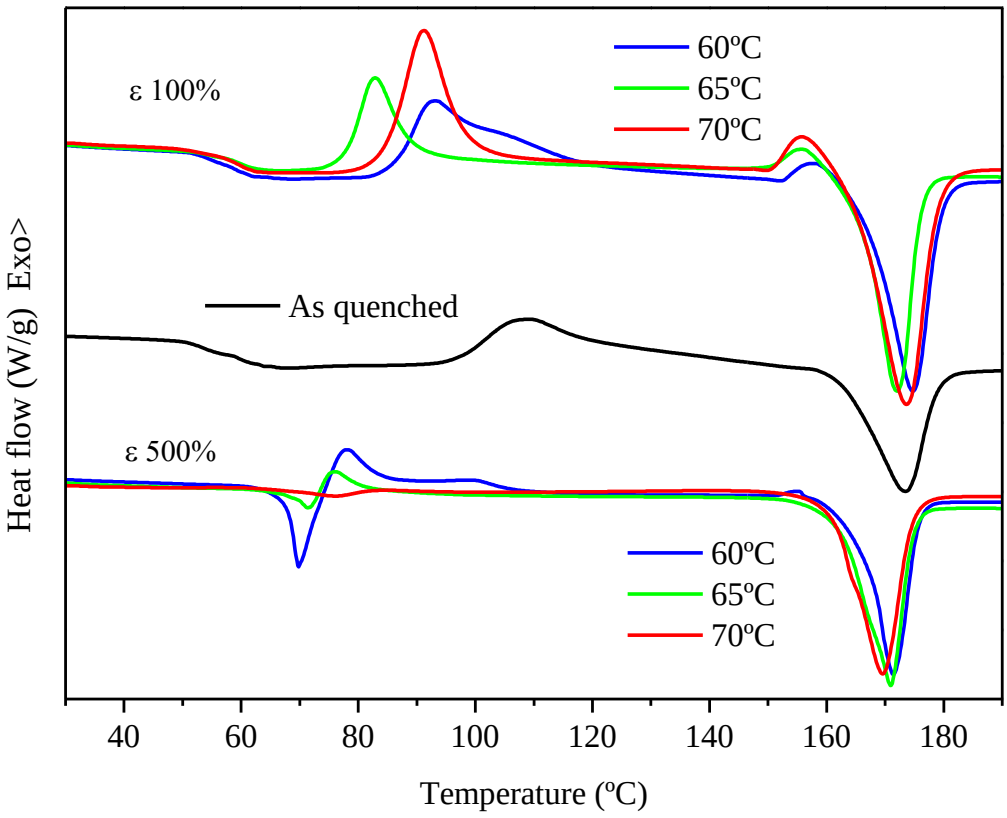

Figure 3.8.- DSC heating scans of as quenched and relaxed samples

Table 3.2.- Glass transition temperature and crystallinity degree determined from DSC heating scans.

	T_g (ºC)				X_c (%)			
	A. Q.	**60ºC**	**65ºC**	**70ºC**	**A. Q.**	**60ºC**	**65ºC**	**70ºC**
ε=0	56.4				7.9			
ε=100%		59.0	60.5	59.7		9.9	22.6	13.5
ε=200%		64.0	63.9	64.3		32.0	47.4	52.3
ε=300%		66.5	65.9	67.6		31.0	45.1	52.3
ε=400%		66.0	67.0	71.7		23.6	46.2	54.3
ε=500%		68.4	69.7	73.0		27.4	45.8	53.7

The overall crystallinity degree was increased. The highest change was observed between 100 and 200% elongation. Except for the 100% strain, the highest values were obtained at 70ºC.

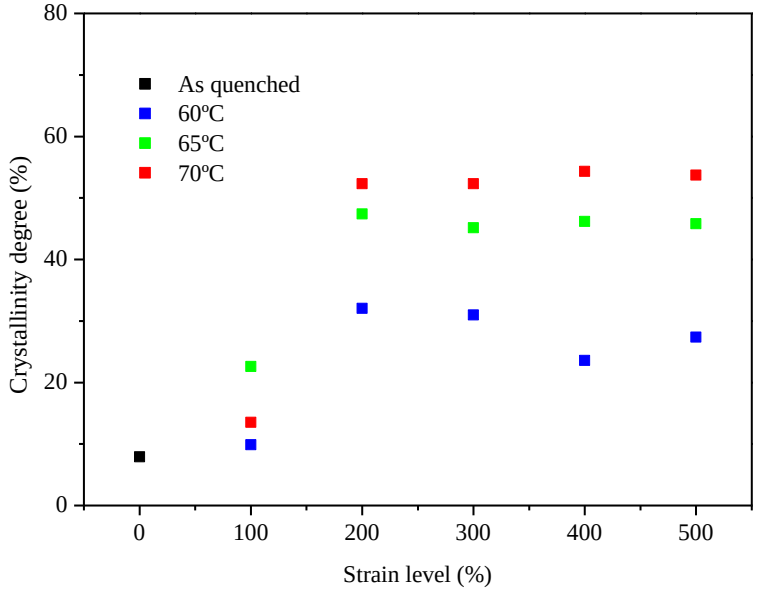

Figure 3.9.- Crystallinity developed as a consequence of temperature and strain combined effects

X-ray diffraction

Accordingly, to gain more insight in the morphology of the crystals, the X-ray powder diffraction patterns of the stretched and relaxed samples were collected and are represented in figures 3.10 and 3.11. For the sake of discussion, additional diffraction patterns corresponding to as quenched and annealed samples are also included. Annealing treatments consisted on exposure to the indicated temperature (100ºC or 60ºC) in order to induce crystallization on quenched PLLA samples. The diffraction patterns were interpreted based on the following fundamentals. In an ideally perfect crystal, in which all atoms throughout its entire extent are placed accurately at the points of an undistorted space lattice, the crystal is considered to have negligible absorption of the x-ray beam.

Therefore, the reflected wavelets at the various atomic planes interact with each other and with the incoming beam, and the observed intensity of the reflected beam is the result of this interaction [54]. Up to a certain angle θ' only a few seconds of arc from the angle θ which satisfies the Bragg equation for the plane under consideration, the resultant intensity is zero [54]. Then, within the small range θ' to θ, the intensity rises sharply to total reflection [54]. Conversely, in an ideally imperfect crystal, which is considered to

be made up of tiny crystal fragments in completely random arrangement (powder), these fragments are so small that each one extracts only a negligible amount of energy from the beam [54]. In this situation, no phase relationships exist between the waves reflected from different fragments, and the complete reflection, being the sum of contributions from individual fragments, shows the featuring powder diffraction halo [54]. Accordingly, an intermediate situation is that of imperfect or distorted crystals. In this case, randomness in the population of atomic sites in three-dimensional structures leads to distortion and broadening of powder reflections, as well as to an increased background [54]. Figures 3.10 and 3.11 show the above mentioned situation. Samples labelled "as quenched" in figure 10, "80'-60ºC" and "60ºC" produced plain patterns, indicating amorphous microstructures, whereas diffraction peaks were detected in samples labelled "3h-100ºC", "65ºC" and "70ºC". Amorphous spectra are supported on DSC traces of figure 3.8 and table 3.2 in that the crystallinity degree is too low to produce observable diffraction patterns. Regarding the low temperature annealed sample, emphasis is laid on the fact that the isolated effect of temperature is not enough to cause crystallization, as, according to the DSC of the as quenched sample, the onset of cold crystallization is located at 93ºC.

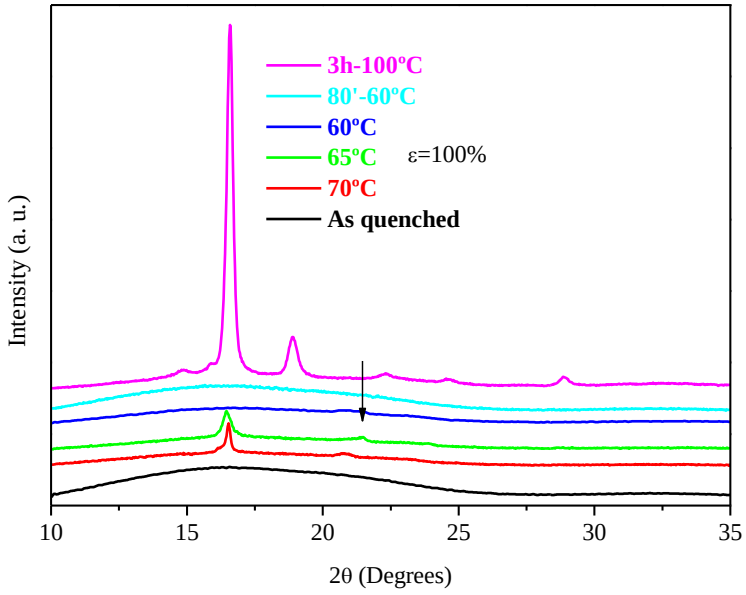

Figure 3.10.- Diffractograms of PLLA

Conversely, the diffraction pattern of sample labelled "3h-100ºC" showed the typical main peaks at 2θ= 16.6º and 18.9º which characterize the crystalline structure of

PLLA [6, 26, 27, 55-58]. These peaks were also distinguishable in samples stretched at 65 and 70ºC. However, from their lesser intensity and slightly deviated positions, their scarce presence and imperfect nature are inferred respectively, in accordance with DSC observations.

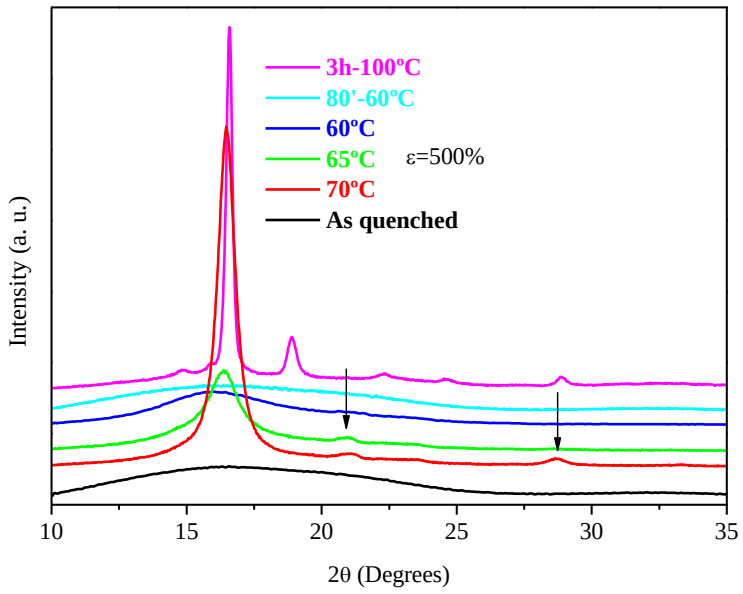

Figure 3.11.- Diffractograms of PLLA

As it can be noted in figure 3.11, further stretching increases the intensity of the main peak at 2θ=16.4º, which is also discernible in sample stretched at 60ºC, and causes the apparition of a third secondary peak in sample stretched at 70ºC. With this additional information, interpretation of DSC traces is straightforward. Due to the combined effect of strain and temperature, the initially amorphous chains of PLLA are stretched and oriented preferentially in the draw direction. From this preferential arrangement, cold crystallization progresses at the stretching temperature, leading to the development of imperfect crystalline domains that manifest themselves by diffraction patterns, the more similar to the typical α form of PLA, the more extreme stretching conditions. At the same time, the development of these crystals takes place at the expense of a diminished and hindered amorphous phase as deducted from the significantly delayed glass transition temperature (table 3.2).

On the other hand, the least altered microstructure corresponds to samples stretched at 60ºC, where a reduced cold crystallization kinetics [59] has been demonstrated after X-ray and DSC observations. At the light of the described picture, if shape recovery is an entropic driven phenomenon linked to reversible coiling of the amorphous chains [26], the development of a crystalline phase [6, 26, 27, 55, 57, 60] is expected to avoid it, unless the recovery stress [27] of the amorphous chains, stored during deformation, overcomes the resistance opposed by the crystalline network [61]. In this regard, from relaxation tests illustrated in figures 3.4 and 3.6 and resumed in table 3.1, it is easily seen that samples stretched at 60ºC store more stress than their counterparts for the same strain level.

Isothermal cyclic tests

Hence, the recovery ratio as well as the fixity ratio were calculated from cyclic isothermal tests conducted at these temperatures, two strain levels and two elapsed times allowed for recovery (herein forth recovery time). As already defined, the strain fixity ratio (R_f) quantifies the capability to maintain the deformed strain whereas the strain recovery ratio represents the shape recovery. Values resumed in table 3.3 correspond to the arithmetic media extracted from five measurements. Tests conducted at 60, 65 and 70ºC for 400% strain and 6' recovery time are illustrated in figure 3.12.

Table 3.3.- Strain recovery and strain fixity rates for isothermal cyclic tests

	60ºC		**65ºC**		**70ºC**	
	R_f	**R_r**	**R_f**	**R_r**	**R_f**	**R_r**
σ=0.33MPa	**%**	**%**	**%**	**%**	**%**	**%**
ε=200%; t=6'	93.1±2.6	94.6±1.3	46.7±5.8	86.3±1.9	69.8±2.2	32.4±3.2
ε=400%; t=6'	96.5±0.3	70.1±10.9	87.0±0.5	61.8±12.1	88.0±0.4	20.2±1.4
ε=400%; t=60'	96.3±0.4	94.6±1.0	86.4±0.6	56.0±3.7	87.8±0.6	20.0±0.8

According to table 3.3, it can be seen that for both levels of strain, samples stretched at 60ºC showed the highest values, whereas 65ºC samples the lowest, and samples at 70ºC yielded intermediate values. The highest values showed by samples

stretched at 60ºC are expected since at this temperature molecular chains are in the least mobile scenario, as indicated by the higher drawing stress, contributing to fix the impinged strain. Following the same reasoning, samples stretched at 65ºC showed less fixity ratio suggesting a temperature enhanced mobility and, in consequence, recovery. Interestingly, samples stretched at 70ºC did not follow this trend, suggesting the development of a stabilising structure that contributes to fix the strain against the recovery force, in agreement with previous analyses. In all cases, increasing the strain led to an enhanced fixity ratio.

The strain recovery, calculated from the onset of the second cycle revealed that, as expected, samples tested at 60ºC yielded the highest ratio. In all cases, the effect of increasing the strain led to a reduction of the recovery which was only seen to improve by extending the recovery time to 60minutes in the 60ºC tests. To further characterize the structure-properties relationships, samples from intermediate stages of the tests were analysed by DSC (figures 3.13 to 3.15) and x-ray diffraction (figures 3.16 to 3.18).

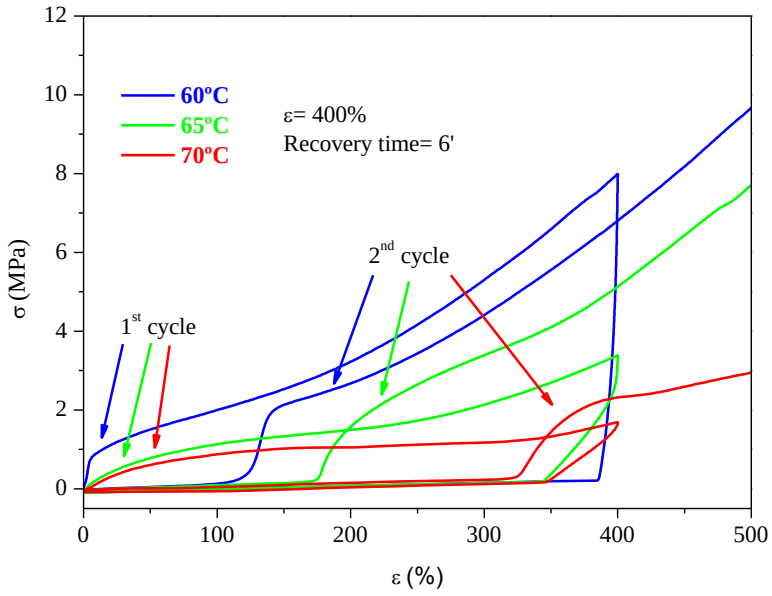

Figure 3.12.- Isothermal stretch and recovery cyclic tests until 400% strain and further elongation until rupture

Thermal analysis

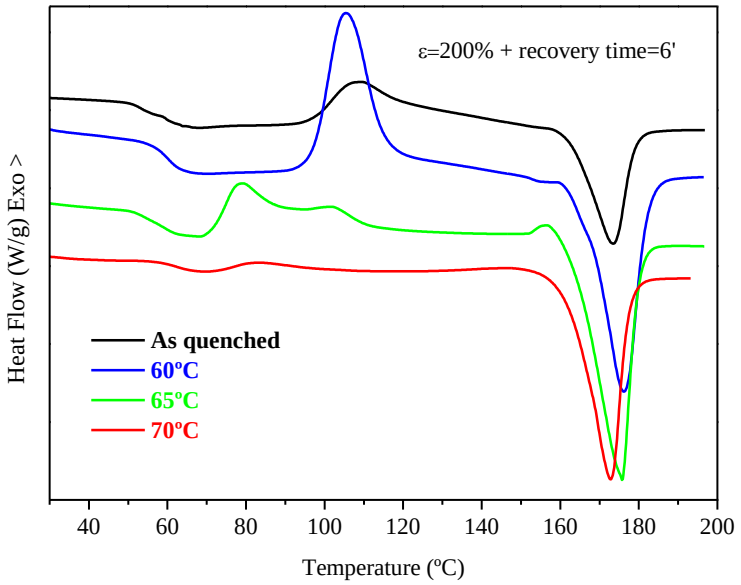

Figure 3.13.- DSC of samples extracted from stretched samples at the indicated temperatures after a recovery time of 6 minutes (just before the beginning of the second cycle).

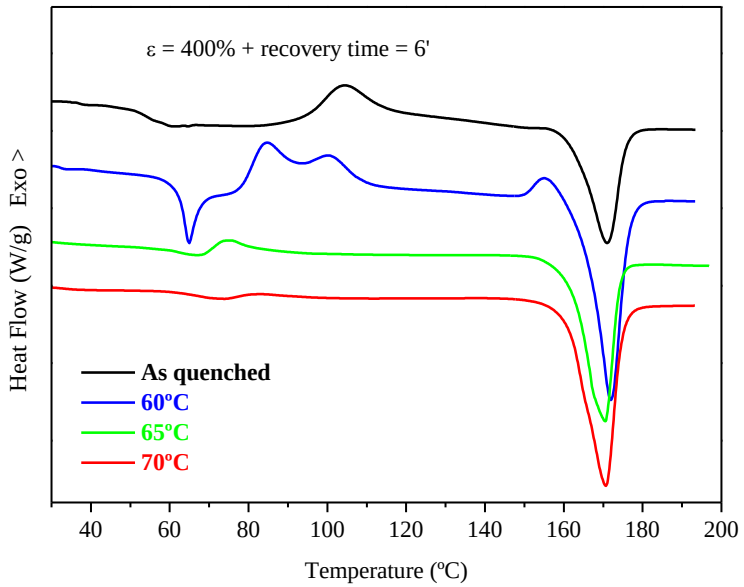

Figure 3.14.- DSC of samples extracted from stretched samples at the indicated temperatures after a recovery time of 6 minutes (just before the beginning of the second cycle).

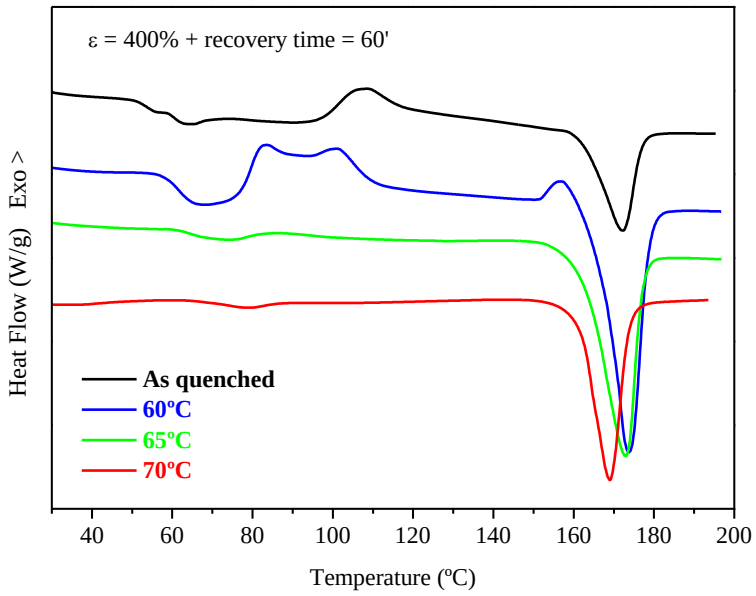

Figure 3.15.- DSC of samples extracted from stretched samples at the indicated temperatures after a recovery time of 60 minutes (just before the beginning of the second cycle).

From the calorimetric analysis, the most illustrating traces are those corresponding to 60ºC tests. Starting with ε= 200% and 6' recovery time, the heating scan shown in figure 13 and resumed in table 3.4, shows a nearly amorphous microstructure with a calculated X_c=2.6%, and a featuring powder diffraction as seen in figure 3.16, which supports the outlined theory of low conformational entropic recovery.

When strain is doubled (ε=400%), the corresponding DSC trace shows a delayed glass transition, followed by an endotherm ascribed to relaxation of oriented chains. A few degrees after the baseline is evenly restored, a bimodal exothermic peak is observed, indicating a strain induced nucleation and further prompted cold crystallization. Finally, before the melting peak another exotherm is also seen, giving an overall X_c=12.4%. Bringing back the reported recovery values of table 3.3, and putting them together with figure 3.14 and 3.17, deduction is straightforward.

As indicated by the delayed glass transition and enthalpic relaxation, a portion of molecular chains persist in an oriented conformation as a consequence of previous stretching step and insufficient recovery time. As the heating ramp during the DSC scan proceeds faster than recovery, oriented chains do not recoil but stabilise in a crystalline

network that is progressively developed and improved by continued heating until they are caused to melt. Further analysing the corresponding DSC of 60' recovery time sample brings more light into the matter. In there, the obtained R_r equalled that registered for ε=200% as a consequence of extended recovery time. However, the forwarded bimodal crystallization, and the missing enthalpic recovery make us infer that chains relaxed in an extended conformation [62], becoming nucleus of subsequent crystallization as the heating ramp in the DSC proceeded.

Table 3.4.- Crystallinity degree calculated from DSC traces

	$X_{c\ (60ºC)}$ %	$X_{c(65ºC)}$ %	$X_{c(70ºC)}$ %
ε=200%; t=6'	2.6	30.3	51.6
ε=400%; t=6'	12.4	46.3	52.3
ε=400%; t=60'	15.4	46.5	51.2

X-ray diffraction

The slightly displaced and broadened diffraction peaks in figures 3.16 to 3.18 strongly support the idea of imperfect crystals. As it can be seen in table 3.4 and corresponding diffraction patterns, higher test temperatures promoted the apparition of the crystalline phase at earlier stages.

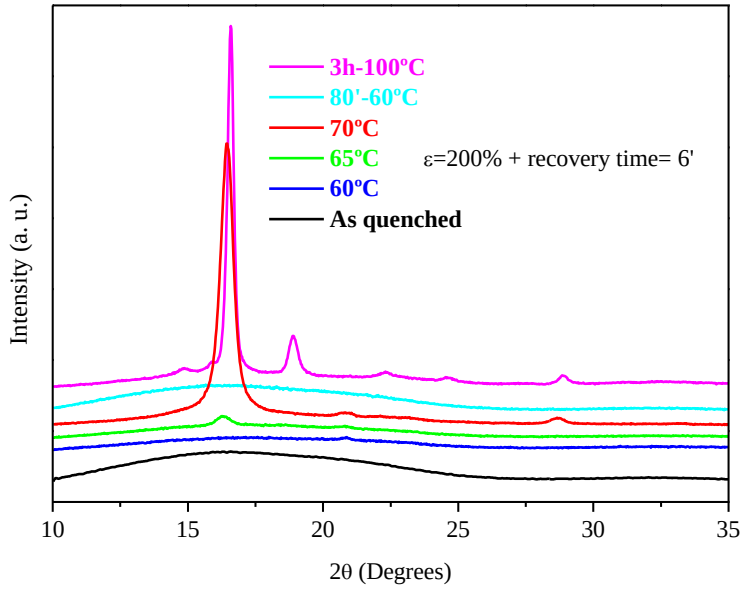

Figure 3.16.- Diffractograms of PLLA

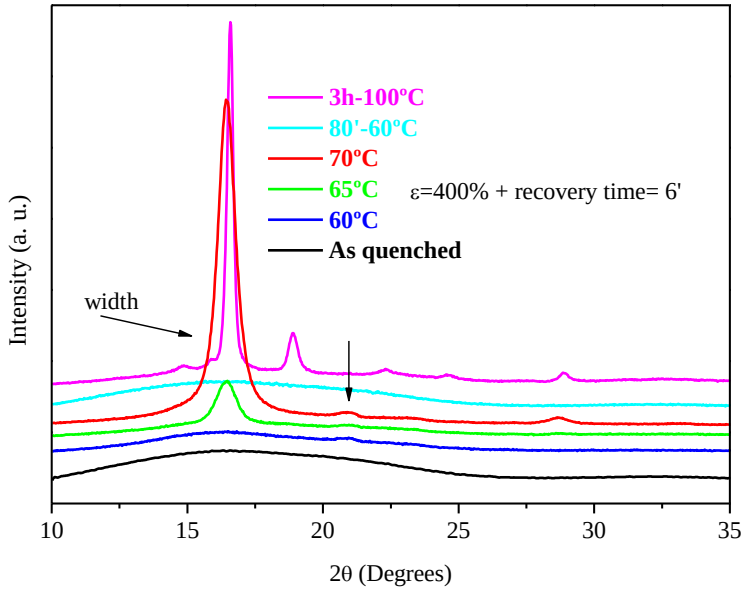

Figure 3.17.- Diffractograms of PLLA

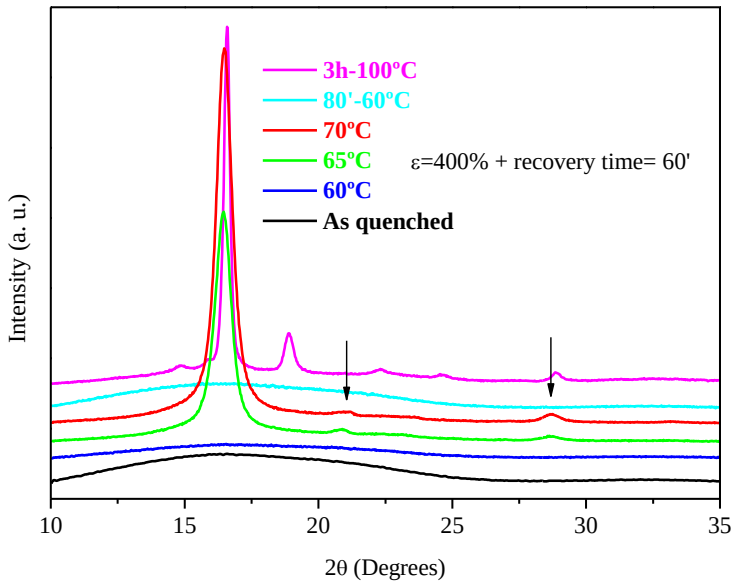

Figure 3.18.- Diffractograms of PLLA

Isothermal cyclic tests

Following, cyclic life over consecutive cyclic tests was assessed over 4 cycles at 60, 65 and 70ºC. As it can be noted in the three dimensional graph of figure 3.19, samples were stretched until ε=400% and allowed for 60' to recover before the start of successive cycle. Strain fixity and recovery ratios between successive cycles as well as total values were calculated and are resumed in table 3.5.

Focusing on the recovery values obtained after the first cycle, the deleterious effect of increased crystallinity associated to the combined action of strain and temperature are more readily seen in 70ºC samples. As it can be noted in figure 3.19, the corresponding onset of the second loading cycle was the last to take off, indicating a residual strain and therefore a poor R_r value. However, in the same table, better values of R_r are registered in subsequent cycles, suggesting a training effect [28, 33, 63] by means of which the "damages", in this case, the residual strain caused by the development of a crystalline network, occur during the first cycle, after which, high and stable recovery is achieved.

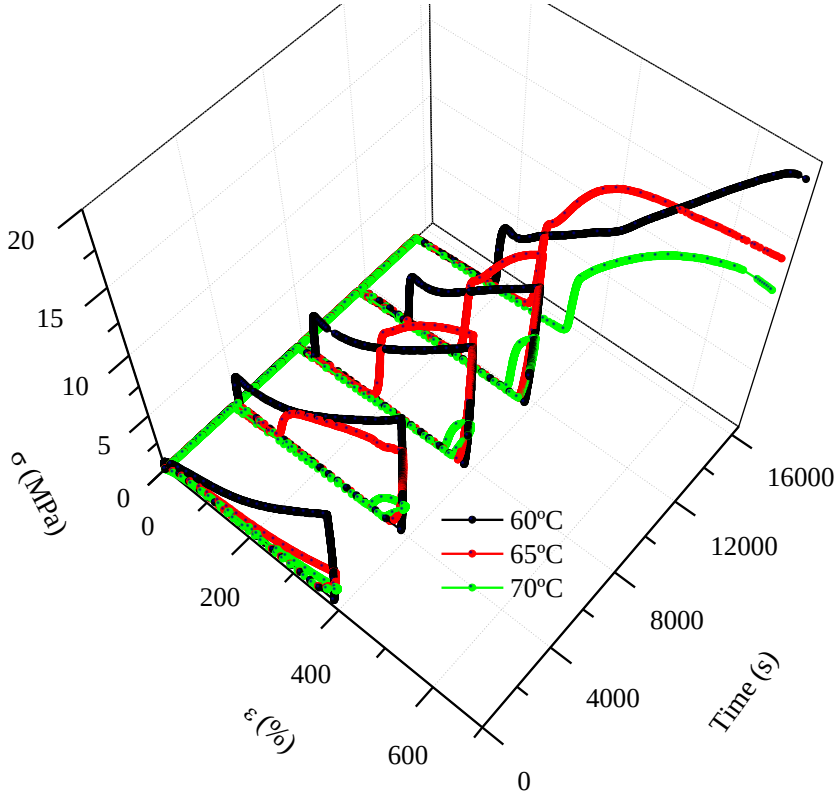

Figure 3.19.-Isothermal cyclic tests

Table 3.5.- Partial and total shape recovery and shape fixity values

	1st Cycle		2nd Cycle		3rd Cycle		4th Cycle		Total
	R_r %	R_f %	R_r %	R_f %	R_r %	R_f %	R_r %	$R_f=R_{f,T}$ %	R_r %
60ºC	95.4	96.8	92.7	96.7	78.7	97.0	74.8	97.1	52.1
65ºC	72.1	88.0	72.1	90.7	74.3	93.7	80.5	93.8	31.1
70ºC	20.6	87.8	71.6	87.7	83.5	90.4	95.3	94.0	11.7

For the ease of clarity, recorded values of R_r are plotted in figure 3.20 at the corresponding number of cycle, respectively. The total recovery values are also included in the same graph and represented by coloured discontinuous lines. In it, the training effect is easily seen in 70ºC test, where recovery is enhanced by successive cycles, whereas in 65ºC test it was more subtle, and in 60ºC it seemed to have an adverse effect.

Based on above described analyses and conclusions extracted thereof, it is suggested that whereas the crystalline network is fulfilled after the first cycle (all crystallisable segments have done so) in 70ºC test, it is progressively developing in lower temperature tests, markedly on 60ºC. As already described, the crystallization kinetics at 60ºC runs slower [64], maintaining the high percentage of amorphous phase (X_a=1-X_c) after the first cycle, which is, at the same time responsible of the high recovery values reported [65]. This very amorphous phase is also responsible of the strain hardening effect observed in figure 19 as a consequence of chain entanglements and limited chain extensibility [60, 66, 67], whereas the maximum observed in higher temperature tests, is associated to plastic deformation of the crystalline domain [27]. Therefore, had further cycling been performed at 60ºC, it is inferred that the decreasing trend would have persisted until the whole crystallisable phase had developed a stable network [6].

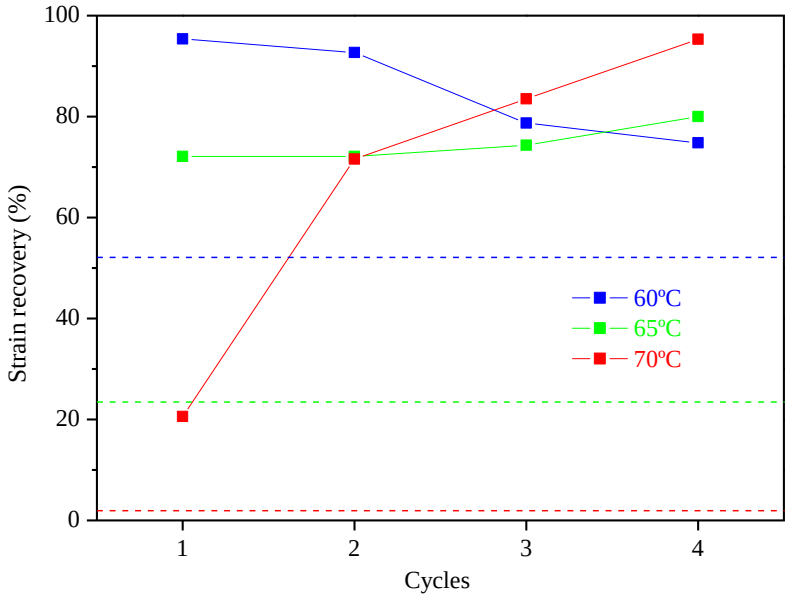

Figure 3.20.-Strain recovery rate

In order to further evaluate the effect of the programming condition, PDLGA copolymer was tested at different levels of strain (ε=50; 200 and 300%) and programming temperatures (T_{HIGH}=45ºC and T_{HIGH}=60ºC) maintaining the temperature for fixation of the temporary shape (T_{LOW}=29ºC). Values of strain at a negligible stress=0.33MPa allowed the calculation of relevant parameters listed in table 3.6.

Table 3.6.- Partial and total shape recovery and fixity ratios

		1st cycle		2nd cycle		
		R_r	**R_f**	**R_r**	**$R_f=R_{fT}$**	**Rr**
	ε=50%	48.2±2.6	99.6±0.1	97.8±7.0	99.6±0.1	47.2±9.2
45ºC	**ε=200%**	63.0±6.8	99.5±0.1	97.2±3.2	99.5±0.1	61.2±6.4
	ε=300%	81.4±1.1	99.6±0.0	97.2±0.5	99.6±0.0	79.1±1.4
	ε=50%	64.8±0.5	99.8±0.1	91.6±0.5	99.8±0.1	59.4±0.6
60ºC	**ε=200%**	82.2±0.2	99.9±0.1	92.6±0.3	99.9±0.1	79.1±0.2
	ε=300%	83.5±0.7	99.8±0.1	94.3±0.1	99.8±0.1	78.7±0.6

Table 3.6 shows high recovery values under the selected conditions. In all cases, recovery obtained after the first cycle was enhanced by further training. Comparing values recorded at 45ºC with those recorded at 60ºC, higher recovery is achieved with increasing the strain level. In all cases fixity approached the 100%.

In order to gain further insight in the molecular mechanism behind the fixity and recovery effects, some tests were interrupted at an intermediate stage and further characterized by modulated DSC. Figure 3.21 represents the stress evolution during the programming step in a shape memory test protocol. Specifically, samples were stretched at 60ºC at a constant strain rate=50mm/min. Once the indicated strain level was achieved, temperature was lowered to T_{LOW} under constant strain, while the stress relaxation behaviour was recorded. As it can be seen, stress decreased a little in the vicinity of T_{HIGH}, but increases with a decrease in temperature below the glass transition temperature T_g. As it can be noted, this thermal stress that opposes to thermal contraction [32, 33] is more readily seen on the lower strain sample, where stress relaxation in the early period of the cooling process is small and the thermal stress $\Delta\sigma_{th}= E\alpha*\Delta T$ (equation 14) due to the temperature change ΔT is large [32]. The reason why stress increases significantly at temperatures below T_g in the cooling process is due to the fact that E is large at low temperature [32].

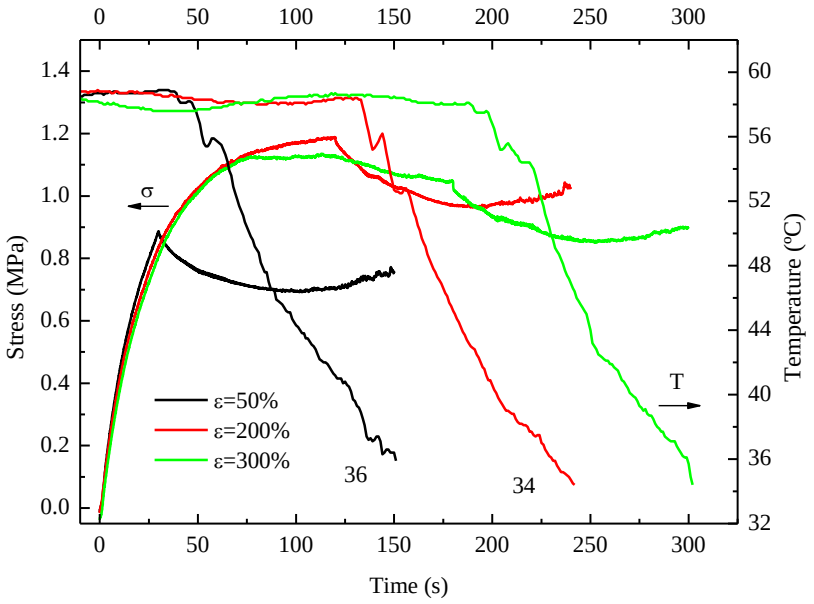

Figure 3.21.- Shape fixation protocol

Figure 3.22 shows the non-reversing C_p of two consecutive heating scans performed in modulated DSC in order to separately analyse the contribution of orientation to relaxation from that associated to aging effects. In order to correct the frequency effect, after the heating process above T_g, samples were cooled under the same MDSC conditions as used for heating. Any peak area in the non-reversing signal on cooling can only be caused by the frequency effect. Thus, this area was subtracted from the peak area obtained on heating to calculate the peak area that corresponds just to the enthalpic recovery. Obtained values are summarized in table 3.7. In all cases, the enthalpic recovery of the first scan makes its apparition before it does in the second, indicating that relaxation of orientation (shape recovery) starts at a lower temperature [17, 68, 69]. Presumably, segmental mobility is advanced due to an enhanced heat transfer during the low rate heating scan (0.5ºC/min) of small scale samples [34]. Thus, activated molecular segments "try" to shorten the distances between their ends at a lower temperature. In the same graph, the area of the enthalpic recovery grows with increasing strain, markedly on samples programed at 45ºC. It is suggested that chain relaxation occurred during the programming step at 60ºC lead to a decrease in the local orientation. Nevertheless, as resumed in table 3.6, shape recovery was not spoiled and a better recovery was observed for ε=50% and ε=200%.

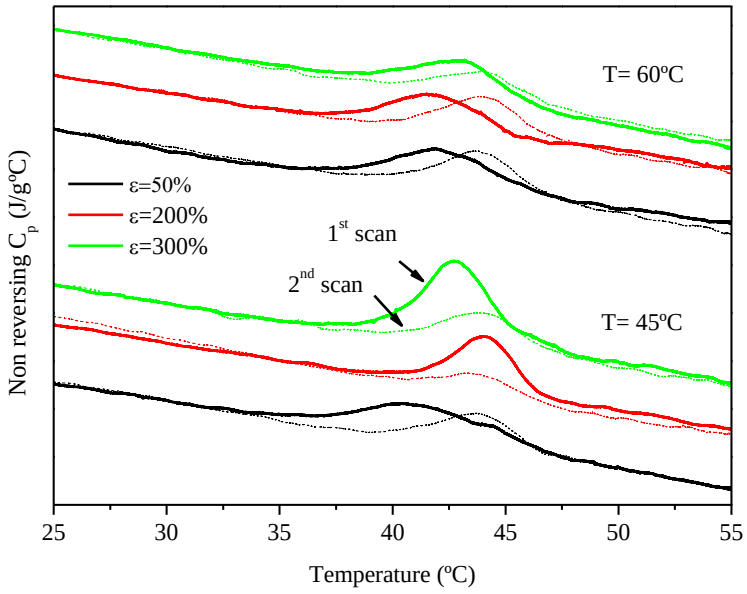

Figure 3.22.- MDSC heating scans

Table 3.7.- Corrected enthalpies

		1st scan ΔH J/g	2nd scan ΔH J/g
45	ε=50%	1.176	0.342
	ε=200%	1.555	0.112
	ε=300%	2.118	0.195
60	ε=50%	0.886	0.298
	ε=200%	0.525	0.455
	ε=300%	1.215	0.095

For the sake of illustrating the multiple relaxation modes, the complex moduli obtained from isothermal frequency scans on PDLGA samples were plotted according to Mavridis and Shroff's [70] procedure in order to identify thermorheological complexity.

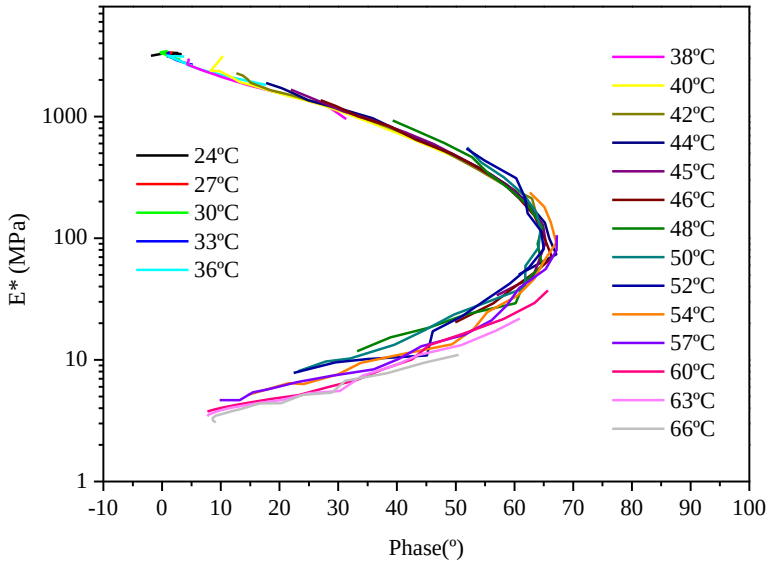

Figure 3.23.- Mavridis and Shroff's plot of PDLGA

Figure 3.23 shows the Mavridis and Shroff's plot of a PDLGA sample without further treatment after compression moulded, whereas figure 3.24 shows the corresponding of a stretched sample up to ε=50% at 60ºC. Accordingly, the lack of superposition in both figures, revealed the different dependence on temperature of existing relaxation modes, where the relaxation of orientation in figure 3.24 is more than obvious.

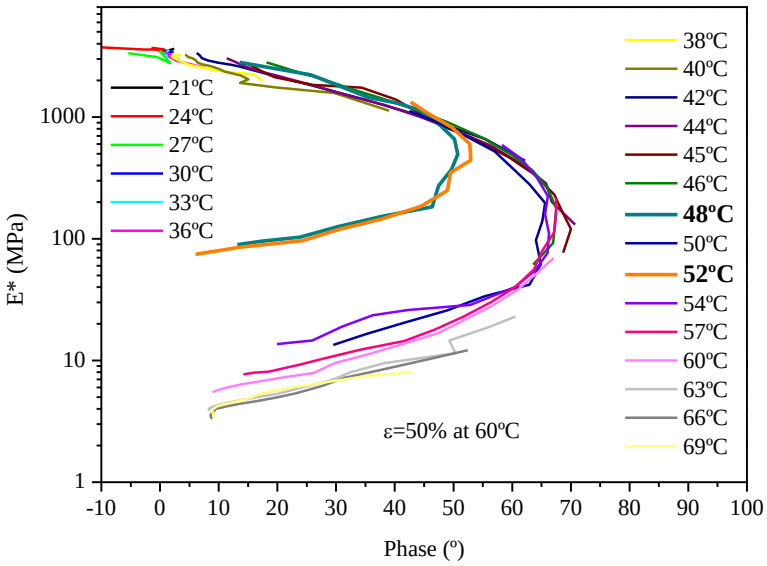

Figure 3.24.- Mavridis and Shroff's plot of stretched PDLGA

Effects of comonomer

In order to evaluate the influence of the type of comonomer in the shape memory behaviour of PLLA, shape memory tests were performed on PLLA, PLCL and PDLGA. Therefore, tests were conducted at $T_{HIGH}=T_g$ and $T_{LOW}=T_g$-16ºC. In all cases, the training effect between successive cycles as well as the total recovery and fixity values were calculated. For the ease of clarity, table 3.8 resumes the arithmetic media, calculated from at least five measurements whereas both arithmetic media and corresponding standard deviation are represented in figure 3.25. It must be noted in table 8 that the strain fixity ratio of the last cycle corresponds to the total fixity ratio ($R_f(5)=R_{f,T}$).

Table 3.8.- Partial and total shape recovery and fixity ratios

Cycle	1st cycle		2nd cycle		3rd cycle		4th cycle		5th cycle		T
	R_r %	R_f %	R_r %	R_f %	R_r %	R_f %	R_r %	R_f %	R_r %	$R_f=R_t$ %	R_r %
PLLA	72.9	99.5	99.3	99.5	99.4	99.2	99.4	99.2	100	99.2	71.5
PLCL	91.8	62.8	99.3	64.7	99.5	64.5	99.7	64.6	99.7	63.6	89.6
PDLGA	85.5	54.5	98.7	55.13	99.0	55.6	99.61	56.4	99.6	56.3	82.6

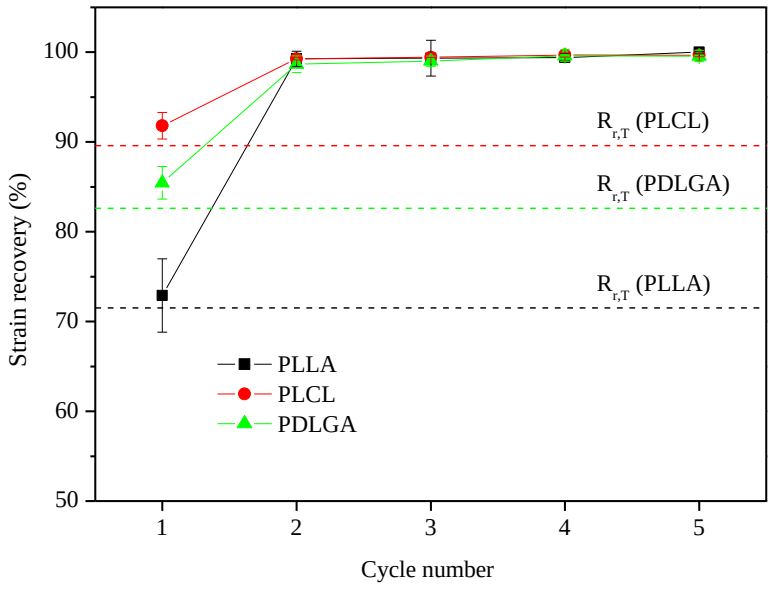

Figure 3.25.- Calculated strain recovery ratio

According to figure 3.25 and table 3.8, the introduction of soft segments (CL) and irregularity (DL) significantly enhances the shape recovery as compared to values of pure PLLA. Again, the training effect is identified by the progressive improvement of strain recovery values.

Effects of chain topology

In order to evaluate the influence of the sequence length over the SME and related properties, segments of ε-caprolactone were introduced in the rigid backbone of PLLA [61, 71-73] by copolymerization. As already described in the materials and methods section, variations in sequence length were achieved by separately conducting two copolymerization reactions with different catalysts. The number average sequence lengths (li) of LA and CL building blocks, the Bernoullian random number-average sequence lengths and the randomness character (R) were calculated from the recorded proton nuclear magnetic resonance (^{1}H NMR) spectra and are resumed in table 3.9. Additionally, the molecular weights (M_w) and polydispersity index (D) are also included. Herein forth, the copolymer with the highest randomness character will be named PLCL-R whereas the copolymer with the lowest, PLCL-B.

Table 3.9.- NMR characterization and GPC measurements of the PLCL copolymers

Sample	**Catalyst**	**Copolymer Molar composition**		**M_w (x10^3)**	**D**	**Microstructure**		
		%LA	**%CL**	**g/mol**	**-**	**l_{LA}**	**l_{CL}**	**R**
PLCL-R	BiSS	69.1	30.9	80.4	1.84	3.22	1.44	1.01
PLCL-B	$Sn(Oct)_2$	69.6	30.4	133.7	1.77	7.94	3.47	0.41

[1] Calculated from H^1 NMR. l_{LA} and l_{CL} are the LA and CL number average sequence lengths. These values are compared to the Bernoullian random number-average sequence lengths (l_A=1/B), obtaining the randomness character value (R).

Their corresponding phase structure and thermal behaviour was also determined by DSC as shown in figure 3.29. The first noticeable effect of copolymerization with

flexible segments of CL [18, 47] is the shift to lower temperatures of the glass transition temperature, compared to that of pure PLLA. Secondly, whereas the shorter and more randomly distributed sequences yielded an amorphous microstructure featured by a single thermal event, namely a sharp glass transition at 15ºC, longer sequences caused the glass transition to delay and span over a wider temperature range. Besides, the apparition of the cold crystallization peak further supports the presence of phase segregated domains.

Tensile tests were conducted at several temperatures (0, 15, 21, (30), 37ºC). Elastic modulus were determined from the elastic part of the stress/strain curve, where the glassy to rubbery transition was demonstrated by the decay of the elastic modulus, as it can be seen in figure 3.26. Interestingly, the effect of sequence length was more readily seen at intermediate and higher temperatures, where the greatest values were recorded for PLCL-B, whereas this difference seems to annihilate for decreasing test temperature, where both values seem to converge.

To gain further insight in the molecular dynamics, Dynamic mechanical analysis was performed for both copolymers in a temperature range from below to above their respective glass transition temperatures. Corresponding storage modulus E' and tan δ are represented in figure 3.27.

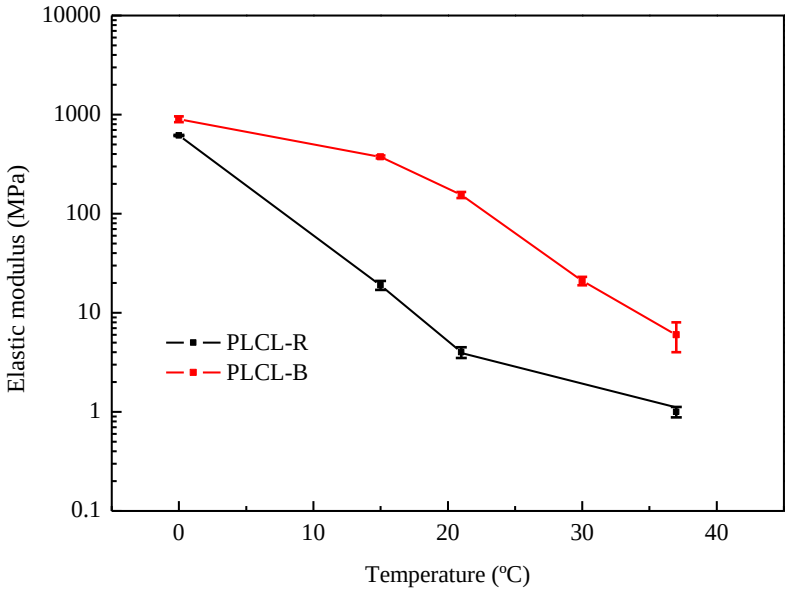

Figure 3.26.- Elastic modulus calculated as the secant modulus at ε=2%.

In general, both copolymers show the characteristic behaviour of non-crystalline thermoplastic polymers with high storage modulus and small damping at low temperature and a softening range where the modulus decreases very rapidly while the damping becomes very large and shows a maximum. In accordance with DSC measurements, the glass transition of PLCL-R is narrower while the corresponding of PLCL-B starting at lower temperatures as suggested by the cross point needs a broader range to complete. The cross point agrees with figure 3.26 too, where intersection was expected at lower temperatures. Close observation to tan δ curves indicate higher damping at low temperature for PLCL-B whereas its peak height is significantly lower as compared to PLCL-R. These observations suggest that longer sequences induce a heterogeneous behaviour that contributes to broaden the transition region.

The origin of this heterogeneity can be found in the course of the polymerization reaction whereby the different reactivity of the components cause differences in the composition between the first and the last molecules formed. Accordingly, the first molecules formed would be rich in the more reactive component while the molecules formed at the end of the reaction would be rich in the less reactive component [45]. When an heterogeneous copolymer formed thereof is submitted to subsequent heating scans (as in DSC or DMA) the molecules that are rich in the lower melting component start to soften earlier than they would in a homogeneous copolymer where all molecular segments are in a similar environment [45], whereas molecules rich in the higher melting component take longer to soften. The consequence of this heterogeneity is a broadening of the transition range and higher damping, whereas a homogeneous copolymer (PLCL-R) exhibits a narrower transition and a sharper damping peak, which are associated with enhanced shape memory properties [14, 26, 33, 45].

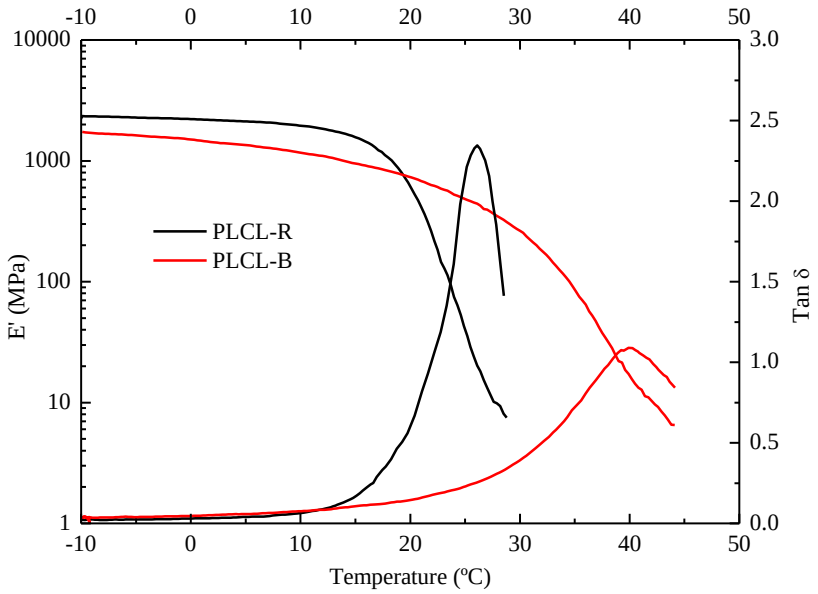

Figure 27.-Dynamic mechanical thermal analysis

Therefore, in order to quantify the shape memory properties of both copolymers, isothermal cyclic tests were carried out at their corresponding glass transition temperatures, as shown in three dimensional graph in figure 3.28. As it can be noted, PLCL-R shows higher recovery than PLCL-B, suggesting an enhanced recovery linked to the highest randomness character, whereas the more ordered structure of PLCL-B due to longer sequences evokes irreversible strains linked to plastic deformation of hard segments or strain induced crystallization [6].

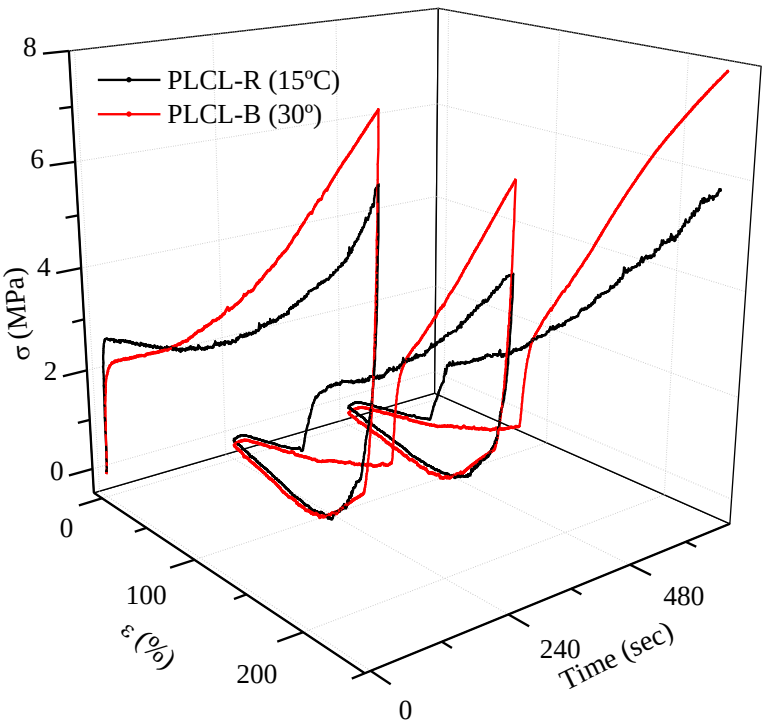

Figure 3.28.- Isothermal cyclic tests

As shown in the DMA, due to the heterogeneous nature, short segments of the lower melting temperature comonomer (CL) start to relax (move) under the application of strain well below the corresponding glass transition of the copolymer, therefore, the onset of yielding in the PLCL-B appears at a lower stress than in PLCL-R. After the soft segments with a lower modulus have extended, stress is transferred to the hard segments [18, 55] causing the strain hardening effect, more markedly in PLCL-B as suggested by the intersection point after which the stress run above that of PLCL-R. Subsequent increase of deformation strain, increases the irreversible deformation [27, 46, 55] that leads to superior fixity and poorer recovery as resumed in table 3.10.

Table 3.10.- Partial and total shape fixity and recovery ratios

	R_{r1} %	R_{f1} %	R_{r2} %	R_{f2} %	R_{rt} %	R_{ft} %
PLCL-R	70.3±4.3	67.5±1.6	92.6±0.6	68.4±1.6	65.2±4.0	68.4±1.6
PLCL-B	40.1±0.8	80.0±1.3	81.5±4.3	80.5±1.1	32.7±1.5	80.5±1.1

In both samples the training effect is observed when strain recovery values of the second cycle are compared to those recorded in the first cycle. In this regard, despite the higher recovery of PLCL-R, signs of irreversible strain are also perceived.

The DSC scans conducted on tested samples evidenced the presence of a melting peak in both samples, whose location was strongly influenced by the sequence length of the corresponding blocks. Due to the strain induced crystallization, the amorphous phase content has diminished, as inferred by the reduced step height of the glass transition temperature. The shorter sequences of PLA in PLCL-R yielded a melting peak at 96ºC with an estimated crystallinity associated to the LA content 2.4%. The DSC of PLCL-B further discloses the phase segregation and strain induced crystallization with an estimated value of 27.5%.

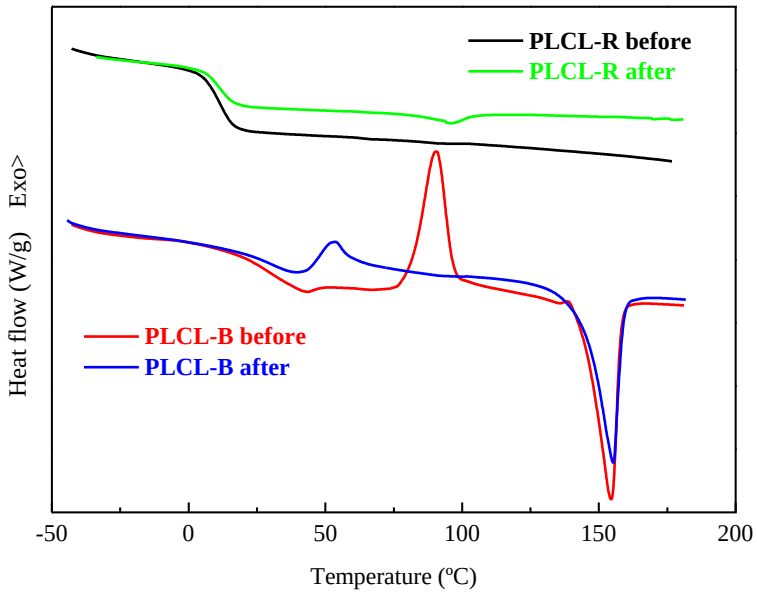

Figure 3.29.- DSC heating scans as quenched (before) and after cyclic tests

Table 3.11.-Thermal properties and crystallinity degree

		T_g ºC	T_m ºC	X_c %
PLCL-R	**Before**	12	-	-
	After	11	95.8	2.4
PLCL-B	**Before**	30	154.4	3.4
	After	31	154.6	27.5

In an analogous fashion as in segmented polyurethanes, in which fixity was associated to the hard segment [1, 11, 28, 74-76], in PLCL copolymers, it is associated to PLA segments [18], whereas recovery to soft PCL segments [18].

Effect of entanglements

Finally, in order to characterize the role of entanglements on SME of an amorphous glassy polymer [77], a range of increasing molecular weight series of PDLLA were synthesised, whose molecular and thermal properties are resumed in table 3.12.

Table 3.12.- Molecular weight (M_w), polydispersity index (D) and glass transition temperatures (T_g)

Reference	**M_w(*10^3) g/mol**	**D**	**T_g ºC**
PDLLA67	67.1	1.70	47
PDLLA100	101.3	1.76	46
PDLLA129	129.8	1.77	46
PDLLA155	155.8	1.75	44
PDLLA190	186.3	1.75	46

As a consequence of the increased irregularity caused by the randomly distributed enantiomers of opposite configuration [52, 78, 79] along the chain backbone, the resulting copolymers were totally amorphous [52, 57] whose only thermal event was the T_g. As the

molecular weight exceeds 20,000 [80], the corresponding glass transition temperatures laid around a constant value of ~46ºC independently of their molecular weight [81].

Dynamic mechanical analysis

The evolution of storage modulus within the test temperature range obtained from dynamic mechanical analysis is illustrated in figure 3.30. In all cases, the sharp transition from glassy state to rubbery state is completed within a narrow temperature range (ΔT_{Tran} ≈17ºC), as listed in table 3.10, indicating a high sensitivity to temperature variation [28]. From these curves, the elasticity ratio ($E_{glassy}/E_{rubbery}$) was calculated and included in table 3.13. As it can be noted, all values were well above 100, whereby outstanding shape fixity [15, 28, 33, 34] is inferred. Another interesting feature from figure 3.30 is the progressive extension of the rubbery plateau with increasing molecular weight. According to molecular theories of undiluted polymers [82], the plateau zone is the intermediate region limited by configurational rearrangements between and beyond entanglements, whose extension is a strong function of the molecular weight distribution [29]. However illustrating figure 3.30 may be, offers limited information regarding the terminal zone of the lower molecular weight samples, as DMA is a solid state characterization method.

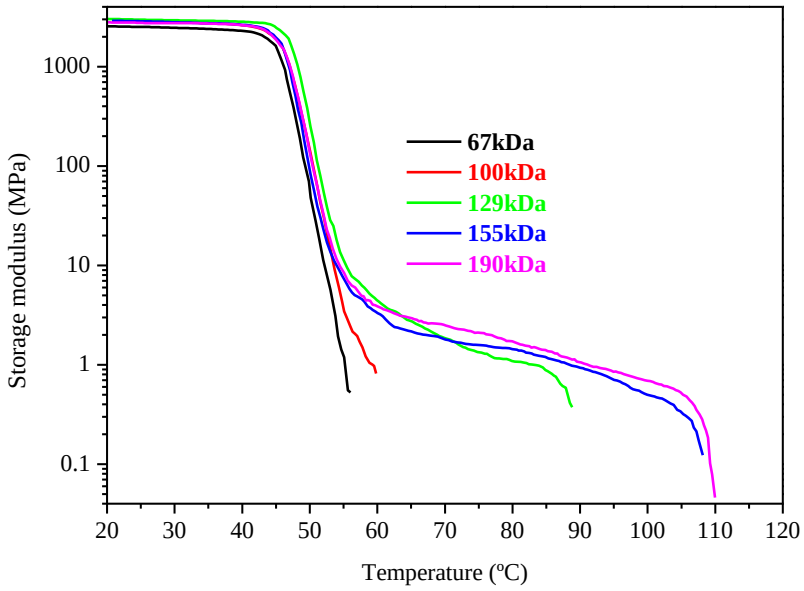

Figure 3.30.- Storage modulus evolution with temperature

Table 3.13.- Glassy to rubbery temperature transition range (ΔT_{Tran}) and elastic ratio (E_g/E_r)

	ΔT_{Tran}	E_g/E_r
	ºC	-
PDLLA67	13	1545
PDLLA100	15	1290
PDLLA129	19	650
PDLLA155	18	760
PDLLA190	18	665

Dynamic viscoelastic analysis

Therefore, for a better characterization of the terminal zone, rheologic measures were conducted in the molten state in the linear viscoelastic regime. From these, their corresponding master curves were constructed and the rubbery plateau modulus, G_N^0, the molecular weight between entanglements, M_e, as well as the flow activation energy were calculated and resumed in table 3.14.

Firstly, the thermorheological simplicity was evaluated according to the Mavridis and Shroff construction that, as shown in figures 3.31 to 3.35 superimposed satisfactorily.

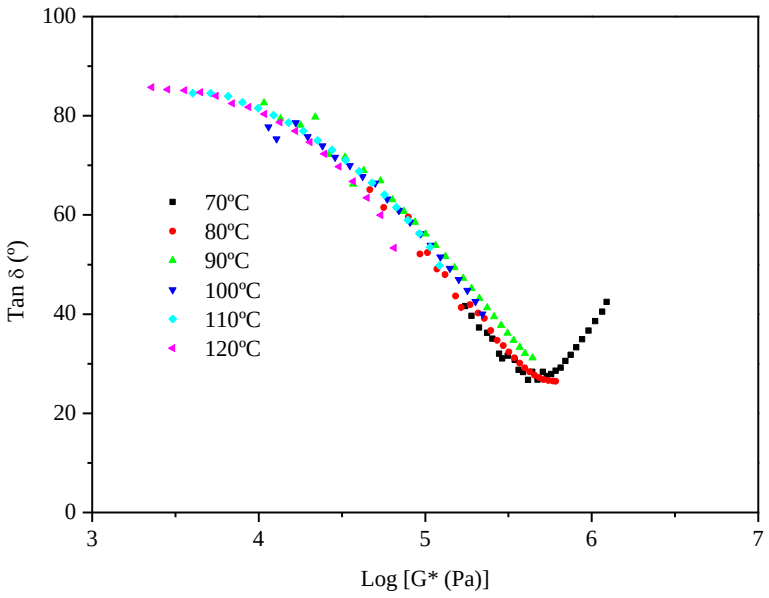

Figure 3.31.- Mavridis and Shroff's plot of a PDLLA67

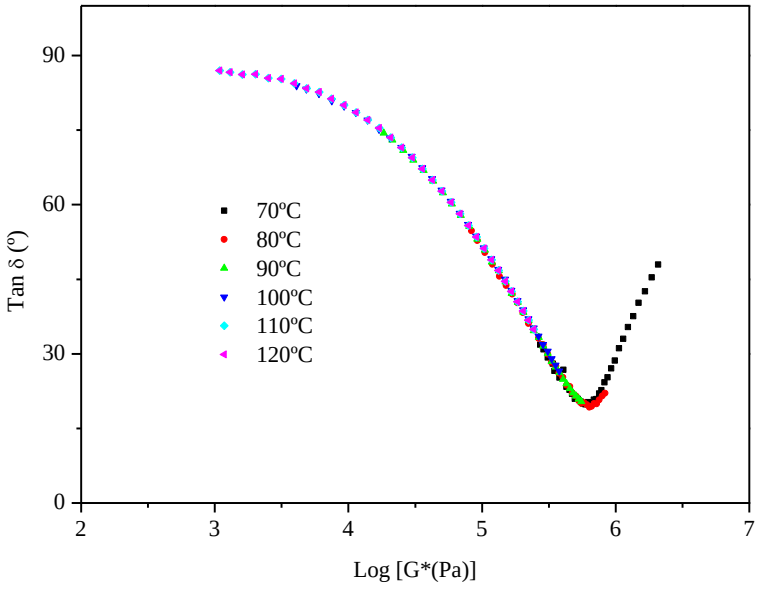

Figure 3.32.- Mavridis and Shroff's plot of a PDLLA100

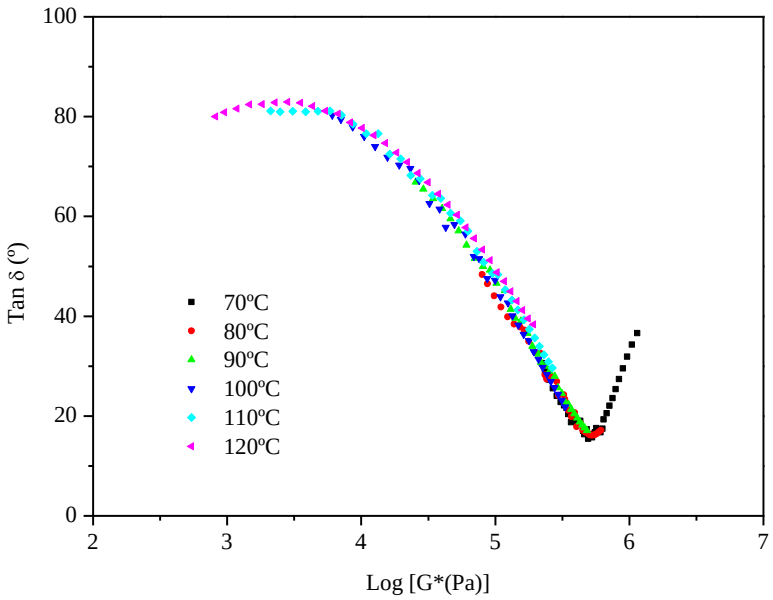

Figure 3.33.- Mavridis and Shroff's plot of a PDLLA129

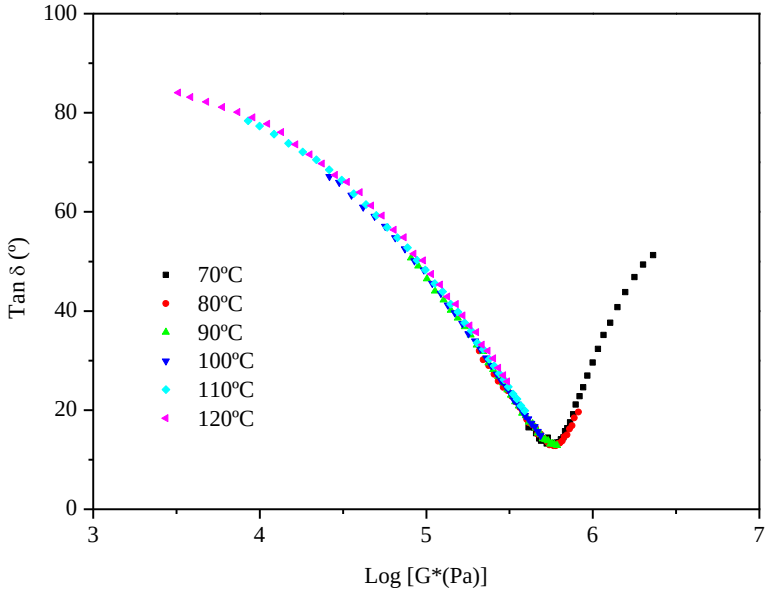

Figure 3.34.- Mavridis and Shroff's plot of a PDLLA155

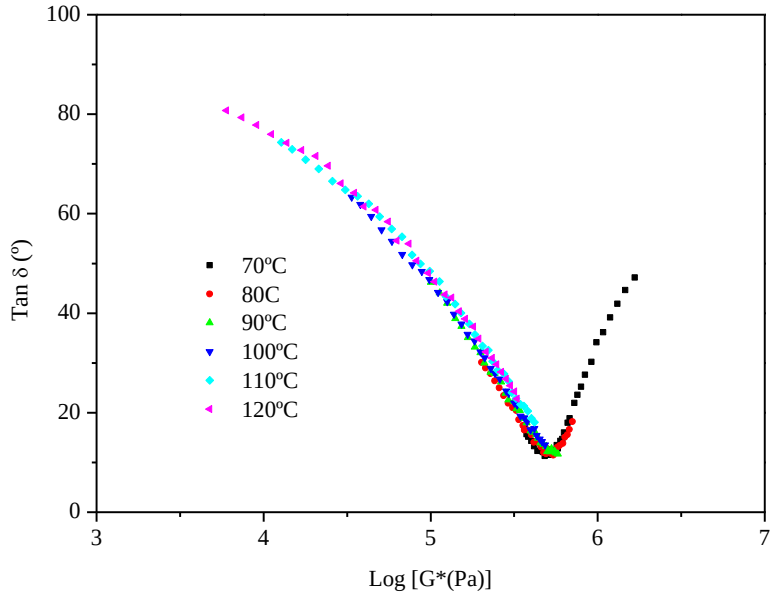

Figure 3.35.- Mavridis and Shroff's plot of PDLLA190

Hence, their corresponding master curves were constructed as shown in figures 3.36 to 3.42. From these, the corresponding G_N^0 values were calculated according to equation 15 $G_N^0 = [G']_{tan\delta \rightarrow minimum}$ (equation 15) [83] and listed in table 3.14. In the melt state and for long chains, the plateau modulus G_N^0 is essentially a property of the

species arising from the uncrossability of the backbone contours in covalent chain molecules [84]. Therefore, calculated values laid as expected, around a constant value. Taking G_N^0=5.8*10^{5}Pa, the entanglement molecular weight was calculated according to equation 16 $M_e = \frac{\rho RT}{G_N^0}$ (equation 16) with ρ=10^6 g/m^3; R=8.31(Pa*m^3)/(mol*K) and a reference temperature of 363K. Thus M_e=5200g/mol. As in all cases, the molecular weight (M_w) exceeded the critical value for chain entanglements, M_c, being M_c=2M_e (equation 17) [82, 85] the presence of a network of entanglements was demonstrated.

The shift factor a_T used to apply the time-temperature superposition is very well adjusted to an Arrhenius-like equation 18 a_T=Bexp(E_a/RT) (equation 18), where E_a, the activation energy of flow constitutes an indirect tool to evaluate the characteristic ratio, that is to say, the chain rigidity [85]. Therefore, upon knowing E_a, the characteristic ratio C_∞ was estimated according to E_a=4.3 exp(4.65log C_∞/2) (equation 19), and included in table 3.14. Comparing with reported values for pure PLLA (C_∞=7-12) [68, 70, 86], it must be reckoned that, within experimental error, the obtained value of C_∞=12 was slightly higher than expected, as the incorporation of L-D junctions is known to increase chain flexibility [61, 87]. Accordingly, a recently published article listed G_N^0 = 2*10^{5}Pa and C∞=10.32 for a commercial PDLLA (M_w=320000g/mol) [88]. Nevertheless, as the higher value of G_N^0 is consistent with the higher value of C_∞ coherence behind reported values hitherto must be claimed.

Further, according to the strong and fragile classification of glass forming liquids [89] the dynamic fragility, m, was calculated from values of C_1 and C_2 according to equation m=$T_g C_1/C_2$ (equation 20) [90] and considering a T_g=46ºC to be 24.6±1.5; which is stronger than previously reported for the aforementioned commercial PDLLA from DMA measurements [90].

Following, the crossover values (ω_x, G_x) at which G'(ω)=G"(ω) the corresponding relaxation times (equation 21) were determined from figures 3.36 to 3.42 and included in table 3.14.

$\tau=1/\omega_x$ (equation 21)

A remarkable feature from these figures lays on the prevalence of storage modulus over the loss modulus, anticipating good recovery values from the shape memory standpoint.

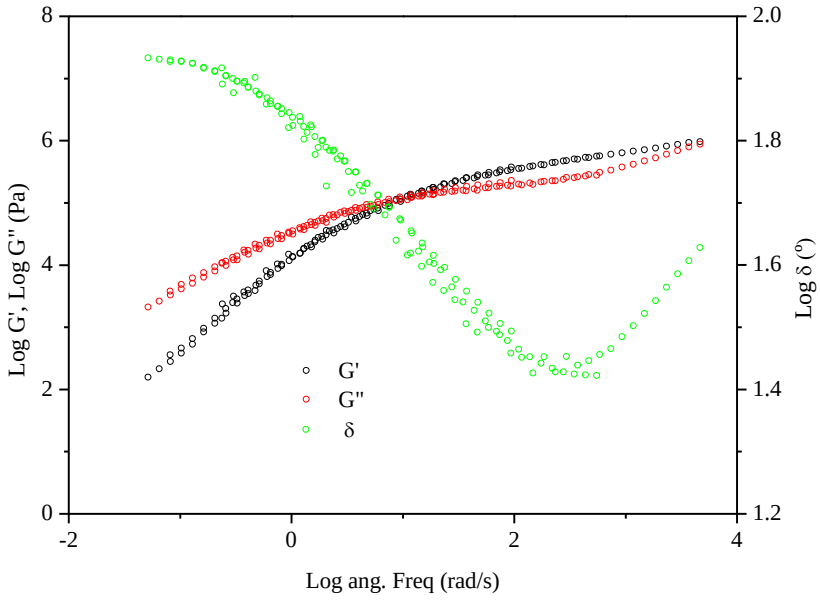

Figure 3.36.-Master curves of PDLLA67

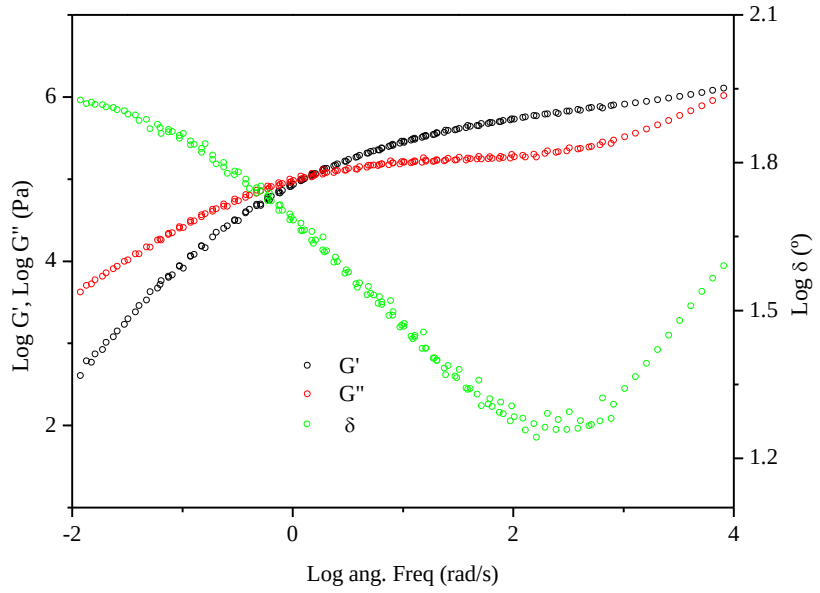

Figure 3.37.- Master curves of PDLLA100

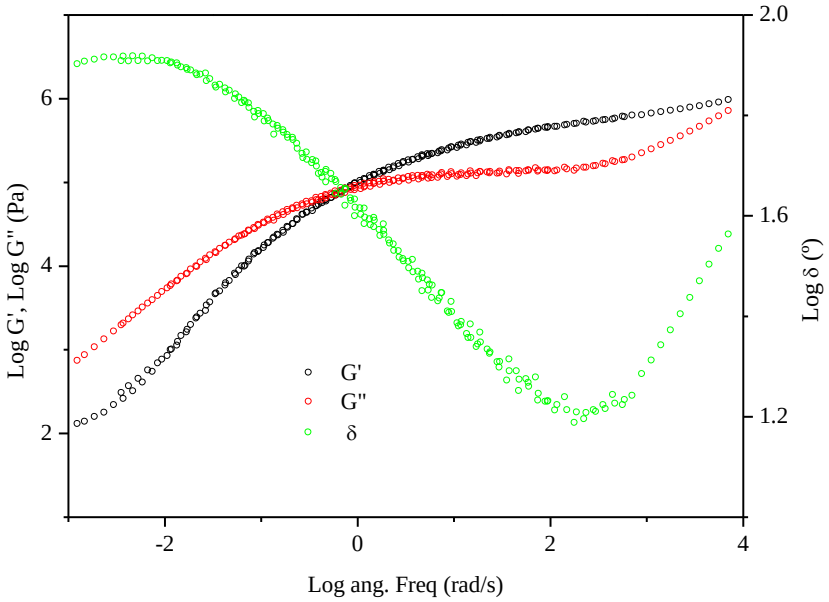

Figure 3.39.- Master curves of PDLLA129

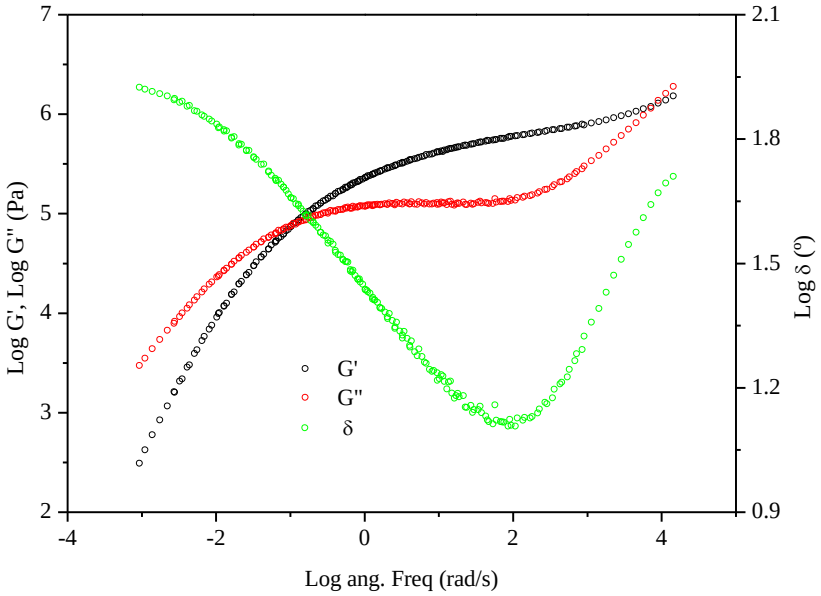

Figure 3.40.- Master curves of PDLLA155

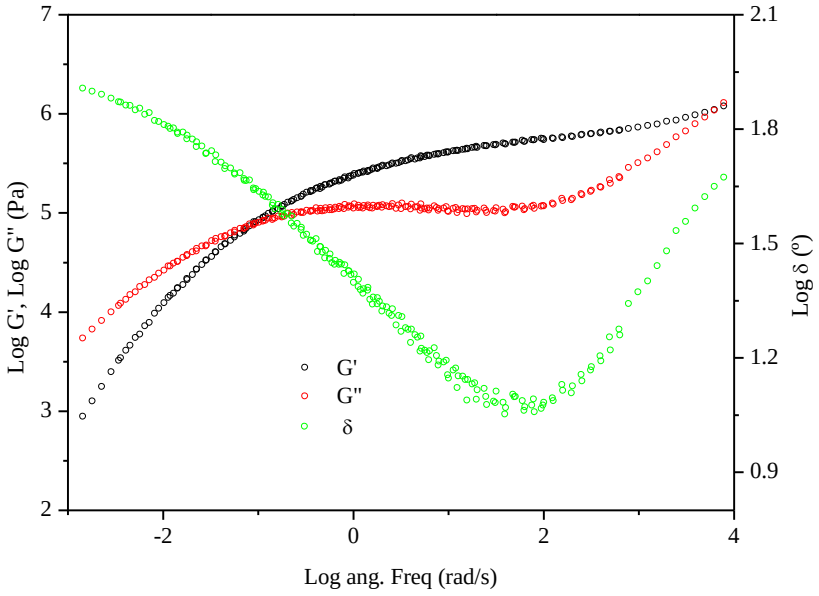

Figure 3.41.- Master curves of PDLLA190

Table 3.14.- Rheological parameters of the terminal zone: entanglement modulus (G_N^0), cross over frequency (ω_x), flow activation energy (E_a), fitting parametres (C_1 and C_2), reference temperature for master curves construction (T_{ref}), characteristic ratio ($C\infty$), and relaxation time (τ)

Mw	G_N^0 ***10^5**	**Log (ang. Frequency)**	**E_a**	**C_1**	**C_2**	**T_{ref}**	**C_∞**	**τ**
kDa	**Pa**	**Rad/s**	**kJ/mol**			**ºC**		**s**
67	5.7	0.9	158.6	8.494	119.8	90	11.9	0.126
100	5.8	0.1	171.9	7.447	91.70	90	12.4	0.794
129	5.7	-0.1	161.6	7.458	99.86	90	12.05	1.259
155	5.8	-1.0	173.7	7.059	84.56	90	14.5	10.0
190	5.7	-1.1	162.6	7.289	96.10	90	12.1	12.589

As it can be noted in table 3.14, relaxation times evolve toward higher values with increasing molecular weight as predicted by the reptation model [85], which is as the same time, proportional to the disentanglement time τ_d.

Shape memory tests

Accordingly, shape memory properties were determined from a 2 cycles test protocol that consisted on a programming step whereby a strain ε=200% was impinged at a constant strain rate=50mm/min at $T_{HIGH}=T_g+10ºC$ (as resumed in table 3.15), subsequently fixed by cooling to $T_{LOW}=T_g-16ºC$ in 2minutes afterwards clamps were approached to their original position of 0% strain to allow for recovery at $T=T_{HIGH}$ before the start of the second cycle. From these, the strain fixity ratio and the strain recovery ratio were calculated and listed in table 3.16.

Table 3.15.- Glass transition temperature (T_g) and corresponding temperatures for strain (T_{HIGH}) and fixation (T_{LOW}) of the temporary shape.

Name	**T_g** **ºC**	**$T_{HIGH}=T_g+10ºC$** **ºC**	**$T_{LOW}=T_g-16ºC$** **ºC**
PDLLA67	47	57	31
PDLLA100	46	56	30
PDLLA129	46	56	30
PDLLA155	44	54	28
PDLLA190	46	56	30

For the ease of clarity, only the most significant curves have been plotted in figure 3.42. As it can be seen during the first cycle and up to ~0.2MPa, three curves overlapped, although herein forward the lowest molecular weight sample deviated significantly, whereas 100kDa did at ~0.5MPa. Interestingly, the lowest molecular weight sample was the last to upturn during the second cycle, whereas sample labelled 190kDa was the first one at a significantly lower strain value, thus reflecting a higher recovery as resumed in table 3.16. In the same graph, the sudden increase of stress at ε=200% is caused by the thermal stress [33, 32] originated during the cooling down to $T=T_{LOW}$, in coherence with the high elasticity ratios resumed in table 3.13 and associated fixity ratios of table 3.16.

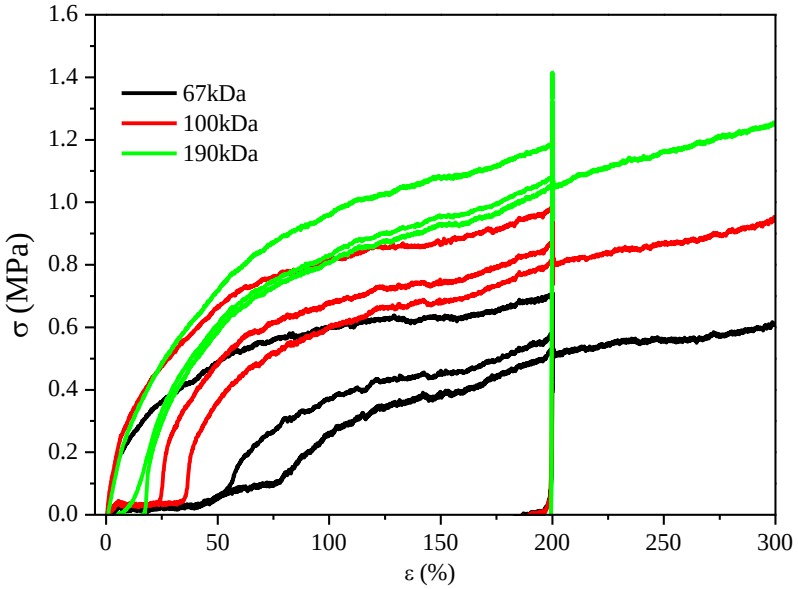

Figure 3.42.- Shape memory tests

Table 3.16.- Partial and total strain fixity and recovery values

	Cycle 1		Cycle 2		Total	
	R_f	R_r	R_f	R_r	R_f	R_r
σ=0.1MPa	**%**	**%**	**%**	**%**	**%**	**%**
PDLLA67	99.8±0.1	73.4±0.9	99.8±0.1	85.3±1.0	99.8±0.1	62.6±0.6
PDLLA100	99.6±0.1	88.4±1.3	99.7±0.1	93.4±0.4	99.7±0.1	82.6±1.6
PDLLA129	99.7±0.1	91.1±1.3	99.7±0.1	94.9±0.4	99.7±0.1	86.6±1.4
PDLLA155	99.5±0.7	94.0±0.7	99.7±0.2	96.4±0.2	99.7±0.2	90.7±0.9
PDLLA190	99.8±0.0	95.0±0.7	99.8±0.0	97.0±0.8	99.8±0.0	92.1±0.9

The relationship between molecular weight and shape memory properties is highlighted in figures 3.43 and 3.44 where R_r and R_f are plotted correspondingly.

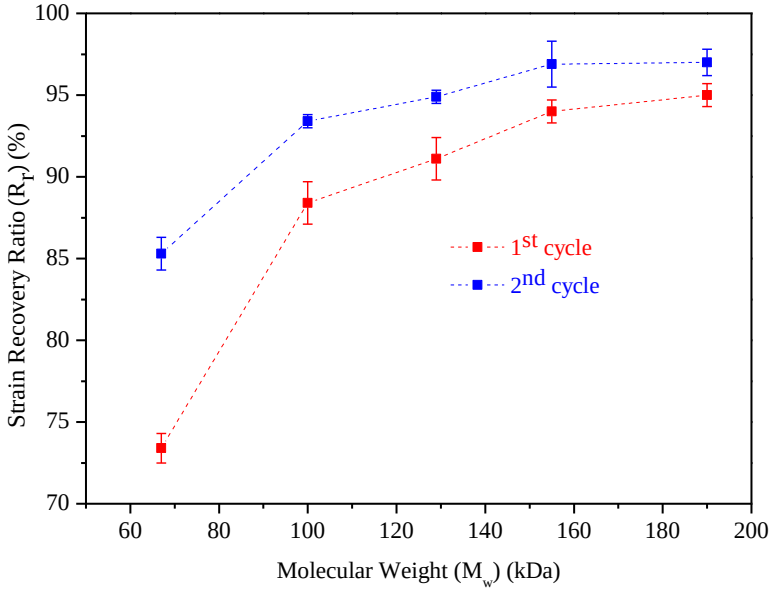

Figure 3.43.- Strain recovery ratio

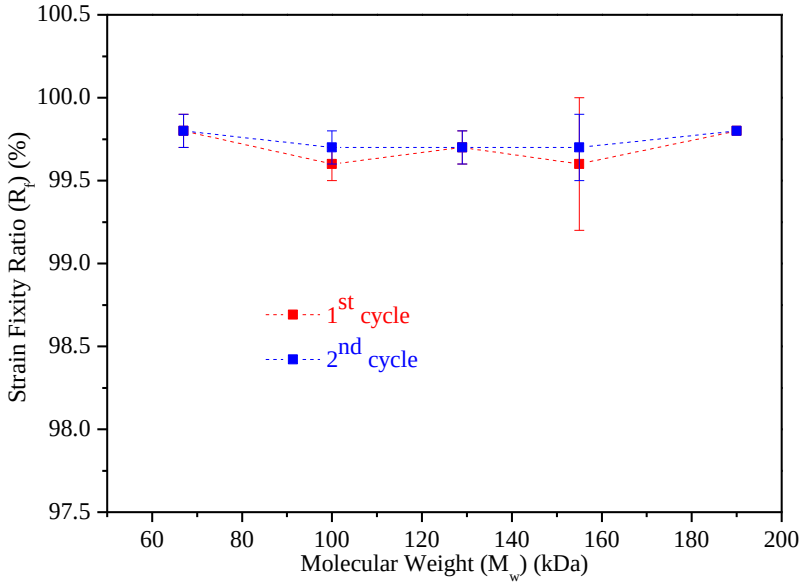

Figure 3.44.- Strain fixity ratio

As it can be noted from figures 3.43 and 3.44, besides the training effect, strain recovery showed a strong dependence on molecular weight, whereas this dependence was negligible for strain fixity. The later was expected, as the capacity to fix the temporary shape relies on the sharpness of the rubbery to glassy transition that, showed to be

remarkable in all cases. Conversely, despite the reasonable values of recovery for all samples, they showed a clear trend as highlighted in figure 4.43. It is reasoned that under the test conditions, irreversible strain ascribed to chain slippage opposed to recovery. Being chain slippage dictated by chain disentangling, it follows that samples with shorter relaxation time in the terminal zone (τ) showed the poorer values of recovery. Thus, it is suggested that beyond the featuring value of G_N^0, the relaxation time of entanglements in the terminal zone, is the relevant parameter in the design of glassy polymers with enhanced shape recovery.

Conclusions

The aim of this chapter was to gain further insight into the shape memory effect (SME) of polylactides, as due to their biocompatibility and biodegradability they have settled as ideal candidates for the development of medical devices.

Thus, two approaches have been followed in order to study the thermally triggered SME based on the glass transition as the switching phase. On the one hand, the effects of temperature, strain and recovery time during the shape memory creation procedure have been disclosed. On the other, making use of the synthetic route, molecular parameters such as the comonomer type, sequence length or molecular weight have been explored.

It has been shown that the capacity to fix the temporary shape is associated to temperature sensitivity, whereby the sharper the transition, the higher the fixity of the temporary shape.

Instead, the capacity to recover the permanent shape is sensitive to irreversible changes in the amorphous phase caused during the programming procedure that, oppose to entropic elasticity. Two sources of these irreversible changes such as strain induced crystallization and chain slippage in the terminal zone have been investigated.

It has been proved that strain induced crystallization causes the main detrimental effect in semicrystaline polymers, as its development reduces the available amount of amorphous phase, which is responsible for shape recovery.

Conversely, in amorphous polymers where crystallization is prohibited as a consequence of a highly irregular topology, chain slippage associated with disentanglement of chains and relaxation of these in an unstretched state, has been identified to be the cause of reduced recovery effect.

However, upon fully development of these, both families of polymers demonstrated a stable and enhanced recovery during subsequent tests, evidencing the relevance of the training effect as a previous step upon a practical situation.

References

[1] Lendlein, A., Kelch, S., Angewandte chemie international edition, 2002, 41, 2034-2057

[2] Jiang, H., Kelch, S., Lendlein, A., Advanced materials, 2006, 18, 1471-1475

[3] Bellin, I., Kelch, S., Langer, R., Lendlein, A., Proceedings of the national academy of sciences of the United States of America, 2006, 28, 18043-18047

[4] Wagermaier, W., Kratz, K., Heuchel, M., Lendlein, A., Advances in polymer science, 2010, 226, 97-145

[5] El Feninat, F., Laroche, G., Fiset, M., Mantovani, D., Advanced engineering materials, 2002, 4, 91-104

[6] Wong, Y. S., Venkatraman, S. S., Acta materialia, 2010, 58, 49-58

[7] Behl, M., Lendlein, A., Materials today, 2007, 10, 20-28

[8] Liu, C., Qin, H., Mather, P. T., Journal of materials chemistry, 2007, 17, 1543-1558

[9] Behl, M., Lendlein, A., Soft matter, 2007, 3, 58-67

[10] Paakinaho, K., Heino, H., Pelto, M., Hannula, M., Törmälä, P., Kellomäki, M., Journal of materials science: materials in medicine, 2012, 23, 613-621

[11] Wang, W., Ping, P., Chen, X., Jing, X., European polymer journal, 2006, 42, 1240-1249

[12] Qi, H. J., Nguyen, T. D., Castro, F., Yakacki, C. M., Shandas, R., Journal of the Mechanics and Physics of Solids, 2008, 56 1730-1751

[13] Kusy, R. P., Whitley, J. Q., Thermochimica acta, 1994, 243, 253-263

[14] Nagahama, K., Ueda, Y., Ouchi, T., Ohya, Y., Biomacromolecules, 2009, 10, 1789-1794

[15] Rousseau, I., Polymer engineering and science, 2008, 48, 2075-2089

[16] Monkman, G. J., Mechatronics, 2000, 10, 489-498

[17] Beloshenko, V. A., Varyukhin, V. N., Voznyak, Y. V., Russian chemical reviews, 2005, 74, 265-283

[18] Min, C., Cui, W., Bei, J., Wang, S., Polymers for advanced technologies, 2005, 16, 608-615

[19] Williams, D. F., Essential biomaterials science, Cambridge university press, UK, 2014, pp 118-120

[20] Nguyen, T. D., Qi, H. J., Castro, F., Long, K. N., Journal of the mechanics and physics of solids, 2008, 56, 2792-2814

[21] Barot, G., Rao, I.J., Zeitschrift für angewandte Mathematik und Physik, 2006, 57, 652-681

[22] Barot, G., Rao, I. J., Rajagopal, K. R., International journal of engineering science, 2008, 46, 325-351

[23] Zini, E., Scandola, M., Biomacromolecules, 2007, 8, 3661-3667

[24] Wong, Y. S., Xiong, Y., Venkatraman, S. S., Boey, F. Y., Journal of biomaterials science, polymer edition, 2008, 19, 175-191

[25] Zheng, X., Zhou, S., Li, X., Weng, J., Biomaterials, 2006, 27, 4288-4295

[26] Lu, X., Sun, Z., Cai, W., Physica scripta, 2007, T129, 231-235

[27] Lu, X. L., Sun, Z. J., Cai, W., Gao, Z. Y., Journal of materials science: materials in medicine, 2008, 19, 395-399

[28] Kim, B. K., Lee, S. Y., Xu, M., Polymer, 1996, 37, 5781-5793

[29] Tuminello, W. H., Polymer engineering and science, 1986, 26, 1339-1347

[30] Hornbogen, E., Advanced engineering materials, 2006, 8, 101-106

[31] Cui, J., Kratz, K., Heuchel, M., Hiebl, B., Lendlein, A., Polymers advanced technologies, 2011, 22, 180-189

[32] Tobushi, H., Hashimoto, T., Hayashi, S., Yamada, E., Journal of intelligent material systems and structures, 1997, 8, 711-718

[33] Tobushi, H., Hara, H., Yamada, E., Hayashi, S., Smart materials and structures, 1996, 5, 483-491

[34] Xu, J., Shi, W., Pang, W., Polymer, 2006, 47, 457-465

[35] Liu, Y., Gall, K., Dunn, M. L., McCluskey, P., Mechanics of materials, 2004, 36, 929-940

[36] Lu, X. L., Cai, W., Gao, Z. Y., Journal of applied polymer science, 2008, 108, 1109-1115

[37] Agrawal, C. M., Haas, K. F., Leopold, D. A., Clark, H. G., Biomaterials, 1992, 13, 176-182

[38] Hietala, E. M., Salminen, U. S., Ståhls, A., Välimaa, T., Maasilta P., Törmälä, P., Nieminen, M. S., Harjula, A.L.J., Journal of vascular research, 2001, 38, 361-369

[39] Tamai, H., Igaki, K., Kyo, E., Kosuga, K., Kawashima, A., Matsui, S., Komori, H., Tsuji, T., Motohara, S., Uehata, H., Circulation, 2000, 102, 399-404

[40] Sweeney, J., Bonner, M., Ward, I. M., Journal of the mechanical behaviour of biomedical materials, 2014, 37, 12-23

[41] Peng, T., Gibula, P., Yao, K. D., Goosen, M. F., Biomaterials, 1996, 17, 685-694

[42] Paakinaho, K., Hukka, T. I., Kastinen, T., Kellomäki, M., Journal of applied polymer science, 2013, 130, 4209-4218

[43] Prospiech, D., Komber, H., Jehnichen, D., Häussler, L., Eckstein, K., Scheibner, H., Janke, A., Kricheldorf, H. R., Petermann, O., Biomacromolecules, 2005, 6, 439-446

[44] Shikinami, Y., et al. US patent 6281262, 2001

[45] Nielsen, L. E., Journal of the American chemical society, 1953, 75, 1435-1439

[46] Lu, X. L., Cai, W., Gao, Z. Y., Zhao, L. C., Materials science and engineering A, 2006, 438-440, 856-861

[47] Min, C., Cui, W., Bei, Wang, S., Polymers for advanced technologies, 2007, 18, 299-305

[48] Bobel, A. C., Petisco, S., Sarasua, J. R., Wang, W., McHugh, P. E., Computational bench testing to evaluate the short-term mechanical performance of a polymeric stent, Cardiovascular engineering and technology 2015, 10.1007/s13239-015-0235-9

[49] Fernández, J., Etxeberria, A., Ugartemendia, J. M., Petisco, S., Sarasua, J.R, Journal of Mechanical Behavior of Biomedical Materials, 2012, 12, 29-38

[50] Fernández, J., Etxeberría, A., Sarasua, J.R., Journal of the Mechanical Behavior of Biomedical Materials, 2012, 9, 100-112

[51] Herbert, I. R., Statistical analysis of copolymer sequence distribution. In NMR Spectroscopy of Polymers. Ibbet, R.N. Ed.: Blackie Academic & Professional, London, 1993, pp.50-79

[52] Sarasua, J. R., Prud'homme, R. E., Wisniewski, M., Le Borgne, A., Spassky, N., Macromolecules, 1998, 31, 3895-3905

[53] Abu-Abdeen, M., Materials and design, 2012, 34, 469-473

[54] Klug, H., Alexander, L. E., X-ray diffraction procedures for polycrystalline and amorphous materials, John Wiley & sons, New York, 1974, pp.137-139 & 489-499

[55] Li, L. X., Cai, W., Gao, Z., Jun, T. W., Polymer bulletin, 2007, 58, 381-391

[56] Jeon, O., Lee, S. H., Kim, S. H., Lee, Y. M., Kim, Y. H., Macromolecules, 2003, 36, 5585-5592

[57] Pluta, M., Galeski, A., Biomacromolecules, 2007, 8, 1836-1843

[58] Sarasua, J. R., López-Rodríguez, N., Zuza, E., Petisco, S., Castro, B., del Olmo, M., Palomares, T., Alonso-Varona, A., Journal of materials science: materials in medicine, 2011, 22, 2513-2523

[59] Khonadar, H. A., Morshedian, J., Mehrabzadeh, M., Wagenknecht, U., Jafari, S. H., European polymer journal, 2003, 39, 1729-1734

[60] Lee, J. K., Lee, K. H., Jin, B. S., European polymer journal, 2001, 37, 907-914

[61] Aou K., Kang S., Hsu S.L., Macromolecules, 2005, 38, 7730-7735

[62] Tobolsky, A. V., Andrews, R. D., The journal of chemical physics, 1945, 13, 3-27

[63] Ohki, T., Ni, Q. Q., Ohsako, N., Iwamoto, M., Composites: Part A, 2004, 35, 1065-1073

[64] Khonakdar, H. A., Morshedian, J., Mehrabzadeh, M., Wagenknecht, U., Jafari, S. H., European polymer journal, 2003, 39, 1729-1734

[65] Smith, P. B., Leugers, A., Kang, S., Hsu, S. L., Yang, X., Journal of applied polymer science, 2001, 82, 2497-2505

[66] Tervoort, T. A., Govaert, L. E., Journal of rheology, 2000, 44, 1263-1277

[67] van Melick, H. G. H., Govaert, L. E., Meijer, H. E. H., Polymer, 2003, 44, 2493-2505

[68] Wang, W., Ping, P., Chen, X., Jing, X., Polymer international, 2007, 56, 840-846

[69] Petisco S., Larrañaga, A., Gracia, C., Sarasua, J. R., Eurotec 2013-Proceedings of the 2nd European technical conference & exhibition, Lyon, France, July 4-5, 2013, 488-493

[70] Mavridis, H.; Shroff, R.N., Polymer engineering and science, 1992, 32, 1778-1791

[71] Yang, X., Kang, S., Yang, Y., Aou, K., Hsu, S. L., Polymer, 2004, 45, 4241-4248

[72] Kang, S., Hsu, S. L., Stidham, H. D., Smith, P. B., Leugers, M. A., Yang, X., Macromolecules, 2001, 34, 4542-4548

[73] Yang, X., Kang, S., Hsu, S. L., Stidham, H. D., Smith, P. B., Leugers, A., Macromolecules, 2001, 34, 5037-5041

[74] Zhuohong, Y., Jinlian, H., Yeqiu, L., Lapyan, Y., Materials chemistry and physics, 2008, 98, 368-372

[75] Lin, J. R., Chen, L. W., Journal of Applied Polymer Science, 1998, 69, 1563-1574

[76] Lin, J. R., Chen, L. W., Journal of Applied Polymer Science, 1998, 69, 1575-1586

[77] Petisco, S., Fernández, J., Amestoy, H., Ugartemendia, J. M., Santamaría, A., Sarasua, J. R., 5TH International conference on mechanics of biomaterials and tissues, Sitges, Spain, December 8-12, 2013

[78] Andreopoulos, A. G.; Hatzi, E.; Doxastakis, M. Journal of materials science: materials in medicine, 1999, 10, 29-33

[79] Urayama, H.; Kanamori, T.; Kimura, Y., Macromolecular Materials and Engineering, 2001, 286, 705-713

[80] Gordon, M., Taylor, J. S., Journal of Applied Chemistry, 1952, 2, 493-500

[81] Gibbs, J. H., DiMarzio, A., The journal of chemical physics, 1958, 28, 373-383

[82] Ferry, J. D., Viscoelastic properties of polymers. Third edition. John Wiley & sons, Inc. New York, 1980, pp. 254, 352, 378

[83] Wu, S., Journal of polymer science: part B: polymer physics, 1989, 27, 723-741

[84] Graessley, W. W., Polymer liquids & networks: Dynamics and rheology. Graessley, W. W., Garland Science Taylor & Francis group, New York, 2008, pp. 151, 152

[85] Florez, S., Muñoz, M. E., Santamaría, A., Macromolecular materials and engineering, 2006, 291, 1194-1200

[86] Meaurio, E., Zuza, E., López-Rodriguez, N., Sarasua, J. R., The journal of physical chemistry B, 2006, 110, 5790-5800

[87] Pan, P., Zhu, B., Inoue, Y., Macromolecules, 2007, 40, 9664-9671

[88] Ugartemendia, J. M., Muñoz, M. E., Sarasua, J. R., Santamaria, A., Rheologica acta, 2014, 53, 857-868

[89] Angell, C. A., Science, 1995, 267, 1924-1935

[90] Zuza, E., Ugartemendia, J. M., Lopez, A., Meaurio, E., Lejardi, A., Sarasua, J. R., Polymer, 2008, 49, 4427-4432

General conclusions

Due to their molecular structure, polymers offer a wide spectrum of properties that can be easily modified in order to match those demanded by application. In this Thesis, several strategies have been explored in order to tune the viscoelastic properties and shape memory of several polylactide based polymers, whose effects have been rationalised taking into consideration the observed microstructural changes.

Copolymerization and blending

It has been shown that compared to pure PLLA, the introduction of a second copolymer during the synthesis step, has hindered and even prohibited the crystallization capacity of the copolymer and promoted the glass transition event.

The importance of the glass transition and, more specifically, their relative position to the temperature of use, relies on the three orders of magnitude change of i. e. storage modulus that takes place on its vicinity categorizing polymers into glasses and elastomers.

In compatible and not to strongly polar systems, the glass transition temperature can be derived from the assumption of the law of mixtures, so that a tailor glass transition copolymer can be easily designed.

Blending has proven to be a useful strategy to attain a full spectrum of properties flanked by those of pure copolymers even when miscibility is not achieved. In such cases, it is the majoritarian component which determines the resultant properties of the blend.

Thermoconformation

Following synthesis, the necessary step towards a useful device is processing the polymer. One of such techniques is based on easily shaping polymers above their melting temperature and fixing by solidification on cooling below their corresponding glass transition temperature.

Here, the rate of cooling has a decidedly strong influence over the microstructure.

More explicitly, in those polymers with crystallization capacity, the resulting crystalline (X_c) and amorphous (X_a=1-X_c) fractions are consequence of rapid (X_c=0%) or

slow cooling. Although crystallization is favoured in linear polymer chains, polymers do not achieve 100% crystallinity as the ability of chains to diffuse from the melt regions to regions around the nuclei severely decreases with the rapid increase in viscosity while the melt is cooled, so that an amorphous region is always present.

In polymers that inherently lack crystallization capacity, it is the glass transition temperature which reflects the deviation from thermodynamic equilibrium.

Thus, the resulting structural state constitutes an undercooled liquid with excess of thermodynamic properties that kept under constant temperature (or pressure) gradually approaches to equilibrium according to a process termed physical aging.

Amongst the peculiarities of physical aging are its thermal reversibility, its memory (nonlinearity), and its kinetics. Moreover, it has been claimed to be the responsible of ductile to brittle transition in polymers.

Though physical aging is a universal phenomenon associated to the extremely local rearrangements of the frozen amorphous phase, it has been shown that in polymers, a more irregular chain microstructure (higher randomness character) shows a faster aging kinetics. It has been rationalised that these irregularities act as joint points providing further flexibility to the chain backbone so that it can more easily accommodate the corresponding rearrangements of its segments in search of thermodynamic equilibrium.

Self-reinforcing

Behind this term is the observed enhancement in toughness and ductile behaviour of polylactide based polymers as a consequence of molecular orientation impinged by stretching at temperatures in the vicinity of the glass transition temperature. It was speculated that this arrangement favoured physical bonds between adjacent chains, which contributed to the spectacular raise of the elastic modulus, and upon application of sufficient stress, yielding.

Unexpectedly, in semicrystalline polymers, this stretching procedure caused a higher crystallization degree than that achieved by thermal treatment.

Plasma polymerization and compounding

Surface modification of Hydroxyapatite powder by plasma polymerization starting from two different monomers has showed to have a positive influence from many standpoints.

Regarding processing by thermoconformation, plasma coating has improved the thermal stability of the polymeric matrix, retarding the onset of thermal degradation, therefore extending the achievable processing temperature.

On the other hand, from the mechanical properties of the composite viewpoint, plasma polymerization has enhanced the interface adhesion between polymeric matrix and inorganic particles, leading to superior properties of the composite, yet preserving the character of the matrix.

In fact, the polymeric matrix composites demonstrated a higher resemblance to the neat polymeric matrix (damping, homogeneous nucleation and crystallization kinetics) than neat particles composites did.

Thermally triggered shape memory

Deeping into the fascinating shape memory effect based on the glass transition as the switching phase, it has been concluded that those factors that cause a deleterious effect on the entropic elasticity or on the amorphous phase will have so upon the shape memory effect. Amongst these, a distinction has been made between extrinsic conditions such as the programming procedure (temperature, temporary strain, recovery time) and intrinsic factors such as chain topology and molecular weight.

Interestingly, after fully development of these detrimental effects, (training effect), stable recovery has been achieved.

Appendix

A1. List of figures

A2. List of tables

A3. List of Symbols and abbreviations

%wt	Weight percentage
$(l_{CL})_{random}$	Bernoullian random number average sequence length of CL
$(l_{LA})_{random}$	Bernoullian random number average sequence length of L-LA
$(\tan \delta)_c$	Damping factor of the composite
$(\tan \delta)_m$	Damping factor of the matrix
ΔH_m^0	Enthalpy of fusion of the polylactide crystal (106J/g)
G_N^0	Plateau modulus in the rubbery region
$\dot{\varepsilon}$	Strain rate
A	Proportionality adjustment coefficient
ACL	Anterior cruciate ligament
a_T	Horizontal displacement
b	Instrumental width
b	Fibre matrix interface adhesion parameter
B	Observed width
C_1	Fitting parameter
C_2	Fitting parameter
C_∞	Aspect ratio
CAD	Coronary artery disease
CE	Conformité Européenne

$CHCl_3$	Chloroform
CL	ε-caprolactone
CL	Molar fraction of ε-caprolactone
Coll/HA/PCL	collagen-hydroxyapatite-poly(L-lactide-co-ε-caprolactone)
C_p	Heat capacity
DLA	D,L-lactide
DMTA	Dynamic mechanical thermal analysis
DSC	Differential scanning calorimetry
E	Elastic modulus
E*	Complex modulus (in tensile mode)
E’	Storage modulus (in tensile mode)
E'_a	Storage modulus(in tensile mode) after the transition
E'_b	Storage modulus (in tensile mode) before the transition
E’(T)	Temperature dependent storage modulus (in tensile mode)
E”	Loss modulus (in tensile mode)
E”(T)	Temperature dependent loss modulus (in tensile mode)
$E_{2\%}$	Secant modulus at 2% strain
E_a	Activation energy of flow
ECM	Extracellular matrix
E_{glassy}	Storage modulus in the glassy state
$E_{rubbery}$	Storage modulus in the rubbery state

EU	European Union
ε_B	Strain at break
ε_m	Maximum mechanical deformation
ε_p	Permanent strain after thermally triggered shape recovery
ε_u	Remanent strain after sudden elastic recovery
f	Test frequency
FWHM	Full width at half maximum
GA	Glycolic acid, glycolide
g-HA	Grafted hydroxyapatite
G_x	Crossover storage modulus (in shear mode)
HA	Hydroxyapatite ($Ca_{10}(PO_4)_6(OH)_2$)
HA_{AA}	Plasma polymerized poly(acrylic acid) functionalized hydroxyapatite
$HA_{\varepsilon\text{-cap}}$	Plasma polymerized ε-caprolactone functionalized hydroxyapatite
K	Shape factor
k_B	Boltzmann's constant
KBr	Potassium bromide
LARS	Ligament advanced reinforcement system
l_{CL}	Number average sequence length of caprolactone building blocks
LA	Molar fraction of lactide

l_{LA}	number-average sequence length of L-Lactide building blocks
LA-CL	Average dyad relative molar fraction
m	Dynamic fragility
M_c	Critical value for chain entanglements
Mc	molecular weight between cross-links
MDSC	Modulated differential scanning calorimetry
MDSC	Modulated scanning calorimetry
MDW	Molecular weight distribution
M_e	Molecular weight between entanglements
MS	Mass spectrometry
MWCNT	Multiwall carbon nanotubes
PDLGA	Poly(racD,L-lactide-co-glycolide)
PGA	Polyglicolide
PLA	Poly(lactide), polylactides
PLCL	Poly(L-lactide-co-ε-caprolactone)
PLCL-B	Blocky poly(L-lactide-co-ε-caprolactone)
PLCL-R	Random poly(L-lactide-co-ε-caprolactone)
PLLA	Poly(L-lactic acid)
PTCA	Percutaneous transluminal coronary angioplasty
PXX_a	Amorphous state obtained by quenching from the melt

PXX_c	Crystalline state obtained by annealing above the glass transition temperature
PXX_o	Oriented state obtained by stretching at temperature ≥ Glass transition temperature
PXX_oHT	Temperature triggered shrunk state starting from an oriented state
Q_E	Maximum energy absorption
Q_t	Net energy absorption after "t" annealing time
r	Cooling rate
R	Randomness character
R	Universal gas constant (8.32J/Kmol)
R^2	Coefficient of determination according to linear least squares fitting
R_f	Strain fixity ratio
ROP	Ring opening polymerization
R_r	Strain recovery ratio
RSF	Relative sensitivity factors
RT	Room temperature
S	Intensity of the glassy to rubbery transition
SEM	Scanning electron microscope
SMA	Shape memory alloy
SME	Shape memory effect
SMP	Shape memory polymer

T	Temperature
tan δ	Damping factor
TCP	β-tricalcium phosphate
T_{def}	Deformation temperature
T_{fix}	Temporary shape fixing temperature
T_g	Glass transition temperature
TGA	Thermo gravimetry analysis
T_{HIGH}	Programming temperature
T_m	Melting temperature
T_{mp}	Normal melting temperature
T_{onset}	Thermal degradation onset temperature
T_p	Peak temperature
T_{perm}	Processing temperature
T_{switch}	Switching temperature
T_{trans}	Transition temperature; either melting, crystallization or glass
TRL	Technology readiness level
TTS	Time temperature superposition principle
UTS	Ultimate tensile strength
V_f	Fibre volume content
w_x	Weight fraction
Xa	Amorphous fraction

X_c	Crystallinity degree
XPLLA	Fraction of PLLA
XPS	X-ray photoelectron spectroscopy
α	Thermal expansion coefficient
β_τ	line broadening at half the maximum intensity
δ	Phase angle
Δ	Relaxation strength
ΔEc	Crystallization activation energy
ΔG_{mix}	Gibbs free energy of mixing
ΔH	Enthalpy of activation
ΔH_{cc}	Enthalpy of cold crystallization
ΔH_m	Enthalpy of fusion
ΔH_{mix}	Enthalpy of mixing
ΔH_r	Enthalpy relaxation
ΔT_p	Undercooling
ΔT_{rec}	Recovery temperature interval
$\Delta\sigma_{th}$	Thermal stress
η_{dp}	Melt viscosity of the dispersed phase
η_m	Melt viscosity of the polymer matrix
θ	Bragg angle
λ	X-ray wavelength

ν	Frequency
ν	Number density of network chains
νr	Maximum recovery rate
ρ	Mass density
ρ	Volumetric energy of fracture
σ_0	Initial stress (before stress relaxation)
σ_B	Stress at break
σ_c	Tensile strength of the composite
σ_d	Drawing stress
σ_f	Final stress (after stress relaxation)
σ_m	Tensile strength of the matrix
τ	Relaxation time
τ	Relaxation time, coherent diffraction domain
τ_d	Disentanglement time
τ_E	Experiemtal time
τ_S	Structural lifetime
Φ	Nucleating activity
ω	Angular frequency
Ω	Number of configurations
ω_x	Crossover frequency

A4. List of Scientific contributions and patents

Scientific papers

Petisco, S., Zuza, E., Aldazábal, P., Eizaguirre, I., Arrieta, A., Sarasua, J. R., In search of a flexible biomaterial for urologic applications *(in progress).*

Petisco, S., Sánchez, M. B., Meaurio, E., Sarasua, J. R., Plasma polymerization of HA *(in progress).*

Bobel, A. C., Petisco, S., Sarasua, J. R., Wang, W., McHugh, P. E., Computational bench testing to evaluate the short-term mechanical performance of a polymeric stent, Cardiovascular engineering and technology 2015, 10.1007/s13239-015-0235-9

Larrañaga, A., Petisco, S., Sarasua, J. R., Improvement of thermal stability and mechanical properties of medical polyester composites by plasma Surface modification of the bioactive glass particles, Polymer degradation and stability, 98, 1717-1723 (2013)

Lizundia, E., Petisco, S., Sarasua, J. R., Phase-structure and mechanical properties of isothermally melt-and cold-crystallized poly(L-lactide). Journal of the mechanical behavior of biomedical materials, 17, 242-251, (2013).

Petisco, S., Larrañaga, A., Gracia, C., Sarasua, J. R., Evaluation of shape memory of a poly(racDL-lactide-co-glycolide) Amorphous Copolymer. EUROTEC® 2013 – Proceedings of the 2nd European Technical Conference & Exhibition, Lyon, France, July 4-5, 488-493 (2013)

Petisco, S., Larrañaga, A., Sarasua, J. R., Effects Of Thermo-Mechanical Treatments On Mechanical Properties Of Lactide Derived (Co)Polymers, EUROTEC® 2013 – Proceedings of the 2nd European Technical Conference & Exhibition, Lyon, France, July 4-5, 482-487 (2013)

Fernández, J., Etxeberria, A., Ugartemendia, J. M., Petisco, S., Sarasua, J. R., Effects of chain microstructures on mechanical behavior and aging of a poly(L-lactide-

co-caprolactone) biomedical thermoplastic-elastomer. Journal of the mechanical behavior of biomedical materials, 12, 29-38, (2012).

Sarasua, J. R., Petisco, S., Fernández, J., Etxeberria, Lejardi, A., Ugartemendia, J. M., Aging Effects, Crystallinity and Phase Structure of Polylactides, European Conference on Biomaterials, 24th, Dublin, Ireland, Sept. 4-8, 2011, 135-142 (2012).

Petisco, S., Zuza, E., Ugartemendia, J. M., Arrieta, A., Eizaguirre, I., Aldazábal, P., Sarasua, J. R., Biodegradation and Mechanical Properties of Polylactides For Urological Applications, European Conference on Biomaterials, 24th, Dublin, Ireland, Sept. 4-8, 2011, 127-133 (2012).

Petisco, S., González, J. J., Sarasua, J. R., Viscoelastic Behavior and Shape Memory Properties of Medical Polylactides, European Conference on Biomaterials, 24th, Dublin, Ireland, Sept. 4-8, 2011, 143-150, (2012).

Larrañaga, A., Sarasua, J. R., Petisco, S., Rubio, E., Palomares, T., Alonso-Varona, A. Mechanical properties and cell viability of lactide and caprolactone based 3-Dimensional scaffolds filled with inorganic bioactive particles. Journal of tissue engineering and regenerative medicine, 5 (suppl. 1), 213-213 (2012)

Congresses and workshops

Petisco, S., Sarasua, J. R., Structure-Property Relationships in Lactide Derived Biodegradable Polymers, ALBA Synchrotron: new tools for materials characterization Barcelona, 13-14 Nov. 2014

Petisco, S., Fernández, J., Amestoy, H., Ugartemendia, J. M., Santamaría, A., Sarasua, J. R. An evaluation of the role of entanglements on thermo-mechanical and shape memory behaviour of an amorphous copolylactide, 5th International Conference on Mechanics of Biomaterials and Tissues, Sitges, España, 8-12 Diciembre, 2013

Petisco, S., Bobel, A., Mc Mahon, S., Mc Hugh, P., Wang, W., Sarasua, J. R. Structural Changes induced by stress relaxation tests on PLLA. 5th International Conference on Mechanics of Biomaterials and Tissues, Sitges, España, 8-12 Diciembre, 2013

Petisco, S., Fernández, J., Sarasua, J. R. Viscoelasticity and Mechanical Properties of Poly (L-lactide-co-ε-caprolactone) Copolymers with Well Resolved Chain Microstructures. 25th European Conference on Biomaterials, Madrid, España, 8-12, Septiembre, 2013

Petisco, S., Larrañaga, A., Gracia, C., Sarasua, J. R. Evaluation of shape memory of a poly(racDL-lactide-co-glycolide) Amorphous Copolymer. EUROTEC® 2013 – 2nd European Technical Conference & Exhibition, Lyon, France, July 4-5, 2013

Petisco, S., Larrañaga, A., Sarasua, J. R. Effects Of Thermo-Mechanical Treatments On Mechanical Properties Of Lactide Derived (Co)Polymers. EUROTEC® 2013 – 2nd European Technical Conference & Exhibition, Lyon, France, July 4-5, 2013

Larrañaga, A., Petisco, S., Sarasua, J. R., Rubio, E., Palomares, T., Alonso-Varona, A. Mechanical properties and cell viability of lactide and caprolactone based 3-dimensional scaffolds filled with inorganic bioactive particles. 3rd TERMIS World Congress, Viena (Austria), 2012

Sarasua, J. R., Petisco, S., Fernández, J., Meaurio, E., Larrañaga, A., Ugartemendia, J. M., Polylactides for tissue engineering: synthesis, structure and properties. International Forum of Biomedical Materials: Nanobiomaterials for Tissue Regeneration, Hangzhou, China, May 29-June 1, 2012

Fernández, J. Ugartemendia, J. M., Petisco, S., Etxeberria, A., Sarasua, J. R. Effects of Chain Microstructure on Physical Aging, Mechanical Properties, and Thermal Stability of a poly(L-lactide-co- e-caprolactone) Elastomer Thermoplastic Copolymer. 9th World Biomaterials Congress: Innovative Biomaterials and Crossing Frontiers in Biomaterials and Regenerative Medicine, Chengdu, China, 2012

Sarasua, J. R., Ugartemendia, J. M., Petisco, S., Fernández, J., Effects of physical aging on enthalpy relaxation and embrittlement of elastomer thermoplastic biodegradable poly(L-lactide/ε-caprolactone). SPE Eurotec 2011, Barcelona (Spain), 14-15 November 2011

Larrañaga, A., Petisco, S., Villanueva, R., Iturri, J., Moya, S., Meaurio, E., Sarasua, J. R., Physicochemical Properties of Plasma Polymerized Acrylic Acid, ε-caprolactone and lactic acid films. SPE Eurotec 2011, Barcelona (Spain), 14-15 Noviembre 2011

Sarasua, J. R., Zuza, E., Ugartemendia, J. M., Petisco, S., Arrieta, A., Eizaguirre, I., Aldazábal, P. Biodegradation and Mechanical Properties of Polylactides in Urological Medium. ESB 24th European Conference on Biomaterials, Dublin (Ireland), 4th-9th September 2011

Sarasua, J. R., Petisco, S., González-Martínez, J., Fernández, J. Viscoelastic behavior and shape memory properties of medical polylactides. ESB 24th European Conference on Biomaterials, Dublin (Ireland), 4th-9th September 2011

Sarasua, J. R., Petisco, S., Fernández, J., Ugartemendia, J. M., Aging effects, crystallinity and phase structure of polylactides. ESB 24TH European Conference on Biomaterials, Dublin (Ireland), 4th-9th September 2011

Petisco, S., Ugartemendia, J. M., Lejardi, A., Sarasua, J. R., Elastomer Thermoplastic Behavior of a biodegradable poly(lactide caprolactone) multiblock copolymer. SPE European Medical Polymers Conference 2010, Belfast (UK), 7th-9th September 2010

Patents

"Biodegradable Bioglass-polymer composite having improved thermal stability", Larrañaga Espartero, A., Petisco Ferrero, S., Sarasua Oiz, J. R., ES2457991 (A1); WO2014049190 (A1), 2012.

"Sistema y método para el tratamiento de partículas sólidas en un ambiente de especies activadas por plasma", Petisco Ferrero, S., Larrañaga Espartero, A., Sarasua Oiz, J. R., Spanish application number 201430447.